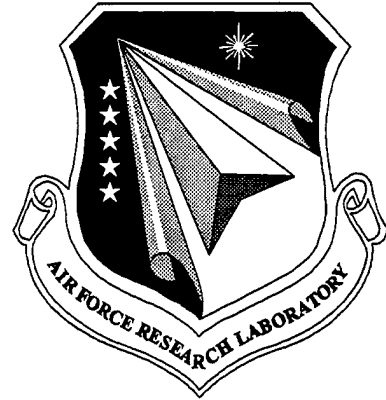


AFRL-ML-WP-TR-1998-4097

**AN EXPERT SYSTEM FOR DESIGN
OF PLASTIC INTEGRATED CIRCUIT
PACKAGES AGAINST LATENT
MOISTURE INDUCED DEFECTS**



**An-Yu Kuo
Structural Integrity Associates
3315 Almaden Expressway, Suite 24
San Jose, California 95118**

**Luu T. Nguyen
Kuan-Luen Chen
National Semiconductor
2900 Semiconductor Drive
Santa Clara, California 950522**

FEBRUARY 1998

FINAL REPORT FOR PERIOD JANUARY 1995 – DECEMBER 1997

Approved for public release; distribution unlimited

19980727 023

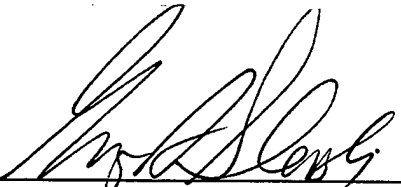
**MATERIALS & MANUFACTURING DIRECTORATE
AIR FORCE RESEARCH LABORATORY
AIR FORCE MATERIEL COMMAND
WRIGHT-PATTERSON AIR FORCE BASE, OH 45433-7734**

NOTICE

WHEN GOVERNMENT DRAWINGS, SPECIFICATIONS, OR OTHER DATA ARE USED FOR ANY PURPOSE OTHER THAN IN CONNECTION WITH A DEFINITE GOVERNMENT-RELATED PROCUREMENT, THE UNITED STATES GOVERNMENT INCURS NO RESPONSIBILITY OR ANY OBLIGATION WHATSOEVER. THE FACT THAT THE GOVERNMENT MAY HAVE FORMULATED OR IN ANY WAY SUPPLIED THE SAID DRAWINGS, SPECIFICATIONS, OR OTHER DATA, IS NOT TO BE REGARDED BY IMPLICATION, OR OTHERWISE IN ANY MANNER CONSTRUED, AS LICENSING THE HOLDER, OR ANY OTHER PERSON OR CORPORATION; OR AS CONVEYING ANY RIGHTS OR PERMISSION TO MANUFACTURE, USE, OR SELL ANY PATENTED INVENTION THAT MAY IN ANY WAY BE RELATED THERETO.

THIS REPORT IS RELEASABLE TO THE NATIONAL TECHNICAL INFORMATION SERVICE (NTIS). AT NTIS, IT WILL BE AVAILABLE TO THE GENERAL PUBLIC, INCLUDING FOREIGN NATIONS.

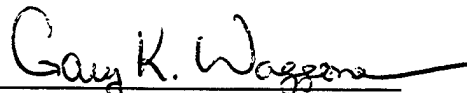
THIS TECHNICAL REPORT HAS BEEN REVIEWED AND IS APPROVED FOR PUBLICATION.



GEORGE A. SLENSKI
Struct. & Electr. FA section
Materials Integrity Branch
System Support Division
MATERIALS AND MANUFACTURING
DIRECTORATE



MICHAEL F. HITCHCOCK
Branch Chief
Materials Integrity Branch
Systems Support Division
MATERIALS AND MANUFACTURING
DIRECTORATE



GARY K. WAGGONER
Chief
Systems Support Division
MATERIALS AND MANUFACTURING
DIRECTORATE

Publication of this report does not constitute approval or disapproval of the ideas or findings. It is published in the interest of scientific and technical information exchange.

REPORT DOCUMENTATION PAGE			Form Approved OMB No. 0704-0188	
Public reporting burden for this collection of information is estimated to average 1 hour per response, including the time for reviewing instructions, searching existing data sources, gathering and maintaining the data needed, and completing and reviewing the collection of information. Send comments regarding this burden estimate or any other aspect of this collection of information, including suggestions for reducing this burden, to Washington Headquarters Services, Directorate for Information Operations and Reports, 1215 Jefferson Davis Highway, Suite 1204, Arlington, VA 22202-4302, and to the Office of Management and Budget, Paperwork Reduction Project (0704-0188), Washington, DC 20503.				
1. AGENCY USE ONLY (Leave blank)		2. REPORT DATE February 1998		3. REPORT TYPE AND DATES COVERED Final Report Jan 95 - Dec 97
4. TITLE AND SUBTITLE An Expert System for Design of Plastic Integrated Circuit Packages Against Latent Moisture Induced Defects			5. FUNDING NUMBERS F33615-95-C-5623 PE 65502F PR 3005 TA 05 W U E5	
6. AUTHOR(S) An-Yu Kuo * Kuan-Luen Chen** Luu T. Nguyen**				
7. PERFORMING ORGANIZATION NAME(S) AND ADDRESS(ES) Structural Integrity Associates* 3315 Almaden Expressway, Suite 24 San Jose, California			8. PERFORMING ORGANIZATION REPORT NUMBER SIR-94-130	
9. SPONSORING/MONITORING AGENCY NAME(S) AND ADDRESS(ES) Materials & Manufacturing Directorate Air Force Research Laboratory Air Force Materiel Command Wright-Patterson Air Force Base, OH 45433-7734 POC: George Slenski, AFRL/MLSA, 937-656-9147			10. SPONSORING/MONITORING AGENCY REPORT NUMBER AFRL-ML-WP-TR-1998-4097	
11. SUPPLEMENTARY NOTES This is a Small Business Innovation Research Report (SBIR), Phase II				
12a. DISTRIBUTION AVAILABILITY STATEMENT Approved for Public Release; Distribution Unlimited			12b. DISTRIBUTION CODE	
13. ABSTRACT (Maximum 200 words) This program examined the feasibility of developing a model for predicting cracking of plastic integrated circuit packages. It was demonstrated that moisture induced hydro-thermal stresses during soldering operations can cause plastic package cracking or "pop coming." A crack propagation model was developed using fracture mechanics parameters coupled with hydrostatic stresses. Selected plastic packages were characterized using the developed model and segregated according to crack susceptibility during a solder reflow process. Model results compared favorably with laboratory testing on actual parts. Also developed was a computer based expert system that incorporates the crack prediction model.				
14. SUBJECT TERMS Thermal Stress, Plastic Integrated Circuits, Electronic Packaging, Expert System			15. NUMBER OF PAGES 161	
			16. PRICE CODE	
17. SECURITY CLASSIFICATION OF REPORT UNCLASSIFIED	18. SECURITY CLASSIFICATION OF THIS PAGE UNCLASSIFIED	19. SECURITY CLASSIFICATION OF ABSTRACT UNCLASSIFIED	20. LIMITATION OF ABSTRACT SAR	

TABLE OF CONTENTS

1	Introduction.....	1-1
2	A Brief Review of Theories and Equations Used in EPACK.....	2-1
2.1	Heat Transfer.....	2-1
2.1.1	Governing Equations.....	2-1
2.1.2	Boundary Conditions.....	2-2
2.1.3	Finite Element Formulation of Heat Transfer Problems.....	2-5
2.2	A Brief Review of Thermal Stress Theories.....	2-7
2.2.1	Governing Equations.....	2-7
2.2.2	Boundary Conditions.....	2-10
2.2.3	Finite Element Formulation of Thermal Stress Problems.....	2-10
2.3	A Brief Review of Fracture Mechanics Theories.....	2-12
2.3.1	Fundamental Concepts.....	2-12
2.3.2	Determination of Applied K for IC Packages.....	2-15
2.4	A Brief Review of Moisture Diffusion and Evaporation.....	2-21
2.4.1	Governing Equations.....	2-21
2.4.2	Boundary and Initial Conditions.....	2-21
2.4.3	1-D Moisture Diffusion Solutions for Thin Packages.....	2-22
2.4.4	Moisture Diffusion Material Constants.....	2-22
2.5	Effects of Moisture on Plastic Package Reliability.....	2-25
2.5.1	Adhesion Strength and Delamination Criterion.....	2-25
2.5.2	EMC Fracture Toughness (see Chapter 3 for details).....	2-26
2.5.3	Interface Fracture Toughness (see Chapter 3 for details).....	2-26
2.5.4	Molding Compound Swelling Coefficients.....	2-27
3	Fracture Strength of Epoxy Molding Compounds.....	3-1
3.1	Fracture Toughness (K_{IC}) of EMC.....	3-1
3.2	Specimen Preparation.....	3-3
3.3	Test Procedures.....	3-5
3.4	Measured Results.....	3-6
3.5	SUMMARY ON RESULTS.....	3-12
4	INTERFACIAL FRACTURE TOUGHNESS IN PLASTIC PACKAGES.....	4-1
4.1	INTRODUCTION.....	4-1
4.2	EXPERIMENTAL.....	4-2
4.2.1	Test Conditions.....	4-2
4.2.2	Test Procedures.....	4-3
4.3	RESULTS AND DISCUSSION.....	4-9
4.3.1	Interface Fracture Toughness.....	4-9
4.3.2	J-Integral for Thermoelasticity.....	4-10
4.3.3	Stress Intensity Factors of Interface Cracks with an Open Crack Tip.....	4-11
4.3.4	Stress Intensity Factor of Closed Interface Cracks.....	4-12

4.3.5. Fracture Mode Separation for Open Interface Cracks	4-13
4.3.6. Elastic Properties of Tested Materials.....	4-13
4.3.7. Mixed-Mode Interface Fracture Toughness	4-14
4.3.8. Discussion.....	4-15
4.4 CONCLUSIONS	4-17
5. Desorption and Absorption Diffusivity of Mold Compounds	5-1
5.1. Objective	5-1
5.2. Introduction.....	5-1
5.3. Procedure	5-1
5.4. Test Specimens	5-2
5.5. Calculation of Diffusivity	5-2
5.6. Results and Discussion.....	5-4
5.7. Conclusion.....	5-6
6. The Effect of Reflow Ramp Rate on Popcorning.....	6-1
6.1. Objective	6-1
6.2. Package Specifications.....	6-1
6.3. Procedure	6-1
6.4. Discussion	6-2
6.5. Conclusion.....	6-4
7. GaAs Package Thermal Shock and Thermal Cycling Experiment.....	7-1
7.1. Overview	7-1
7.2. Package Description	7-1
7.3. Equipment	7-1
7.3.1. Scanning Procedure.....	7-2
7.3.2. Preconditioning	7-2
7.3.3. Thermal Shock Procedure	7-2
7.3.4. Thermal Cycling Procedure	7-3
7.4. Discussion	7-3
7.5. Conclusion.....	7-7
8. Popcorning Evaluation of Plastic Packages	8-1
8.1. Objective	8-1
8.2. Part Descriptions	8-1
8.3. Procedure	8-2
8.4. Discussion	8-2
8.5. IR Reflow Temperature Profile	8-5
8.6. Micrographs of cross-sectioned parts	8-6
8.7. Example C-SAM Images of PBGA parts at 0-hour.....	8-8
8.8. Conclusion.....	8-9
9. Hygrothermal Reliability Evaluation of Plastic IC Packages with EPACK	9-1
9.1. Introduction.....	9-1
9.2. EPACK Program Structure.....	9-2
9.3. Automatic Finite Element Mesh Generation	9-3
9.4. Moisture Diffusion Analysis	9-6

9.5. Hygrothermal Stress Analysis.....	9-7
9.6. Initial Delamination.....	9-8
9.7. Propagation of Interface Cracks.....	9-10
9.8. Steam Pressure	9-11
9.9. Penetration of the EMC Layer.....	9-12
9.10. Model Verification and Validation.....	9-13
9.11. Conclusions	9-18
10. References.....	10-1

1 Introduction

Plastic encapsulated microcircuits (PEM) accounts for more than 95% of the worldwide electronic packaging market, and that number is growing. PEM have gained wide acceptance by the military in recent years for reliability (Gallo, 1995). In 1993, over 97% of all integrated circuits were packaged in plastic (Pecht, 1995). Substantial cost savings, lightweight, and wide availability are the principal reasons for the gradual adoption of PEM over the ceramic packages by electronics and computer industries (Mei, 1995).

Although PEM have many advantages, they are not problem free. Among these problems, the well known "popcorning" failure appears to be the most serious for many PEM manufacturers. Plastic packages are permeable to moisture due to the hygroscopic nature of the epoxy molding compound (EMC). The absorbed moisture will reduce the material interface adhesion strengths and fracture toughnesses, making the wet packages susceptible to delamination and cracking. During the older reflow, a process which is commonly used in assembling surface mount devices, a popping sound is often heard when the internal drack/delamination penetrate through the molding compound layer and becomes an external crack. This phenomenon, commonly referred to as popcorning, is a critical reliability problem with the PEM packaging.

Baking the plastic packages at a relatively low temperature prior to surface mount would eliminate the popcorning problem. However, the baking is a very undesirable and expensive option to the electronic companies because it would dramatically slow down the assembly thru-put. Currently, a common solution used in industry to avoid popcorning is to place the PEM in a dry aluminized pack containing a desiccant. These packs are used to ship moisture-sensitive PEM. The RH inside the pack is kept below 20% in order to keep the contained PEM from absorbing additional moisture from the surrounding environment. This arrangement, though effective, requires several processes which have many restrictions on their uses (Mei, 1995). The disposal of the dry bags also creates environmental problems, in addition to the burden of bookkeeping to the manufacturers.

An effort was initiated by this SBIR Phase I and II project to develop a reliable analytical/numerical model to simulate the thermo-hygro-mechanical behavior of PEM exposed to moisture diffusion from the surrounding environment. Ideally, the popcorning can be incorporated into a design expert system so that IC package designers can easily and accurately predict the moisture behavior of

his or her target package design. Such an expert system requires the following key ingredients:

- accurate and reliable input of material characteristics, such as the fracture strength of EMC at various temperatures and with various moisture contents in the materials,
- a physically sound model for the complicated popcorning mechanism,
- assemblies of numerical simulation methods and software for the multiple physics phenomena (see Figure 1-1) associated with popcorning, such as heat transfer, moisture diffusion, strength of materials, fracture mechanics, and thermodynamics,
- a package design library for most, if not all, existing package types,
- a material library containing all material hygro, thermal, mechanical, and electrical constants and coefficient for the commonly used materials in IC packaging,
- quick turn around cycle for each design simulation (less than one hour),
- it can be used by most of the packaging engineers, not the specially trained analysts, and
- thorough verification and validation of the prediction results.

Electronic Packaging Simulation requires multi-discipline

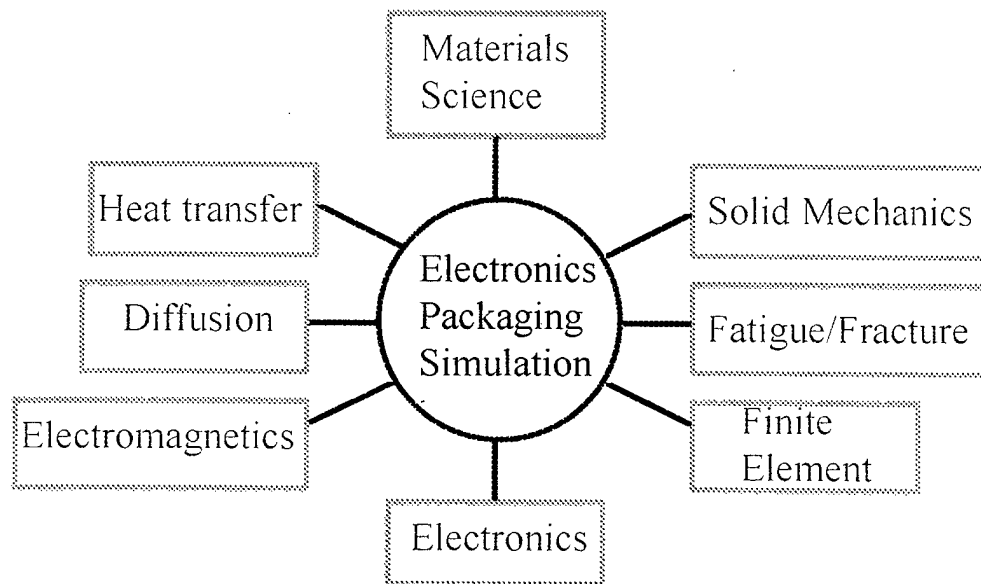


Fig 1-1 Multi-Discipline Requirement on IC Packaging Simulation

After a successful Phase II R&D, Optimal Corporation and its project team members (National Semiconductor, Ford Motor Company, San Jose State University, Quanta Laboratory, and Southwest Research Institute) have developed a commercially available design expert system, EPACK, for plastic IC packaging design.

A brief description of the resulting design software, EPACK, is presented by a product brochure attached as the last two pages of this Chapter. It can be seen from this brochure that, through additional internal funding, EPACK covers not only the popcorning problem but also other important packaging design issues, such as thermal resistance, delamination, solder joint fatigue, die cracking, molding flow simulation (wire sweep), package warpage, parasitic extraction, and electrical signal integrity.

This report present technical details employed in EPACK, while usage of the computer software is contained in a separate user's manual. Chapter 2 briefly review the theories and equations used in EPACK. Chapter 3 presents testing and results of molding compound fracture toughness. Chapter 4 describes material interface fracture toughness testing and results. Chapter 5 contains results of molding compound moisture absorption and desorption. Chapter 6 illustrates effects of temperature ramp rates during solder reflow on plastic package popcorning resistance. Chapter 7 describes testing results of thermal shocks on GaAs packages. Chapter 8 presents testing results of PBGA popcorning resistance . Chapter 9 delineates popcorning evaluation procedures of plastic packages employed by EPACK. Finally, Chapter 10 contains references cited throughout this report. Appendix I contains the user's manual.

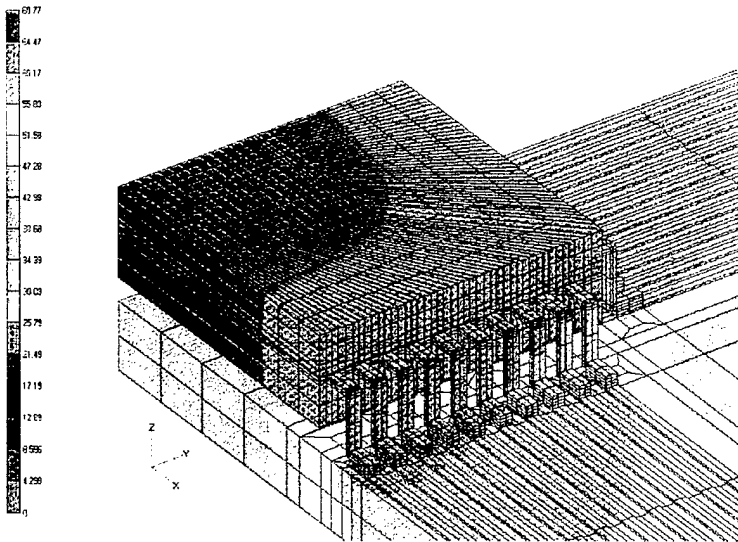


Thermal, Moisture & Mechanical Simulation of IC Packaging

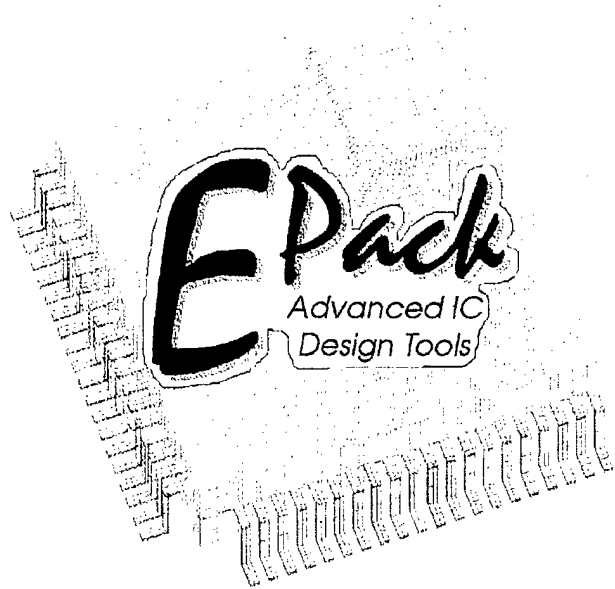
Physics-Based Simulation Tool for

- Thermal Resistance (θ_{ja} , θ_{jc}) Analysis
- JEDEC Package Popcorning Level Prediction
- Die Cracking Evaluation
- Material Delamination Evaluation
- Wire Sweep Analysis
- Moisture Diffusion Prediction
- Solder Joint Fatigue Evaluation
- Package Warpage Analysis
- Parasitic Extraction/Signal Integrity

Output Set: EPACK FINITE ELEMENT RES:Contour MODAL TEMPERATURE

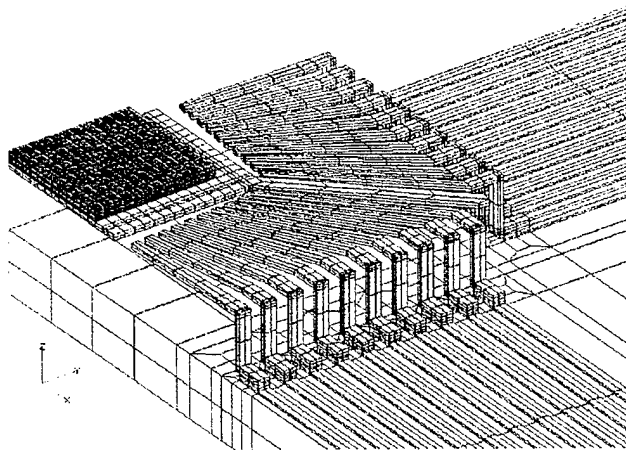
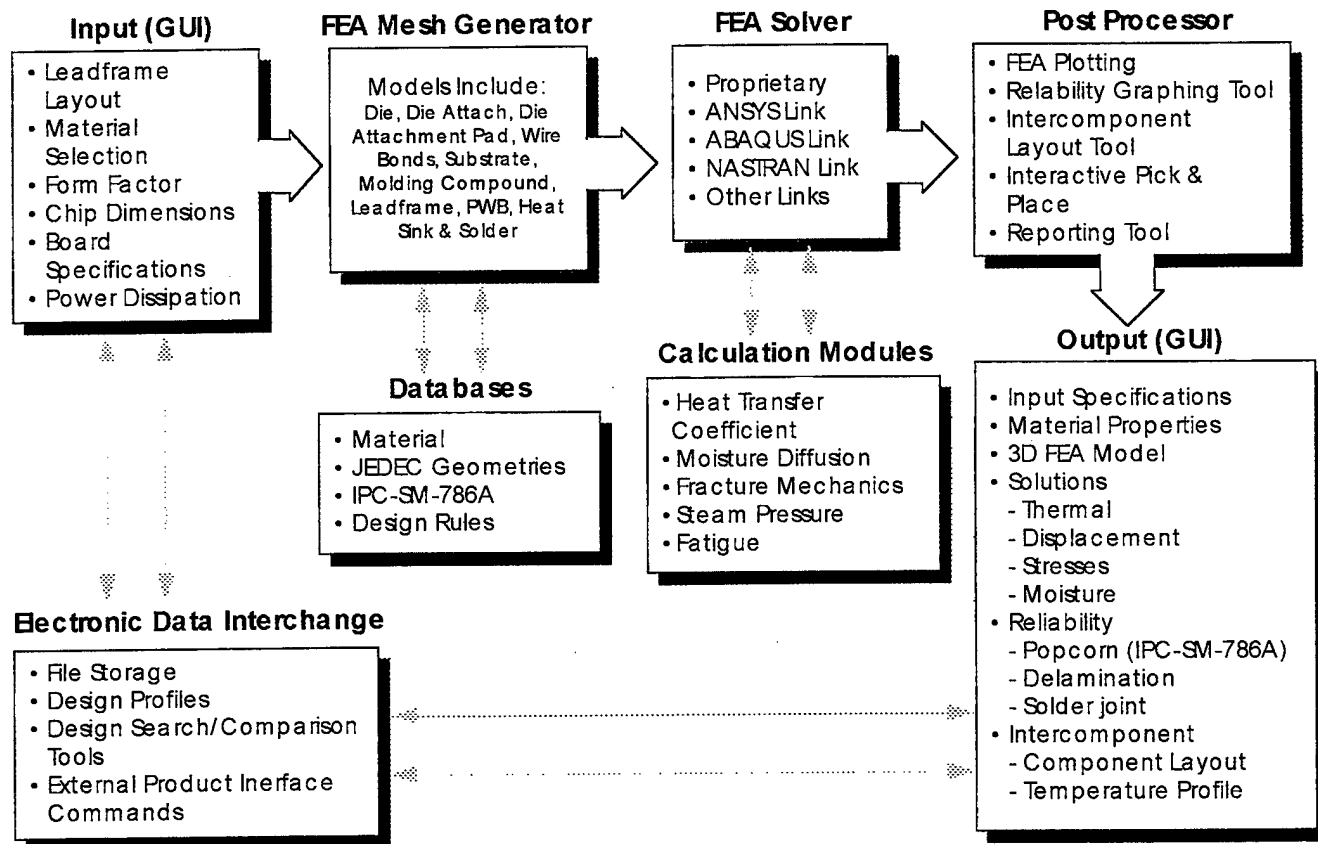


In less than 2 minutes, you can accurately predict the package's thermal resistance at different air speeds.



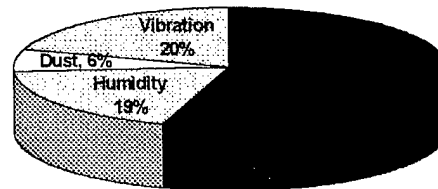
Unique Features in EPACK :

- Automatic FEM and CFD Model Generator for All JEDEC Packages (BGA, QFP, PLCC, SOJ, PGA, CSP, ...)
- Built-In Material Data Base and Failure Criteria
- Interactive, User-Friendly Data Input for Packaging Engineers
- Super-Fast Computational Speed (Less Than 15 Minutes for Most Analyses)
- Pre-Configured Figures, Tables, and Text for Cut & Paste in Report Writing
- Thoroughly Validated and Calibrated Against Thousands of Test Data Points



EPACK's model includes all the details in a plastic IC package. Components such as die, die attach, die pad, leadframe, molding compound, solder joints, metal traces, and PWB are automatically generated by EPACK in a few seconds. Even with such a complex and complete model, EPACK's super fast solver (5 minutes for a typical thermal stress problem with 45,000 degrees of freedom) makes it possible to perform design optimization and virtual prototyping of IC packages with the physics-based simulation.

Hygro-thermal-mechanical factors account for more than 30% of IC package failures (U.S. Air Force Avionics Integrity Program). EPACK's solution oriented approach provides IC packaging engineers with an expert system to assess hygro-thermal-mechanical reliability of their IC packages. EPACK combines material properties testing, IC package reliability results, and physics-based numerical simulation in a user-friendly framework.



2 A Brief Review of Theories and Equations Used in EPACK

2.1 Heat Transfer

2.1.1 Governing Equations

Anisotropic and Transient

$$\frac{\partial}{\partial x} \left(K_x \frac{\partial T}{\partial x} \right) + \frac{\partial}{\partial y} \left(K_y \frac{\partial T}{\partial y} \right) + \frac{\partial}{\partial z} \left(K_z \frac{\partial T}{\partial z} \right) = \rho c \frac{\partial T}{\partial t} \quad (2-1)$$

$T = T(x,y,z;t)$ = Temperature Distribution
 K_x = Thermal Conductivity in the x-direction
 K_y = Thermal Conductivity in the y-direction
 K_z = Thermal Conductivity in the z-direction
 ρ = Mass Density
 c = Heat Capacity

Anisotropic and Steady-State

$$\frac{\partial}{\partial x} \left(K_x \frac{\partial T}{\partial x} \right) + \frac{\partial}{\partial y} \left(K_y \frac{\partial T}{\partial y} \right) + \frac{\partial}{\partial z} \left(K_z \frac{\partial T}{\partial z} \right) = 0 \quad (2-2)$$

Isotropic Materials with Constant Thermal Conductivity (Transient)

$$K \left(\frac{\partial^2 T}{\partial x^2} + \frac{\partial^2 T}{\partial y^2} + \frac{\partial^2 T}{\partial z^2} \right) = \rho c \frac{\partial T}{\partial t} \quad (2-3)$$

$$K_x = K_y = K_z = K \quad (2-4)$$

Isotropic Materials with Constant Thermal Conductivity (Steady-State)

$$K \left(\frac{\partial^2 T}{\partial x^2} + \frac{\partial^2 T}{\partial y^2} + \frac{\partial^2 T}{\partial z^2} \right) = 0 \quad (2-5)$$

Table 2-1 Typical Material Thermal Properties

	K (W/m-°C)	ρ (g/cm ³)	c (J/Kg-°C)
Si Die	150	2.33	712
Die Attach	2	1.2	2000
Olin-194 Lead Frame	262	8.5	380
Molding Compound	0.6	1.2	1000
Sn63 Solder	51	8.47	160
FR-4 PWB	0.18	1.94	879
Pure Copper	400	8.9	385
Pure Silver	419	10.3	235
Pure Gold	318	19.3	129

2.1.2 Boundary Conditions

Fixed Temperature

$$T(x_o, y_o, z_o; t) = F(t) \quad (2-6)$$

- Seldom used in packaging simulation except for vapor-phase solder reflow simulation

Heat Flux/Power Generation

$$Q = -KA \frac{\partial T}{\partial n} \quad (2-7)$$

Q = Heat Flux in the units of Watts
A = Surface Area in the units of mm²
n = Outer Normal of the Surface Area

- Typically used in IC power dissipation on the die surface.
- For highly conductive dies, such as Si (K=150 W/m-°C), it is a good approximation to assume that the total power is dissipated uniformly on the entire die surface.
- For less conductive dies, such as GaAs (K=34 W/m-°C), the heat generation areas should reflect to actual circuit designs on the die surface.

Heat Convection & Radiation

$$q = -K \frac{\partial T}{\partial n} = (h + h_r)(T - T_{\infty}) \quad (2-8)$$

- n = outer normal of the surface
- T = package surface temperature
- T_{∞} = ambient temperature
- h = heat transfer coefficient due to convection
- h_r = heat transfer coefficient due to radiation
- q = surface heat flux

Determination of Heat Transfer Coefficients

Table 2-2 Fluid Dynamics Constants Used

Symbol	Description	Units
h	Heat Transfer Coefficient	$W/m^2 \cdot ^\circ C$
g	Acceleration of Gravity	m/sec^2
K	Thermal Conductivity	$W/m \cdot ^\circ C$
L	Significant Length	M
q	Surface Heat Flux	W/m^2
T	Package Surface Temperature	$^\circ C$
T_{∞}	Ambient (Air) Temperature	$^\circ C$
U	Air Speed	m/Sec
ρ	Mass Density	Kg/m^3
β	Compressibility	$1/^\circ C$
ν	Kinematic Viscosity	m^2/sec
μ	Molecular Viscosity	$N \cdot Sec/m^2$
σ	Stefan-Boltzmann Constant	$W/m^2 \cdot ^\circ C^4$
ϵ	Surface emissivity	dimensionless
Gr	Grashof Number	dimensionless
Nu	Nussalt Number	dimensionless
Pr	Prandtl Number	dimensionless
Re	Renolds Number	dimensionless
St	Stanton Number	dimensionless

Pr = Physical Property of Cooling Medium
 ≈ 0.71 for room temperature air

$$Gr = \frac{g\beta(T - T_{\infty})L^3}{\nu^2} \quad (2-9)$$

$$Re = \frac{\rho UL}{\mu} \quad (2-10)$$

$$St = \frac{Nu}{Re \cdot Pr} \quad (2-11)$$

$$Nu = \frac{hL}{K} \quad (2-12)$$

- Heat transfer coefficients h and h_r are determined with empirical relationships derived from heat transfer experiments and calibration with actual package thermal resistance measurements.
- There are three parts in the heat transfer coefficients: natural convection, forced convection, and radiation.

Natural Convection

$$Nu = \frac{hL}{K} = \begin{cases} c \cdot Gr^a \cdot Pr^b & \text{heated surface upward} \\ c \cdot \frac{Pr^a \cdot Gr^b}{(d + Pr)^a} & \text{heated vertical surface} \end{cases} \quad (2-13)$$

Forced Convection

$$Nu = \frac{hL}{K} = c \cdot Re^a \cdot Pr^b \quad (2-14)$$

Radiation

$$q = \sigma A \epsilon (T^4 - T_{\infty}^4) \quad (2-15)$$

- For convenience, the radiation heat transfer effect is often combined with convection heat transfer by

$$q = -K \frac{\partial T}{\partial n} = (h + h_r)(T - T_\infty) \quad (2-16)$$

$$h_r = \text{radiation heat transfer coefficient} \\ = \sigma \epsilon (T^2 + T_\infty^2)(T + T_\infty)$$

- For a package with an emissivity of 0.8 at 25°C above ambient radiating to a black enclosure, $h_r = 5.44 \text{ W/m}^2\text{-}^\circ\text{C}$.
- The radiation effect is important only in natural convection condition. The radiation effect becomes negligible in forced convection.

Iteration Procedure

- Since heat transfer coefficients depend on the package surface temperatures, finding the heat transfer coefficient becomes a nonlinear process.

2.1.3 Finite Element Formulation of Heat Transfer Problems

$$([K_T] + [K_h])\{T\} = \{R_\infty\} \quad (2-17)$$

$$[K_T] = \sum_{\text{ele}} [k_T] \quad (2-18)$$

$$[K_h] = \sum_{\text{ele}} [k_h] \quad (2-19)$$

$$\{T\} = \sum_{\text{ele}} \{T_e\} \quad (2-20)$$

$$\{R_\infty\} = \sum_{\text{ele}} \{r_\infty\} \quad (2-21)$$

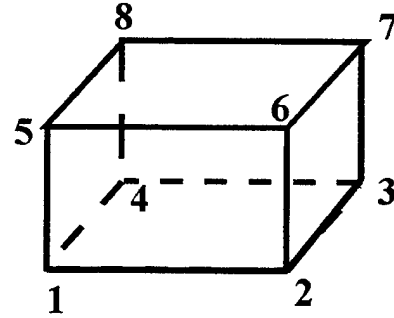
$$[k_T] = \int_V [B_T]^T [C] [B_T] \cdot dv \quad (2-22)$$

$$[k_h] = \int_A [N_T]^T [N_T] \cdot h \cdot dA \quad (2-23)$$

$$\{r_\infty\} = \int_A (N_T)^T \cdot h \cdot T_\infty \cdot dA \quad (2-24)$$

$$[C]_{3 \times 3} = \begin{bmatrix} K & 0 & 0 \\ 0 & K & 0 \\ 0 & 0 & K \end{bmatrix} \quad (2-25)$$

8-Node Isoparametric Brick Element



$$(N_T)_{1 \times 8} = (N_1 \quad N_2 \quad N_3 \quad N_4 \quad N_5 \quad N_6 \quad N_7 \quad N_8) \quad (2-26)$$

$$\{T_e\}_{8 \times 1}^T = (T_1 \quad T_2 \quad T_3 \quad T_4 \quad T_5 \quad T_6 \quad T_7 \quad T_8) \quad (2-27)$$

$$[B]_{3 \times 8}^T = \begin{bmatrix} \frac{\partial N_1}{\partial x} & \frac{\partial N_2}{\partial x} & \frac{\partial N_3}{\partial x} & \frac{\partial N_4}{\partial x} & \frac{\partial N_5}{\partial x} & \frac{\partial N_6}{\partial x} & \frac{\partial N_7}{\partial x} & \frac{\partial N_8}{\partial x} \\ \frac{\partial N_1}{\partial y} & \frac{\partial N_2}{\partial y} & \frac{\partial N_3}{\partial y} & \frac{\partial N_4}{\partial y} & \frac{\partial N_5}{\partial y} & \frac{\partial N_6}{\partial y} & \frac{\partial N_7}{\partial y} & \frac{\partial N_8}{\partial y} \\ \frac{\partial N_1}{\partial z} & \frac{\partial N_2}{\partial z} & \frac{\partial N_3}{\partial z} & \frac{\partial N_4}{\partial z} & \frac{\partial N_5}{\partial z} & \frac{\partial N_6}{\partial z} & \frac{\partial N_7}{\partial z} & \frac{\partial N_8}{\partial z} \end{bmatrix} \quad (2-28)$$

$$N_m = \frac{1}{8} (1 + \xi \cdot \xi_m + \eta \cdot \eta_m + \zeta \cdot \zeta_m) \quad (2-29)$$

2.2 A Brief Review of Thermal Stress Theories

2.2.1 Governing Equations

Strain-Displacement Relationship

$$\begin{Bmatrix} \epsilon_x \\ \epsilon_y \\ \epsilon_z \\ \gamma_{xy} \\ \gamma_{yz} \\ \gamma_{zx} \end{Bmatrix} = \begin{bmatrix} \frac{\partial}{\partial x} & 0 & 0 \\ 0 & \frac{\partial}{\partial y} & 0 \\ 0 & 0 & \frac{\partial}{\partial z} \\ \frac{\partial}{\partial y} & \frac{\partial}{\partial x} & 0 \\ 0 & \frac{\partial}{\partial z} & \frac{\partial}{\partial y} \\ \frac{\partial}{\partial z} & 0 & \frac{\partial}{\partial x} \end{bmatrix} \begin{Bmatrix} u \\ v \\ w \end{Bmatrix} \quad (2-30)$$

Compatibility Equations

$$2 \frac{\partial^2 \epsilon_x}{\partial y \partial z} = \frac{\partial}{\partial x} \left(-\frac{\partial \gamma_{yz}}{\partial x} + \frac{\partial \gamma_{zx}}{\partial y} + \frac{\partial \gamma_{xy}}{\partial z} \right) \quad (2-31)$$

$$2 \frac{\partial^2 \epsilon_y}{\partial x \partial z} = \frac{\partial}{\partial y} \left(\frac{\partial \gamma_{yz}}{\partial x} - \frac{\partial \gamma_{zx}}{\partial y} + \frac{\partial \gamma_{xy}}{\partial z} \right) \quad (2-32)$$

$$2 \frac{\partial^2 \epsilon_z}{\partial x \partial y} = \frac{\partial}{\partial z} \left(\frac{\partial \gamma_{yz}}{\partial x} + \frac{\partial \gamma_{zx}}{\partial y} - \frac{\partial \gamma_{xy}}{\partial z} \right) \quad (2-33)$$

$$\frac{\partial^2 \epsilon_x}{\partial y^2} + \frac{\partial^2 \epsilon_y}{\partial x^2} = \frac{\partial^2 \gamma_{xy}}{\partial x \partial y} \quad (2-34)$$

$$\frac{\partial^2 \epsilon_y}{\partial z^2} + \frac{\partial^2 \epsilon_z}{\partial y^2} = \frac{\partial^2 \gamma_{yz}}{\partial z \partial y} \quad (2-35)$$

$$\frac{\partial^2 \epsilon_x}{\partial z^2} + \frac{\partial^2 \epsilon_z}{\partial x^2} = \frac{\partial^2 \gamma_{zx}}{\partial x \partial z} \quad (2-36)$$

Stress-Strain Relationship

$$\begin{Bmatrix} \sigma_x \\ \sigma_y \\ \sigma_z \\ \tau_{xy} \\ \tau_{yz} \\ \tau_{zx} \end{Bmatrix} = \frac{E(1-\nu)}{(1+\nu)(1-2\nu)} \begin{bmatrix} 1 & \frac{\nu}{1-\nu} & \frac{\nu}{1-\nu} & 0 & 0 & 0 \\ & 1 & \frac{\nu}{1-\nu} & 0 & 0 & 0 \\ & & 1 & 0 & 0 & 0 \\ & & & \frac{1-2\nu}{2-2\nu} & 0 & 0 \\ & \text{sym} & & & \frac{1-2\nu}{2-2\nu} & 0 \\ & & & & & \frac{1-2\nu}{2-2\nu} \end{bmatrix} \begin{Bmatrix} \epsilon_x = \alpha' \Delta T \\ \epsilon_y = \alpha' \Delta T \\ \epsilon_z = \alpha' \Delta T \\ \gamma_{xy} \\ \gamma_{yz} \\ \gamma_{zx} \end{Bmatrix} \quad (2-37)$$

$$\alpha' = \alpha + \alpha_s$$

α = Coefficient of Thermal Expansion (CTE)

α_s = Equivalent CTE Due to Moisture Swelling (Section 6.0)

$\Delta T = T - T_{REF}$

T_{REF} = Reference Temperature (Stress Free)

Table 2-3 E, ν , and CTE of A Few Packaging Materials

Material	E (GPa)	ν	CTE (ppm/ $^{\circ}$ C)
Si Die	128.2	0.30	3.60
GaAs Die	85.3	0.49	5.72
Typical Die Attach	2.4	0.30	50.0
Typical Leadframe	110.3	0.33	16.3
Typical Molding Compound	12.0	0.35	17.0/50.0
Sn 63 Solder	14.9	0.40	24.7
FR-4 PWB	17.2	0.30	16.0
Gold	110.3	0.42	14.2
Silver	75.8	0.36	18.0

- Special attention should be taken in setting T_{REF} .
- For die attach materials, T_{REF} is usually set as the cure temperature.
- For molding compounds, T_{REF} is usually set as the molding temperature.

- For solder and PWB materials, T_{REF} is usually set as the solder solidification temperature.
- For die and leadframe, T_{REF} is usually set as the adhesive cure temperature.
- For die attach and molding compound materials with a glass transition temperature, the CTE value (α_1) below T_g and the CTE value (α_2) above T_g are quite different. In this case, the following T_{REF} should be used for analyses at different temperature ranges:

$$T_{REF}^* = T_o - [\alpha_2(T_g - T_o) + \beta C] / \alpha_1 \quad T < T_g < T_o \quad (2-38a)$$

$$T_{REF}^* = T_o - (\beta C) / \alpha_1 \quad T_g < T_o < T \quad (2-38b)$$

T_o = molding or cure temperature
 β = Swelling Coefficients
 C = Moisture Concentration

Equilibrium Equations

In Terms of Stresses

$$\frac{\partial \sigma_x}{\partial x} + \frac{\partial \tau_{xy}}{\partial y} + \frac{\partial \tau_{xz}}{\partial z} = 0 \quad (2-39)$$

$$\frac{\partial \tau_{xy}}{\partial x} + \frac{\partial \sigma_y}{\partial y} + \frac{\partial \tau_{yz}}{\partial z} = 0 \quad (2-40)$$

$$\frac{\partial \tau_{zx}}{\partial x} + \frac{\partial \tau_{zy}}{\partial y} + \frac{\partial \sigma_z}{\partial z} = 0 \quad (2-41)$$

In Terms of Displacements

$$(1 - 2\nu)\nabla^2 u + \frac{\partial^2 u}{\partial x^2} + \frac{\partial^2 v}{\partial x \partial y} + \frac{\partial^2 w}{\partial x \partial z} = 2\alpha(1 + \nu) \frac{\partial T}{\partial x} \quad (2-42)$$

$$(1 - 2\nu)\nabla^2 v + \frac{\partial^2 u}{\partial x \partial y} + \frac{\partial^2 v}{\partial y^2} + \frac{\partial^2 w}{\partial y \partial z} = 2\alpha(1 + \nu) \frac{\partial T}{\partial y} \quad (2-43)$$

$$(1 - 2\nu)\nabla^2 w + \frac{\partial^2 u}{\partial z \partial x} + \frac{\partial^2 v}{\partial z \partial y} + \frac{\partial^2 w}{\partial z^2} = 2\alpha(1 + \nu) \frac{\partial T}{\partial z} \quad (2-44)$$

2.2.2 Boundary Conditions

To reduce the size of finite element model, only a quarter (sometimes 1/8) of the package is modeled with finite element. Since there are usually no mechanical loading, the most common boundary conditions of a thermoelastic finite element analysis of an IC package are the symmetry conditions along the symmetry lines and restraints of the rigid body motion. A sample finite element model is shown in Figure 2-1 below.

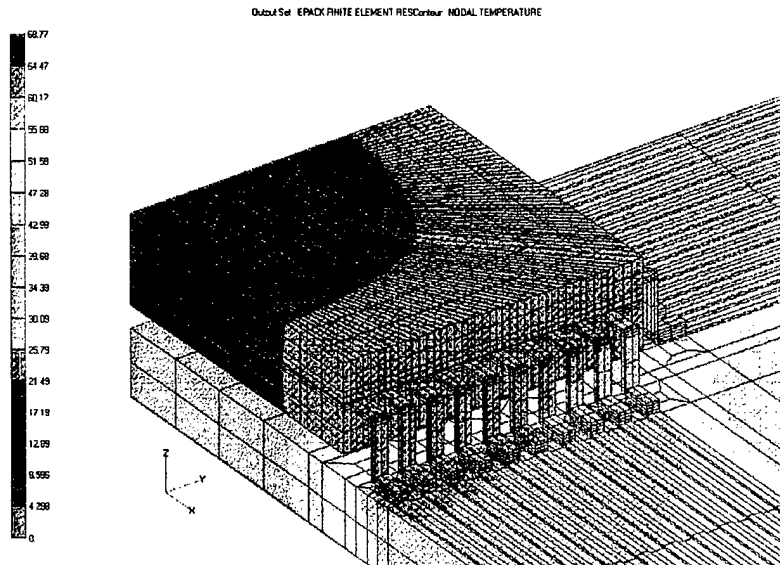


Fig 2-1 A Sample Finite Element Model and Results

2.2.3 Finite Element Formulation of Thermal Stress Problems

$$[K]\{U\} = \{R\} \quad (2-45)$$

$$[K] = \sum_{ele} [k] \quad (2-46)$$

$$\{R\} = \sum_{ele} \{r\} \quad (2-47)$$

$$\{U\} = \sum_{ele} \{U_e\} \quad (2-48)$$

8-Node Isoparametric Brick Element

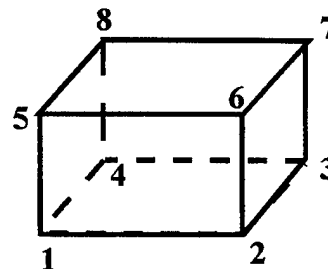


Fig 2-2 Eight-Node Brick Element

$$[k] = \int_V [B]^T [C] [B] \cdot dV \quad (2-49)$$

$$\{r\} = \int_V [B]^T [C] \{\epsilon_o\} \cdot dV \quad (2-50)$$

$$[C]_{6 \times 6} = \frac{E(1-\nu)}{(1+\nu)(1-2\nu)} \begin{bmatrix} 1 & \frac{\nu}{1-\nu} & \frac{\nu}{1-\nu} & 0 & 0 & 0 \\ & 1 & \frac{\nu}{1-\nu} & 0 & 0 & 0 \\ & & 1 & 0 & 0 & 0 \\ & & & \frac{1-2\nu}{2-2\nu} & 0 & 0 \\ & & & & \frac{1-2\nu}{2-2\nu} & 0 \\ & \text{sym} & & & & \frac{1-2\nu}{2-2\nu} \end{bmatrix} \quad (2-51)$$

$$\{\epsilon_o\}_{6 \times 1}^T = (\alpha \Delta T \quad \alpha \Delta T \quad \alpha \Delta T \quad 0 \quad 0 \quad 0) \quad (2-52)$$

$$\Delta T = T - T_{REF} \quad (2-53)$$

$$\{U_e\}_{24 \times 1}^T = (u_1 \quad v_1 \quad w_1 \quad u_2 \quad \dots \quad u_8 \quad v_8 \quad w_8) \quad (2-54)$$

$$[B]_{6 \times 24} = [[B_1] \quad [B_2] \quad [B_3] \quad [B_4] \quad [B_5] \quad [B_6] \quad [B_7] \quad [B_8]] \quad (2-55)$$

$$[B_m]_{6 \times 3} = \begin{bmatrix} \frac{\partial N_m}{\partial x} & 0 & 0 \\ 0 & \frac{\partial N_m}{\partial y} & 0 \\ 0 & 0 & \frac{\partial N_m}{\partial z} \\ \frac{\partial N_m}{\partial y} & \frac{\partial N_m}{\partial x} & 0 \\ 0 & \frac{\partial N_m}{\partial z} & \frac{\partial N_m}{\partial y} \\ \frac{\partial N_m}{\partial z} & 0 & \frac{\partial N_m}{\partial x} \end{bmatrix} \quad (2-56)$$

$$N_m = \frac{1}{8} (1 + \xi \cdot \xi_m + \eta \cdot \eta_m + \zeta \cdot \zeta_m) \quad (2-57)$$

2.3 A Brief Review of Fracture Mechanics Theories

2.3.1 Fundamental Concepts

- Why a steel rod of diameter D is weaker than a steel rope of the same diameter made of thousands of small steel wires of diameter d ?
- Why most of the engineering materials can never achieve their "theoretical strength" ?
- Why delamination in a plastic package propagate to areas where the stresses are much lower than the interface strength ?
- Cracks and dislocations are the answer !!
- There are three fracture modes (see Figure 2-2 below)

Mode I - Opening or tensile mode where the crack surface move directly apart

Mode II - Sliding or in-plane shear mode, where the crack surfaces slide over on another in the direction perpendicular to the leading edge of the crack

Mode III - Tearing or antiplane shear mode, where the crack surfaces move relative to on another and parallel to the leading edge of the crack

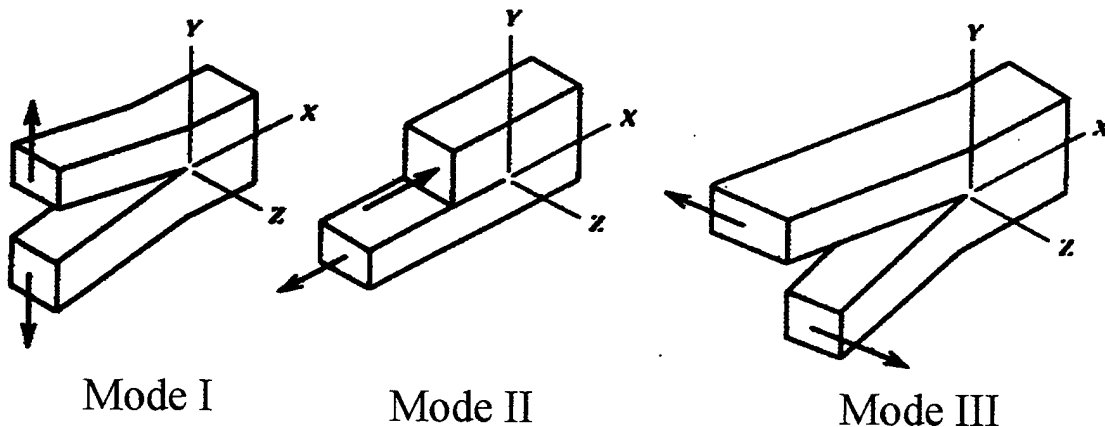


Figure 2-3 Three Crack Fracture Modes

$$\sigma_{ij} = \sum_{M=1}^{\text{III}} \frac{K_M}{\sqrt{2\pi r}} f_{ij}^M(\theta) \quad (2-58)$$

$$u_i = \sum_{M=1}^{\text{III}} \frac{K_M}{G} \sqrt{\frac{r}{2\pi}} g_{ij}^M(\theta) \quad (2-59)$$

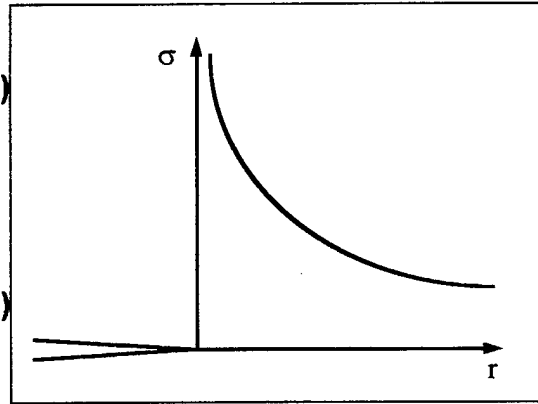


Figure 2-4 Crack-tip Singularity

Asymptotic Stress Field at the Crack-Tip

$$\begin{aligned} \sigma_x = & \frac{K_I}{\sqrt{2\pi r}} \cos \frac{\theta}{2} \left(1 - \sin \frac{\theta}{2} \sin \frac{3\theta}{2} \right) \\ & - \frac{K_{II}}{\sqrt{2\pi r}} \sin \frac{\theta}{2} \left(2 + \cos \frac{\theta}{2} \cos \frac{3\theta}{2} \right) \end{aligned} \quad (2-60)$$

$$\begin{aligned} \sigma_y = & \frac{K_I}{\sqrt{2\pi r}} \cos \frac{\theta}{2} \left(1 + \sin \frac{\theta}{2} \sin \frac{3\theta}{2} \right) \\ & - \frac{K_{II}}{\sqrt{2\pi r}} \sin \frac{\theta}{2} \cos \frac{\theta}{2} \cos \frac{3\theta}{2} \end{aligned} \quad (2-61)$$

$$\begin{aligned} \tau_{xy} = & \frac{K_I}{\sqrt{2\pi r}} \sin \frac{\theta}{2} \cos \frac{\theta}{2} \cos \frac{3\theta}{2} \\ & - \frac{K_{II}}{\sqrt{2\pi r}} \cos \frac{\theta}{2} \left(1 - \sin \frac{\theta}{2} \sin \frac{3\theta}{2} \right) \end{aligned} \quad (2-63)$$

$$\sigma_z = \nu(\sigma_x + \sigma_y) \quad (2-64)$$

$$\tau_{xz} = \frac{K_{III}}{\sqrt{2\pi r}} \sin \frac{\theta}{2} \quad (2-65)$$

$$\tau_{yz} = \frac{K_{III}}{\sqrt{2\pi r}} \cos \frac{\theta}{2} \quad (2-66)$$

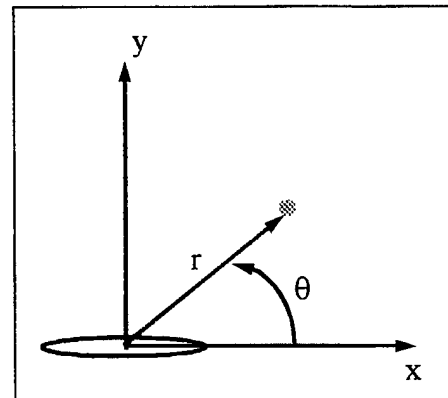


Fig. 2-5 Crack-tip Coordinates

Asymptotic Displacement Field at the Crack-Tip

$$\begin{aligned}
 u = & \frac{K_I}{G} \sqrt{\frac{r}{2\pi}} \cos \frac{\theta}{2} \left(1 - 2\nu + \sin^2 \frac{\theta}{2} \right) \\
 & + \frac{K_{II}}{G} \sqrt{\frac{r}{2\pi}} \sin \frac{\theta}{2} \left(2 - 2\nu + \cos^2 \frac{\theta}{2} \right)
 \end{aligned}
 \tag{2-67}$$

$$\begin{aligned}
 v = & \frac{K_I}{G} \sqrt{\frac{r}{2\pi}} \sin \frac{\theta}{2} \left(2 - 2\nu + \cos^2 \frac{\theta}{2} \right) \\
 & + \frac{K_{II}}{G} \sqrt{\frac{r}{2\pi}} \sin \frac{\theta}{2} \left(-1 + 2\nu + \sin^2 \frac{\theta}{2} \right)
 \end{aligned}
 \tag{2-68}$$

$$w = \frac{K_{III}}{G} \sqrt{\frac{r}{2\pi}} \sin \frac{\theta}{2}
 \tag{2-69}$$

$$G = \frac{E}{2(1+\nu)}
 \tag{2-70}$$

- To avoid dealing with infinite stresses, the stress intensity factors, K_I , K_{II} , and K_{III} , are used to characterize cracks (delaminations).
- The criterion of crack initiation (formation of delamination) is that the interface stresses are greater than the interface strength.
- The criterion of crack propagation (growth of delamination) is that the applied stress intensity factors are greater than the material fracture toughness.

2.3.2 Determination of Applied K for IC Packages

Common Package Delamination (Crack) Types

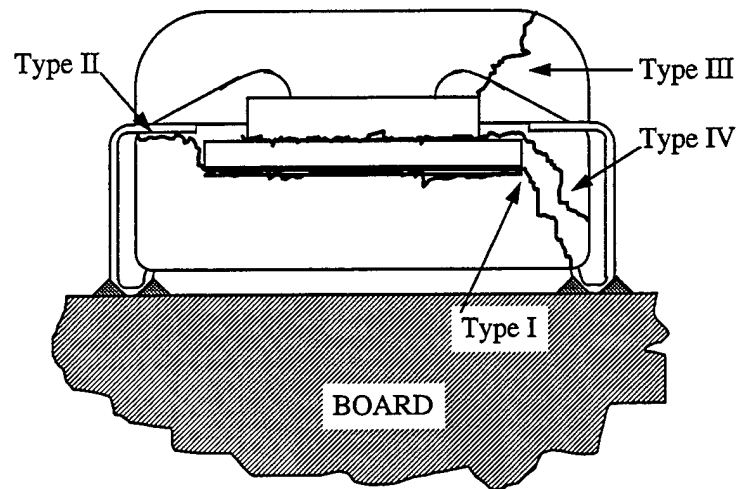


Fig. 2-6 Common Crack Types in Plastic IC Packages

Two-Dimensional Approximation

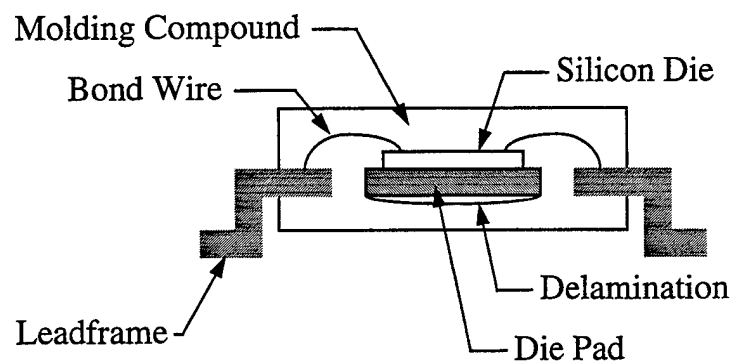


Figure 2-7 2D Approximation of IC Package Cracking

2D Crack Model and Solutions

$$\sigma_y(x) = \sigma_o + \sigma_1 \left(\frac{x}{W}\right) + \sigma_2 \left(\frac{x}{W}\right)^2 + \sigma_3 \left(\frac{x}{W}\right)^3, \quad \text{or} \quad (2-71)$$

$$\sigma_z(r) = \sigma_o + \sigma_1 \left(\frac{r}{W}\right) + \sigma_2 \left(\frac{r}{W}\right)^2 + \sigma_3 \left(\frac{r}{W}\right)^3 \quad (2-72)$$

$$K_I^{2D} = \sqrt{\pi a} \sum_{n=0}^3 F_n \sigma_n \quad (2-73)$$

$$\delta^{2D} = \frac{a(1-\nu^2)}{E} \sum_{n=0}^3 V_n \sigma_n \quad (2-74)$$

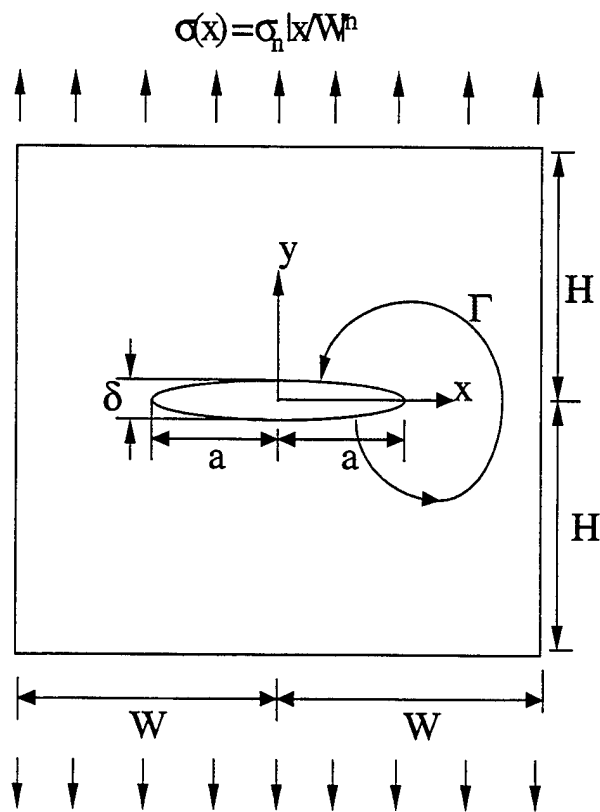


Fig. 2-8 A Plane-Strain Crack

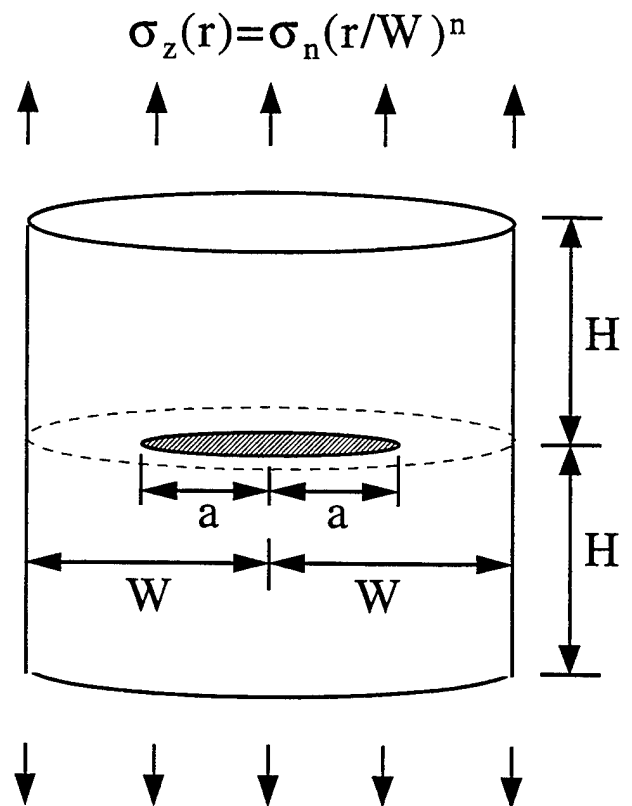


Fig. 2-9 An Axisymmetric Crack

J-Integrals

Plane-Strain:

$$J = \int_{\Gamma} (W n_1 - T_i u_{i,1}) ds = \frac{(1-\nu^2) K_I^2}{E}, \quad i, j = 1 \text{ or } 2 \quad (2-75)$$

Axisymmetric:

$$J_A = \int_{\Gamma} (W x_{\alpha} n_{\alpha} - T_{\alpha} u_{\alpha\beta} x_{\beta} - \frac{1}{2} T_{\alpha} u_{\alpha}) \frac{ds}{R_c^2} = \frac{(1-\nu^2) K_I^2}{E}, \quad \alpha, \beta = r, z \quad (2-76)$$

3D Crack:

$$G(s) = \frac{\hat{G}}{\int_{s_a}^{s_b} \lambda(s) ds} = \frac{(1-\nu^2) K_I^{3D}(s)^2}{E} \quad (2-77)$$

$$\hat{G} = \int_V (\sigma_{ij} u_{i,k} q_{k,j} - W q_{k,k}) dV, \quad (2-78)$$

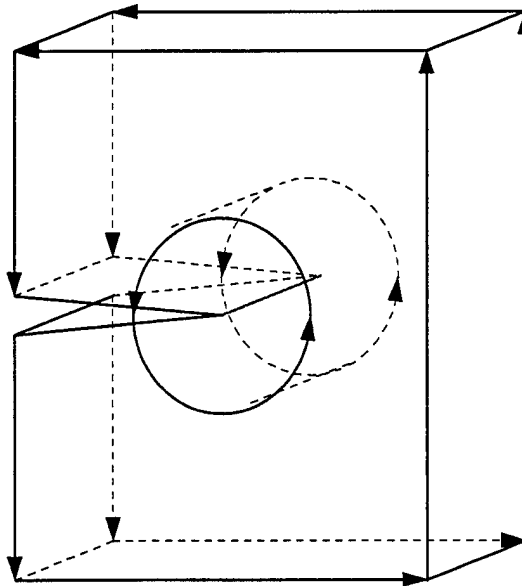


Figure 2-10 3D Crack-Tip J-Integral

3D Crack Model and Solutions

The 2D solution is a good approximation for slender packages (packages with large W_1/W_2 or W_2/W_1 ratios such as SOJ and DIP). For square or almost square packages (QFP, BGA), the 2D crack solution is too severe and the more realistic 3D solution is required.

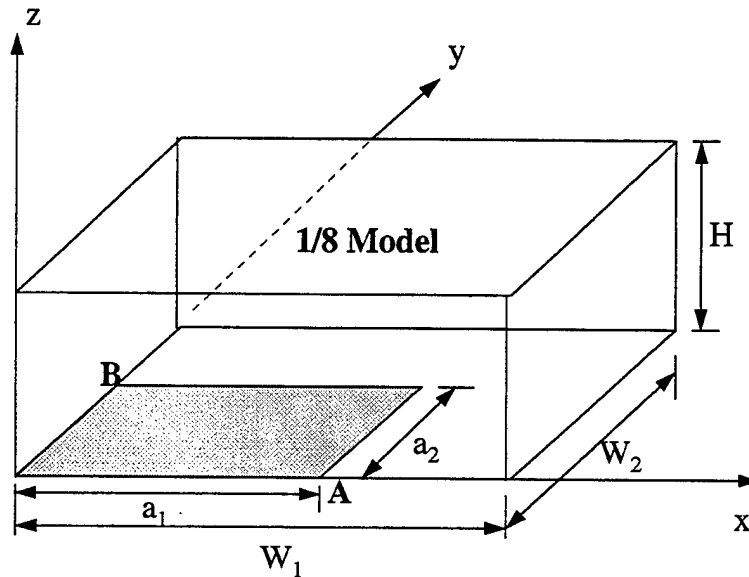


Figure 2-11 A Rectangular Crack in a Plastic IC Package

$$K_I^{3D} = f \cdot K_I^{2D} \quad (2-79)$$

$$K_I^{3D} = f\left(\frac{a_2}{W_2}, \frac{W_2}{W_1}, \frac{H}{W_1}\right) \cdot \sqrt{\pi a} \cdot \sum_{n=3}^3 F_n \cdot \sigma_n \quad (2-80)$$

$$\delta_I^{3D} = g\left(\frac{a_2}{W_2}, \frac{W_2}{W_1}, \frac{H}{W_1}\right) \cdot \frac{a(1-\nu^2)}{E} \cdot \sum_{n=3}^3 V_n \cdot \sigma_n \quad (2-81)$$

Function f and g are tabulated in Appendix I of this report.

$$f\left(\frac{a_2}{W_2}, \frac{W_2}{W_1}, \frac{H}{W_1}\right) = f_1 + \frac{5}{3}\left(1 - \frac{W_2}{W_1}\right)(f_2 - f_1) \quad (2-82)$$

$$f_1\left(\frac{H}{W_1}, \frac{a_2}{W_2}\right) = \begin{pmatrix} 1 & \frac{H}{W_1} & \frac{H^2}{W_1^2} \end{pmatrix} \begin{bmatrix} 0.4996 & 0.5213 & -0.2463 \\ 0.1578 & -1.7944 & 0.2778 \\ 0.6630 & 0.6482 & 0.1852 \end{bmatrix} \begin{Bmatrix} 1 \\ \frac{a_2}{W_2} \\ \frac{a_2^2}{W_2^2} \end{Bmatrix} \quad (2-83)$$

$$f_2\left(\frac{H}{W_1}, \frac{a_2}{W_2}\right) = \begin{pmatrix} 1 & \frac{H}{W_1} & \frac{H^2}{W_1^2} \end{pmatrix} \begin{bmatrix} 0.9316 & 0.2733 & -0.1222 \\ -0.9622 & 2.1556 & -2.7222 \\ 2.4444 & -6.3333 & 7.2222 \end{bmatrix} \begin{Bmatrix} 1 \\ \frac{a_2}{W_2} \\ \frac{a_2^2}{W_2^2} \end{Bmatrix} \quad (2-84)$$

$$g\left(\frac{a_2}{W_2}, \frac{W_2}{W_1}, \frac{H}{W_1}\right) = g_1 + \frac{5}{3}\left(1 - \frac{W_2}{W_1}\right)^m (g_2 - g_1) \quad (2-85)$$

$$m = \begin{cases} 1 & , H/W_1 > 0.2 \\ 0.4 & , H/W_1 < 0.2 \end{cases} \quad (2-86)$$

$$g_1\left(\frac{H}{W_1}, \frac{a_2}{W_2}\right) = \begin{pmatrix} 1 & \frac{H}{W_1} & \frac{H^2}{W_1^2} \end{pmatrix} \begin{bmatrix} 0.5039 & 0.1302 & -0.097 \\ 0.4417 & -2.4417 & 1.9167 \\ 0.0574 & 2.7315 & -3.4259 \end{bmatrix} \begin{Bmatrix} 1 \\ \frac{a_2}{W_2} \\ \frac{a_2^2}{W_2^2} \end{Bmatrix} \quad (2-87)$$

$$g_2\left(\frac{H}{W_1}, \frac{a_2}{W_2}\right) = \begin{pmatrix} 1 & \frac{H}{W_1} & \frac{H^2}{W_1^2} \end{pmatrix} \begin{bmatrix} 1.0600 & -0.0819 & 2.6926 \\ -1.5200 & 3.9583 & -9.3981 \\ 2.6926 & -9.3981 & 11.759 \end{bmatrix} \begin{Bmatrix} 1 \\ \frac{a_2}{W_2} \\ \frac{a_2^2}{W_2^2} \end{Bmatrix} \quad (2-88)$$

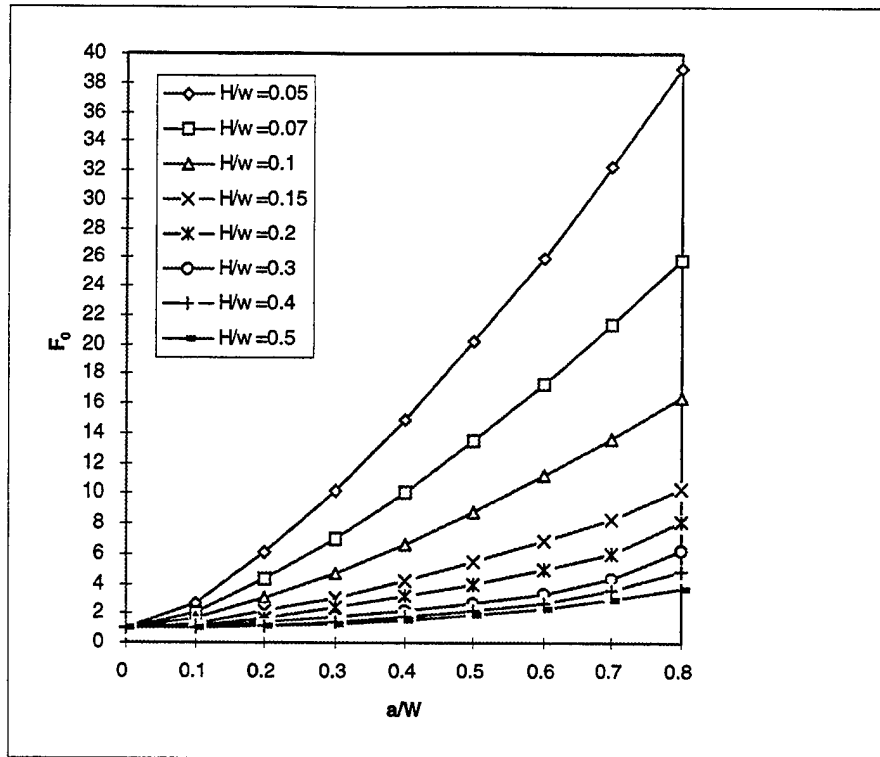


Figure 2-12 F_0 of a Plane Strain Crack

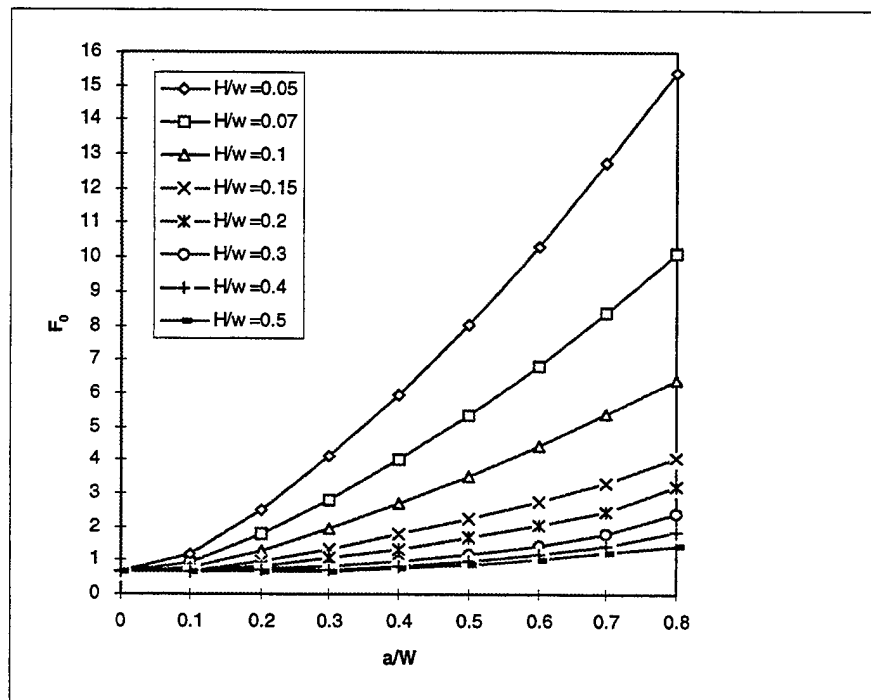


Figure 2-13 F_0 of an Axisymmetric Crack

2.4 A Brief Review of Moisture Diffusion and Evaporation

2.4.1 Governing Equations

$$D \left(\frac{\partial^2 C}{\partial x^2} + \frac{\partial^2 C}{\partial y^2} + \frac{\partial^2 C}{\partial z^2} \right) = \frac{\partial C}{\partial t} \quad (2-89)$$

C = Moisture Concentration (mg/cm^2)

D = Diffusivity (cm^2/sec)

2.4.2 Boundary and Initial Conditions

$$C(x,y,z;0) = C_o \quad (2-90a)$$

$$C(x,y,z;t) = C_{\text{sat}} \quad (2-90b)$$

$$D \frac{\partial C(x,y,z;t)}{\partial n} = 0 \quad (2-90c)$$

C_o = Initial Moisture Concentration

C_{sat} = the equilibrium saturation

D and C_{sat} can be derived from EIAJ EDX-4701 and the paper by Richard Shook, "Moisture Sensitivity Characterization of Plastic Surface Mount Device Using Scanning Acoustic Microscopy", Proc. 30th Rel. Phys. Sym., 157-168, 1992

2.4.3 One-D Moisture Diffusion Solutions for Thin Packages

$$C(t)_{\text{pad}} = C_{\text{sat}} \left[1 - \frac{4}{\pi} \sum_{n=0}^{\infty} \frac{(-1)^n}{2n+1} \text{Exp} \left(\frac{-(2n+1)^2 \pi^2 D t}{4d^2} \right) \right] \quad (2-91)$$

$$M(t) = M_{\infty} \left[1 - \frac{8}{\pi^2} \sum_{n=0}^{\infty} \frac{1}{(2n+1)^2} \text{Exp} \left(\frac{-(2n+1)^2 \pi^2 D t}{4d^2} \right) \right] \quad (2-92)$$

d = mold compound thickness under the pad
 $M(t)$ = total absorbed moisture

2.4.4 Moisture Diffusion Material Constants

Determining C_{sat} and D from measurement data is the most accurate and reliable approach. A curve fitting module is available in EPACK.

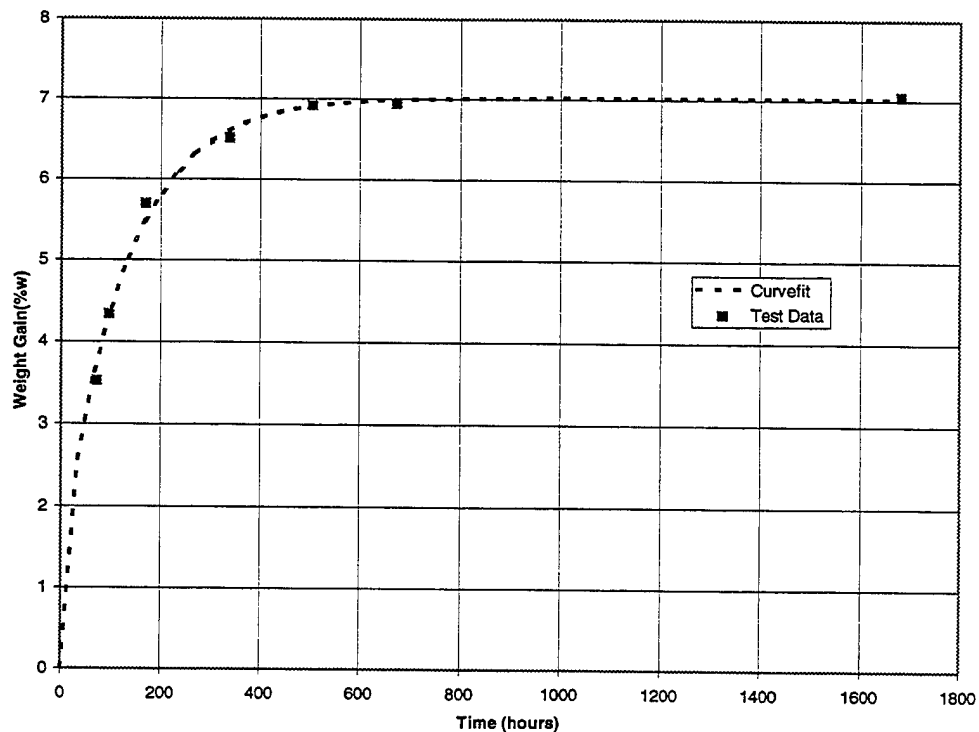


Figure 2-14 Determining D and C_{sat} by Curvefitting Test Results

C_{sat}

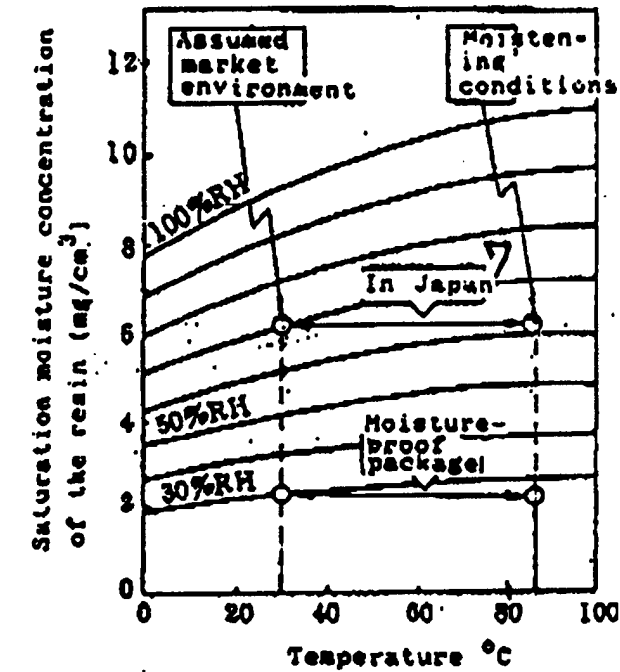


Figure 2-15 C_{sat} per EIAJ EDX-4701

Moisture Diffusivity (Intel Formula)

$$D = \frac{0.031\sqrt{T} \exp(-2740/T)}{0.063 + H\rho_{sat} \exp(2940/T)} \quad (2-93)$$

D = Diffusivity in cm^2/Hr

T = Temperature in $^{\circ}\text{K}$

H = Relative Humidity

ρ_{sat} = density of saturated water vapor at temperature T

(Bhattacharyya, et al, 1988, "Moisture Absorption and Mechanical Performance of Surface Mountable Plastic Packages," Proc. 38th Electronics Components Conference, pp.49-58)

Moisture Diffusivity (Lucent Formula)

$$D = 17.95 \cdot \text{EXP}\left(\frac{-0.4546\text{ev}}{kT}\right) \quad \text{Novalac} \quad (2-94)$$

$$D = 11.11 \cdot \text{EXP}\left(\frac{-0.4464\text{ev}}{kT}\right) \quad \text{Biphenyl} \quad (2-95)$$

$$D = 1.492 \cdot \text{EXP}\left(\frac{-0.3533\text{ev}}{kT}\right) \quad \text{Multifunctional} \quad (2-96)$$

Where D is in (mm²/s), $k=8.617 \times 10^{-5}$ ev/°K, and T is in °K.

(Shook, R.L., and Sastry, V.S., 1997, "Influence of Preheat and Maximum Temperature of Solder Reflow Profile on Moisture Sensitive IC's). As illustrated in the following figure, the Lucent formula has better correlation with experimental data. Therefore, the Lucent formula is used as the default equations for EMC's moisture diffusivity.

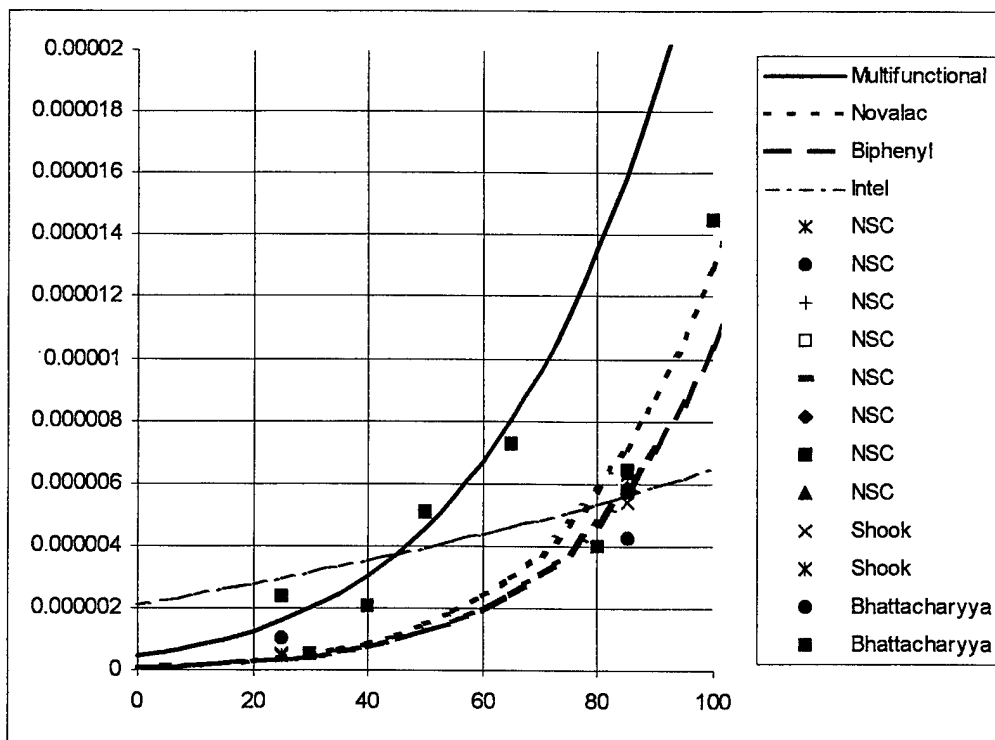


Figure 2-16 Moisture Diffusivity Correlation Versus Test Data

2.5 Effects of Moisture on Plastic Package Reliability

- Reduce adhesion strength between EMC/Cu and EMC/Die
- Reduce fracture toughness of EMC and interfaces
- Introduce addition hygro stress due to material swelling
- Introduce steam pressure under rapid heating such as solder reflow process
- Provide an environment more susceptible to corrosion

2.5.1 Adhesion Strength and Delamination Criterion

(Ohizumi, et al., 1990)

$$\left(\frac{\sigma_{peel}}{\sigma_C} \right)^2 + \left(\frac{\tau_{shear}}{\tau_C} \right)^2 = 1 \quad (2-97)$$

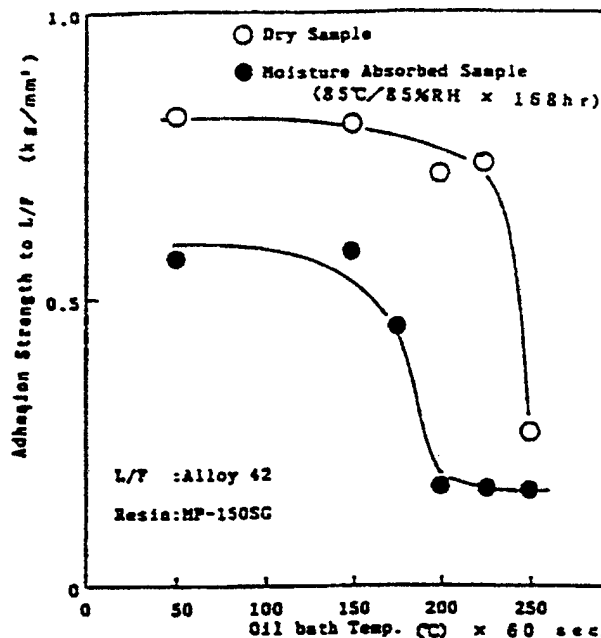


Fig. 2-17 Alloy42/MP150 Adhesion

Kim(1991) Adhesion Ratios

EMC/Cu : EMC/Alloy-42 : EMC/Cu-Ni Plated = 1.56 : 1 : 0.12

2.5.2 EMC Fracture Toughness (see Chapter 3 for details)

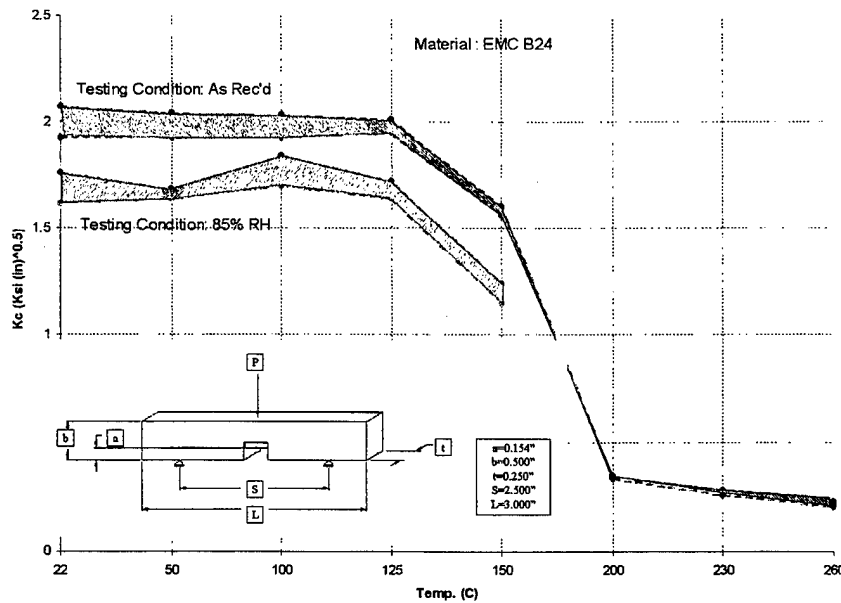


Figure 2-18 Fracture Toughness of a Typical Molding Compound

2.5.3 Interface Fracture Toughness (see Chapter 3 for details)

B8/Olin-7025 Interface Fracture Toughness

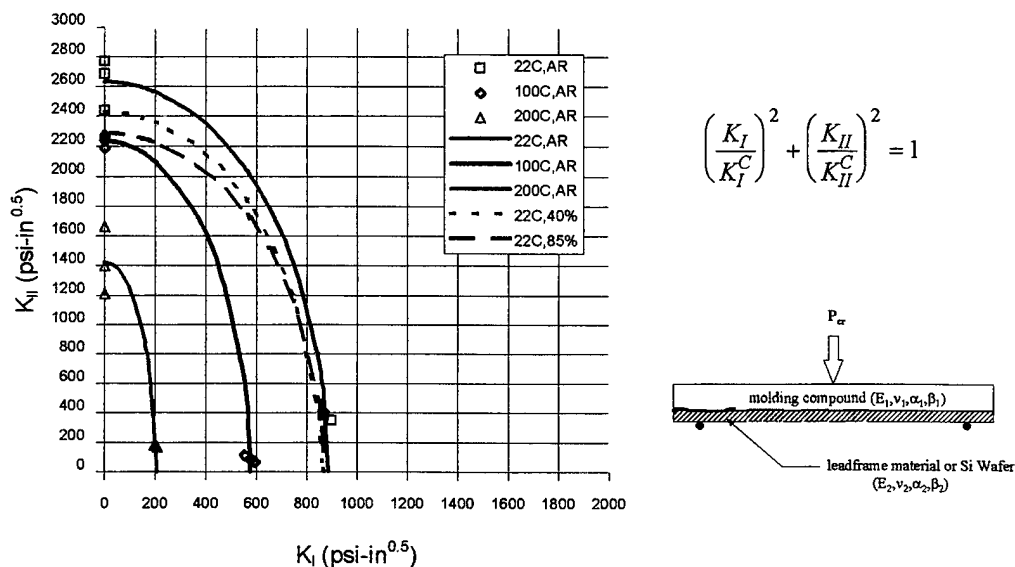


Figure 2-19 Typical Interface Fracture Toughness

2.5.4 Molding Compound Swelling Coefficients

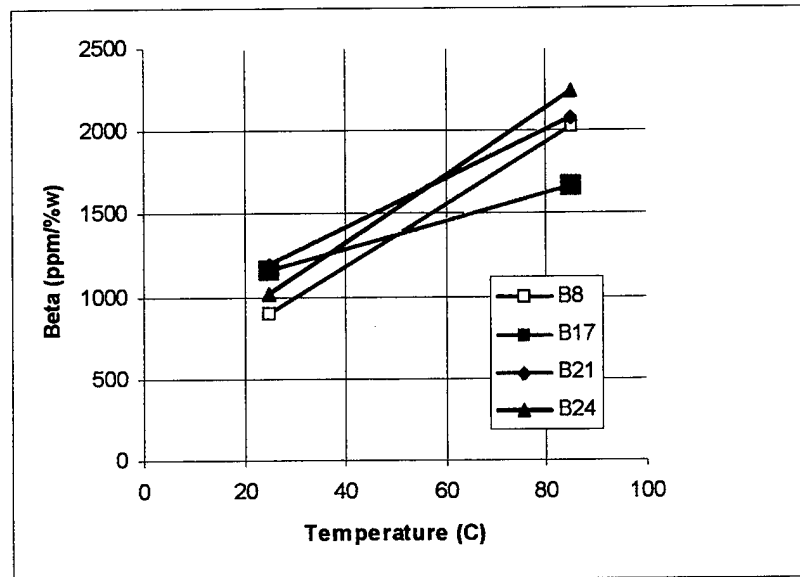


Figure 2-20 Molding Compound Swelling Coefficients

3 Fracture Strength of Epoxy Molding Compounds

Fracture toughness (K_{Ic}) of four molding compounds used for encapsulation in integrated circuits were measured. These measurements were made within a temperature range that varied from room temperature to 260°C. Specimens were pre-soaked in an environmental chamber with temperature and relative humidity (RH) up to 80°C and 85% respectively. Measured results indicated significant decreases in fracture toughness with increasing temperatures and moisture contents in the specimens. A reduction of as much as 30% in measured K_{Ic} values were observed with specimens saturated at 80% RH prior to the test.

3.1 Fracture Toughness (K_{Ic}) of EMC

Fracture toughness, K_{Ic} may be defined as the stress intensity, K_I , of a material at which an existing crack begins to propagate. One of the commonly used methods for determining K_{Ic} for a crack opening mode fracture of a material is to apply a three-point bending to a beam specimen as illustrated in Fig. 3-1. The beam specimen contains a line crack initiating from the lower edge of the beam and perpendicular to its longitudinal axis.

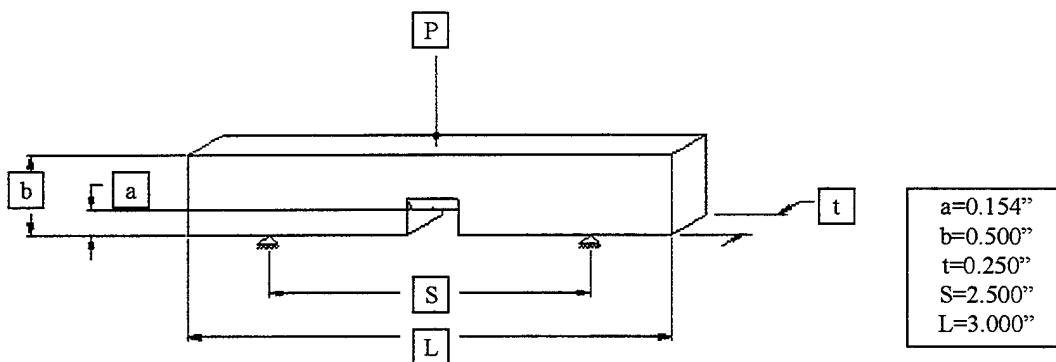


Fig. 3-1 Three-point bending specimens with chevron notch for EMC materials

The K value of the beam specimen with a line crack may be calculated by the following formula (Tada, 1973):

$$K = \sigma \sqrt{\pi a} F(a/b) \quad (3-1)$$

in which the maximum bending stress:

$$\sigma = 6M/(tb^2) \quad (3-2a)$$

and the bending moment:

$$M = Ps/4 \quad (3-2b)$$

The function:

$$F(a/b) = 1.09 - 1.735(a/b) + 8.2(a/b)^2 - 14.18(a/b)^3 + 14.57(a/b)^4 \quad (3-3a)$$

for $s/b = 4$, and

$$F(a/b) = 1.107 - 2.12(a/b) + 7.71(a/b)^2 - 3.55(a/b)^3 + 14.25(a/b)^4 \quad (3-3b)$$

for $s/b = 8$.

where a, b, P and t , as well as the distance s , which denotes the distance between two supports are shown in Fig. 3-1.

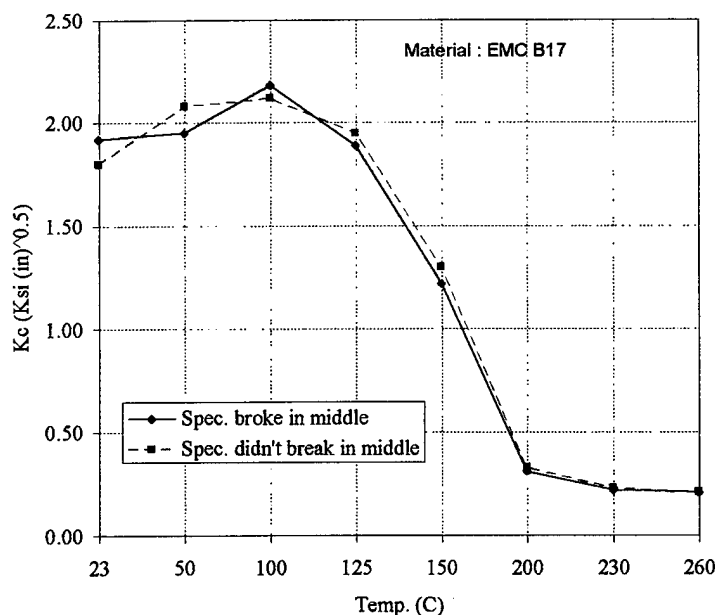
The applied load, P in Eq. (3-2b) is replaced by the critical load at which the crack in the specimen propagates through the material. In such case, the stress intensity factor K in Eq. (3-1) is equivalent to the fracture toughness K_c of the material.

3.2 Specimen Preparation

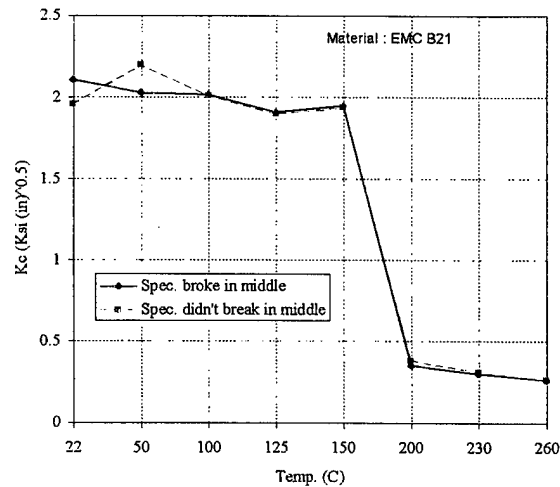
The geometry and dimensions of the EMC specimens used for the tests followed closely to what were used in similar tests by a research team at Ohio State University. As illustrated in Fig. 3-1, a Chevron notch with a depth, $a = 0.154$ " (4 mm) was introduced to a beam specimen. Other nominal dimensions are: $L = 3$ " (76 mm), $t = 0.25$ " (6.35 mm), $b = 0.50$ " (12.7 mm), and $s = 2.5$ " (63.5 mm). The width of the notch was 0.12 " (3 mm).

Specimens made of four types of EMC were fabricated and supplied by National Semiconductor Corporation. These EMC, with designations of: B8, B17, B21 and B24 are used throughout the investigation.

A minute line cut of 0.002 " (0.05 mm) wide x 0.15 - 0.20 " (0.38-0.5 mm) deep was introduced to the tip of the chevron notch using a fine jeweler saw. The purpose of introducing these fine line cracks to the specimens was to initiate fracture at the tip of these line cracks. This procedure was later omitted due to the fact that results obtained for the K_{IC} values indicated that maximum deviation of results from specimens with and without such cuts was less than 6% such as illustrated in Fig. 3-2. However, all specimens fractured within the chevron notched zone.



(a)



(b)

Fig. 3-2. Sensitivity of fracture location in the specimens on K_c measurements

An environmental chamber was used to introduce moisture in the specimens at various temperatures. The chamber could provide an environment of 80° C at 85% RH (relative humidity). Specimens were first weighed by a high resolution scale to determine their initial weight (or weight at the "as-received" state). They were then placed in wire mesh trays in the chamber at 80° C and the desired level of RH. Individual specimens were weighed every 24 hours, and their weight gains were recorded as illustrated in Fig. 3-3 for the case of 85% RH. From these graphs, one could determine the required time for "saturated" moisture diffusion into various groups of specimens.

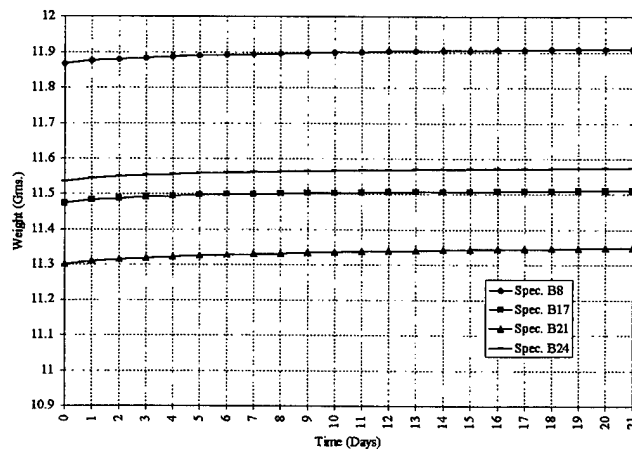


Fig. 3-3 History of moisture absorption in EMC specimens

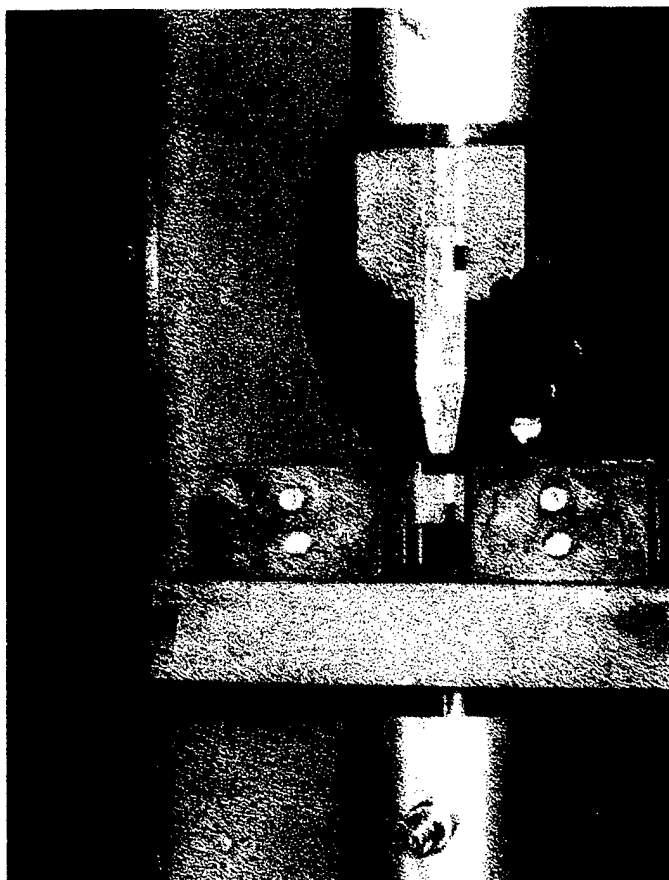


Fig. 3-4 Test set-up for 3-point bending tests in a furnace

3.3 Test Procedures

A universal testing machine was used to provide the loading to the specimen. A special rig for the three-point bending was designed and constructed for the notched beam specimens. The bending rig was placed in an oven which is capable of providing a temperature environment up to 350° C. The loading rate was kept at 20 in (0.5 m)/minute. The set-up is shown in Fig. 3-4 above.

Test conditions for the K_{IC} measurements are presented in Table 3-1.

Table 3-1 Test Conditions for Each Molding Compound

Temperature (C)	22	50	100	125	150	200	230	260
Relative Humidity (%)	AR	AR	AR	AR	AR	AR	AR	AR
	40	40	40	40	40	40	40	40
	60	60	60	60	60	60		
	85	85	85	85	85			
No Conditions	4	4	4	4	4	3	2	2

As can be observed from the above table, 108 tests were performed on each of the four EMC specimens. These conditions with combined temperatures and humidities were set to reflect the conditions that PEM are expected to operate in reality. Each test condition was repeated four times to ensure consistencies of the measured data. A total of 432 tests were successfully performed in this research project.

Effort was made in completing tests on specimens with moisture contents in less than 10 minutes in order to minimize the desorption of moisture in the specimens during the tests. Analysis using Fick's diffusion equation and laboratory experiments had indicated that moisture loss of the specimens to ambient environment is insignificant during normal length of time required to perform the tests. Fig. 3-5 shows the rate of weight losses of EMC specimens at 260° C.

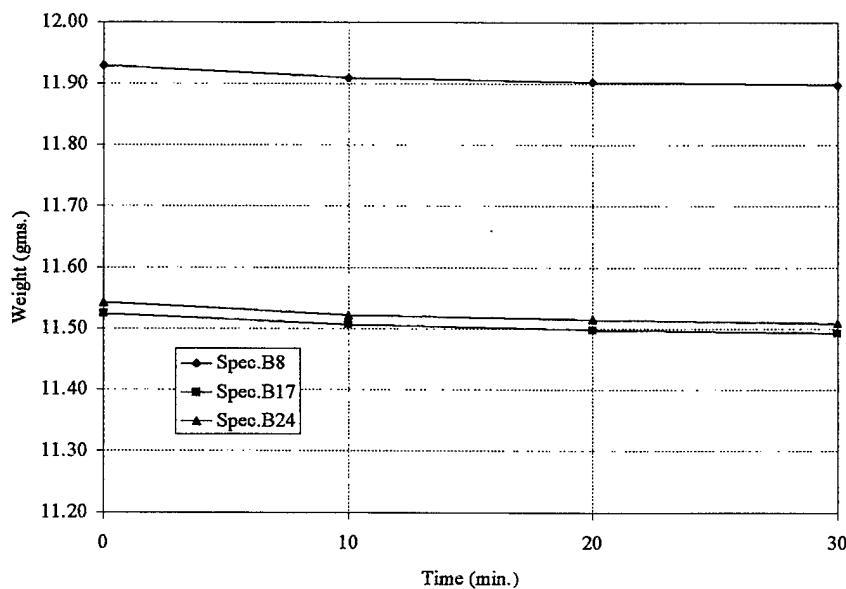
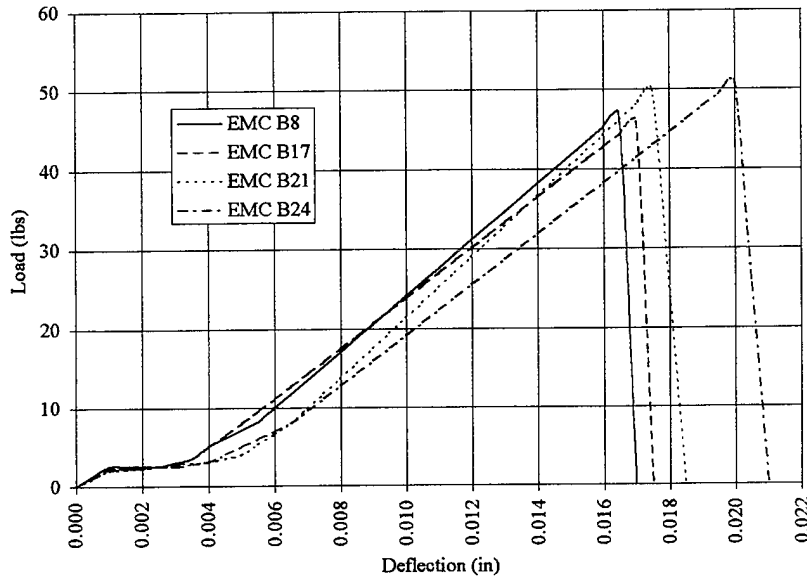


Fig. 3-5. Moisture deposition from specimens at 260° C

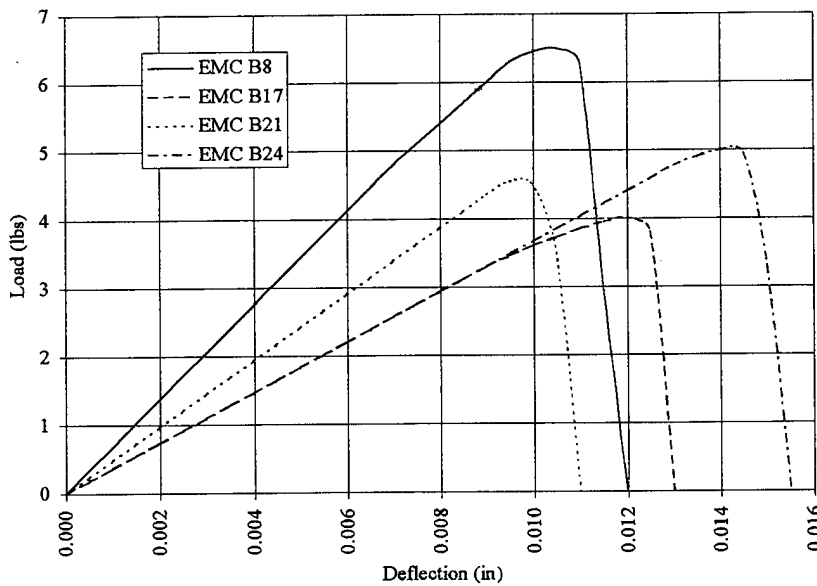
3.4 Measured Results

Figure 3-6 shows typical measured "load vs. deflection" curves for EMC specimens. The peak loads in these curves, at which the specimens fractured, are the critical loads, P_{cr} used to calculate K_c for the specimens. Thus, Figs. 3-

6 (a) gave P_{cr} for four EMC at RT (room temperature) and AR (as received), whereas Fig. 6 (b) shows P_{cr} at 260° C and 40% RH (relative humidity).



(a): Typical load vs. deflection curves of 'as received' specimens at room temperature.



(b): Typical load vs. deflection curves at 260° C and 40% RH.

Fig. 3-6 Measured load vs. deflection curves

The value of all P_{cr} measured on all specimens at all conditions listed in Table 3-1 were used to compute the corresponding fracture toughness, K_{Ic} in Eq. (3-1). Figure 3-7 shows the band widths that illustrate the scattering of measured K_{Ic} values at AR and 85% RH. One may observe moderate scattering of K_{Ic} at low temperatures from this figure. These band widths, however, narrowed substantially after passing the glass transition temperature of the material at about 150°C. Average fracture toughness, K_{Ic} values for all 4 EMC are presented in Figs. 3-8, 3-9, 3-10 and 3-11. Fig. 3-12(a) shows the variation of K_{Ic} among all EMC at "as received" condition (i.e. no additional moisture content), whereas the variation became more pronounced when additional moisture was introduced as illustrated in Fig. 3-12 (b).

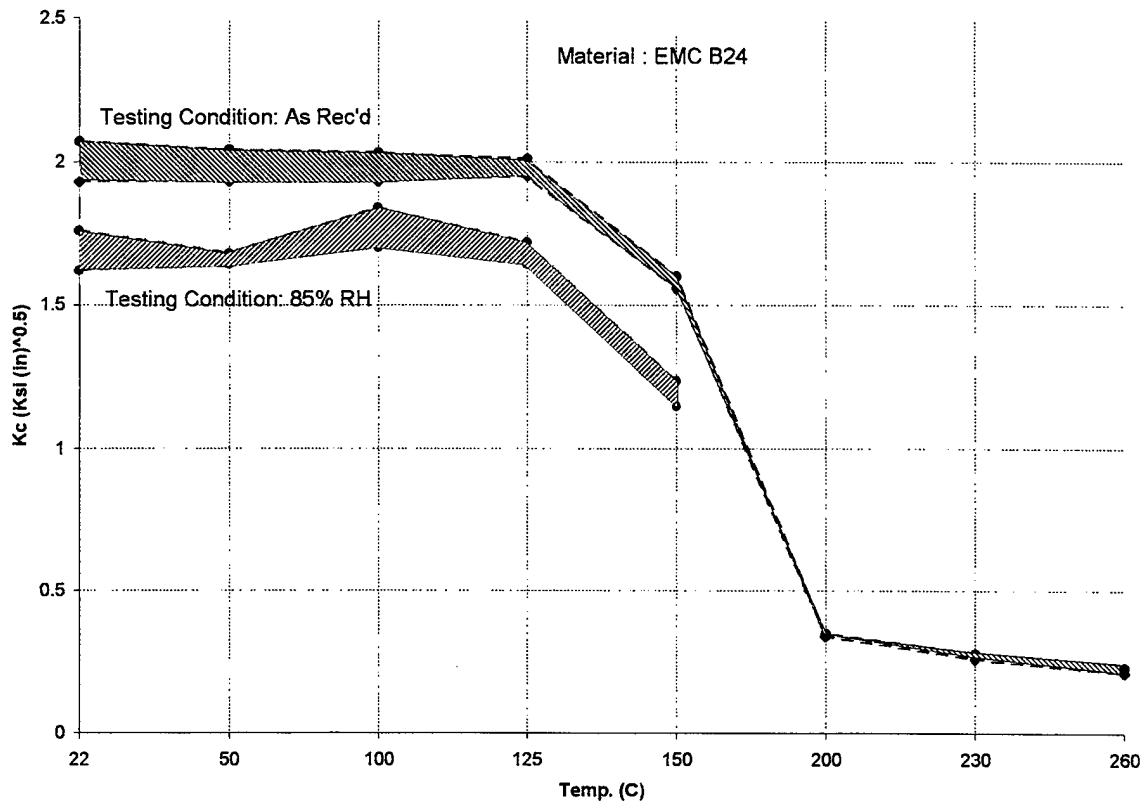


Fig. 3-7 Scattering of measured K_{Ic} values

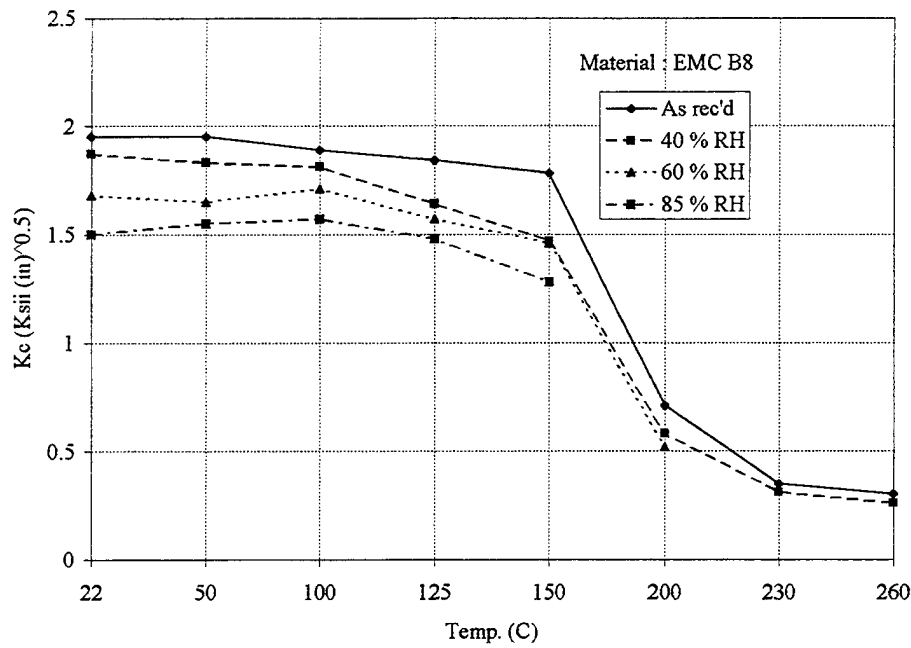


Fig. 3-8 Moisture effect on fracture toughness for EMC B8 specimens

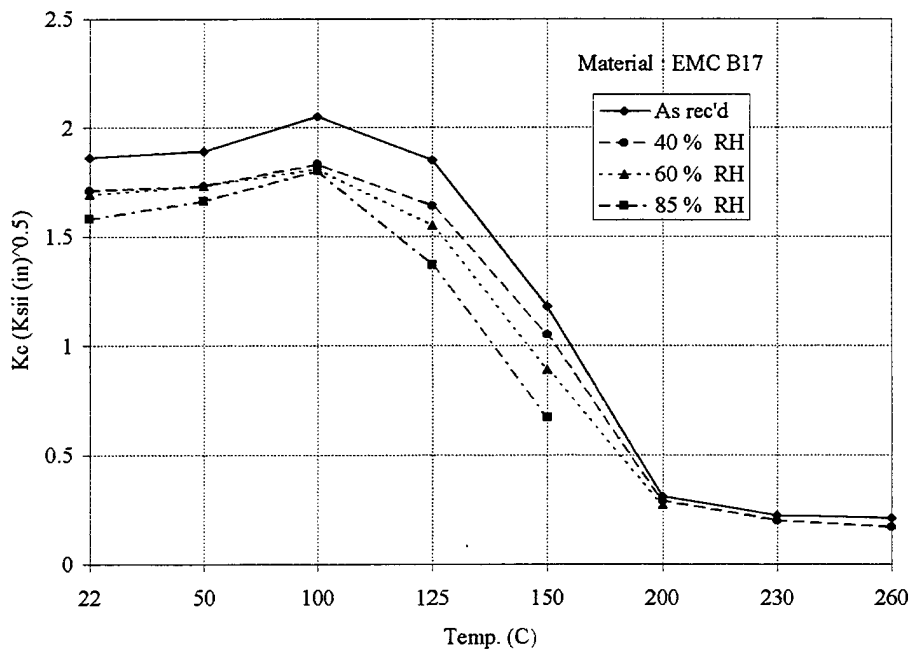


Fig. 3-9 Moisture effect on fracture toughness for EMC B17 specimens

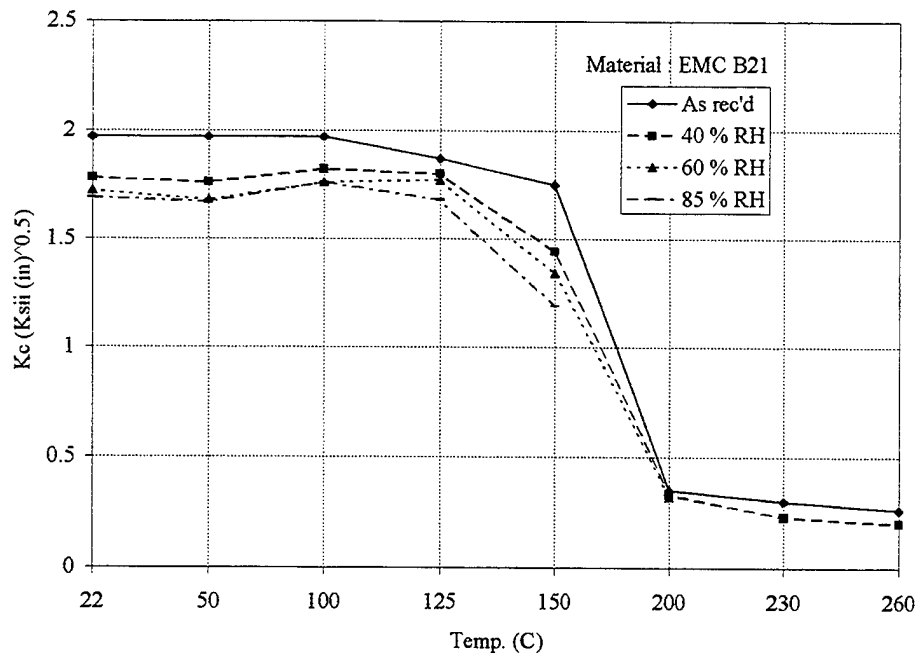


Fig. 3-10 Moisture effect on fracture toughness for EMC B21 specimens

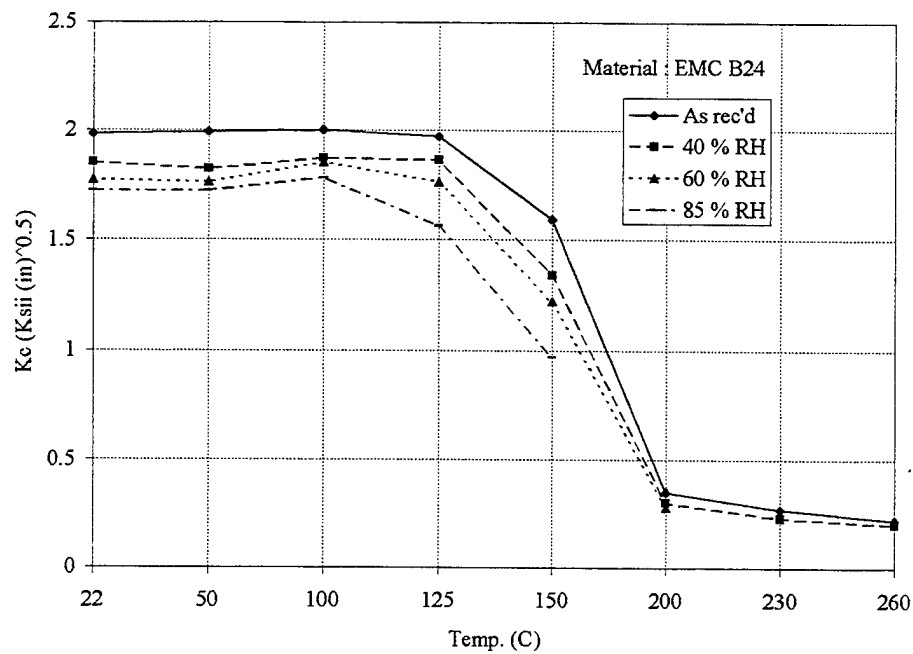
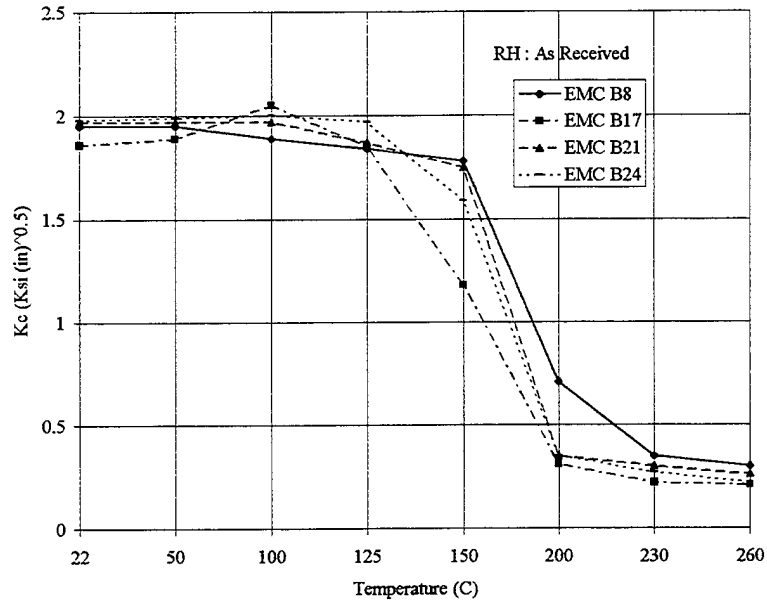
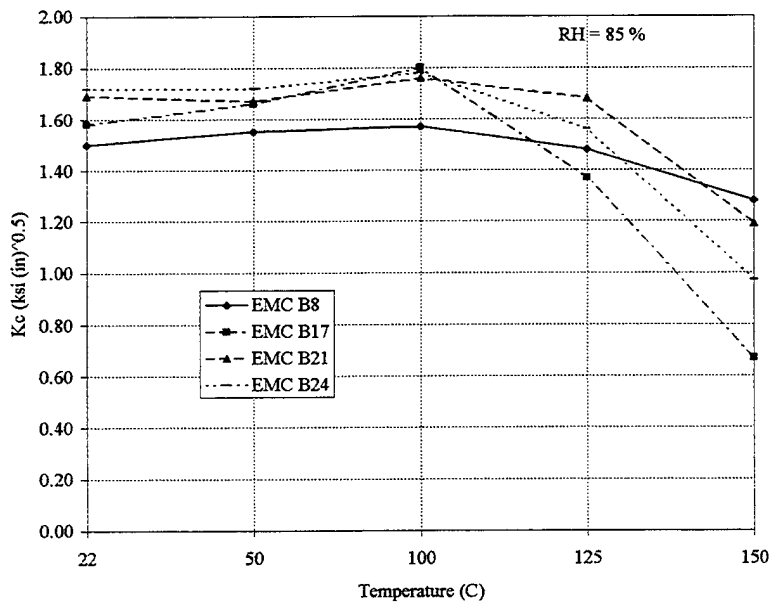


Fig. 3-11 Moisture effect on fracture toughness for EMC B24 specimens



(a) For 'as received' Specimens.



(b) For specimens saturated at 85% RH

Fig. 3-12 Measured average fracture toughness for EMC Specimens

3.5 SUMMARY ON RESULTS

Results obtained from the 432 successful tests on K_{IC} measurements can be summarized as follows:

- (1) The measured average K_{IC} value for the four EMC was at the neighborhood of $2 \text{ Ksi}\sqrt{\text{in}}$ at room temperature in the "as received" condition, which agrees with what was reported by the Ohio State University team on similar EMC at same conditions.
- (2) Temperature has a significant effect on the K_{IC} values. For example, $K_{IC} = 1.94 \text{ Ksi}\sqrt{\text{in}}$ for the "as received" EMC B8 at room temperature. This value dropped to $0.30 \text{ Ksi}\sqrt{\text{in}}$ at 260°C , which represents an 84% decrease in the value! The same effect was observed on other EMC.
- (3) Moisture content also played a major role in K_{IC} value of the materials. The same "as received" EMC B8 specimens had an average $K_{IC} = 1.78 \text{ Ksi}\sqrt{\text{in}}$ at 150°C . This value decreased by 28% to $1.28 \text{ Ksi}\sqrt{\text{in}}$ at the same temperature for specimens saturated in 85% RH environment prior to the tests.
- (4) Variation of K_{IC} values of specimens with different moisture contents reduced drastically at high temperature ranging from 200 to 260°C as shown in Figs. 3-8 to 3-12. Such reduction was mainly attributed to the significant desorption of moisture in the specimens during the 10-minute test duration at these temperatures.
- (5) Results indicated that K_{IC} for all EMC remain relatively constant with moderate temperature increases. Drastic decrease of this value, however, was observed once the temperature exceeds the glass transition temperature of 150°C .
- (6) Of the four molding compounds tested, EMC B8 has the highest fracture toughness, whereas EMC B17 has the lowest values.
- (7) As expected, there were signs of downward shifting of glass transition temperatures of the molding compounds with increasing moisture contents (see Figs. 3-9 to 3-11).

4 INTERFACIAL FRACTURE TOUGHNESS IN PLASTIC PACKAGES

Interfacial adhesion in plastic packages is one of the key requirements to achieving popcorn-resistant packages. As part of an Air Force-funded study to develop an Expert Design System for plastic packages (EPACK[®]), an extensive evaluation of various interfaces in plastic packages is being conducted. Three-point bending testing was conducted on molded composite beams embedded with either Si (with and without polyimide coating), or copper alloy. Two pre-crack lengths were tried. Testing was conducted at different temperatures and humidities. The effect of residual stresses (resulting in curved test specimens) was modeled and accounted for in the evaluation of the critical interfacial fracture toughness. Eventually such material properties, together with package configurations and leadframe designs, will be entered as part of the EPACK database to provide design rules for achieving Level-1 (no dry bag) performance.

4.1 INTRODUCTION

Plastic encapsulated microcircuits (PEMs) offer many advantages over their ceramic counterparts such as low-cost, lightweight, ready availability, and good reliability that accounted for the wider use. However, one key drawback to PEM is the susceptibility to moisture absorption. The epoxy molding compound (EMC) used in the PEM, a typical epoxy cresol novolac blend with up to 70 weight loading of silica fillers, is hygroscopic. When left exposed to a humid environment, the epoxy resin can absorb moisture up to saturation, which can surpass 0.3% for some packages. Under such a scenario, if the packages are then assembled on to the circuit board, the intense heat from the reflow oven will vaporize the absorbed moisture, turning it into high pressure steam, which will escape through the path of least resistance, delaminating and cracking the package along the way. Such popcorning is due to a number of inter-relating factors such as package size, mold compound, die attach, exposure conditions, and reflow profile, as summarized by Nguyen (1993). Although popcorning can be avoided by adopting one of a number of solutions, e.g., dry bagging (storage in aluminized bags with desiccants), baking prior to assembly, or selecting (more expensive) materials of construction, no single cost-effective answer has been obtained yet. Much industry-wide effort has been devoted to finding a solution to this package cracking problem (Umehara *et al.*, 1995; Ganesan *et al.*, 1995; Ganesan and Berg, 1996; Lee and Parthasarathi, 1997; Nguyen *et al.*, 1997a, 1997b).

As part of an Air Force-funded effort to develop an Expert Design System for PEMs to guard against moisture-induced defects, a number of activities have concentrated in the last year on gathering material properties to validate a criterion for package cracking, as summarized by Nguyen *et al.* (1995). Data on fracture toughness for a number of EMCs as a function of temperature and humidities were presented recently, Hsu *et al.*, 1997. This chapter will describe interfacial shear strength data collected on laminated samples of these EMCs with either copper alloy or silicon. Such structures mimic the interfaces encountered in actual packages, such as at the leadframe and mold compound or the silicon die with the mold compound. Working with well-defined and idealized geometries facilitates the interpretation of the data.

4.2 EXPERIMENTAL

4.2.1 Test Conditions:

Two types of interfacial shear strength tests were conducted:

1) Bending of laminated beams of EMC and silicon or EMC and copper alloy strips, with pre-cracks of finite lengths introduced at one end. Pre-cracks were introduced by spraying Teflon powder onto the substrate (e.g., Si or Cu strip) under a mask to provide a known area for weak adhesion. Scanning acoustic microscopy can monitor the ensuing poor coupling between the EMC and the substrate. The acoustic scans indicated that the distance of the "pre-crack" was within the specifications.

TABLE 4-1: Test Samples and Test Conditions for the 3-point Loading.

EM C	Substrate	Pre- crack (cm)	% RH	T (°C)
B8	O-194	1, 2	0	20
B17	C-7025		40	100
B24	Si without PIQ		85	200
	Si with PIQ			

TABLE 4- 2: Shear tests of sandwiched specimens with Cu alloy strips.

Materials	% RH	T (°C)
B17/O-194 B17/C-7025	0, 40, 85	20, 100, 200
B24/O-194 B24/C-7025	0, 40, 85	20, 100, 200
B8/C-7025	0	20, 100, 200

2) Shearing of blocks of EMC sandwiching either silicon or copper alloy strips. The geometry and dimensions of these specimens are shown in *Figure 4-1*. Three EMCs were used in these tests, B8 (a standard epoxy cresol novolac), B17 (a low stress ECN), and B24 (a low stress ECN modified for Quad Packages). The copper alloys included, O-194 and C-7025, are commonly used for both stamped and etched leadframes. The silicon samples included two types, namely, dies with standard nitride passivation (no polyimide) and a coating of polyimide layer for stress buffering. Each test condition was repeated at least 3 times. The total number of tests was: 12 (materials) x 2 (pre-crack) x 3 (RH%) x 3 (temperatures) x 3 (tests) = **648** tests, as shown in *Table 4-1*.

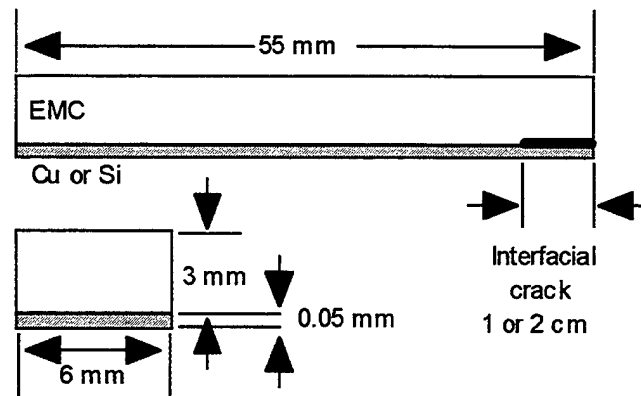
For the tests listed in *Table 4-2*, the total number of tests was: 4 (materials) x 3 (RH%) x 3 (temperatures) x 3 (tests) + 1 (material) x 1 (RH%) x 3 (temperatures) x 3 (tests) = **117**.

For the shearing of the sandwiched specimens with silicon strips, only six samples made of B17/Si with PIQ were used. Room temperature testing was done in this case.

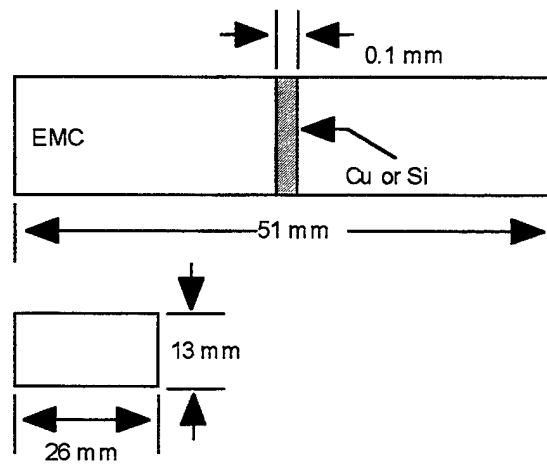
4.2.2 Test Procedures

All the tests were conducted using a universal testing machine with loading capacity up to 1,000 lbs. A furnace which can provide a chamber at temperatures up to 260°C at ± 1 °C accuracy was attached to a loading frame. Three tension/compression load cells with ranges at 0-50, 0-100, and 0-500 lbs were used in these tests. The load cells were first calibrated by means of a tension/compression ring. *Figure 4-2* shows the configuration for the 3-point bending setup with the typical geometries of "concave-upward" and "concave-

downward” due to residual stresses. The fixture for the shear tests is illustrated in *Figure 4-3*.



(a) Laminated samples



(b) Sandwiched samples

Fig 4-1 Geometries of samples tested. a) Laminated beams of EMC and Si or Cu alloy; b) Sandwiched blocks of EMC and Si or Cu alloy.

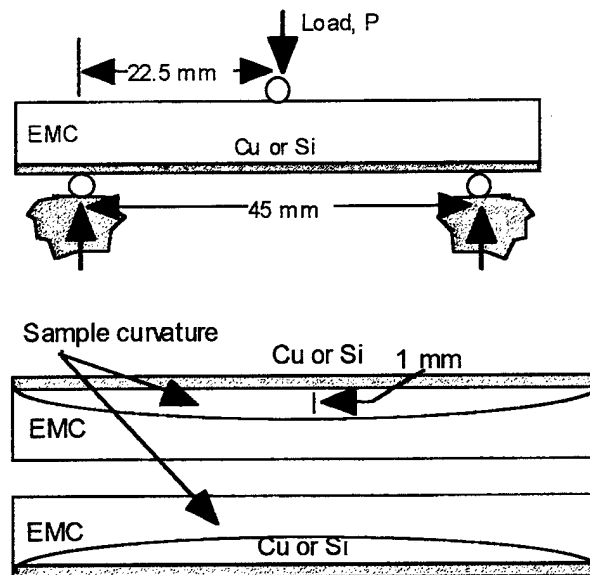


Fig 4-2 Three-point bending of laminated beams with pre-cracks. Residual stresses from thermal mismatch caused the bilayer structures to bend either concave-upward (a) or concave-downward (b).

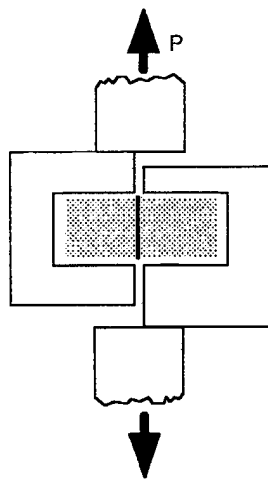


Fig 4-3 Fixture for shearing of sandwiched specimens.

The specimens were exposed to moisture in an environmental chamber, which provided various levels of relative humidity (RH) up to 85% at 80 °C for extended periods. The typical moisture absorption for both types of specimens is shown in *Figures 4-4 and 4-5*. Samples that were placed in the moisture chamber were weighted beforehand (after baking to remove moisture) and at intervals of 24 hours thereafter. Saturation of moisture absorption was recognized at the time when no more weight increase was recorded.

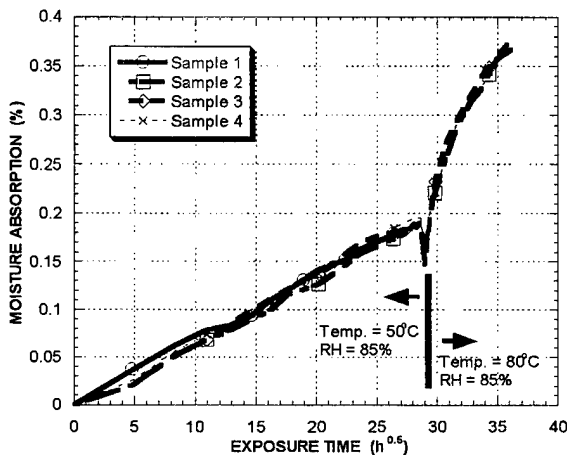


Fig 4-4 Moisture Absorption (B8/Cu)

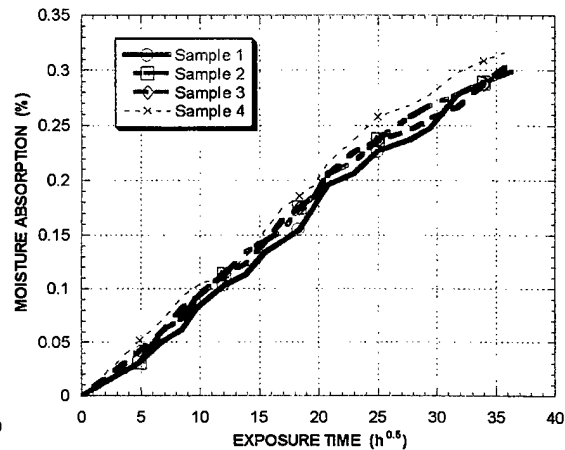


Fig 4-5 Moisture Absorption (B8/Cu)

At pre-determined intervals, samples were removed from the environmental chamber into the test chamber at a pre-set temperature. A 10-15 minute waiting period was allowed for the sample to reach uniform temperature. Such transition period is unavoidable in the current setup unless the test chamber can be modified at greater cost to allow for high temperature and high pressure testing. Bending or shearing loads were then applied to the specimen and the load deflection curves were recorded until the specimens broke. The loads at the breaking points were recorded as the critical loads, P_{cr} . Typical load deflection curves for the 3-point tests are shown in *Figures 4-6 and 4-7*, and shear tests of the sandwiched samples are illustrated in *Figures 4-8 and 4-9*.

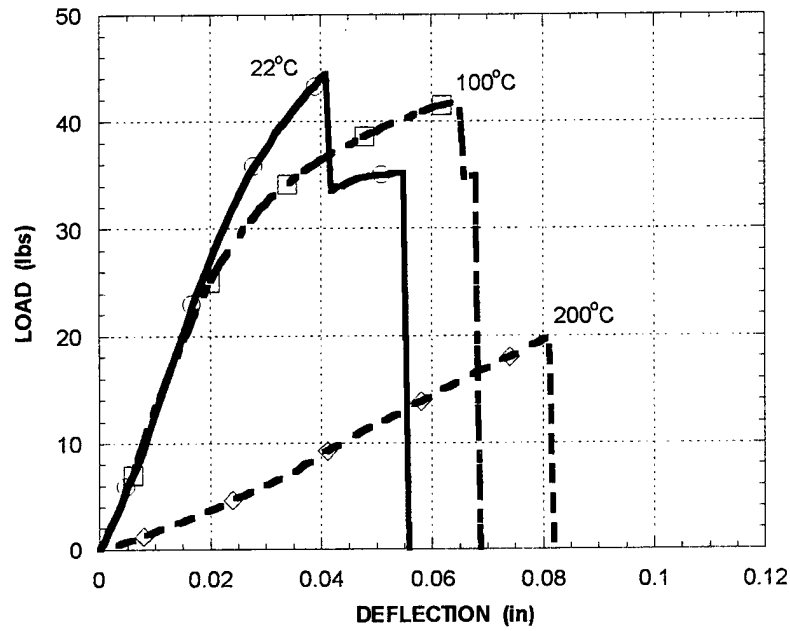


Fig 4-6 Load deflection curves for a composite beam of B24/C-7025 with a 1 cm pre-crack at 40% RH.

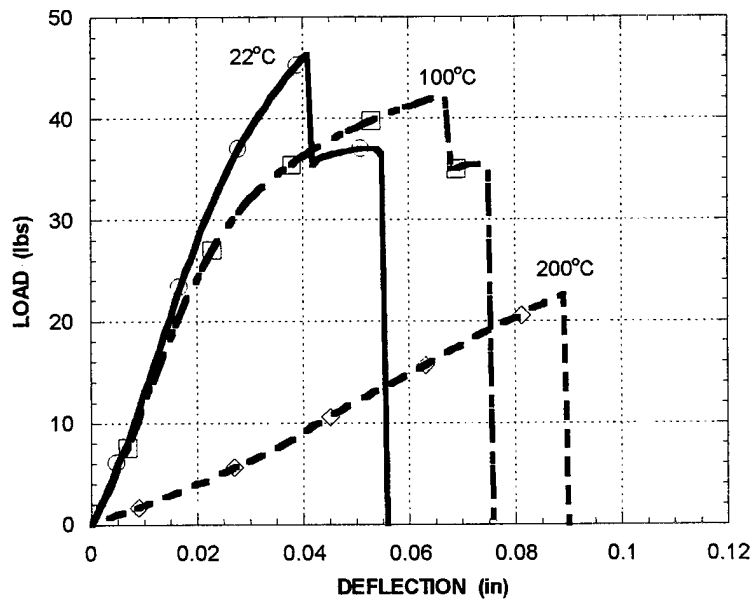


Fig 4-7 Load deflection curves for a composite beam of B24/C-7025 with a 2 cm pre-crack at 40%RH.

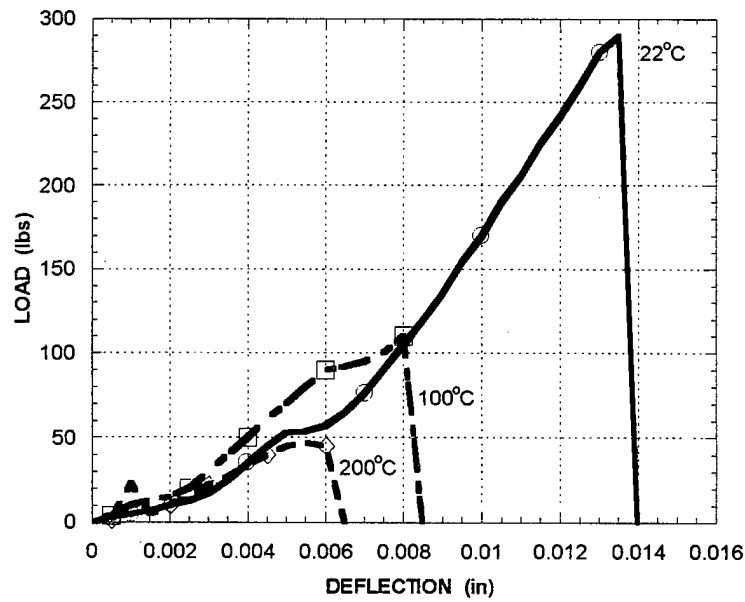


Fig 4-8 Load deflection curve for the sandwiched block of B24 and C-7025 alloy at "as received condition" and different temperatures.

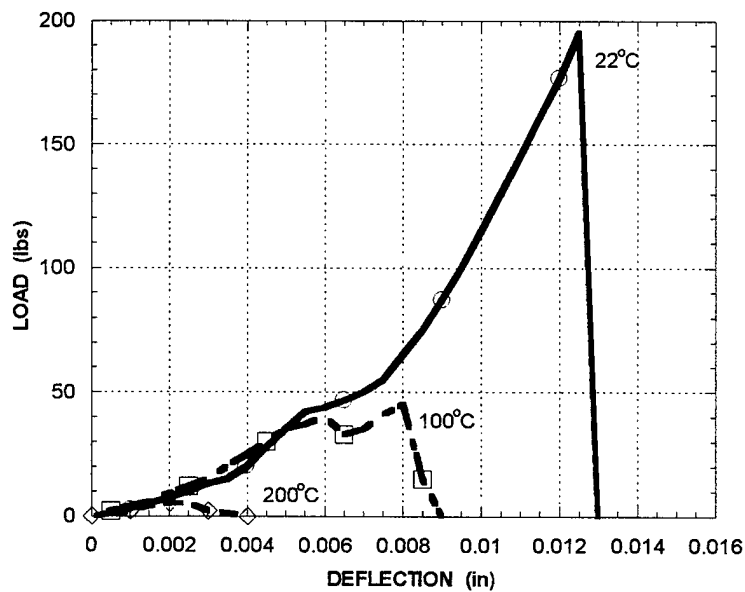


Fig 4-9 Load deflection curve for the sandwiched block of B24 and C-7025 at 85% RH and different temperatures.

4.3 RESULTS AND DISCUSSION

4.3.1 Interface Fracture Toughness

Similar interface fracture toughness tests for electronic materials have been performed and reported recently by Tanaka and Nishimura (1995), and Ikeda *et al.* (1997). As expected, under a combined loading of mechanical force, thermal stress, hygro stress, and residual stress due to molding, the crack-tip of the interface crack in the laminate specimen is under mixed-mode fracture (e.g., Ikeda *et al.* 1997).

Tanaka and Nishimura (1995) used a simple-minded approach to calculate the interface fracture toughness. In their study, an equivalent stress intensity factor was used as the fracture parameter for the mixed-mode fracture problem and the residual stress due to molding was handled by taking the average fracture loads of concave-up and concave-down specimens. For electronic materials, the interface fracture toughness for Mode I and Mode II fractures are quite different. As a result, the critical equivalent stress intensity factors reported by Tanaka and Nishimura (1995), and later re-calculated by Lin and Tay (1997), will not be accurate enough. Although taking the average value of a concave-up and a concave-down specimen as the interface fracture seems intuitive and simple, it is actually not correct due to the fact that fracture mode mixities for the concave-up and concave-down specimens are quite different. The crack surfaces are open in the concave-up specimens but closed in the concave-down specimens.

Ikeda *et al.* (1997) have corrected this shortcoming by using an innovative virtual crack extension approach to separate the Mode I and Mode II stress intensity factors. In addition to the three-point bending testing, these authors have also added a peeling testing with the same laminate specimens. Since many of the IC package popcorning incidents happen very early during the solder reflow process, it is not true to assume that delamination and crack propagation always occur at the reflow temperature. It has been well known that moisture will lower the interface adhesion strength, making the materials more likely to delaminate.

Gledhill *et al.* (1980) reported that moisture would also lower the interface fracture toughness once the moisture level is higher than a threshold value. Unfortunately, Ikeda *et al.* (1997) did not report the effects of temperature and moisture on the mixed-mode fracture toughness.

In this study, the critical mixed mode stress intensity factors of the laminated specimens are calculated by a modified $M(1,2)$ -Integral (Yau and Wang, 1984).

4.3.2 J-Integral for Thermoelasticity:

For thermoelastic 2-D problems, Kuo and Riccardella (1987) have derived a path-independent line integral for a plane strain problem:

$$J = \int_{\Gamma} [Wn_1 - \sigma_{ij}n_j u_{i,1} + (1 + \nu)\alpha\sigma_{i1}n_1 T] ds \quad (4-1)$$

W = Strain energy density

σ_{ij} = Stress tensor

u_i = Displacement vector

n_j = Outer normal of the integration path Γ

E = Young's modulus

G = Shear modulus

ν = Poisson's ratio

α = Coefficient of thermal expansion

$T = T(x,y)$ = steady-state temperature distribution above the reference temperature

Since the hygro stress and the thermal stress are both considered body forces to the elastic solids, the J-Integral for thermoelasticity problems derived by Kuo and Riccardella (1987) can be easily extended to the hygro thermal stress problem as:

$$J = \int_{\Gamma} [Wn_1 - \sigma_{ij}n_j u_{i,1} + (1 + \nu)\sigma_{i1}n_1 (\alpha T + \beta C)] ds \quad (4-2)$$

where β is the material swelling coefficient and C is the moisture content of the material.

The path-independent integral derived by Kuo and Riccardella (1987) does not involve the cumbersome area integral in the J-Integral for thermoelasticity by Wilson and Yu (1979).

4.3.3 Stress Intensity Factors of Interface Cracks with an Open Crack Tip

As discussed by Rice (1988), there are several ways to define the stress intensity factors for the interface cracks. The following definition of the mixed-mode stress intensity factors for the interface cracks is adopted in this paper:

$$(\sigma_{yy} + i\sigma_{xy})_{\theta=0} = \frac{(K_I + iK_{II})}{\sqrt{2\pi r}} \left(\frac{r}{L}\right)^{i\varepsilon} = \frac{(\hat{K}_I + i\hat{K}_{II})r^{i\varepsilon}}{\sqrt{2\pi r}} \quad (4-3)$$

where L is the unit length and ε is the bi-material constant defined as:

$$\varepsilon = \frac{1}{2\pi} \ln \left(\frac{\kappa_1 / \mu_1 + 1 / \mu_2}{1 / \mu_1 + \kappa_2 / \mu_2} \right) \quad (4-4)$$

with subscripts 1 and 2 referring to the upper and lower materials, $\kappa = 3-4\nu$ for plane strain and $(3-\nu)/(1+\nu)$ for plane stress, ν = Poisson's ratio, and μ = shear modulus. Since inch is used as the unit for the length dimension in this study, $L = 1$ inch for all the analysis cases. The stress intensity factors, K_I and K_{II} , defined above have the conventional units of $\text{psi}\sqrt{\text{in}}$ (or $\text{MPa}\sqrt{\text{m}}$) for stress intensity factors while retaining the meaning of stress intensity factors due to Mode I and Mode II loading. It is worth noting that when other values are used for L (e.g., Ikeda *et al.* (1997) used 10 μm instead of 1 mm), the K_I and K_{II} values no longer have a direct link with the crack opening mode and crack shear mode. The above definition for the interfacial crack stress intensity factors is used for the concave-up specimens with a 10 mm edge crack, where the crack-tip is "open" (see Fig 4-10).

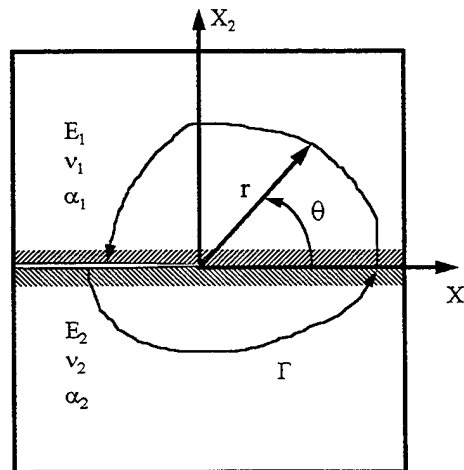


Fig. 4-10 An Interface Crack

4.3.4 Stress Intensity Factor of Closed Interface Cracks

For the concave-down specimens and the concave-up specimens with a 20 mm edge crack, the crack-tip is found to be closed, i.e., the crack surface are in contact. In these cases, the following definitions of stress intensity factors (Comninou, 1977) are used:

$$(\sigma_{yy} + i\sigma_{xy})_{\theta=0} = \frac{(0 + iK_{II})}{\sqrt{2\pi r}} \quad (4-5)$$

$$J = \frac{\pi}{4c} K_{II}^2 \quad (4-6)$$

$$(\sigma_{yy} + i\sigma_{xy})_{\theta=\pm\pi} = \frac{(K_I^* + 0i)}{\sqrt{2\pi r}} = \frac{-\beta|K_{II}|}{\sqrt{2\pi r}} \quad (4-7)$$

$$\alpha = \frac{G_2(1 - \nu_1) - G_1(1 - \nu_2)}{G_2(1 - \nu_1) + G_1(1 - \nu_2)} \quad (4-8)$$

$$\beta = \frac{G_2(1 - 2\nu_1) - G_1(1 - 2\nu_2)}{G_2(2 - 2\nu_1) + G_1(2 - 2\nu_2)} \quad (4-9)$$

$$c = \frac{G_1(1 + \alpha)}{(2 - 2\nu_1)(1 - \beta^2)} \quad (4-10)$$

It is worth noting that the "Mode-I" stress intensity for closed cracks is defined differently from that for the classical open cracks. For closed cracks, the shear stress at the crack-tip approaches infinity with a classical $r^{1/2}$ singularity while the crack opening stress σ_{yy} remains finite in front of the crack-tip ($\theta = 0$) but also approaches infinity with the $r^{1/2}$ singularity along the crack surfaces ($\theta = \pm\pi$). Since, for closed crack, K_I and K_{II} are directly related, they can be calculated with the path-independent J-Integral for hygro thermal stress problems described previously.

4.3.5 Fracture Mode Separation for Open Interface Cracks

With the above J-Integral for the hygrothermal problems, we can extend the conservation integrals derived by Yau and Wang (1984) to the bi-material, thermoelastic problem:

The contribution of the last term in the bracket of the above equations is zero for the cases with $T = \text{constant}$ and/or $C = \text{constant}$. In the laminate specimen analysis, T of the thin strip is set as zero while T of the thick molding compound strip was set as a negative temperature, which will generate the same amount of bowing (about 1 mm for all specimens) observed in the specimens. Detailed definitions of the auxiliary solution fields $u_i^I, u_i^{II}, \sigma_{ij}^I$, and σ_{ij}^{II} are presented in Appendix II of this report.

$$K_I = \frac{1}{\frac{1-\nu_1^2}{2 \cdot E_1} + \frac{1-\nu_2^2}{2 \cdot E_2}} \int_{\Gamma} [\sigma_{ij} \{u_{ij}^I - \delta_{ij}(1+\nu)(\alpha T + \beta C)\} n_i - (\sigma_{ij} n_j u_{i,1}^I + \sigma_{ij}^I n_j u_{i,1}) + (1+\nu) \sigma_{ii}^I n_i (\alpha T + \beta C)] ds \quad (4-11)$$

$$K_{II} = \frac{1}{\frac{1-\nu_1^2}{2 \cdot E_1} + \frac{1-\nu_2^2}{2 \cdot E_2}} \int_{\Gamma} [\sigma_{ij} \{u_{ij}^{II} - \delta_{ij}(1+\nu)(\alpha T + \beta C)\} n_i - (\sigma_{ij} n_j u_{i,1}^{II} + \sigma_{ij}^{II} n_j u_{i,1}) + (1+\nu) \sigma_{ii}^{II} n_i (\alpha T + \beta C)] ds \quad (4-12)$$

4.3.6 Elastic Properties of Tested Materials

Table 4-3 lists the elastic material properties used in the fracture toughness calculation. Except for the swelling coefficients (β_1 and β_2), the material properties are taken from material vendors' data sheets. The swelling coefficients were measured by exposing samples of the EMCs to water up to saturation, and monitoring the dimensions of the samples under an optical microscope. The smaller swelling coefficients (β_a) are measured at room temperature, while the higher swelling coefficients (β_b) are measured at 85°C. Although the swelling coefficients of the molding compound materials are expected to be even higher at 100°C and 200°C, due to lack of test data at higher temperatures, the swelling coefficients measured at 85°C will be used approximately for the 100°C and 200°C test cases.

TABLE 4-3: Elastic materials of the EMCs used in this study

Material I	E (10 ⁶ psi)	ν	T _g (°C)	α_1, α_2 (ppm/°C)	β_a, β_b 1. (ppm/%w)
B8	2.0	0.33	164	24.0, 55.0	901, 2021
B17	2.2	0.33	156	17.5, 55.0	1166, 1676
B24	1.7	0.33	165	16.5, 55.0	1019, 2248
C-7025	19.2	0.30	N/A	17.6	N/A
O-194	17.5	0.30	N/A	16.3	N/A
Si	18.6	0.30	N/A	3.6	N/A

4.3.7 Mixed-Mode Interface Fracture Toughness

The following criterion has been developed in the present study

$$\left(\frac{K_I}{K_I^C}\right)^2 + \left(\frac{K_{II}}{K_{II}^C}\right)^2 = 1 \quad (4-13)$$

where K_I^C and K_{II}^C are, respectively, Mode I and Mode II fracture toughness of the interface. Typical curves of K_I^C and K_{II}^C for three cases are shown: B8/O-194 (Figure 4-11); B8/C-7025 (Figure 4-12); and, B8/Si (Figure 4-13). Similar curves can be generated for the other material combinations used in this study. All the other interface fracture toughness data are contained in Appendix II of This report.

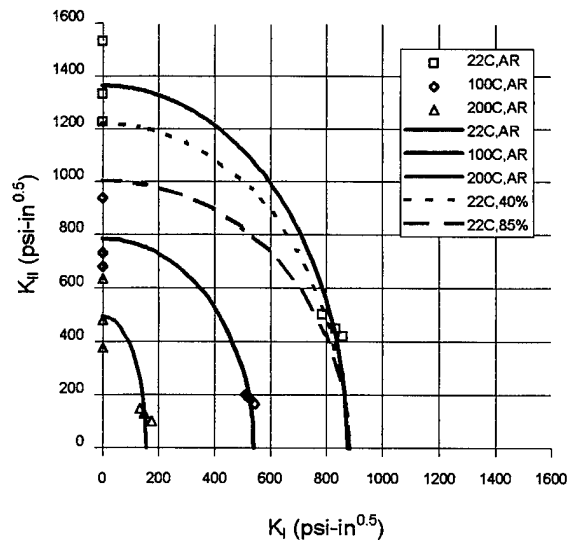


Fig 4-11 Mixed-mode fracture toughness for the combination B8/O-194.

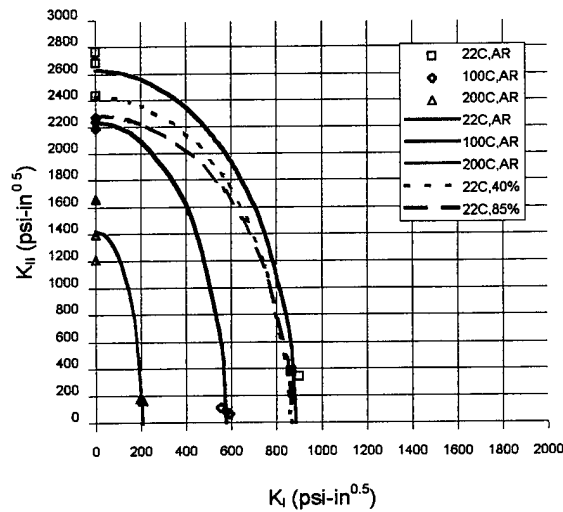


Fig 4-12 Mixed-mode fracture toughness for the combination B8/C-7025.

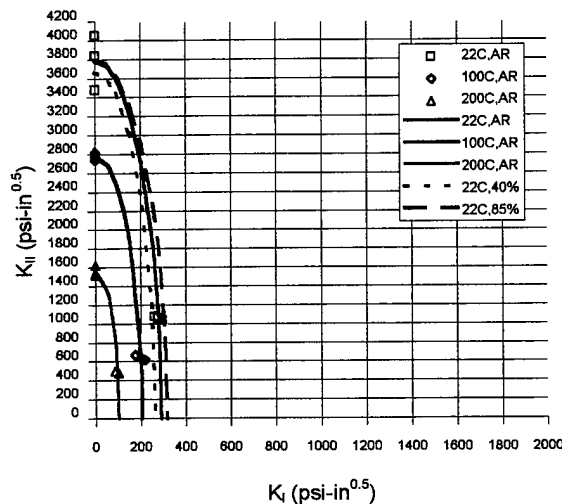


Fig 4-13 Mixed-mode fracture toughness for the combination B8/Si.

4.3.8 Discussion

Results with sandwiched specimens will be reported at a later date. For the laminated samples, residual stresses from molding combined with the thermal mismatch between EMC and either Si or the copper alloy strip imparted curvature to most laminated specimens. The curvature ranged from 0.5 up to 1 mm. Subsequent tests on both concave downward and upward conditions showed significant difference in the measured P_{cr} . For B17/C-7025, for instance, critical load values are listed and shown in *Table 4-4*. Results indicated the following:

- The pre-crack lengths in the laminated beams did not show significant difference in the measured P_{cr} values.
- Temperature contributed a major factor to the adhesion strength, as indicated in *Figures 4-6 and 4-7*.
- Moisture also had a strong effect on the shear strength of the material, as demonstrated in *Figures 4-8 and 4-9* for the sandwiched configuration.
- In the shear test, almost all the EMC/Si specimens fractured at the interfacial material, i.e., silicon layer, whereas "clean" surfaces were observed for the EMC/Cu samples. For example, *Figure 4-14* illustrates the two halves of the fractured Si sample.
- A conservation integral for interface cracks under hygro thermal stresses has been derived to separate stress intensity factors for different fracture modes. All the measured P_{cr} values with moisture contents at various temperatures were used as inputs for assessing the K_{IC} opening mode fracture strength and K_{IIC} for the shear fracture strength of the laminated beams. The present model can account for the differences between concave-up and concave-down specimens.
- For all the material interfaces, the Mode II fracture toughness, K_{II}^C , is much higher than the Mode I fracture toughness, K_I^C .

TABLE 4-4: Critical loads, P_{cr} , for the three-point bending tests of the composite beams.

Geometry	T (°C)	Pre-crack (cm)	P_{cr} (lb)
Down	22	1	32
	100	1	21
Up	22	1	42
	100	1	41
Down	22	2	32
	100	2	21
Up	22	2	43
	100	2	40

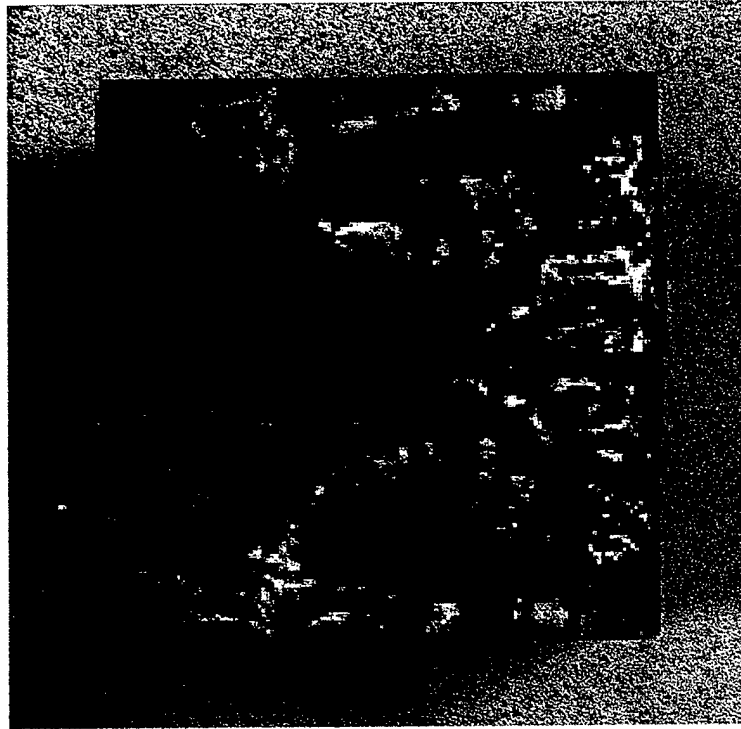


Fig 4-14 Fracture surface within the silicon layer for sandwiched blocks of EMC/Si.

4.4 CONCLUSIONS

The interfacial strength of different material combinations (3 molding compounds and 3 substrates), pre-crack lengths (1 and 2 cm), die coating conditions (with and without polyimide stress buffer coating), preconditioning (3 moisture levels), and test configuration (concave-up and concave-down) have been tested at 3 different temperatures. A conservation integral was derived based on the data collected to predict the mixed-mode fracture toughness. The data indicated typically higher K_{II}^C than K_I^C , with both values decreasing rapidly as the temperature rises. The data also revealed rather weak EMC/Si interfaces compared to the EMC/Cu counterparts.

The database collected will become part of the EPACK software to help the prospective package designer with more *a priori* design and evaluation.

5 Desorption and Absorption Diffusivity of Mold Compounds

5.1 Objective

Determine the desorption and absorption diffusivities for four epoxy mold compounds at different temperature and relative humidity (T/RH) conditions.

5.2 Introduction

The epoxy mold compounds utilized in the microelectronic packaging industry are susceptible to ingress of moisture from the ambient surroundings. The moisture absorbed by the epoxy can cause warping and delamination of the package structure and can lead to "popcorning" of the package upon reflow.

To assist in the design of packages, modeling software is being developed which will factor in the absorption of moisture in order to predict the occurrence of "popcorning". Determining the diffusion rates for the mold compounds of interest is therefore a necessary step in the development of the software.

5.3 Procedure

The test specimens used in the desorption test were baked at 125°C for 24 hours to drive out any moisture they may have absorbed. They were then weighed and placed in an 85°C/85% chamber to absorb moisture. The weight gain of the specimens was monitored until all of the specimens reached approximately 0.4% weight gain. This value was selected as each of the mold compounds could attain this level and it was close to saturation. Once the specimens had absorbed 0.4% moisture, they were separated into five (5) groups and placed in ovens at 100°C, 125°C, 150°C, and 175°C. The fifth group was left in ambient conditions ($T = \sim 23^{\circ}\text{C}$ and $\text{RH} = \sim 35\%$). The weight of each specimen was taken at various times during the desorption process to monitor the weight loss.

The same specimens used in the desorption test were then used in the absorption test. The specimens were first baked at 125°C for 24 hours to drive out any remaining moisture. The specimens were weighed to obtain their "dry"

weight and separated into four (4) groups. The T/RH conditions used were 30°C/60%, 85°C/60%, 85°C/85%, and room temperature water, $T = \sim 23^{\circ}\text{C}$. The specimens were weighed at various times during the absorption process to monitor the weight gain.

5.4 Test Specimens

Epoxy Mold Compounds :	B8	Plaskon 7115
	B17	Sumitomo 6700
	B21	Plaskon PPF165A
	B24	Sumitomo 6300H
Geometry :	Rectangular bar (semi-infinite solid)	
	Length	: 4.973 in
	Width	: 0.497 in
	Thickness	: 0.125 in

5.5 Calculation of Diffusivity

Most practical diffusion situations can be categorized as nonsteady-state; the diffusion flux and the concentration gradient at some particular point in a solid vary with time. In order to solve diffusion problems of this nature, the partial differential equation known as Fick's second law is used (Equation 5-1).

$$\frac{\partial C}{\partial t} = \frac{\partial}{\partial x} \left(D \frac{\partial C}{\partial x} \right) \quad (5-1)$$

If the diffusion coefficient, D , is assumed to be constant, then Equation (5-1) can be simplified to

$$\frac{\partial C}{\partial t} = D \frac{\partial^2 C}{\partial x^2} \quad (5-2)$$

The geometry of the test specimens was such that they could be treated as semi-infinite solids, where the length is much greater than the diffusion distance, $L \gg Dt$. The following assumptions are made for this case:

1. the solids are uniformly distributed with concentration C_0 .
2. the diffusion process begins at time zero ($t = 0$).
3. solid thickness is zero at surface and increases with distance into the solid.

The corresponding boundary conditions for the diffusion process are:

$$\text{For } t = 0 \quad C = C_0 \text{ at } 0 \leq x \leq \infty$$

$$\begin{aligned} \text{For } t > 0 \quad C &= C_s \text{ at } x=0 \text{ (constant surface concentration)} \\ C &= C_0 \text{ at } x=\infty \end{aligned}$$

Application of these boundary conditions to Equation (5-2) yields the following solution,

$$\frac{C_x - C_0}{C_s - C_0} = 1 - \operatorname{erf}\left(\frac{x}{2\sqrt{Dt}}\right) \quad (5-3)$$

where *erf* is the error function.

Following the 24 hour bake at 125°C , the moisture concentration $C_0 = C_s = 0$, and after the T/RH conditioning, the left hand side of Equation (5-3) becomes

$$\frac{C_x - C_0}{C_s - C_0} = C_x$$

From this the diffusivity can be calculated using Equation (4),

$$D = \frac{x^2}{4(z)^2(t)^2} \left[\frac{\text{cm}^2}{\text{sec}} \right] \quad (5-4)$$

where z is the tabulated error function value.

5.6 Results and Discussion

The weight loss/gain data were plotted against the square root of time (hours^{1/2}). The plots and data are included in Appendix III. The amount of diffusing substance entering/leaving the specimen per unit area of its surface varies as the square root of time. Therefore, plotting the percent weight loss/gain vs. time^{1/2} yields a curve which is linear throughout much of the diffusion process. The slope of the linear portion is related to the diffusion coefficient, D.

The desorption data shows a very large temperature dependence in diffusivity for each of the compounds. The room temperature diffusivity at 24 hours was on the order of 3.4E-8cm²/s while at 175°C the value was on the order of 7.3E-8cm²/s. The diffusivity more than doubled at the higher temperature. B8 and B21 tend to desorb slower than B17 and B24 initially, however they are able to desorb more moisture over time. After only 2 days of desorption, B8 and B21 had desorbed more than B17 and B24 for T > 125°C and by day 3 for T > 100°C. The absorption plots show that B17 and B24 tend to absorb moisture more rapidly than B8 and B21 at a given T/H condition. However, for both the 85°C/60% and 85°C/85% conditions the saturation level is higher for B8 and B21. It took approximately 6 days at the higher temperature and humidity for B8 and B21 to absorb more than B17 and B24. At the lower T/RH conditions B8 and B21 remained slightly behind B17 and B24.

B17 and B24 tend to 'react' quicker than B8 and B21, meaning that they initially desorb and absorb moisture faster. B8 and B21, on the other hand, tend to reach a higher saturation level and a lower 'dry' level. The reason for this can not be determined from the present experiment. Techniques such as Nuclear Magnetic Resonance would probably need to be utilized to better understand the mechanisms for desorption and absorption.

The diffusion coefficient was calculated for each epoxy molding compound at various times. Tables 1 and 2 show the calculated values of D for each of the epoxy molding compounds at the various T/RH conditions, at two time durations for desorption and absorption, respectively.

Table 5-1. Diffusion Coefficient (D cm²/s) for Desorption.

EMC	Time	22°C	100°C	125°C	150°C	175°C
B8	4 Hr	2.32E-7	3.43E-7	3.76E-7	4.01E-7	4.22E-7
	24 Hr	3.68E-8	6.63E-8	7.11E-8	7.33E-8	7.36E-8
B17	4 Hr	2.26E-7	3.55E-7	3.85E-7	4.09E-7	4.30E-7
	24 Hr	3.05E-8	6.74E-8	7.05E-8	7.17E-8	7.29E-8
B21	4 Hr	2.23E-7	3.38E-7	3.70E-7	3.96E-7	4.26E-7
	24 Hr	3.30E-8	6.51E-8	7.03E-8	7.33E-8	7.48E-8
B24	4 Hr	2.28E-7	3.48E-7	3.84E-7	4.06E-7	4.29E-7
	24 Hr	3.53E-8	6.73E-8	7.15E-8	7.25E-8	7.26E-8

Table 5-2. Diffusion Coefficient (D cm²/s) for Absorption.

EMC	Time	30°C/60%	85°C/60%	85°C/85%	RT/H2O
B8	4 Hr	2.70E-7	2.94E-7	3.20E-7	2.65E-7
	24 Hr	5.13E-8	5.74E-8	6.30E-8	5.09E-8
B17	4 Hr	2.71E-7	3.09E-7	3.33E-7	2.73E-7
	24 Hr	5.22E-8	5.93E-8	6.51E-8	5.22E-8
B21	4 Hr	2.60E-7	2.90E-7	3.14E-7	2.76E-7
	24 Hr	4.97E-8	5.66E-8	6.21E-8	5.06E-8
B24	4 Hr	2.65E-7	3.06E-7	3.32E-7	2.73E-7
	24 Hr	5.14E-8	5.91E-8	6.51E-8	5.15E-8

For the desorption test, the values were calculated using the average weight loss of two (2) specimens for a given mold compound. The absorption data are based on the weight gain of two (2) specimens which were weighed at alternating intervals. Therefore, only one bar was weighed per mold compound at any given time interval. The small sample size is due in part to the time it takes to weigh the bars and to help minimize the amount of time desorption/absorption was taking place outside the desired environment.

Appendix III contains two tables which compare the current findings to a previous study of the same mold compounds. The desorption diffusivity value at 22C and the absorption diffusivity value at 30C/60% show a fairly large percent difference between the two studies. The desorption diffusivity at 22C in the previous study averaged 22% higher than in the current study. The absorption diffusivity at 30C/60% in the previous study averaged 15% lower than in the current study. The largest percent difference in the remaining categories was only 8% and the average percent difference of these categories was 3%. The average percent difference for all of the categories was 6%. Overall, the data are fairly consistent between the two studies and the discrepancy seen for two of the categories can not be explained at this time.

The T/RH chamber used for the 85°C/85% conditioning failed during the testing and therefore the test had to be restarted for these specimens. The data are not as complete for this condition due to this equipment failure.

5.7 Conclusion

The concentration and temperature dependence of the diffusivity is evident based on the data. Further, the diffusivity varies with time. The diffusivity values calculated for the four epoxy mold compounds fall within a relatively narrow range for a given T/RH condition. The variation of the diffusivity over time covers a much larger range. The values are still within the expected order of magnitude of $10^{-8} \text{ cm}^2/\text{s}$.

6 *The Effect of Reflow Ramp Rate on Popcorning*

6.1 Objective

The effect of the temperature ramp rate during IR reflow was studied using a TQFP-48 lead package. The correlation between ramp rate and popcorning was studied by reflowing parts at three ramp rates for two peak temperatures. Scanning acoustic microscope (C-SAM) images were taken prior to and after IR reflow to monitor the effects of the reflow process. In addition, the parts were weighed after each of the three IR reflow passes to monitor the weight loss per pass.

6.2 Package Specifications

Package	TQFP-48
Mold compound	7320CR
Die attach	Ablestik 84-1
Die size	151x129 mil
DAP size	197x197 mil
Body Size	7x7x1.4 mm
Assembly site	ANAM

6.3 Procedure

The TQFP-48 parts were baked at 125C for 24 hours to drive out any moisture they had absorbed. The parts were then scanned to obtain 0 hour images of the parts. The parts were separated into eight groups and placed in T/RH chambers for various levels of preconditioning (Table 6-1).

Table 6-1. Preconditioning levels

T / RH	Duration (days)	Comments
30C / 60%	4, 7, 10, 14, 18, 21	
85C / 60%	7	JEDEC level 2
85C / 85%	7	JEDEC level 1

After preconditioning, the parts in each group were put into subgroups of four parts total and reflowed using one of six reflow profiles.

Six profiles were developed on the Vitronic IR reflow oven, three for each of the peak temperatures used. Vapor phase reflow was not performed in this study. The peak temperatures were 220C and 240C. Low, medium, and high ramp rates were obtained for both peak temperatures (see Appendix IV for profiles). The ramp rate ranged from 0.6 C/sec to 1.0 C/sec for the 220C reflow and from 0.8 C/sec to 1.6 C/sec for the 240C reflow. Each subgroup passed through the IR oven three times and the parts were weighed after each pass. The parts were scanned after the reflow process to check for the presence of delamination and/or cracking.

6.4 Discussion

The profiles created for the ramp rate test followed JEDEC standards as closely as possible for IR reflow of plastic packages. In order to meet the JEDEC standard, the portion of the reflow profile which could be varied was a relatively narrow section between 183C and the peak temperature. This made it difficult to create profiles with ramp rates that varied by more than 1.0 C/sec between the low and high ramp rates. This was largely do to the number of heating/cooling zones available on the Vitronic IR oven.

The C-SAM images of the reflowed parts were compared to the 0 hour images to determine the effects of the reflow process (see Appendix IV). Scans of the top and bottom side of the parts were made so the various interfaces could be seen. The parts showed no signs of delamination or cracks in the 0 hour scans. The condition of the parts after reflow is listed in Table 6-2. Delamination of the DAP was seen in almost every part tested and therefore the bottom scan was used to discern the effect of ramp rate.

Table 6-2. Results of post reflow C-SAM images. T = top B = bottom.

Precon. days/T/RH	Low / 220C	Med / 220C	Hi / 220C	Low / 240C	Med / 240C	Hi / 240C
4 / 30 / 60	T : clean B : clean	T : clean B : clean	T : clean B : clean	T : DAP B : clean	T : DAP B : clean	T : DAP B : clean
7 / 30 / 60	T : DAP B : clean	T : clean B : clean	T : clean B : clean	T : DAP B : clean	T : DAP B : clean	T : DAP B : clean
10 / 30 / 60	T : DAP B : clean	T : clean B : clean	T : 2/4 DAP B : clean	T : DAP B : leads	T : DAP B : leads	T : DAP B : leads
14 / 30 / 60	T : DAP B : clean	T : DAP B : clean	T : DAP B : clean	T : DAP B : leads	T : DAP B : leads	T : DAP B : leads
18 / 30 / 60	T : DAP B : clean	T : DAP B : clean	T : DAP B : leads	T : DAP B : leads	T : DAP B : leads	T : DAP B : leads
21 / 30 / 60	T : DAP B : leads	T : DAP B : clean	T : DAP B : leads	T : DAP B : leads	T : DAP B : leads	T : DAP B : leads
7 / 85 / 60	T : DAP B : leads	T : DAP B : leads	T : DAP B : leads	T : DAP B : leads	T : DAP B : leads	T : DAP B : leads
7 / 85 / 85	T : DAP B : cracks	T : DAP B : cracks	T : DAP B : cracks	T : DAP B : cracks	T : DAP B : cracks	T : DAP B : cracks

The parts soaked for 7 days or less at 30/60 showed no delamination of the leads or cracking, whereas all of the 7/85/60 parts showed delamination at the leads and all of the 7/85/85 parts had cracks. For the other subgroups, there is some variation in the results for the 220C peak temperature test that correlates with the ramp rate variation. There tends to be delamination at the leads at lower precon levels as the ramp rate increases. The results from the 240C peak temperature test show no ramp rate effect. All three ramp rates resulted in the same damage to the parts. The higher peak temperature seems to be the major factor in the damage seen in the parts.

The subgroups were weighed after each pass through the IR oven in order to monitor the loss of moisture throughout the reflow process. Appendix IV contains a table of the weight loss data. The average weight gain values show a greater variation within the same preconditioning level than expected. Further, the weight gain of the parts in the 30/60 chamber does not directly follow the increase in soak duration. Whether this is a result of a variation in the packages themselves, a spatial variation in T/RH in the chamber, or a variation in the weighing process is unknown.

The parts absorbed between 0.08 - 0.21% moisture. The total percent weight lost during the three passes was generally within 0.02 of the percent weight increase. On average the parts lost 71% of the total weight loss during the first reflow pass. Pass two drove off 22.5% and pass three drove off 6.5%. The

maximum amount lost in pass one was 92% and the minimum amount lost in pass one was 34%. The 92% value was for parts soaked at 7/30/60 and using the 220C, low ramp rate profile. The 34% value was for parts soaked at 7/85/60 and using the 240C, high ramp rate profile. There is not a clear trend in the weight loss data corresponding to ramp rate or peak temperature.

Correlating the moisture content to the damage seen in the C-SAM images is also difficult. All of the packages which cracked had absorbed more than 0.18% moisture. The delamination of the leads however does not show a similar cut-off value. One subgroup which had absorbed 0.13% showed no signs of delamination at the leads while another subgroup that was reflowed using the same profile showed delamination with 0.11% moisture absorption. The spread of the absorption data is relatively narrow and this makes it difficult to discern any cut-off values for delamination.

6.5 Conclusion

The effect of temperature ramp rate on the popcorning of the TQFP-48 package seems to be of a lesser importance than the maximum temperature. The packages reflowed at the 220C peak temperature showed a possible correlation between delamination of the leads and ramp rate; faster ramp rates resulted in damage at lower preconditioning levels. The parts reflowed at the 240C peak temperature showed the same degree of damage for each of the ramp rates. The effect of peak temperature seems to have been greater than the effect of ramp rate at this temperature.

All parts which lost more than 0.18% moisture during the IR reflow process showed evidence of cracking in the C-SAM images. These parts had all been subjected to level 1 preconditioning. The parts subjected to level 2 preconditioning all showed delamination at the leads but no cracking. More parts would have to be tested before this package could be considered a level 2 package.

The weight loss data shows that the parts lose approximately the same amount of moisture as they had absorbed prior to reflow. The largest part of this loss occurs during the first pass through the IR oven. In the future, it might be useful to scan parts that have been reflowed once, twice, and three times to study when the damage occurs.

7 GaAs Package Thermal Shock and Thermal Cycling Experiment

7.1 Overview

Five sets of GaAs packages were subjected to thermal cycling and thermal shock testing. The thermal effects on the packages, both encapsulated and unencapsulated, were examined using a scanning acoustic microscope (C-SAM). The packages were scanned before and after each interval of the thermal conditioning tests.

7.2 Package Description

No part specifications were provided. The parts received were the following:

<u>Type</u>	<u>Qty</u>	<u>Description</u>
A	35	Encapsulated with a die.
B	30	Encapsulated with a die and heat spreader.
C	40	Die attached to leadframe without encapsulation.
D	40	Heat spreader attached to leadframe without encapsulation.
E	40	Die and heat spreader attached to a leadframe without encapsulation.

7.3 Equipment

- SonoScan 3000DX Scanning Acoustic Tomograph
30Mhz transducer for type A and B
100Mhz transducer for type C, D and E
- Moisture chambers for pre-conditioning (Quanta Labs)
- Thermonics T-2500 thermal chambers (Quanta Labs)

7.3.1 Scanning Procedure

All parts were scanned when they were received to assess the 0-hour integrity of the parts. Delamination, cracking, and voiding were checked for where applicable and noted. The parts were scanned at high resolution (256x240) and depending on the part type either the 30Mhz or 100Mhz transducer was used. The C-SAM was not able to adequately penetrate objects such as heat spreaders and because of this not all parts could be effectively scanned from both the top and bottom side.

Type A and B were scanned on the top and bottom side using the 30Mhz transducer. Type C was scanned on the bottom side using the 100Mhz transducer. Type D and E were scanned on the topside using the 100Mhz transducer.

7.3.2 Preconditioning

All parts were weighed as received and then baked at 100C for 8 hours. They were weighed after the bake and then subjected to various levels of preconditioning. The pre-conditioning levels were the following:

<u>Precondition</u>	<u>Temperature/Humidity</u>	<u>Duration</u>
C1	none	none
C3	30C/80%RH	168hrs
C4	30C/80%RH	480hrs

After preconditioning, the parts were weighed and then subjected to the thermal shock and thermal cycling tests.

7.3.3 Thermal Shock Procedure

A total of seven thermal shock conditions were used. Part types A (#21 - 35), B (#16 - 30), and E (#16 - 30) were subjected to the thermal shock testing. The minimum temperature for all of the tests was -55C. The maximum temperatures were -20C, 10C, 40C, 70C, 100C, 130C, and 160C. The parts were scanned after each phase of the thermal shock test to monitor the package integrity and then returned to Quanta for the next phase. The thermal shock profiles are shown in Appendix V.

7.3.4 Thermal Cycling Procedure

The parts underwent a total of 1000 thermal cycles. Part types A (#1 - 20), B (#1 - 15), C (#1 - 15), D (#1 - 15), and E (#1 - 15) were subjected to thermal cycle testing. The parts were cycled between -55C and 195C and removed from the chamber for weighing and scanning at 5, 10, 50, 100, 200, 300,...1000 cycles. After the parts were scanned, they were returned to Quanta to continue the testing. An example of the thermal cycle profile is shown in Appendix V.

7.4 Discussion

The thermal effects associated with the thermal shock and thermal cycling tests were difficult to monitor due to the structure of the parts and limitations of the C-SAM. The small sample size also made it difficult to draw conclusions based on this set of data alone. This played a large role in the thermal shock test where 'virgin' parts were only used for the first phase of the test.

Of the five part types only types A and B, the encapsulated parts, yielded scan images which could be interpreted well and where delamination could be monitored. Further, some of the parts failed completely during the testing (heat spreaders separated from the leadframe) and thus further testing of those parts yielded little to no information. Prior to pre-conditioning, minor delamination was present in 8 of the 35 type A parts and in 16 of the 30 type B parts. All of the type C and E parts showed delamination at the DAP. Some of the type E parts showed major delamination at the DAP. All of the type D parts showed signs of delamination between the heat spreader and leadframe. The 0-hour C-SAM images of all the parts are in Appendix V.

The thermal shock testing was performed with part types A (#21 - 35), B (#16 - 30), and E (#16 - 30). The following tables summarize the damage observed after four of the thermal shock test steps for type A and B. Three categories (minor, moderate, and severe) were used to describe the delamination as seen by scanning the parts with the C-SAM.

Type A:

Precon	-20C	10C	100C	160C
C1	t: moderate b: none	t: minor b: none	t: moderate b: none	t: moderate b: none
C3	t: minor b: none	t: minor b: none	t: minor b: none	t: moderate b: none
C4	t: minor b: none	t: none b: none	t: minor b: none	t: minor b: none

Type B:

Precon	-20C	10C	100C	160C
C1	t: moderate b: moderate	t: moderate b: minor	t: minor b: minor	t: severe b: moderate
C3	t: minor b: minor	t: minor b: minor	t: minor b: minor	t: moderate b: minor
C4	t: severe b: moderate	t: moderate b: minor	t: moderate b: minor	t: severe b: moderate

The C-SAM images of the type E parts were difficult to interpret because of the structure of the parts. The 0-hour images showed minor to severe delamination for many of the parts and after the thermal shock testing the parts tended to have more delamination.

The C-SAM images of the thermal shock parts after the initial thermal shock (-55C to -20C) are in Appendix V. As this was the only phase where virgin parts were tested, these images best show the effect of the thermal shock test. The type A and B parts all showed increased delamination around the die after thermal shock testing. The effect of preconditioning on the parts seems to be minor. Parts that weren't preconditioned showed the same or more delamination than the parts that had been preconditioned. While these data alone can't be used to state that the parts aren't sensitive to moisture, they do suggest that this may be the case. A simple moisture sensitivity test could be conducted to make this determination.

For all three of the part types tested, there were phases of the test where the parts showed less delamination than they had after the previous test. This is reflected in the tables above. The C-SAM images were made using the same settings for a given part type, therefore the reason for this fluctuation between the different test phases is unknown. It seems unlikely that the parts "healed" during phases of the test, yet the images alone would suggest something of this nature. The thermal cycle testing was performed on all of the part types. Again, type A (#1 – 5, 11-20) and B (#1 - 15) allowed for tracking of the delamination process, while images of the other parts proved harder to interpret. Figures 7-1 and 7-2 show the top and bottom images for the type A (#16 - 20) and B (#11 - 15) parts at 5, 500, and 1000 cycles with preconditioning level 4.

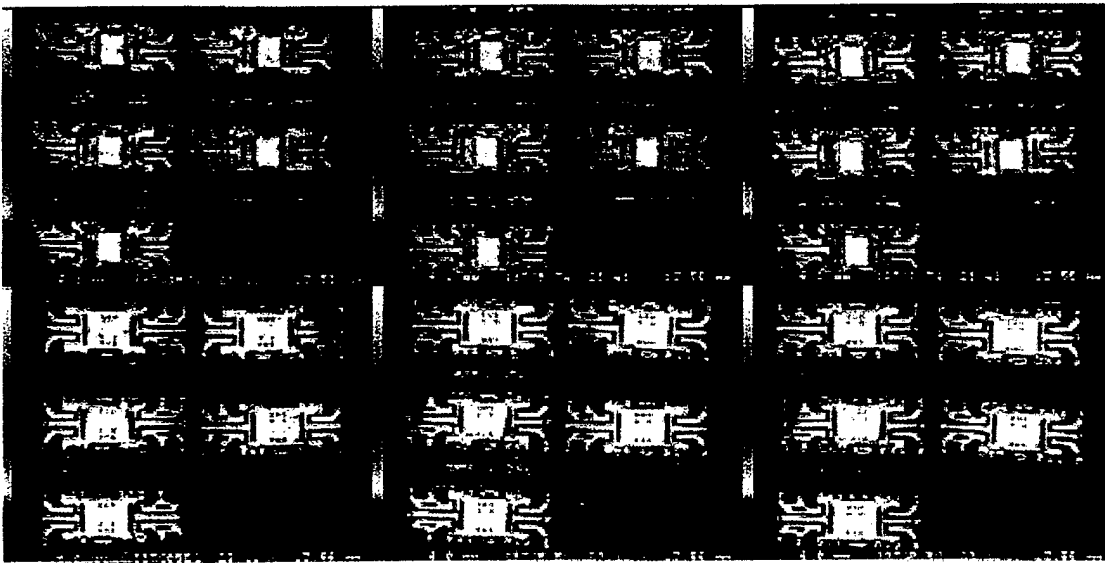


Figure 7-1 : Top and bottom C-SAM Images at 5, 500, and 1000 cycles for part type A.

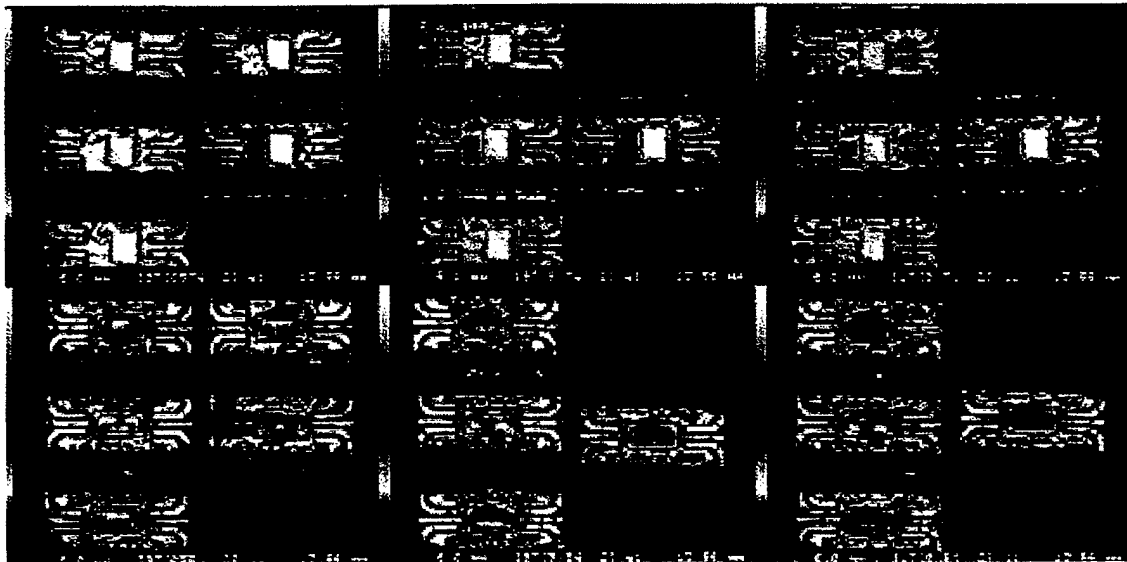


Figure 7-2 : Top and bottom C-SAM Images at 5, 500, and 1000 cycles for part type B.

The progressive increase in delamination of the DAP and the leads can readily be seen in this figure and is typical for the type A and B parts. After only five thermal cycles the parts show moderate amounts of delamination. The pre-conditioning level has a slight influence on the delamination seen after five cycles. The parts preconditioned at level 4 showed more delamination than the C1 or C3 parts. The type B parts tend to show this more than the type A parts.

The images for part types C (#1 - 15), D (#1 - 15), and E (#1 - 15) were more difficult to interpret due to the structure of the parts. However, a general increase of delamination could be seen in these parts. Figures 7-3, 7-4, and 7-5 show the C-SAM images after 5, 500 and 1000 cycles at preconditioning level C4 (#11 - 15) for part types C, D, and E respectively.

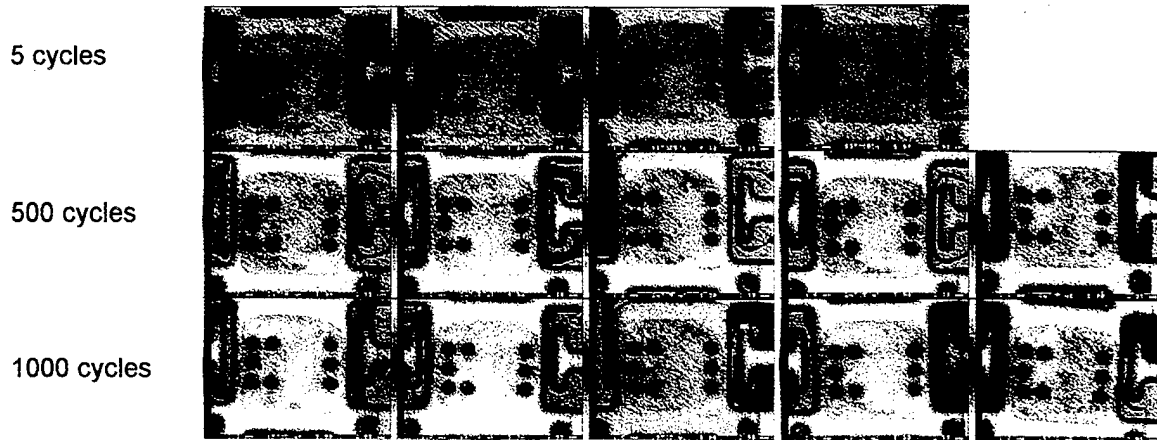


Figure 7-3 : Thermal cycle C-SAM images for part type C (precon 4).

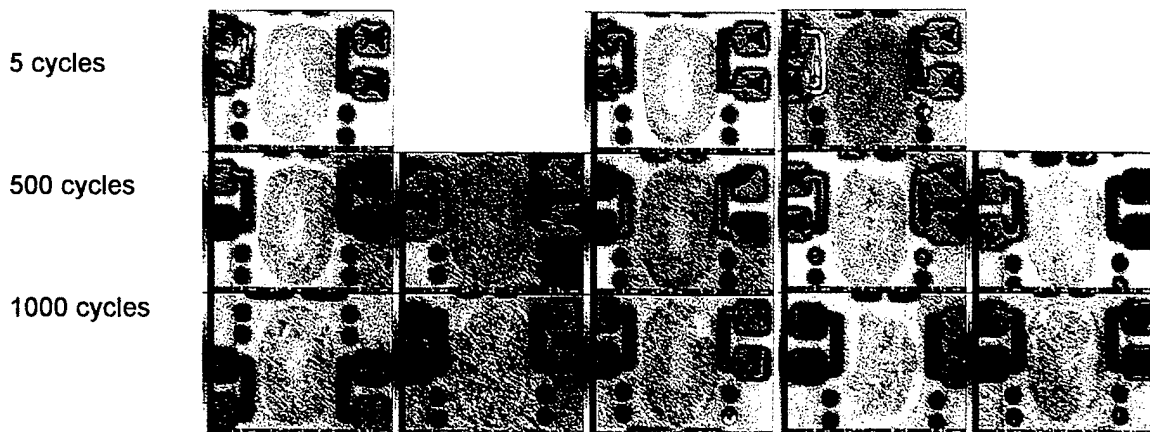


Figure 7-4 : Thermal cycle C-SAM images for part type D (precon 4).

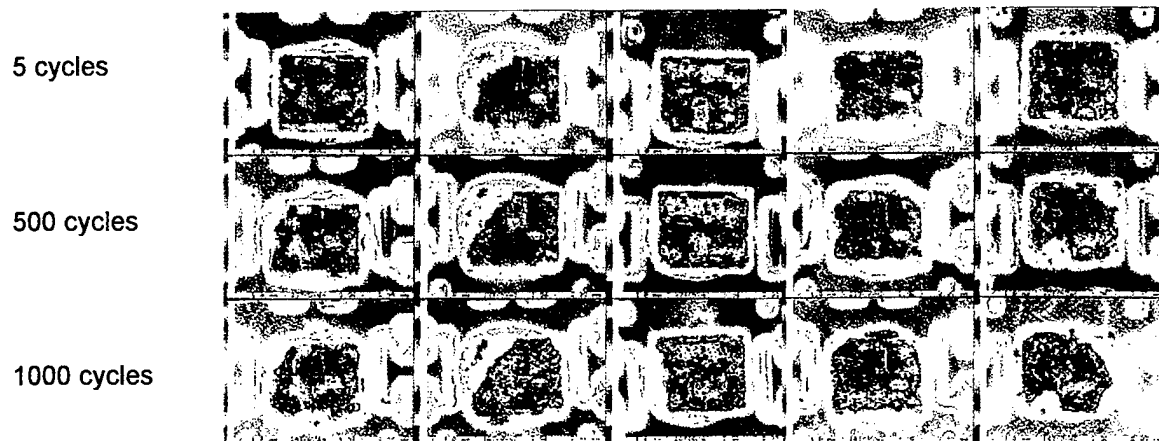


Figure 7-5 : Thermal cycle C-SAM images for part type E (precon 4).

Delamination can be seen around the corners of the die in part type C (the lighter regions), towards the center of the heat spreader in type D (the lighter regions), and across the whole DAP in type E (the yellow and red regions). Preconditioning only seemed to have a slight role in the delamination of these parts, with slightly more delamination seen earlier in the C4 parts than in the C1 parts. The C-SAM images for these parts are in Appendix V.

7.5 Conclusion

The effects of thermal shock and thermal cycling were difficult to monitor for the majority of the GaAs parts subjected to testing. Only two of the five part types were encapsulated, the remainder being bare leadframes with die and/or heat spreaders attached to them. The encapsulated parts, type A and B, showed only a slight effect of preconditioning, with greater delamination seen in the parts preconditioned at level 4 than the non-preconditioned, level 1, parts. Part types C, D, and E seemed to show a similar trend, however the C-SAM images were difficult to interpret due to the heat spreader and die which limited the ability of the C-SAM to scan the interfaces. The limited number of parts available also makes it difficult to draw any substantial conclusions from these tests and in particular for the thermal shock test.

The usefulness of the thermal shock testing was reduced due to the limited number of parts. Virgin parts were only used in the initial phase of the testing (-55C to -20C) and subsequent phases used the parts that had already gone through one or more thermal shock tests. For this reason, only the first phase of the test yielded information that could be interpreted well. Part types A, B, and E all showed an increase in delamination after the initial thermal shock test. The

increase in delamination varied from minor to severe with preconditioning having little to no effect on the results. For type A and B, the delamination was seen around the DAP and only very little on the leads. The delamination fluctuated during the subsequent phases, sometimes increasing and other time decreasing. The reason for this is unknown and based only on the images it would appear that the parts were "healing" during some phases of the test. This is an unlikely possibility due to the nature of epoxy mold compounds in general.

The thermal cycle testing yielded C-SAM images which were more readily interpreted. The delamination seen in all of the part types increased as the testing proceeded and the preconditioning level seemed to affect the amount of delamination seen after the first 5 cycles. The parts preconditioned at C4 tended to show more delamination than the C3 and C1 parts. After only 5 cycles, the type A and B parts showed moderate amounts of delamination and after 500 cycles delamination around the leads and DAP were severe. The type C parts showed an increase in delamination around the corners of the die over the course of the test, yet even after 1000 cycles the delamination was relatively minor. The type D parts showed an increase in delamination under the center of the heat spreader and the heat spreader separated from some parts. With the exception of the parts which separated, the type D parts showed only minor to moderate delamination after 1000 cycles. The images from the type E parts were the most difficult to interpret. The 0 hour images showed minor to severe delamination at the DAP for most of the parts. Subsequent testing tended to increase the amount of delamination seen in the images.

The GaAs parts responded to the thermal shock and thermal cycle testing in a fairly predictable manner. Preconditioning played less of a role than may have initially been thought, although the parts did tend to show increased delamination with increasing preconditioning time. More parts would need to be obtained to draw any conclusions from the thermal shock testing. Virgin parts should be used for each phase of the test.

8 *Popcorning Evaluation of Plastic Packages*

8.1 *Objective*

Conduct popcornning analysis of plastic packages to determine moisture sensitivity level. The main purpose of these popcornning tests is to provide experimental calibration of the resulting EPACK software. Out of thousands of packages tested, only the popcornning test results of PBGA packages are described in this Chapter, while the popcornning test results for other package types (PLCC, QFP, and SO) are contained in a proprietary internal report of Optimal Corporation. The popcornning test procedures described in this Chapter for PBGA packages are similar to those used to test the other packages types.

8.2 *Part Descriptions*

Package	PBGA-388	PBGA-388	PBGA-256
Qty	60	60	60
Device	Dummy die	Dummy die	Dummy die
Mold compound	Nitto HC-100-X2	Nitto HC-100-X2	Nitto HC-100-X2
Die attach material	Ablestik 8360	Ablestik 8360	Ablestik 8360
Die dim.	285x285 mil	445x445 mil	375x375mil
PAD dims.			
Substrate supplier	ACL	ACL	
Substrate material	BT – Bismalimide Trizene	BT – Bismalimide Trizene	
Solder mask	Taiyo PSR-4000- AUS5	Taiyo PSR-4000- AUS5	
Body size	27x27x1.0mm	27x27x1.0mm	
Assembly site	NSSC	NSSC	NSSG

8.3 Procedure

The PBGA packages were scanned using the Sonoscan C-SAM to check the integrity of the packages at hour 0. After scanning, the parts were placed in an oven at 125C for 24 hours to bake out any absorbed moisture. The parts were weighed after the 24-hour bake and then placed in T/RH chambers for preconditioning. The parts were preconditioned according to JEDEC specifications for moisture sensitivity. A manufacturer's exposure time (MET), the time between bake and bag plus the maximum amount of time allowed out of the bag at the distribution facility, of 0 hours was used for these parts. The MET value is added to the base JEDEC preconditioning duration to get the total soak time for levels 3 - 6. National Semiconductor considers PBGA to be moisture sensitive packages and the time between bag and bake is kept as low as possible (< 8 hours) at the assembly sites. The preconditioning levels used in this study are listed in Table 8-1.

Table 8-1. Preconditioning levels and soak times.

Level	T (C) / RH (%)	Duration (days)
1	85 / 85	7
2	85 / 60	7
3	30 / 60	7
4	30 / 60	3
5	30 / 60	1

After preconditioning, the parts were weighed and then reflowed in a Vitronic IR reflow oven using a temperature profile that was in accordance with JEDEC specifications. The profile is shown in Section 8.5. The parts were passed through the oven three times and then scanned to assess the effects of the preconditioning and reflow process.

8.4 Discussion

Only the PBGA-388 packages were tested, as molding of the 256-lead package in Singapore was delayed. The completion of the molding of the PBGA-388 lead packages also took substantially longer than expected, as poor adhesion between the mold compound and substrate was found for the first set of parts. Delamination at the die/DAP interface was also apparent. The ESEC automatic

die attach machine was used for die attach. Figure 8-1 shows the C-SAM image of one of these PBGA packages.

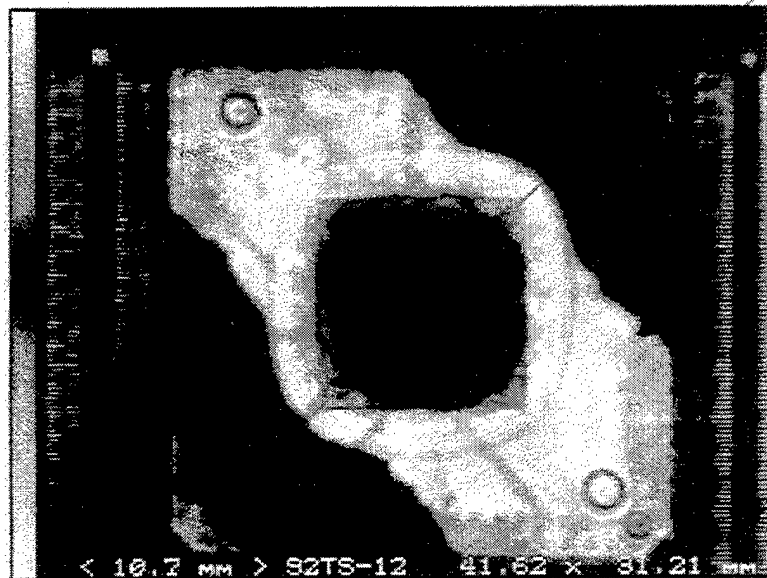


Figure 8-1. C-SAM image showing poor adhesion and delamination at the die/DAP interface.

This part was cross-sectioned to verify the delamination seen in the C-SAM images. The cross-section was made along the body diagonal, from the lower left corner to the upper right corner. Micrographs of the cross-sectioned sample are in Section 8.6. The micrographs showed that the die was almost completely delaminated from the DAP.

Initially it was believed that the poor adhesion was the result of using EMC B24 which is not the compound used in production. The EMC was switched to the production Nitto compound, yet the adhesion problem still existed. It was learned that the substrates used for these packages were prototype substrates that differed from production substrates in the way they were cleaned prior to shipping. Plasma cleaning of the substrates after the die attach process was then performed to see if this improved the adhesion. The substrates that were plasma cleaned prior to molding yielded parts that showed good adhesion between the EMC and substrate. The numerous iterations made before producing adequate packages reduced the overall number of parts tested from 120 per package type to 50. The 0-hour C-SAM images of the parts showed no signs of delamination between the EMC and substrate. Voids were present in a small number of packages, but they were relatively minor. The die/DAP interface had minor delamination for the majority of the parts. Section 8.7 has examples of the 0-hour C-SAM images. The PBGA-388 packages (both die sizes) passed the JEDEC level 3 conditions of 7 days at 30C and 60% RH. The parts that were preconditioned at levels 1 and 2 showed severe delamination for

all parts. Figures 8-2 and 8-3 are typical C-SAM images for parts tested at level 3 and level 2, respectively.

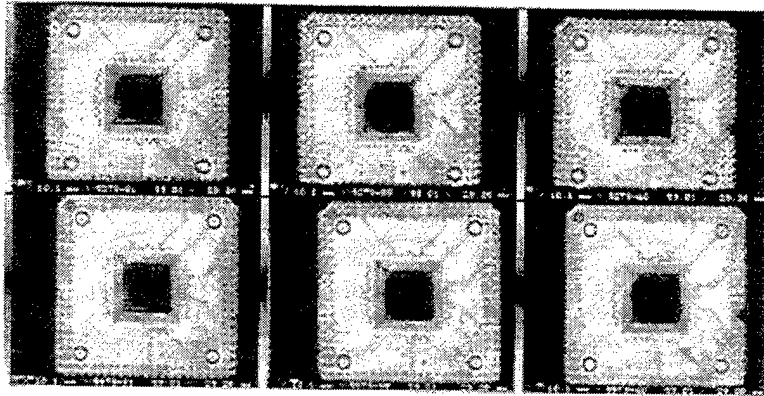


Figure 8-2. C-SAM image of parts tested at JEDEC level 3 conditions.

Top = 0-hour Bottom = after IR reflow

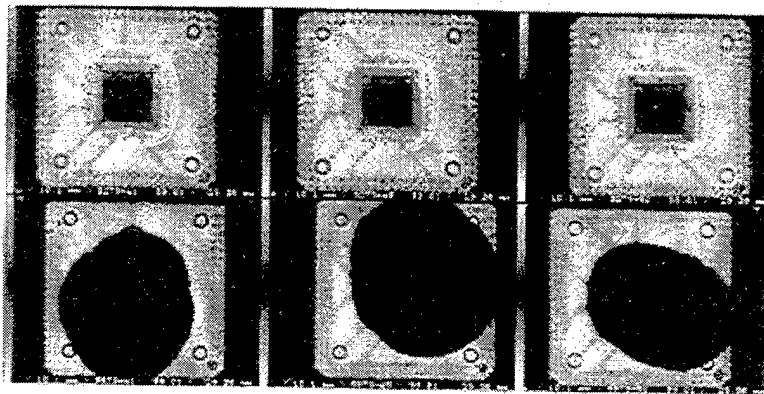


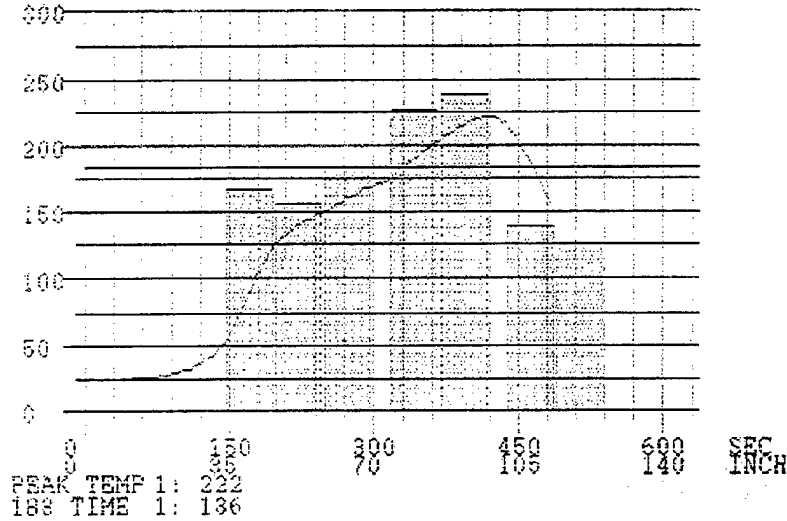
Figure 8-3. C-SAM image of parts tested at JEDEC level 2 conditions.

Top = 0-hour Bottom = after IR reflow

The delamination of the level 1 and 2 parts was often severe enough that the eye could see the separation between the EMC and substrate. On average, the parts preconditioned at level 3 had a weight gain of 0.18 % after preconditioning. The level 1 and 2 parts had weight gains of 0.44 % and 0.27 %, respectively. A popcorning threshold must exist between 0.19 – 0.26% moisture gain for the PBGA-388 packages tested.

8.5 IR Reflow Temperature Profile

Profile: Date: 10-2-1997 Time: 14:37:50



x

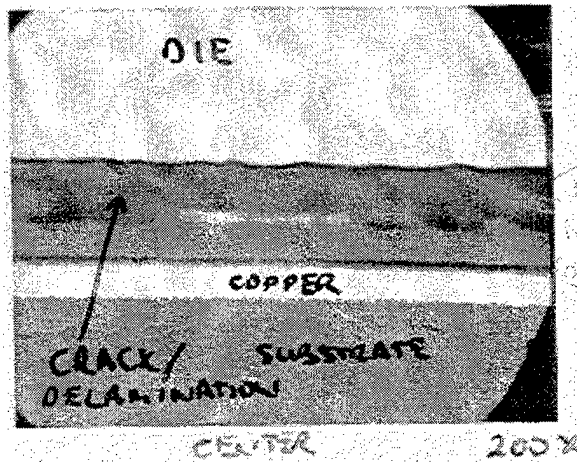
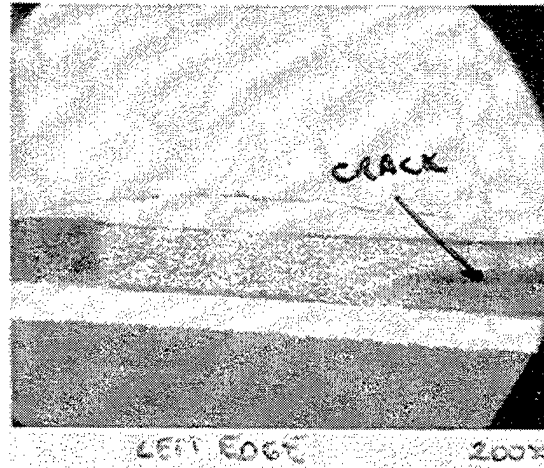
Program Recipe: RCALITE Recipe Directory Set: 1

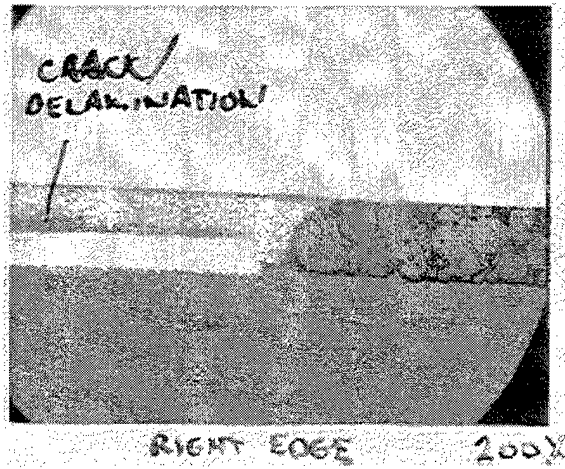
Description: System default recipe.

Convection Cell Fan Speed: 2300
 Outload, Conveyor Speed: 14.0 in/min
 Zone 01: Nitrogen Baffle, Nitrogen Flow: ON
 Zone 02: Heating, top: 157 C bottom: 157 C
 Zone 03: Heating, top: 157 C bottom: 157 C
 Zone 04: Heating, top: 157 C bottom: 157 C
 Zone 05: Heating, top: 225 C bottom: 225 C
 Zone 06: Heating, top: 240 C bottom: 240 C
 Zone 07: Cooling
 Zone 08: Cooling
 Zone 09: Nitrogen Baffle, Nitrogen Flow: ON
 Offload

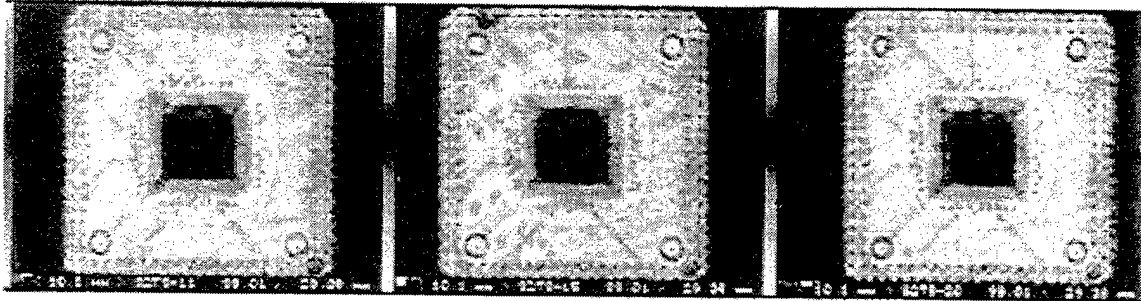
8.6 Micrographs of cross-sectioned parts.

Micrographs of left edge, center, and right edge sections of PBGA showing delamination at the die/DAP interface.

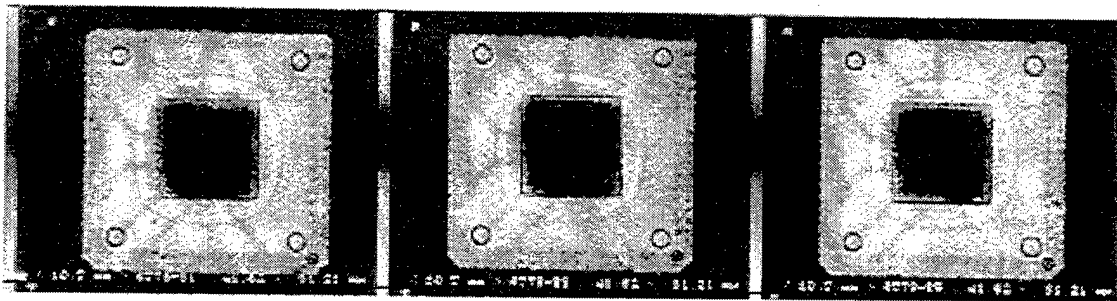




8.7 Example C-SAM Images of PBGA parts at 0-hour.



Thru-scan images of PBGA-388 package with small die at 0-hour.
Images show delamination at die/DAP and small voids.



Thru-scan images of PBGA-388 package with large die at 0-hour.
Images show delamination at die/DAP interface.

8.8 Conclusion

The PBGA-388 lead packages tested passed the level 3 conditions used in this test, but showed severe delamination at level 2. Both the EMC/substrate interface and the die/DAP interface showed delamination after IR reflow. A popcorning threshold between 0.19 – 0.26% moisture exists for these packages. The MET value used in this study was 0 hours and therefore the soak time for a level 3 package could easily be longer for some assembly plants.

The importance of plasma cleaning the substrates prior to molding was made obvious after molding 2 sets of parts that failed to show good adhesion between the EMC and substrate. Plasma cleaning resulted in parts that had good adhesion across the entire EMC/substrate interface. As this step only takes a matter of minutes, it should be done for all subsequent PBGA molding runs using these substrates. The production substrates may not need this step, as they are cleaned and sealed prior to shipping.

9 *Hygrothermal Reliability Evaluation of Plastic IC Packages with EPACK*

This chapter presents the development and application of a computer-aided engineering tool, EPACK™, for hygro-thermal-mechanical performance and reliability evaluation of plastic IC packages. With this user-friendly and fully automated tool, a packaging engineer can perform a reliability evaluation of a plastic IC package in minutes. Usage of EPACK is described in a separate report, "EPACK User's Manual", for this project.

9.1 Introduction

Polymeric materials used in plastic-encapsulated IC packages, such as molding compound and die attach adhesive materials, are highly permeable to moisture. The absorbed moisture becomes detrimental to the package's reliability in three areas: degrading the polymeric material properties (e.g., fracture toughness and interface strength), generating additional hygro stresses due to material swelling, and creating steam pressure during moisture evaporation.

Traditionally, the plastic IC package reliability problem associated with moisture has been handled by performing industry standard tests (such as JESD22-A112-A, JESD22-A113-A, and IPC-SM-786A) to determine moisture susceptibility of the IC package and follow the dry-pack guideline during shipping and storage of the package. However, the reliability testing is very time-consuming and does not offer too many insights into the failure mechanisms of plastic packages. As a result of advancements in computer-aided engineering tool development and computer speed and capacity, using physics-based simulation to assess plastic IC package reliability has become an attractive alternative to IC packaging engineers.

In this paper, development and application of a computer-aided engineering tool, EPACK™, for hygro-thermal-mechanical performance and reliability evaluation of plastic IC packages are presented. With such a user-friendly and fully automated design tool, a packaging engineer can perform a reliability evaluation of a plastic IC package in less than fifteen minutes.

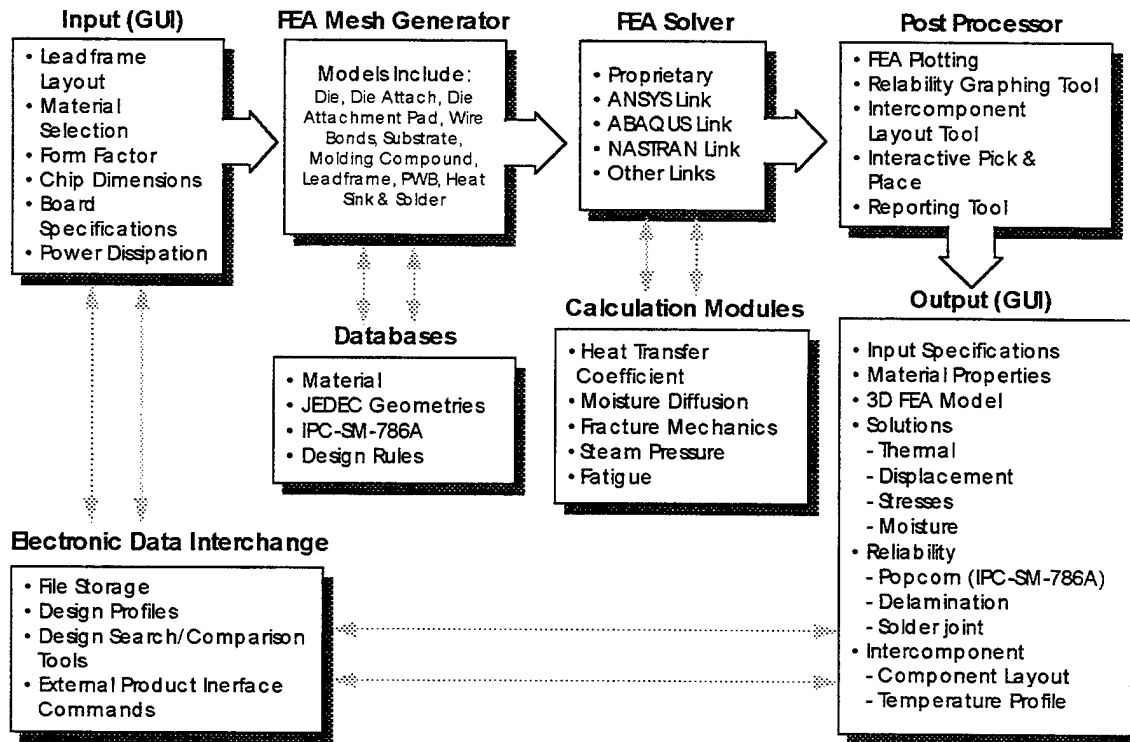


Fig 9-1 Program Structure of the IC Package Design Expert System.

9.2 EPACK Program Structure

As the IC package gets smaller and smaller, and dissipates more power, design cycles of new IC packages are getting shorter for faster time-to-market. As a result, the traditional design approach of testing and prototyping has become too time-consuming for the fast-moving IC industry. Similarly to what happened to the electrical design automation (EDA) about a decade ago, packaging design automation (PDA) with user-friendly computer-aided design tools has become an inevitable trend for the IC packaging industry. With the advancements in processor power and storage capacity, personal computers (PC) have become an economic and effective platform for the packaging design expert system. As a result of a three-year joint R&D effort between Optimal Corp., National Semiconductor Corp., and several subcontractors, a PC-based design expert system for IC packaging, EPACK, has recently been developed. As illustrated in *Figure 9-1*, the first generation of the design expert system focuses on prediction of the hydro-thermal-mechanical performance and reliability of IC packages.

Although most of the numerical analysis capabilities (e.g., heat transfer, thermal stress, and fracture mechanics) implemented in this design expert system can also be found in other commercial analysis tools, EPACK is one of the first few

computer software packages offered as a design tool for IC packaging designers.

The popcorning evaluation module of EPACK is used as an example in this paper to illustrate important features of the design expert system. The package popcorning mechanism implemented in EPACK is shown schematically in *Figure 9-2*. Details are found in Nguyen *et al.*, 1995.

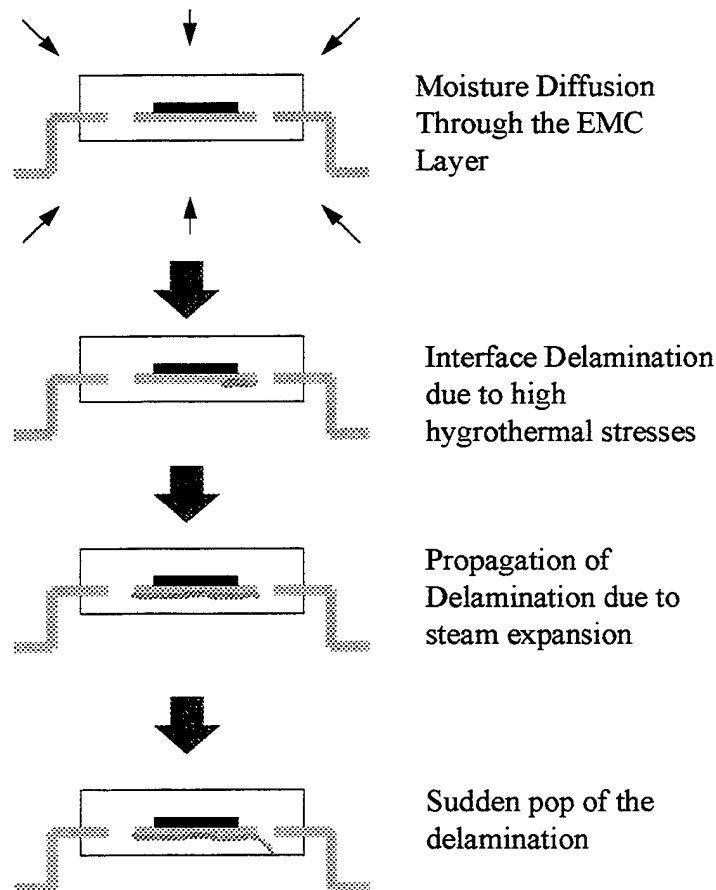


Fig 9- 2 Package Popcorning Failure Mechanism.

9.3 Automatic Finite Element Mesh Generation

With the traditional general purpose analysis tools, building a three-dimensional finite element model, including selecting appropriate material properties and implementing accurate boundary conditions, may take up to two weeks of an analyst's time. Also, the general purpose analysis tools (finite element, boundary element, or computational fluid dynamics (CFD)) are usually so

complicated that analysts with in-depth training in solid mechanics, heat transfer, fluid dynamics, and the finite element method are required to generate meaningful results. To eliminate the time-consuming finite element model generation and the need for a specially trained analyst, the first key feature of EPACK is to generate the three-dimensional finite element model automatically after the users have defined their problems through a user-friendly input module. A similar approach has been demonstrated successfully in a CFD-based design tool, FLOTHERM™, for system cooling analysis.

To ease the data input bottleneck, package dimensions defined in the existing JEDEC standards are pre-stored in a package form factor database. After choosing a package form factor (e.g., QFP, BGA, SO, PLCC, ..., etc.) and its associated parameters (e.g., pin count, pitch, ..., etc.), the users only need to input the package internal dimensions. For example, for a PQFP package, the users are required to go through the input modules for die, die attach, die pad/leadframe, package exterior dimensions, solder, and PWB. In EPACK, geometric definition of a specific problem is done through graphical user submenus for each component of an IC package. In all the submenus, there are graphic illustrations for all the input variables in the input table. For example, *Figure 9-3* is the on-screen illustration for defining the leadframe dimensions of a PQFP.

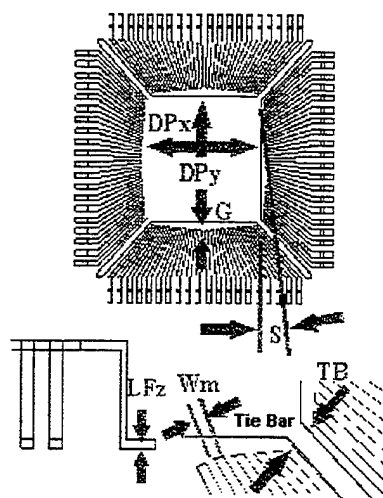


Fig 9-3: On-Screen Picture of Leadframe Dimension Input.

In addition to the geometric dimensions, EPACK also offers a material database. After the users have chosen one of the materials from the material library, temperature-dependent material properties, such as thermal conductivity, Young's modulus, Poisson's ratio, swelling coefficients, and moisture diffusivity, are implemented into the finite element analysis automatically. Alternatively, the users can also choose the user-defined material option and establish a specific temperature-dependent material property table.

The last submenu of the input module is to define the loading. Currently, EPACK users have a choice of performing thermal resistance, package warpage, delamination, popcorning, die cracking, or solder joint fatigue analyses. Additional loading cases, such as parasitic analysis, signal integrity evaluation, and bond wire sweep (molding simulation), will also be offered in the near future. For this example of popcorning analysis, the users need to input package preconditioning level (e.g., 1 through 6) and the maximum reflow temperature.

After the users have completed the input module, the program will automatically generate a three-dimensional finite element model. For the example problem of a 44-lead PQFP, the resulting finite element meshes are depicted in *Figure 9-4*.

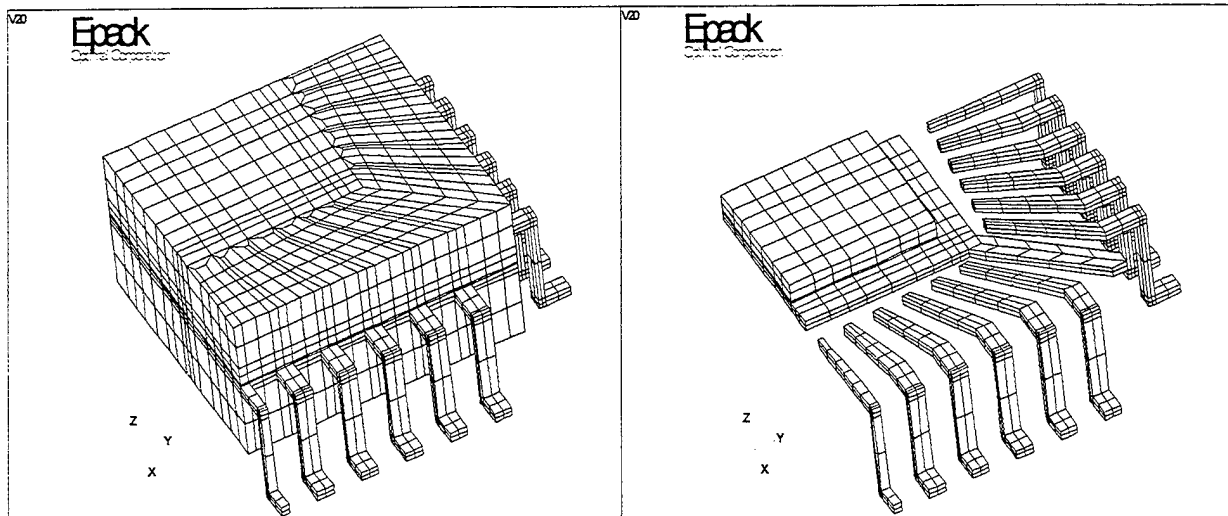


Fig 9-4 Finite Element Mesh Generated by EPACK (PQFP-44).

The example PQFP-44 package has been tested to be a JEDEC Level 3 package. The moisture susceptibility test results of the package are summarized in *Figure 9-5*. Material properties of the example PQFP-44 package are summarized in *Table 9-1*.

Table 9-1: Material Properties of the Package Materials.

	E (GPa)	ν	α (ppm/°C)	T_{ref} (°C)	β (ppm/%wt)
Die	150.0	0.3	2.5	175	0.0
Die attach	4.3	0.3	82.0	90	0.0
Die pad/LF	114.0	0.3	16.3	175	0.0
EMC	12.2	0.3	57.0	175	2000.0

Note: LF: Leadframe; EMC: Epoxy Molding Compound. E: Youngs' modulus; ν : Poisson's ratio; α : Coefficient of thermal expansion; β : Swelling coefficient.

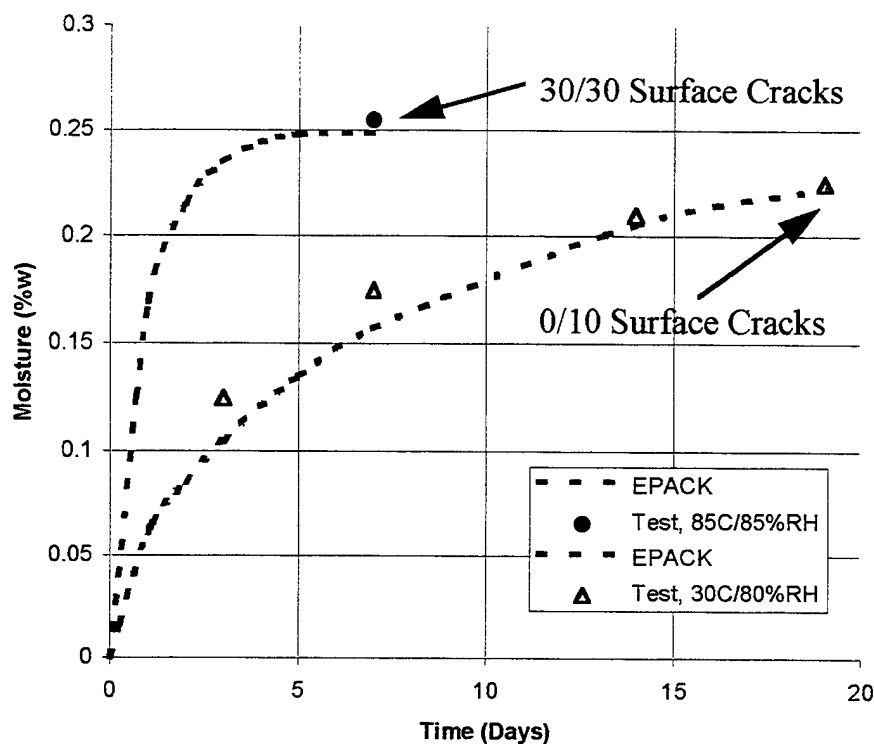


Fig 9-5 Popcorning Test Results of the PQFP-44 Package.

9.4 Moisture Diffusion Analysis

Within EPACK, moisture diffusion is calculated by the classical Fick's law:

$$D \left(\frac{\partial^2 C}{\partial x^2} + \frac{\partial^2 C}{\partial y^2} + \frac{\partial^2 C}{\partial z^2} \right) = \frac{\partial C}{\partial t} \quad (9-1)$$

where,

C = Moisture concentration (mg/cm²)

D = Diffusivity (cm²/sec).

After extensive numerical experiments, it was found that for all IC packages, the EMC (epoxy molding compound) layer is so thin that the following one-

dimensional moisture diffusion can accurately describe the absorption and desorption of moisture:

$$C(t)_{\text{pad}} = C_{\text{sat}} \left[1 - \frac{4}{\pi} \sum_{n=0}^{\infty} \frac{(-1)^n}{2n+1} \text{Exp} \left(\frac{-(2n+1)^2 \pi^2 D t}{4d^2} \right) \right] \quad (9-2)$$

$$M(t) = M_{\infty} \left[1 - \frac{8}{\pi^2} \sum_{n=0}^{\infty} \frac{1}{(2n+1)^2} \text{Exp} \left(\frac{-(2n+1)^2 \pi^2 D t}{4d^2} \right) \right] \quad (9-3)$$

where,

- $C(t)_{\text{pad}}$ = Moisture concentration at the die pad/EMC interface,
- d = Mold compound thickness under the pad,
- $M(t)$ = Total absorbed moisture in the package.

As illustrated in *Figure 9-5*, the predicted moisture absorption agrees very well with experimental results. In this case, the predicted package moisture content, $M(t)$, after the 85°C/85%RH for 168 hour preconditioning, was predicted to be 0.41 %wt, and was multiplied by 2/3 to adjust for the fact that the EMC accounts for about 2/3 of the total package weight.

9.5 Hygrothermal Stress Analysis

The resulting hygrothermal stresses of the example PQFP-44 package:

$$\sigma_{ij} = C_{ijkl} [u_{k,l} - \delta_{kl} (\alpha \Delta T + \beta C)] \quad (9-4)$$

were calculated with a finite element module in EPACK. A proprietary iterative solver was employed by EPACK so that the finite element solution process is extremely fast and disk storage space efficient. For the example PQFP-44 finite element model shown in *Figure 9-4*, the finite element solution took only about two minutes in a relatively slow Pentium-133MHz-based PC for the 17,000⁺ degrees-of-freedom problem. The resulting peeling stress distribution at the die pad/EMC interface is illustrated in *Figure 9-6*.

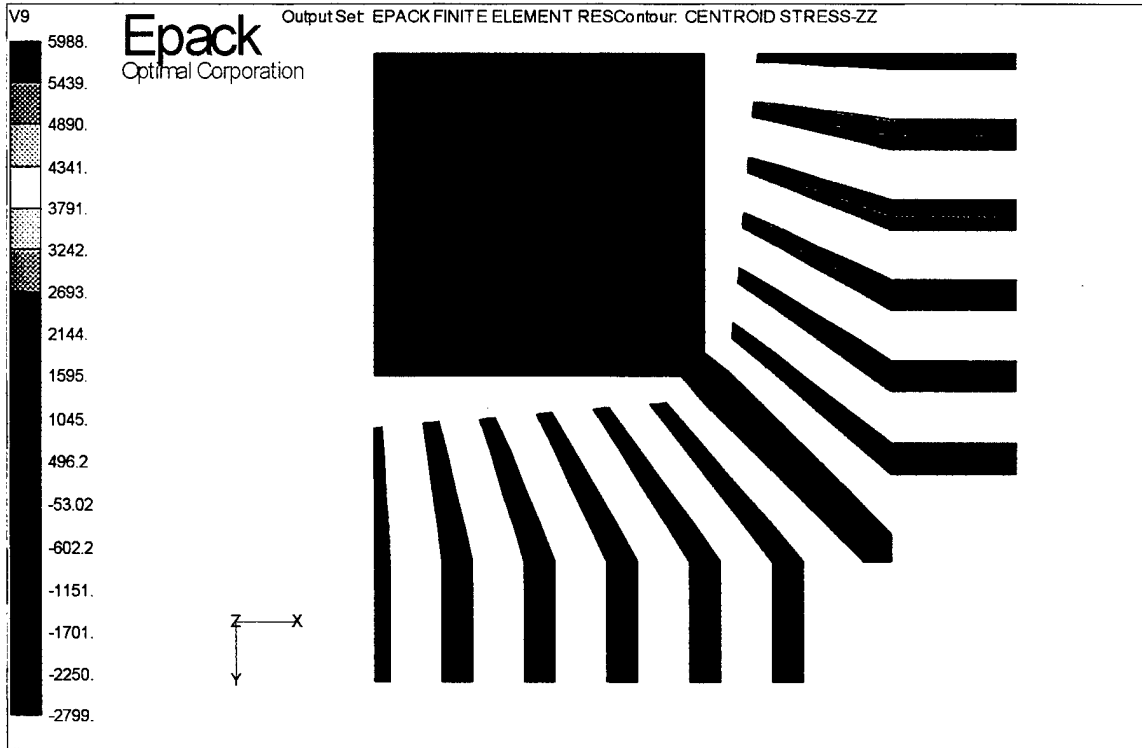


Fig 9-6 Peeling Stress Distribution at the Die Pad/ EMC Interface.

9.6 Initial Delamination

After the hygrothermal stress analysis, EPACK next determined the initial die pad/EMC interface delamination according the following criterion:

$$\left(\frac{\sigma_{\text{peel}}}{\sigma_c} \right)^2 + \left(\frac{\tau_{\text{shear}}}{\tau_c} \right)^2 = 1 \quad (9-5)$$

where σ_c and τ_c are experimentally measured interface adhesion strength at different temperature and moisture conditions. One of the interface adhesion strength data implemented in EPACK is shown in *Figure 9-7*. The resulting initiation delamination of the example PQFP-44 package is illustrated in *Figure 9-8*.

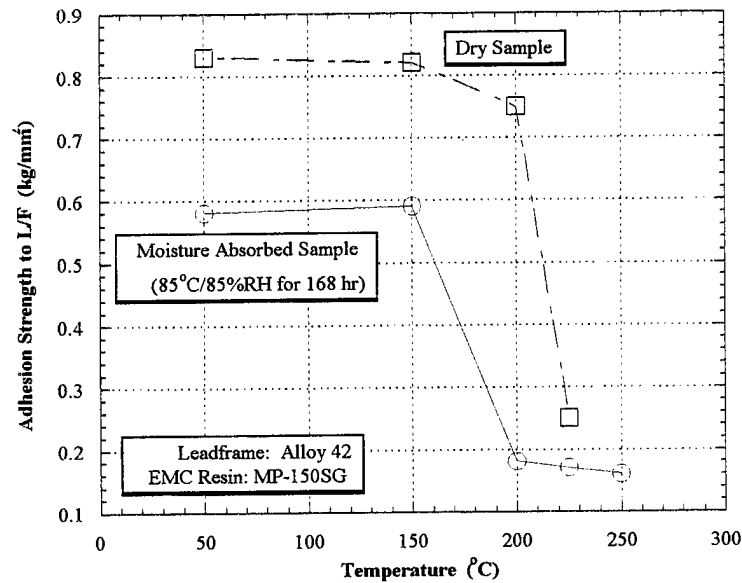


Fig 9-7 Degradation of Adhesion Strength (Ohizumi et al., 1990).

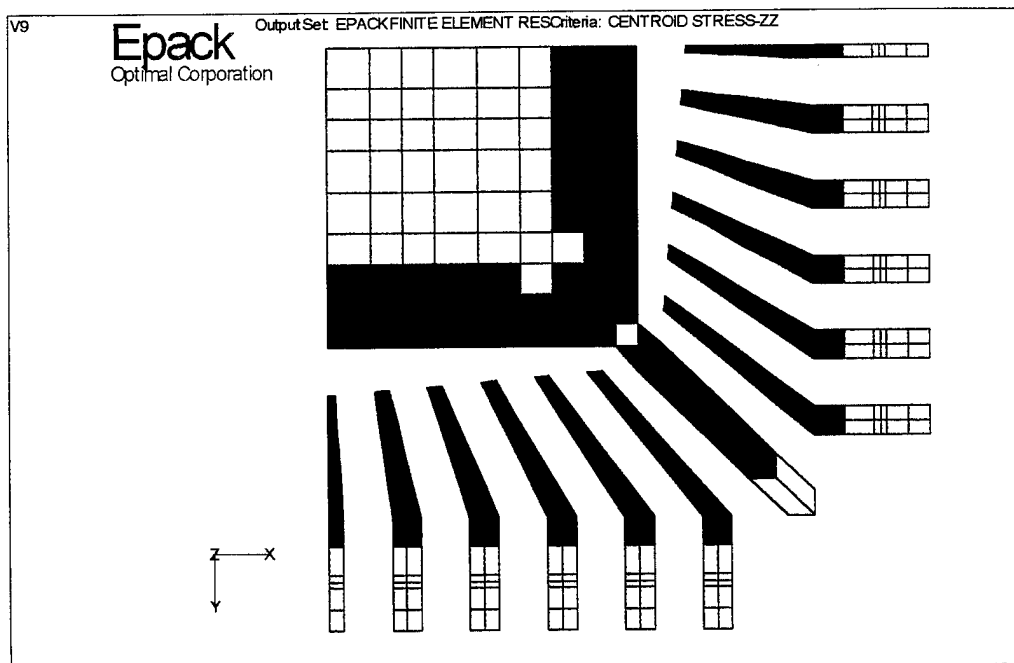


Fig 9-8 Delamination Pattern at Die Pad/EMC Interface
(Dark Color = Delamination)

9.7 Propagation of Interface Cracks

The next step in EPACK for the popcorning evaluation of the example PQFP-44 package is to assess the stability of the initial delamination. Propagation of the initial delamination shown in *Figure 9-8* is determined by the following interface crack stability criterion:

$$\left(\frac{K_I}{K_{IC}}\right)^2 + \left(\frac{K_{II}}{K_{IIC}}\right)^2 = 1 \quad (9-6)$$

where K_I and K_{II} are stress intensity factors of the initial interface crack, and K_{IC} and K_{IIC} are mode I and mode II interface fracture toughness, respectively. For the EMC material used in the example PQFP-44 package, the interface fracture toughness shown in *Figure 9-9* was used by EPACK (see Chapter 4 for details).

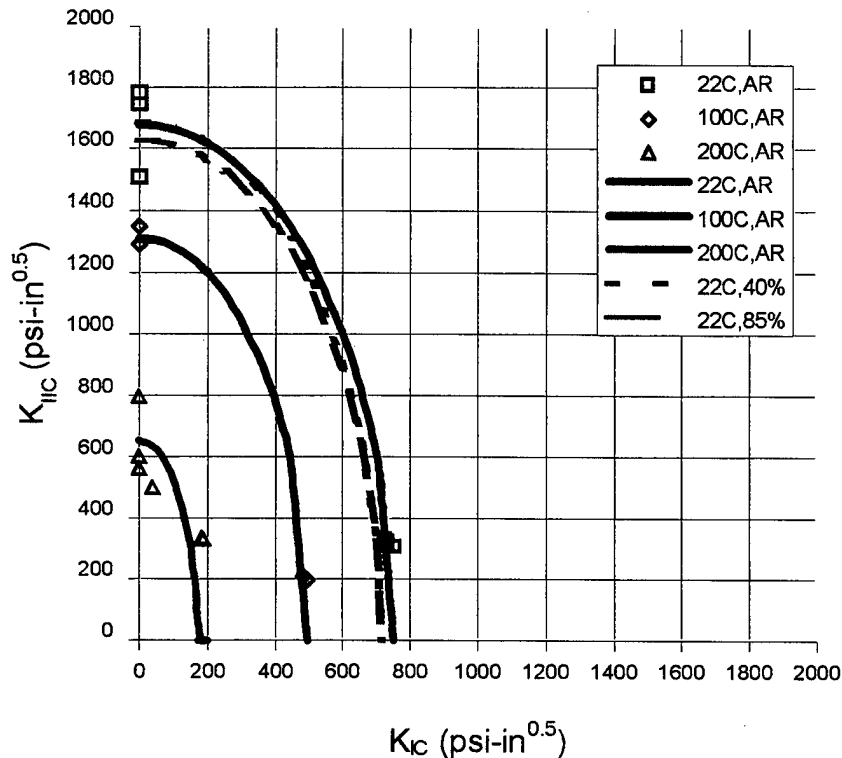


Fig 9-9: Interface Fracture Toughness of the Die Pad/EMC Interface.

In EPACK, the three-dimension stress intensity factors, K_I and K_{II} are calculated by the formulation developed by (see Chapter 2):

$$K_I^{3D} = f\left(\frac{a_2}{W_2}, \frac{W_2}{W_1}, \frac{H}{W_1}\right) \cdot \sqrt{\pi a} \cdot \sum_{n=3}^3 F_n \cdot \sigma_n \quad (9-7)$$

$$K_{II}^{3D} = f\left(\frac{a_2}{W_2}, \frac{W_2}{W_1}, \frac{H}{W_1}\right) \cdot \sqrt{\pi a} \cdot \sum_{n=3}^3 F_n \cdot \tau_n \quad (9-8)$$

where functions f are tabulated in Appendix I.

For the present example PQFP-44 package,

$$K_I = 139.4 \quad \text{psi}\sqrt{\text{in}} \quad K_{II} = 163.2 \quad \text{psi}\sqrt{\text{in}} \quad (9-9)$$

With $K_{IC} = 118.5\text{psi}\sqrt{\text{in}}$, $K_{IIC} = 529.5\text{psi}\sqrt{\text{in}}$ for the materials (see *Figure 9-9*), the initial delamination is predicted to propagate through the entire die pad/EMC interface. This prediction agrees with the experimental observation.

9.8 Steam Pressure

In Sections 9-7 and 9-9 of this report, the crack is under both the hygrothermal stresses described in Section 5 and a steam pressure due to vaporization of the absorbed moisture. EPACK users can choose from two different formulae to calculate the steam pressure, one based on the ideal gas law and the other one based on the thermodynamics theory. The thermodynamics based theory (Sullivan, 1996) was used for the example problem.

For comparison, steam pressures by both the ideal gas law and the thermodynamics-based theory are plotted against each other in *Figure 9-10*.

Pore (Steam) Pressure Due to 0.009g/cm^3 Moisture

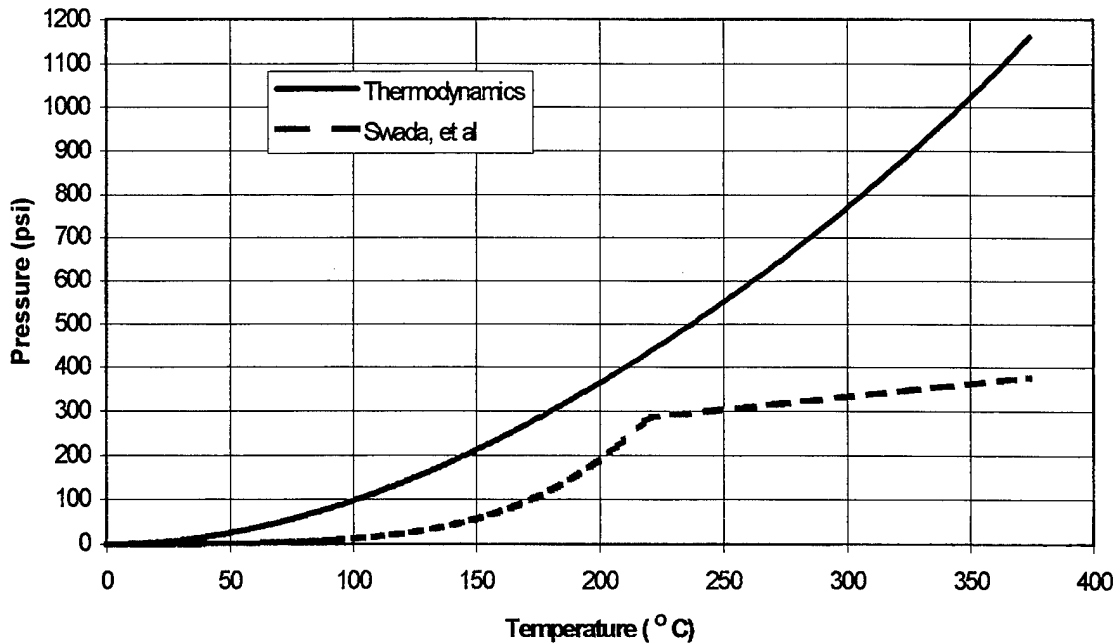


Fig 9-10 Steam Pressure Calculated by Two Different Methods

9.9 Penetration of the EMC Layer

As illustrated in *Figure 9-2*, the last step in the popcorning evaluation by EPACK is to determine whether the delamination will penetrate the EMC layer and become an external crack. EMC fracture toughness at different temperature and moisture conditions for several commonly used molding compounds have been recently measured (Hsu *et al.*, 1997) and have been incorporated into EPACK as part of the material database. For the example PQFP-44 EMC material, the fracture toughness depicted in *Figure 9-11*(refer to *Chapter 3* for details) was used.

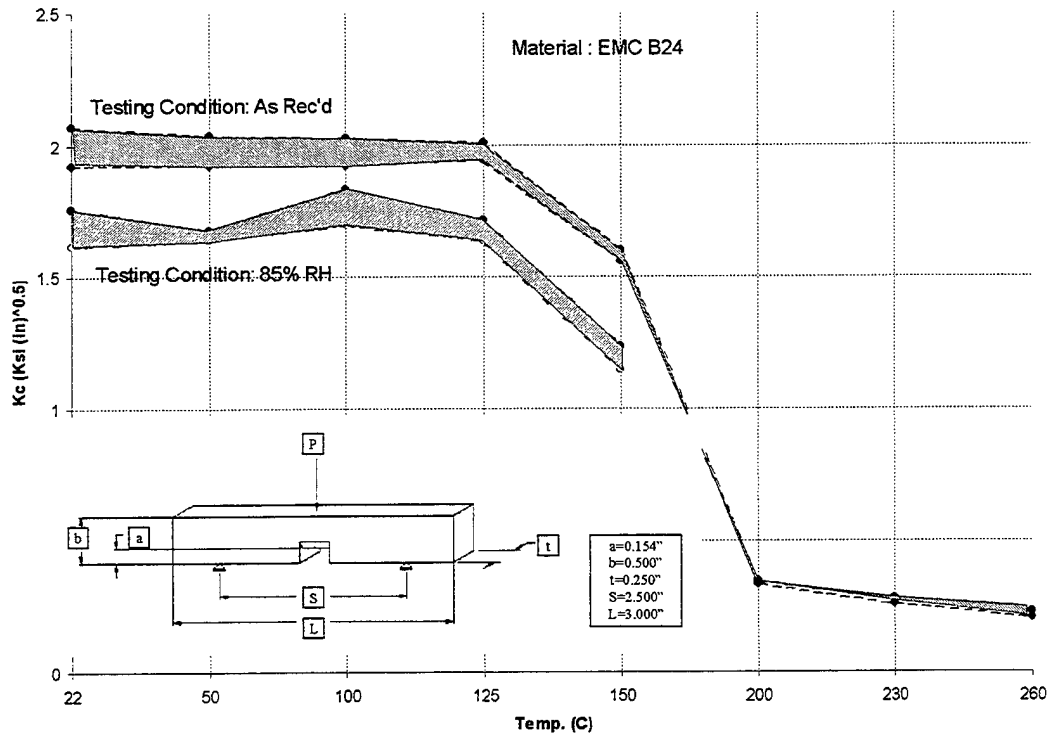


Fig 9-11: Fracture Toughness of the EMC Used in the PQFP-44 Package.

For the present example problem, the Mode I stress intensity factor for the totally delaminated die pad/EMC interface is calculated to be $1345.5 \text{ psi}\sqrt{\text{in}}$, which exceeds the EMC fracture toughness (see *Figure 9-10*) of $200 \text{ psi}\sqrt{\text{in}}$. Therefore, after the Level 1 preconditioning, an external crack will appear in the example PQFP-44 package. The predicted popcorning characteristics agree with this test observation.

9.10 Model Verification and Validation

In addition to the Level 1 preconditioning described above, other preconditioning levels depicted in *Figure 9-5* have also been evaluated by EPACK. Results of these popcorning evaluations are summarized in *Table 9-2*. All the predicted popcorning characteristics agree well with test data.

Table 9-2: Predicted Popcorning Characteristics of the PQFP-44 Package.

Case	Preconditioning
1	85°C/85%RH/168 hr
2	30°C/80%RH/168 hr
3	30°C/60%RH/456 hr

Case	Initial Delam. (%)	Final Delam. (%)	Ext. Crack
1	77	100	Yes
2	63	100	Marginal
3	51	51	No

All the popcorning test data in the proprietary Optimal Corporation internal report have also been analyzed with EPACK and compared against the test results. It has been found that most of the IC package thermal/mechanical predictions by EPACK are within 5% of the experimental data. Representative plots of the EPACK verification and validation are illustrated in Figures 9-12, 9-13, and 9-14 for QFP packages. Verification plots for other packages types are contained in the proprietary Optimal Corporation internal report.

Prediction of QFP Package Popcorning

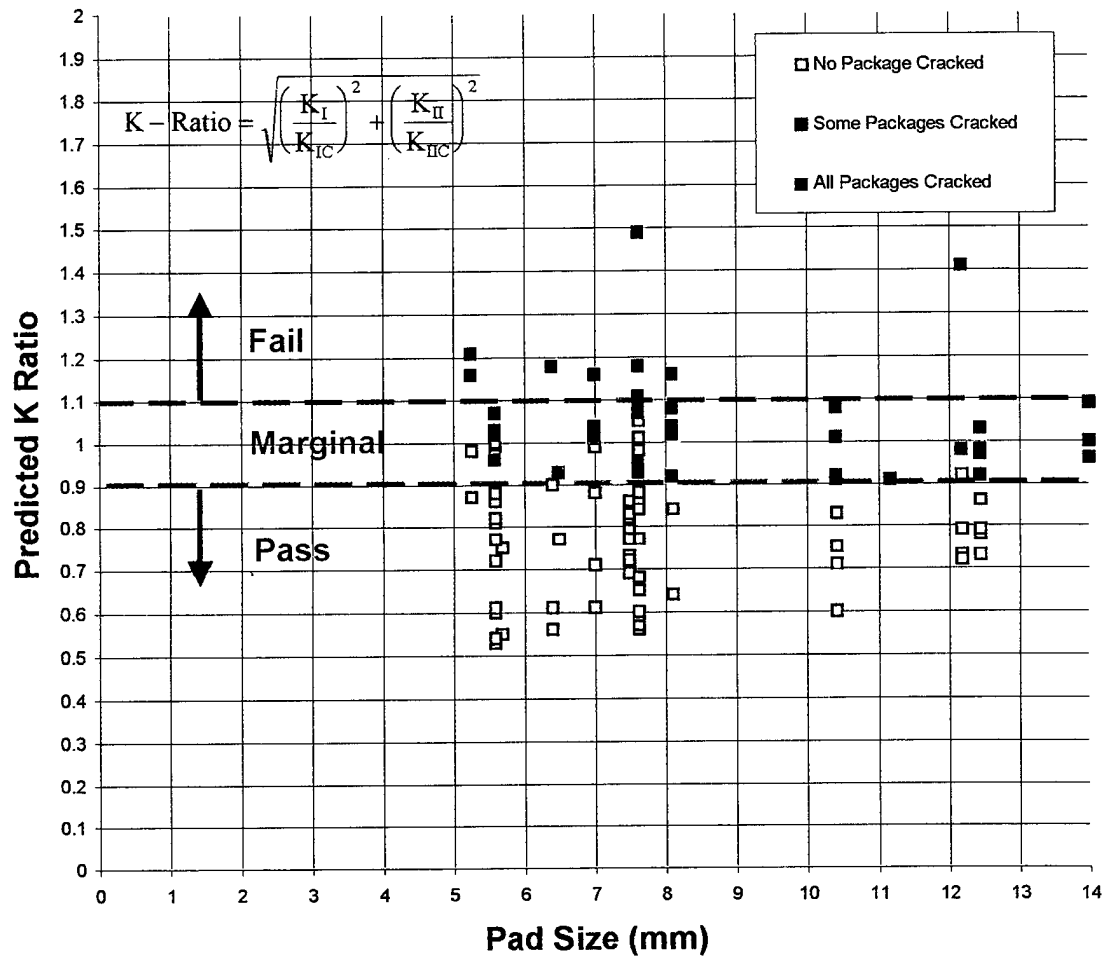


Figure 9-12 EPACK's Popcorning Prediction vs. Test Results

Prediction of QFP Package Moisture Absorption

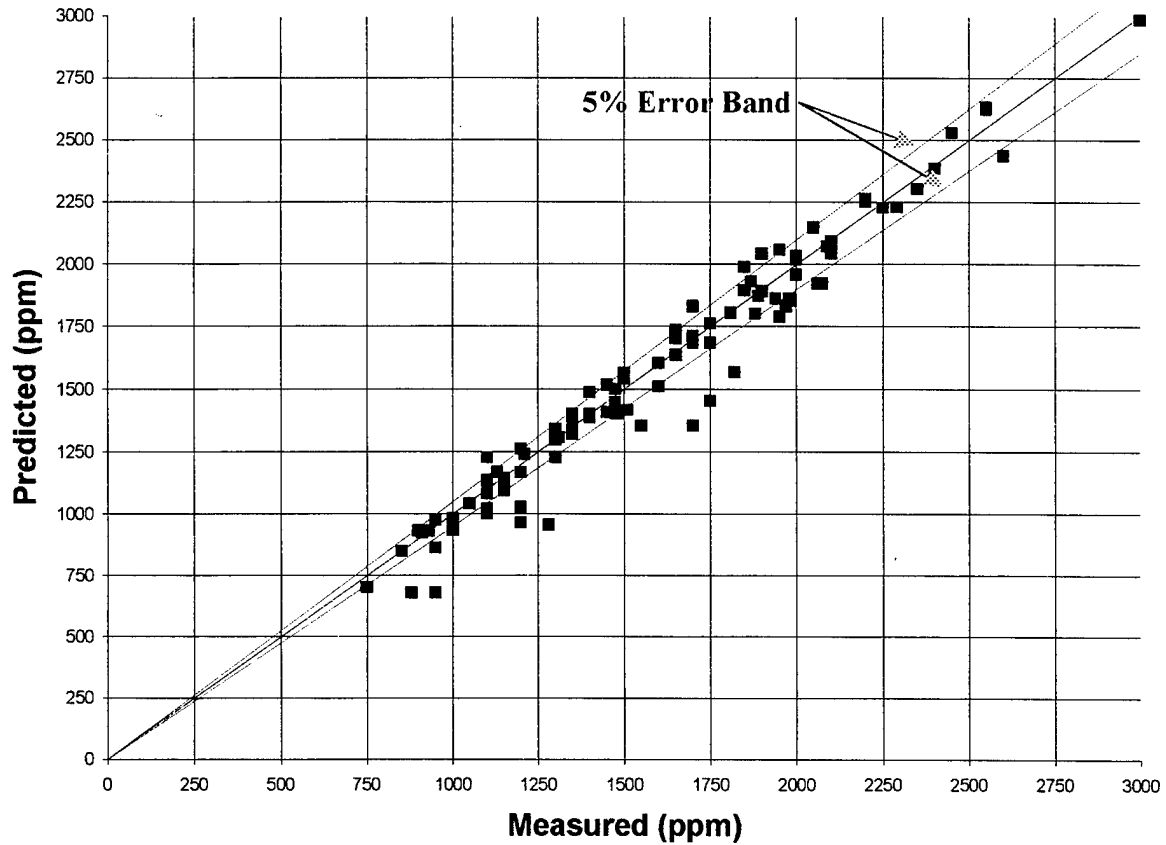


Figure 9-13 EPACK's Moisture Diffusion Prediction vs. Test Results

QFP Packages θ_{JA} at Natural Convection

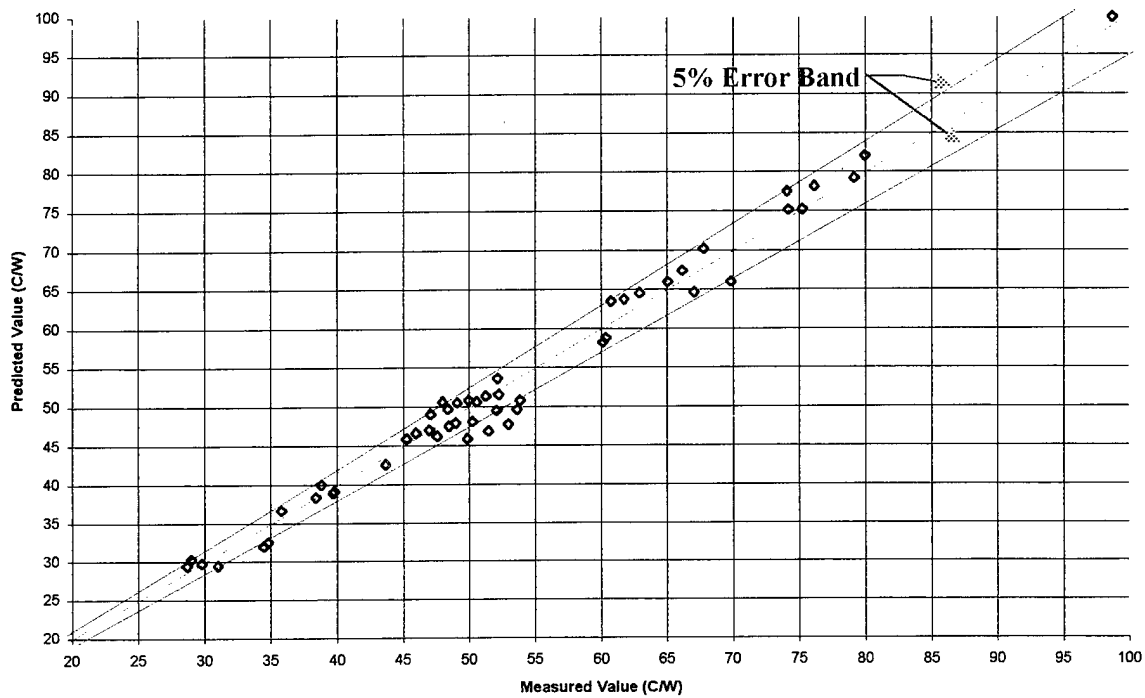


Figure 9-14 EPACK's Thermal Resistance Prediction vs. Test Results

9.11 Conclusions

The following conclusions can be drawn:

- The physics-based computer simulation tool, which combines moisture diffusion, heat transfer, hygrothermal stress analysis, fracture mechanics, molding fluid dynamics, and electromagnetic theories in one package, can accurately and effectively predict the popcorning susceptibility of plastic IC packages.
- The same technique has been extended to other reliability/performance characterization problems of IC packages, such as thermal resistance, die cracking, package warpage, parasitic parameters extraction, ..., etc.
- Incorporation of material characterization results, such as adhesion strength, fracture toughness, interface fracture toughness, material swelling, and moisture diffusivity is essential to the package design expert system.
- Automation in finite element mesh generation, implementation of a material database, implementation of JEDEC package form factors and profiles, and development of a user-friendly input module make the design expert system easy to use and extremely fast.
- Verification and validation of the predicted results by the design expert system with experimental data makes the design expert system even more feasible and appealing to the package design engineers.

10 References

Aoki, K; Kishimoto; and Sakata, M, 1980, Engineering Fracture Mechanics, Vol. 13, pp.841-850.

Comninou, M., 1977, "The Interface Crack," by Maria Comninou, ASME Journal of Applied Mechanics, December, pp.631-636.

Ganesan, C. S., Lewis, G., Woosley, A., Lindsay, W., Berg, H., 1995, "Level-1 Crack-Free Plastic Packaging Technology," 45th ECTC, pp. 450-454.

Ganesan, S. and Berg, H., 1996, "Method and Apparatus for Improving Interfacial Adhesion Between a Polymer and a Metal," U.S. Patent 5,554,569.

Gledhill, R. A., Kinloch, A. J., and Shaw, S. J., 1980, "A Model for Predicting Joint Durability," J. Adhesion, Vol. 11, pp. 3-15.

Hsu, T. R., Fawzi, K. M., Nguyen L. T., and Kuo, A. Y. 1997, "Fracture Strength of Epoxy Molding Compounds," Interpack '97, pp. 261-268.

Hsu, T. R., Nguyen, L., Kuo, A. Y., and Fawzi, K., "Fracture Strength of Molding Compounds," Interpack '97, pp. 261-268, Kohala Coast, Hawaii, June 15-19 (1997).

Hsu, T.R.; Fawzi, K.; and Rong Fang; and 1997, San Jose State Test Report on Laminate Specimens.

Ikeda, T.; Komohara, Y.; and Miyazaki, N., 1997, "Measurement of Mixed Mode Fracture Toughness of An Interface Crack in Electronic Devices," ASME EEP-Vol.19-2, Advances in Electronic Packaging.

Kuo, A. Y. and Riccardella, P. C., 1987, "Path-Independent Line Integrals for Steady-State, Two-Dimensional Thermoelasticity," Int. J. Fracture, Vol. 35, pp. 71-79.

Kuo, A.Y., Chen, W. T., and Chiang, M., "Stress Intensity Factor Solutions for Plastic IC Package Delamination," to be published.

Lee, C. and Parthasarathi, A., 1997, "Investigation of a Novel Leadframe Treatment for "Dry-Pack Free" Packaging," 47th ECTC, pp. 1049-1060.

Lin, T. Y. and Tay, A. A. O., 1997, "A J-Integral Criterion for Delamination of Bi-Material Interfaces Incorporating Hygrothermal Stress," ASME-EEP, Vol. 19-2.

Nguyen, L. T., 1993, "Reliability of Postmolded Packages," ASME Trans. J. of Electron. Packaging, pp. 346-355.

Nguyen, L. T., Chen, A., Giberti, R., Breedis, J., Parthasarathi, A., Peterson, J., Gallo, A., Sweet, J., Hsia, A., Richardson, S., and Staab, P., 1997b, "Plastic Package Ruggedization," SEMICON West, J-1.

Nguyen, L. T., Chen, K. L., Schaefer, J., Kuo, A. Y., and Slenski, G., 1995, "A New Criterion for Package Integrity under Solder Reflow," 45th ECTC, pp. 478-490.

Nguyen, L. T., Giberti, R. W., Chen, A. S., Staab, P. C., Peterson, J. O., Gallo, A., 1997a, "Molding Compound Development in the TRP Plastic Packaging Consortium," SAMPE '97, pp. 402-410.

Nguyen, L. T., Lee, G., Jones, C., Hsu, T. R., Fang, R., Kuo, A. Y., and Chen, W. T., "Interfacial Fracture Toughness in Plastic Packages," ASME Int. Mech. Eng. Congress & Exposition, Dallas, TX, Nov. 16-21 (1997).

Ohizumi, S., Nagasawa, M., Igarashi, K., and Kohmoto, M., "Analytical and Experimental Study for Designing Molding Compounds for Surface Mounting Devices," 40th Electron. Comp. & Tech. Conf., pp. 632-640 (1990).

Rice, J. R., 1988, "Elastic Fracture Mechanics Concepts for Interface Cracks," ASME J. Appl. Mechanics, Vol. 55, pp. 98-103.

Sullivan, R. M., "The Effect of Water on Thermal Stresses in Polymer Composites," ASME J. of Applied Mechanics, Vol. 63, pp. 173-179 (1996).

Tanaka, N. and Nishimura, A., 1995, "Measurement of IC Molding Compound Adhesion Strength and Prediction of Interface Delamination with Package," ASME EEP, Vol. 10-2.

Umebara, N., Inomata, S., Umeda, Y., Naeshiru, M., and Sakamoto, K., 1995, "S-Pad Implementation: Total Plastic Package Crack Solution for Non-Moisture Sensitive Package," 45th ECTC, pp. 470-477.

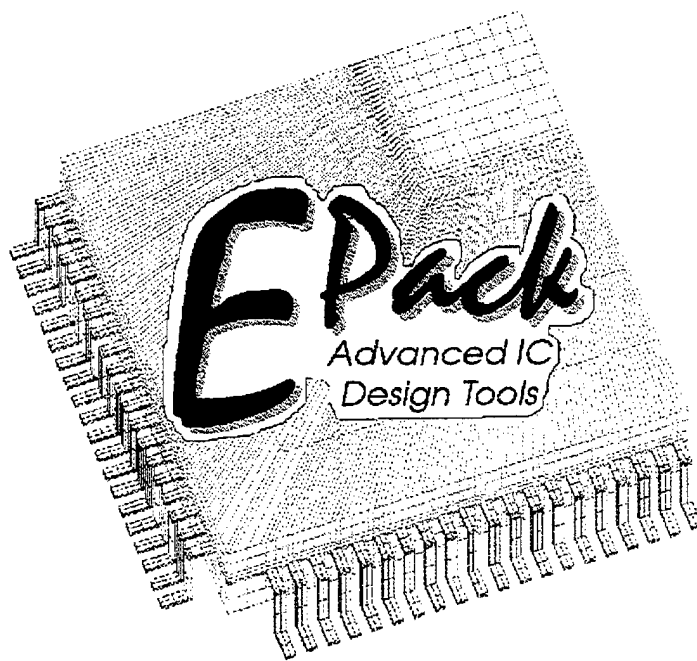
Wilson, W. K. and Yu, I. W., 1979, "The Use of J-Integral in Thermal Stress Crack Problems," Int. J. Fracture, Vol. 15, pp. 377-387.

Yau, J. F. and Wang, S. S., 1984, "An Analysis of Interface Cracks between Dissimilar Isotropic Materials using Conservation Integrals in Elasticity

APPENDIX I

Epack User's Manual

Version 1.1



Optimal Corporation
3150 Almaden Expressway, Suite 100A
San Jose, CA 95118-1217
TEL : (408)264-8900
FAX : (408)264-8996

Table of Contents

1	INTRODUCTION	1-1
2	GETTING STARTED	2-1
3		3-4
4	BGA	4-5
4.1	PBGA	4-5
4.1.1	Die	4-6
4.1.2	Die Attach	4-7
4.1.3	Substrate Metallization	4-8
4.1.4	Substrate Metallization Top Layer	4-9
4.1.5	Substrate Metallization Bottom Layer	4-9
4.1.6	Substrate Thermal Via	4-10
4.1.7	LID (Molding Compound Encapsulation)	4-10
4.1.8	Package	4-11
4.1.9	Solder Balls	4-11
4.1.10	Solder Masks	4-12
4.1.11	Printed Wire Board (PWB)	4-12
4.1.12	PWB Metallization	4-13
4.1.13	Loading, Running, and Results	4-14
5	SUPER BGA	5-15
5.1	PBGA	5-15
5.2	SBGA	5-16
5.2.1	Die	5-17
5.2.2	Die Attach	5-18
5.2.3	Substrate Metallization	5-19
5.2.4	Substrate Thermal Via	5-20
5.2.5	LID (Molding Compound Encapsulation)	5-20
5.2.6	Package	5-21
5.2.7	Solder Balls	5-21
5.2.8	Solder Masks	5-22
5.2.9	Heat Sink	5-22
5.2.10	HS Attach	5-23
5.2.11	Substrate Attach	5-23
5.2.12	Printed Wire Board (PWB)	5-24
5.2.13	PWB Metallization	5-24
5.2.14	Loading, Running, and Results	5-25
6		6-26
7	PBGA	7-26
8	QFP	8-27
8.1	PQFP	8-27
8.1.1	Die	8-28
8.1.2	Die Attach	8-29
8.1.3	Leadframe	8-30
8.1.4	Package	8-31
8.1.5	Solder	8-31
8.1.6	PWB Metal Trace	8-32
8.1.7	PWB	8-32

8.1.8	Heat Sink	8-33
8.1.9	Loading, Running, and Results	8-34
9	9-35
10	PBGA	10-35
11	QFP	11-35
11.1	PQFP	11-35
11.2	TQFP	11-36
11.2.1	Die	11-37
11.2.2	Die Attach	11-38
11.2.3	Leadframe	11-39
11.2.4	Package	11-40
11.2.5	Solder	11-40
11.2.6	PWB Metal Trace	11-41
11.2.7	PWB	11-41
11.2.8	Heat Sink	11-42
11.2.9	Loading, Running, and Results	11-43

1 Introduction

EPACK is a multi-physics design simulation program for IC packages. When you choose EPACK as one of your package design tools, you have achieved 80% of the work for your package design automation.

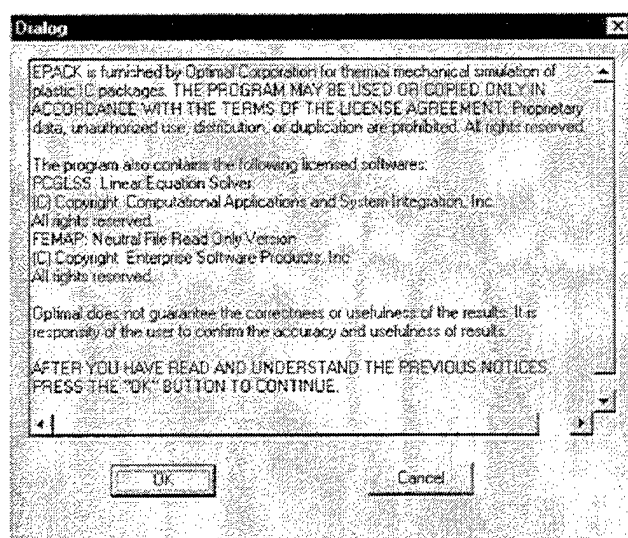
- EPACK is a component-level, multi-physics simulation expert system for IC packages. All package components such as die, die attach, die attachment pad, leadframe, substrate, mask, solder, PWB,...etc., will all be modelled three-dimensionally in EPACK.
- In one single software, EPACK can perform electrical, thermal, hygro (moisture), fluid dynamics (molding) and mechanical simulations of your IC packages.
- EPACK's solution oriented and user-friendly interface design enables average packaging engineers without any computer simulation training to run the software in an hour. EPACK can perform thermal resistance, popcornning, die cracking, delamination, warpage & coplanarity, solder joint fatigue, molding, parasitic parameters extraction, and signal integrity analyses of a given package.
- EPACK's solver is superfast. For a 100,000 degrees of freedom finite element problem, it takes less than 60 minutes to run in a modest Pentium-150 PC.
- EPACK covers all JEDEC standard packages, QFP, SO, BGA, CSP,..., etc., with flexibilities for customized package designs.
- With an extensive material base containing most commonly used molding compound, die attach, leadframe, substrate, solder, and PWB materials by different materials vendors, EPACK serves as a valuable source book for packaging design.
- EPACK's predictions are highly reliable since its results have been validated against thousands of test data (see the verification manual).
- EPACK's prediction results and their supporting information, both text and graphics, can be cut and pasted directly into another Microsoft Windows program for reporting and presentation.

System requirements for running EPACK are

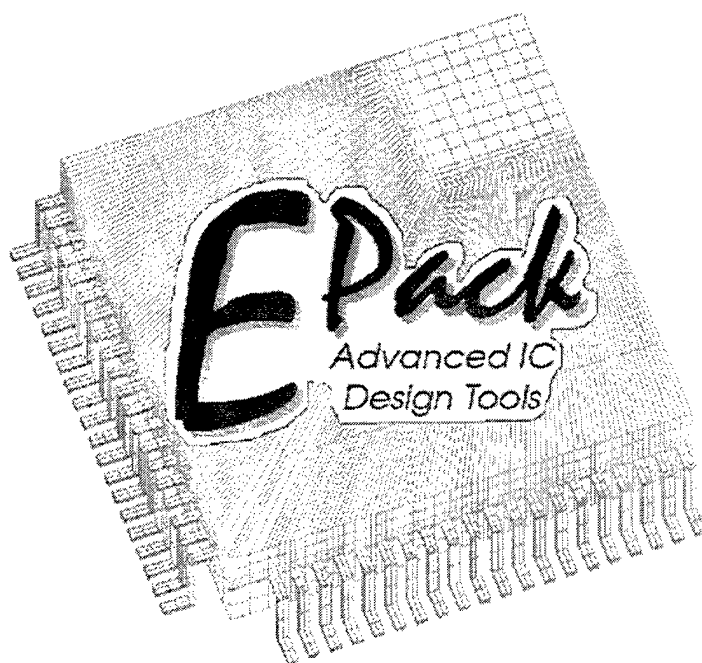
- PC with Intel's 80486 or Pentium processors
- Microsoft Windows-95 or Windows-NT system
- A monitor with 1024x768 resolution in 256 colors
- 96 MB or more RAM
- 100 MB harddisk space

2 Getting Started

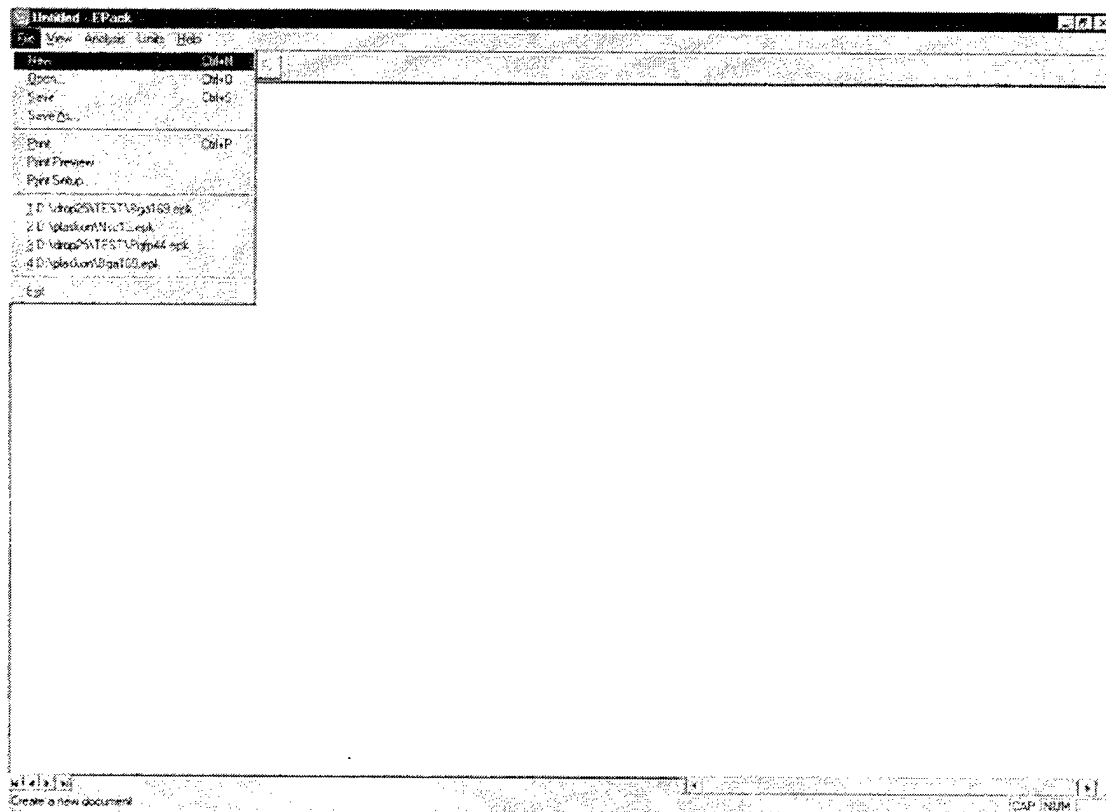
- (1) To start the program, simply double click the EPACK shortcut icon or launch **Start-Program-EPACK** from the Windows-95 or Windows-NT screen.
- (2) The following screen for licensing and disclaimer will appear on screen at the start of the program.



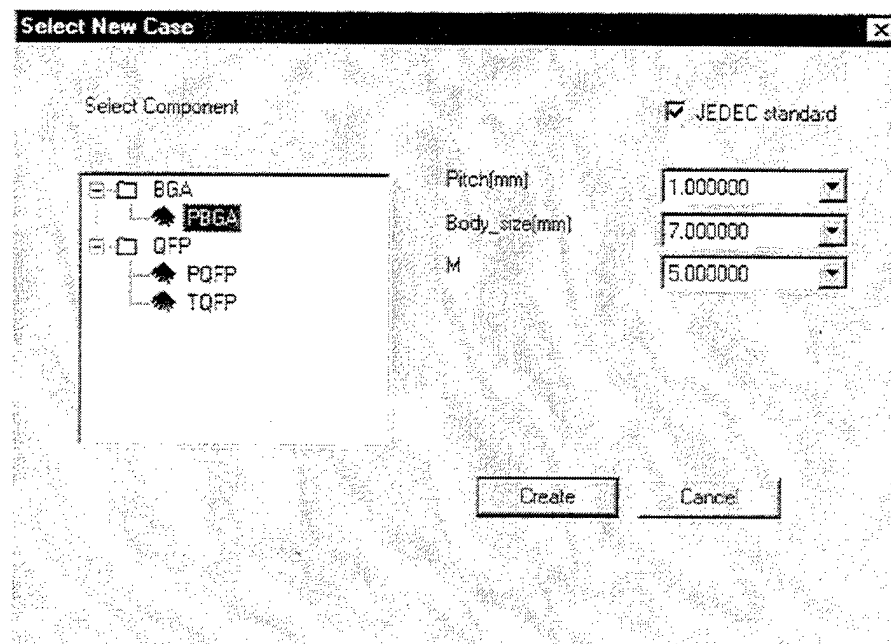
- (3) Review the on-screen and press **OK** to accept it or press **Cancel** to decline it.
- (4) Upon clicking **OK** acceptance of the on-screen disclaimer, the following EPACK logo will appear on screen. Simply click the mouse or press any key to enter the program main menu.



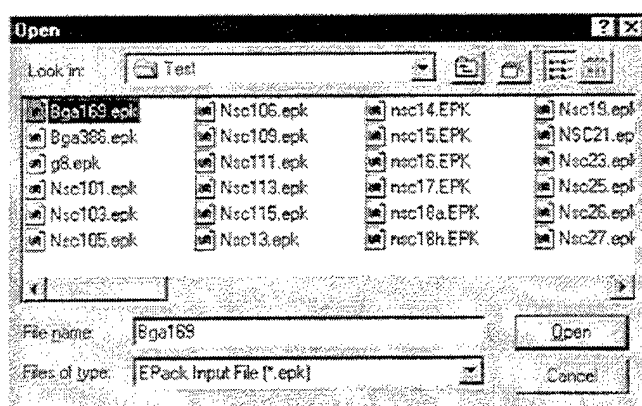
- (5) For a new problem, click **File-New** to start the analysis (see the figure below).



- (6) For a new problem, double click the matching package types from the tree of package form factors.



- (7) To restart a saved file, click **File-Open** and choosed a previously saved file from the screen menu.

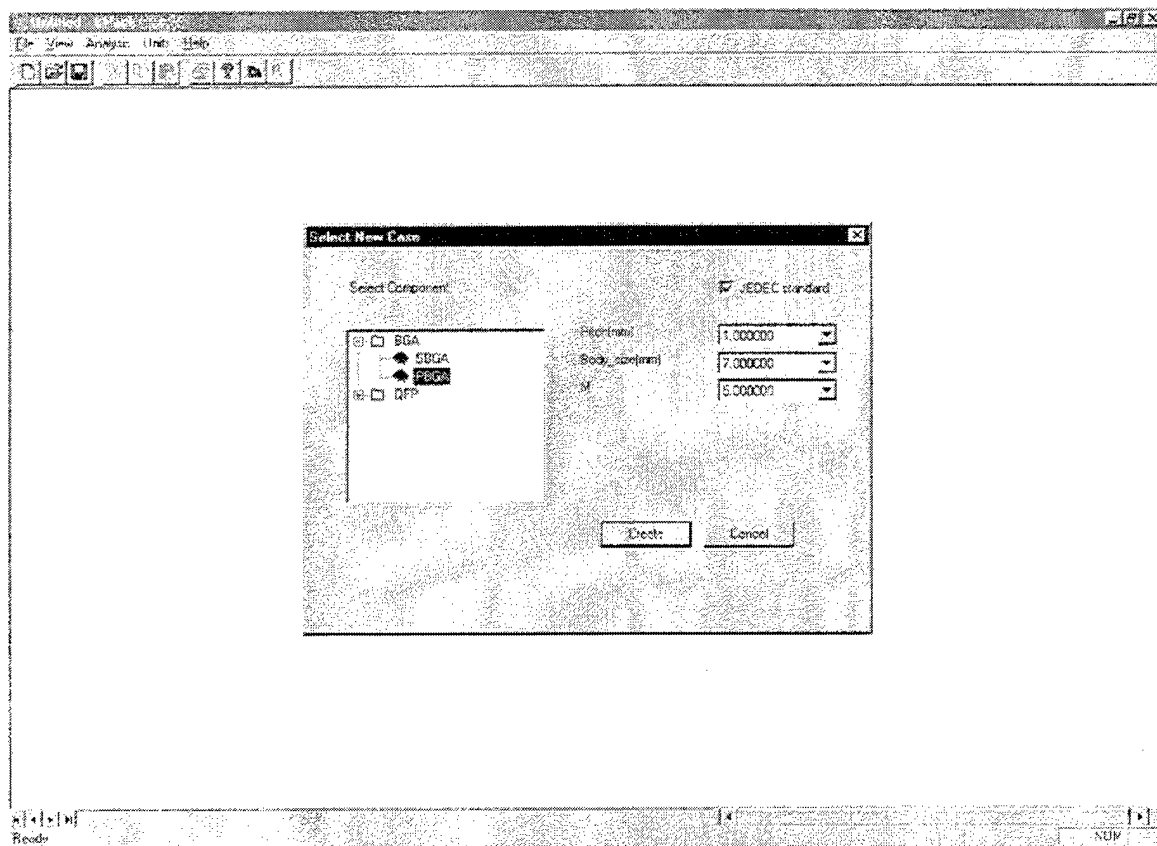


- (8) For each package form factor, continue to a corresponding chapter in this manual for the remaining instruction. For example, for a PBGA package, go to Chapter 3.

3. BGA

3.1 PBGA

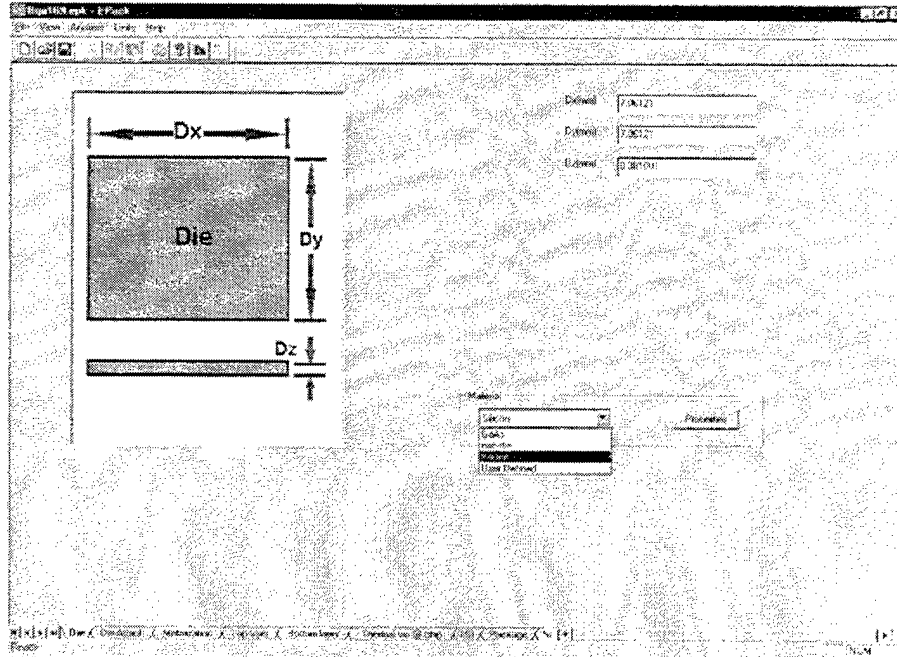
From **File-New** in the main menu, click **BGA-PBGA**, pick appropriate **Pitch** (solder ball pitch), **Body_size** (package widths) and **M** (number of outer rows of the solder balls) sequentially from the menu, and click Create to start the analysis for a JEDEC standard PBGA package. For PBGA packages no registered in JEDEC, simply click the **JEDEC Standard** dialog box to clear the check mark and enter **Pitch**, **Body_size**, and **M** in the same way. A check mark in the **JEDEC Standard** dialog box means that the package is a JEDEC registered package, and an empty **JEDEC Standard** dialog box indicates that the package is a Non-JEDEC registered customized PBGA package.



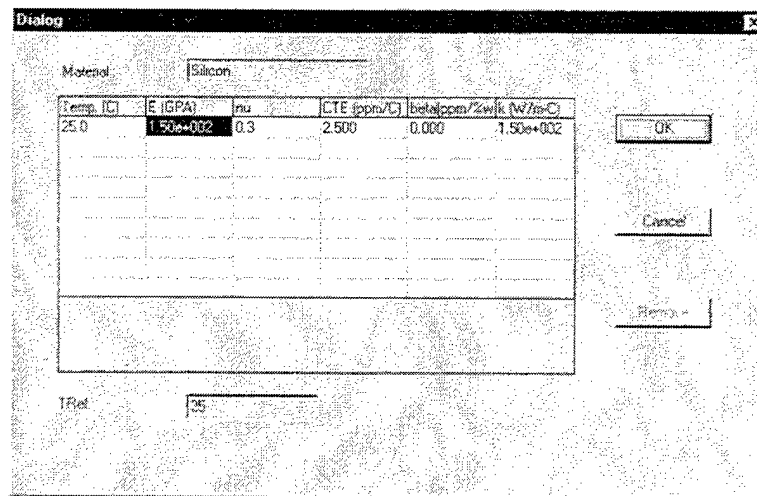
As illustrated near the bottom edge of the following figure, there are 14 sub-menus for PBGA packages: **Die**, **Die Attach**, **Metallization** (in substrate), **Top Layer**, **Bottom Layer**, **Thermal via @ chip**, **LID**, **Package**, **Solder**, **Mask**, **PWB**, **PWB Metal**, **Loading**, and **Results**. Go through all the submenus to complete the analysis journey.

3.1.1 Die

- (1) Input die widths (**Dx** and **Dy**) and thickness (**Dz**) into the corresponding dialog boxes on screen.
- (2) Click Unit on top of the screen to switch between **Metric** and **English** units at any time.
- (3) Click the Material dialog box and choose a die material from the library.

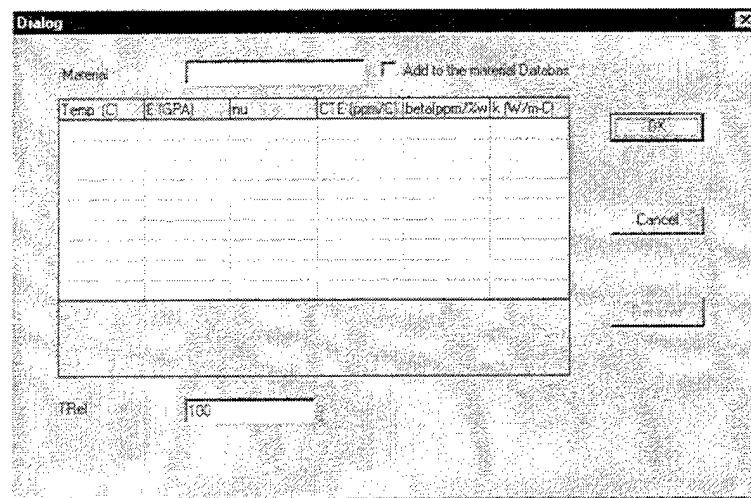


- (4) Click the Properties button to review the temperature material properties.



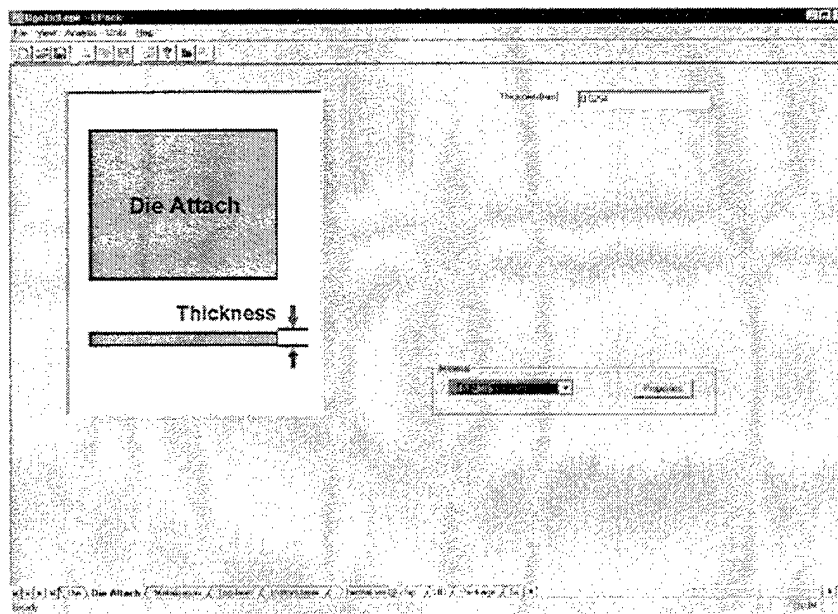
- (5) For new materials or materials not listed in the material library, choose User Defined as the material from the Material dialog box and click Properties to define the material properties.
- (6) Enter a name as the material ID and check the Add to the material Database box if you want to include the new material in the material database for future use.
- (7) Enter **Temp**, **E** (Young's modulus), **nu** (Poisson's ratio), **CTE** (coefficient of thermal expansion), **beta** (moisture swelling coefficient), and **TRef** (reference temperature) at up to nine different temperatures in an ascending order. For materials with constant material properties, simply complete one row of the table.

- (8) The newly defined material can be removed at any time by choosing the material and press the Remove button.



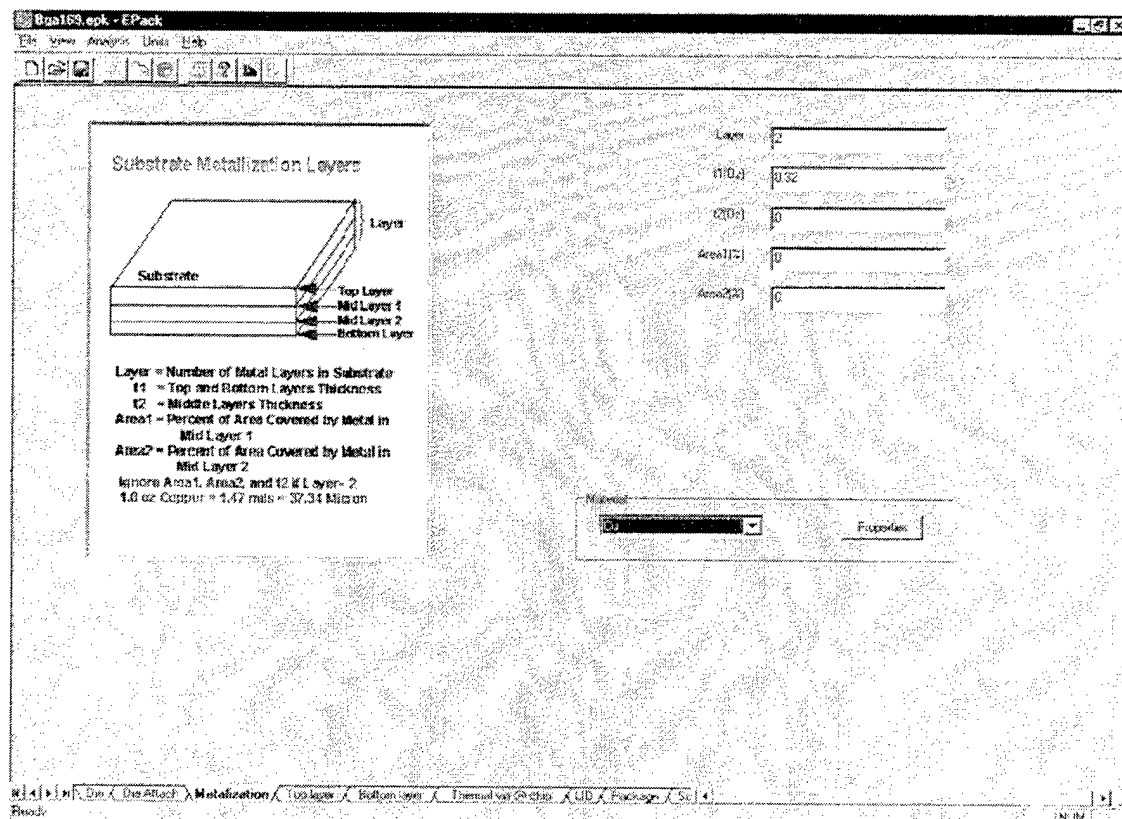
3.1.2 Die Attach

- (1) Input die attach thickness in the dialog box.
- (2) Select or define the die attach material with the same procedure as Step (2) to (8) in Section 3.1.1.



3.1.3 Substrate Metallization

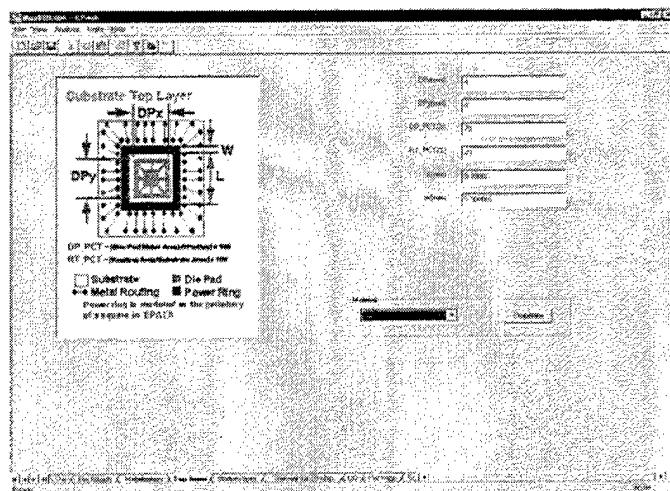
- (1) Input **Layer** (number of metalization layers enter either 2 or 4), **t1** (top and bottom layers thickness), **t2** (middle layers thickness), **Area1** (percent area covered by metal in the upper mid-layer), and **Area2** (percent area covered by metal in the lower mid-layer) in the dialog box. **t2**, **Area1** and **Area2** can be left empty if **Layer** equals to 2. The units for **t1** and **t2** are oz. As indicated in the on-screen illustration, 1 oz of copper (1 oz per square foot) equals to 1.47 mils (37.34 Microns) in thickness.
- (2) Select or define the substrate metalization material with the same procedure as Step (2) to (8) in Section 3.1.1.



In the present EPACK version, it is assumed that the substrate has either 4 or 2 metalization layers. It is also assumed that the top and bottom layers have the same thickness, and the two middle layers (if any) are in the same thickness.

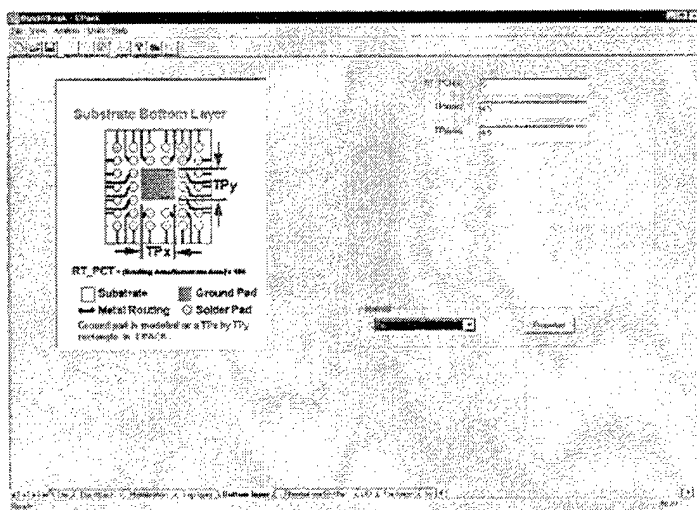
3.1.4 Substrate Metallization Top Layer

- (1) Input **DPX**, **DPY** (die pad widths), **DP_PCT** (percent die pad area covered by metal, = [die pad metal area/DPX/DPY]), **RP_PCT** (percent substrate area covered by metal routing = [metal routing area/substrate area]) and **L** and **W** (dimensions of an equivalent square power ring). Ignore **L** and **W** if there is no power ring in the design.
- (2) Select or define the top layer metalization material with the same procedure as Step (2) to (8) in Section 3.1.1.



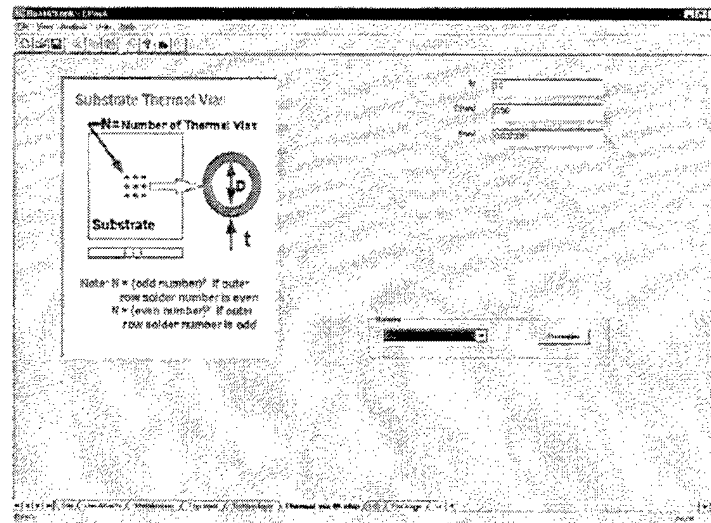
3.1.5 Substrate Metallization Bottom Layer

- (1) Input **RP_PCT** (percent substrate area covered by metal routing = [metal routing area/substrate area]) and **TP_x** and **TP_y** (dimensions of the equivalent rectangular ground pad). Ignore **TP_x** and **TP_y** if there is no ground pad in the design.
- (2) Select or define the bottom layer metalization material with the same procedure as Step (2) to (8) in Section 3.1.1.



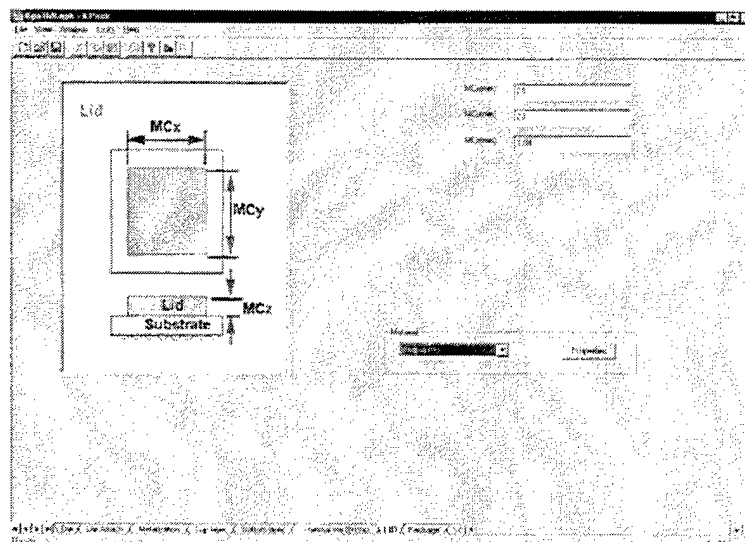
3.1.6 Substrate Thermal Via

- (1) Input **D**, **t** (inside diameter and thickness of the thermal vias) and **N** (number of thermal vias in the substrate). Input **N** as 0 and ignore the inputs for **D** and **t** if there is no thermal via in the substrate. In the current EPACK version, the number of substrate thermal vias, **N**, must be the square of an even number if the outer row solder ball number is an odd number and the square of an odd number if the outer row solder ball number is an even number.
- (2) Select or define the substrate thermal via material with the same procedure as Step (2) to (8) in Section 3.1.1.



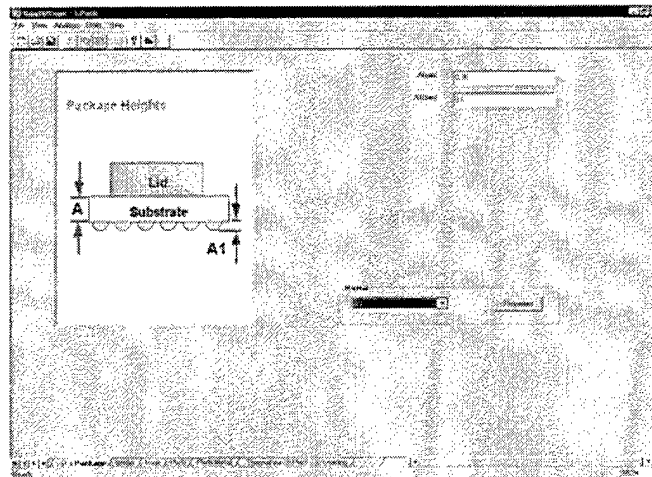
3.1.7 LID (Molding Compound Encapsulation)

- (1) Input **MCx**, **MCy** (widths of the encapsulation) and **MCz** (thickness of the encapsulation).
- (2) Select or define the encapsulation molding compound material with the same procedure as Step (2) to (8) in Section 3.1.1.



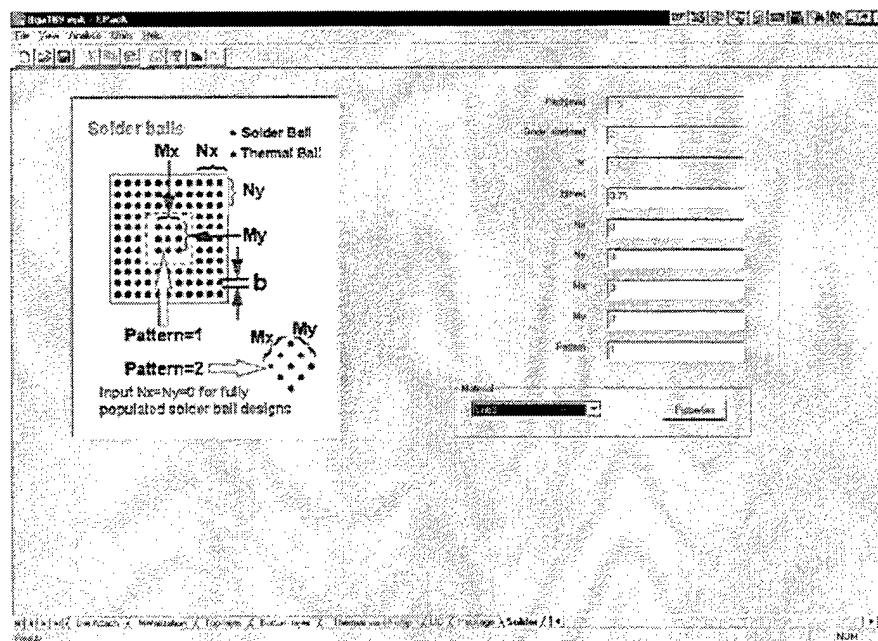
3.1.8 Package

- (1) Input A (substrate thickness) and $A1$ (solder height after reflow collapse). In other words, $A1$ is the gap between the substrate and the PWB.
- (2) Select or define the substrate material with the same procedure as Step (2) to (8) in Section 3.1.1.



3.1.9 Solder Balls

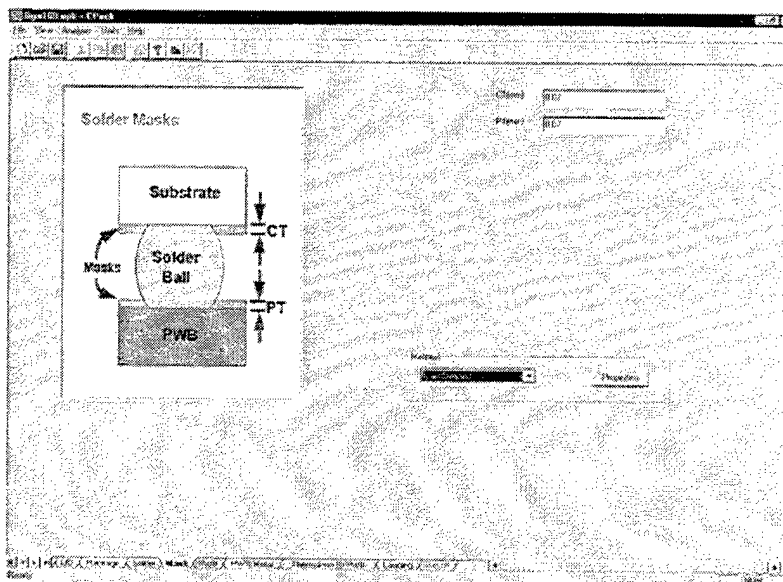
- (1) Input b (solder ball diameter) and Nx , Ny (column and row numbers of outer solder balls) and Mx , My (column and row numbers of inner thermal balls). For packages with populated solder balls (no inner thermal balls), input 0 for Nx and Ny .
- (2) Select or define the solder/thermal ball material with the same procedure as Step (2) to (8) in Section 3.1.1.



Pitch, Body_size and M can not be changed in this menu. However, advanced users can change these numbers by modifying an existing *.EPK files according to the instruction described in Appendix IV.

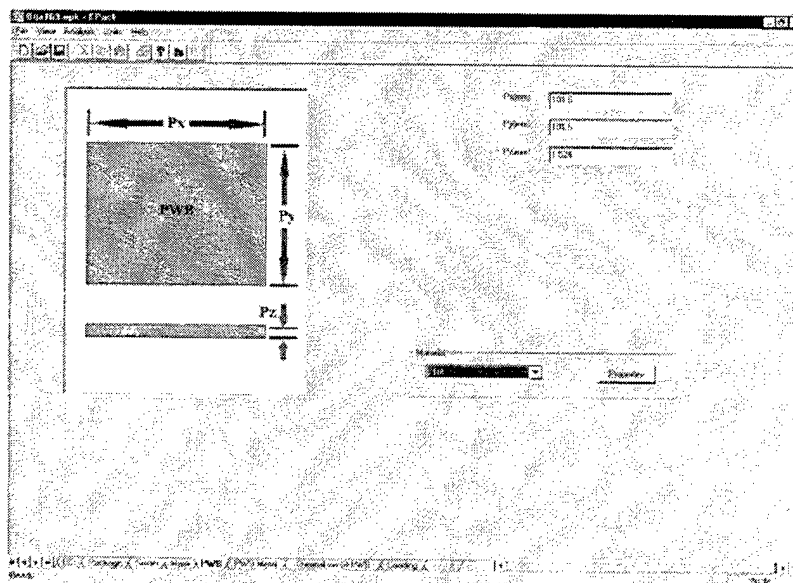
3.1.10 Solder Masks

- (1) Input **CT** and **PT** (solder mask thicknesses).
- (2) Select or define the solder mask material with the same procedure as Step (2) to (8) in Section 3.1.1.



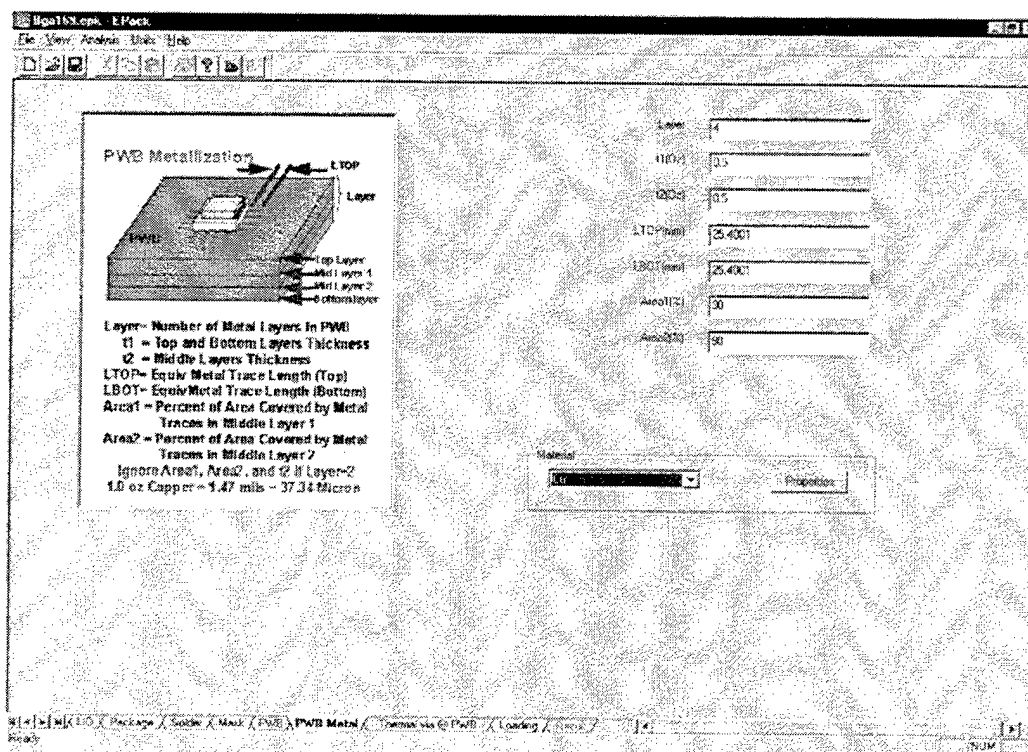
3.1.11 Printed Wire Board (PWB)

- (1) Input **Px**, **Py** (PWB widths) and **Pz** (PWB thickness).
- (2) Select or define the PWB material with the same procedure as Step (2) to (8) in Section 3.1.1.



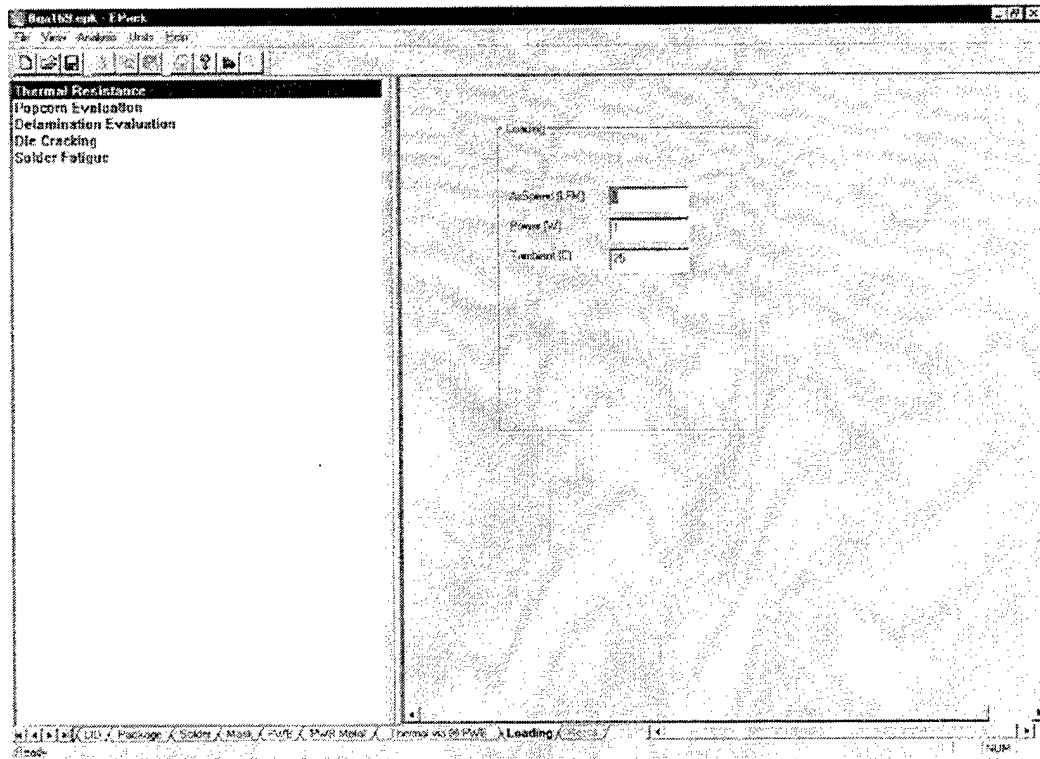
3.1.12 PWB Metallization

- (1) Input **Layer** (number of metalization layers enter either 2 or 4), **t1** (top and bottom layers thickness), **t2** (middle layers thickness), **LTOP** (equivalent metal trace length on the top surface of the PWB), **LBOT** (equivalent metal trace length on the bottom surface of the PWB), **Area1** (percent area covered by metal in the upper mid-layer), and **Area2** (percent area covered by metal in the lower mid-layer) in the dialog box. **t2**, **Area1** and **Area2** can be left empty if **Layer** equals to 2. The units for **t1** and **t2** are oz. As indicated in the on-screen illustration, 1 oz of copper (1 oz per square foot) equals to 1.47 mils (37.34 Microns) in thickness. For a typical thermal test board, **LTOP** and **LBOT** are usually between 0.5" to 1.0".
- (2) Select or define the PWB metalization material with the same procedure as Step (2) to (8) in Section 3.1.1.



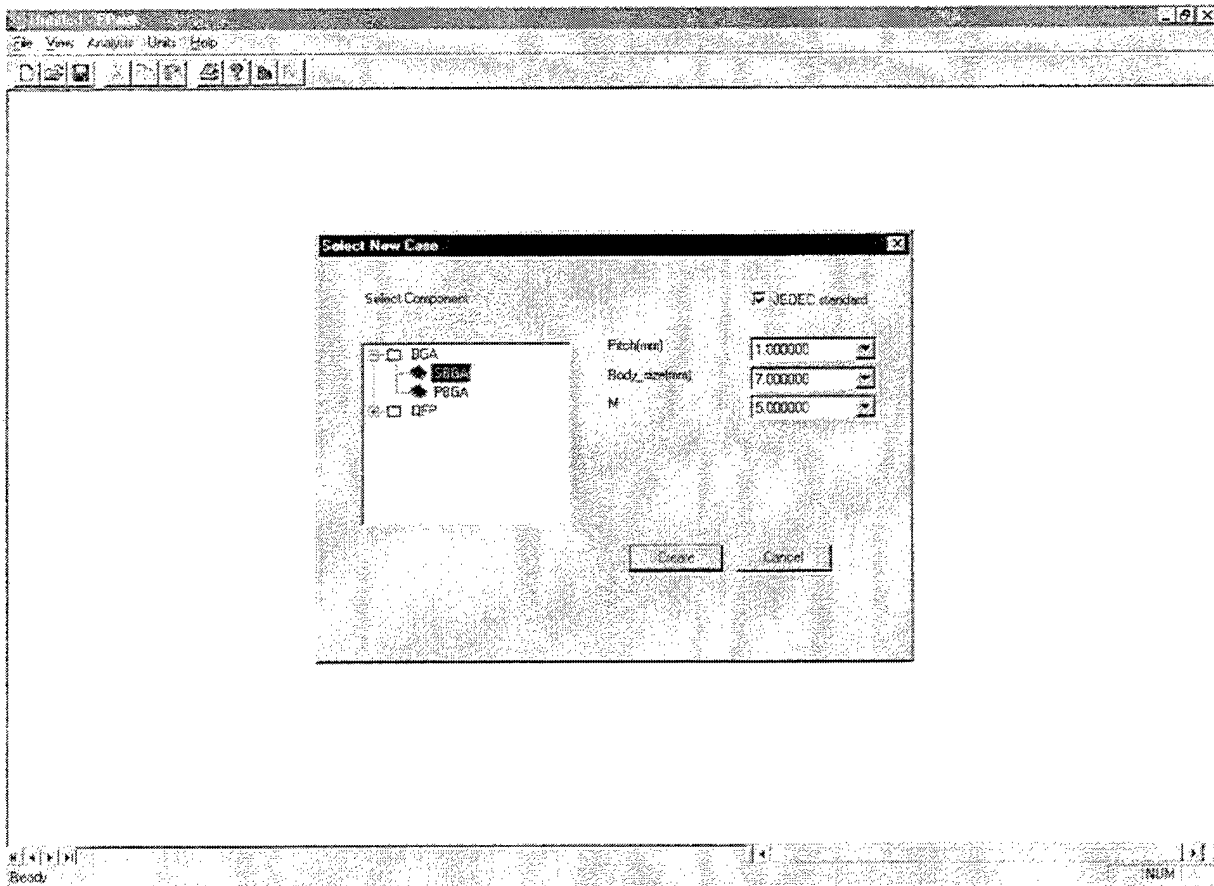
3.1.13 Loading, Running, and Results

- (1) Pick the desired evaluation item from the on-screen menu.
- (2) Please refer to Appendix I for detailed input instructions of each analysis item.
- (3) Please refer to Appendix II for instructions of launching the analysis.
- (4) Please refer to Appendix III for results reviewing and plotting.



3.2 SBGA

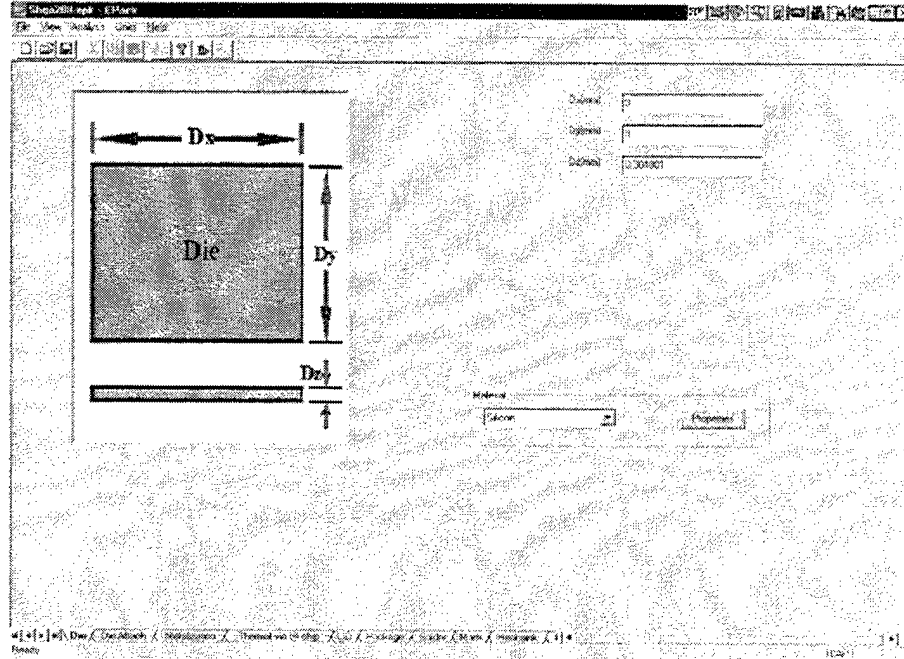
From **File-New** in the main menu, click **BGA-SBGA**, pick appropriate **Pitch** (solder ball pitch), **Body_size** (package widths) and **M** (number of outer rows of the solder balls) sequentially from the menu, and click **Create** to start the analysis for a JEDEC standard PBGA package. For PBGA packages no registered in JEDEC, simply click the **JEDEC Standard** dialog box to clear the check mark and enter **Pitch**, **Body_size**, and **M** in the same way. A check mark in the **JEDEC Standard** dialog box means that the package is a JEDEC registered package, and an empty **JEDEC Standard** dialog box indicates that the package is a Non-JEDEC registered customized PBGA package.



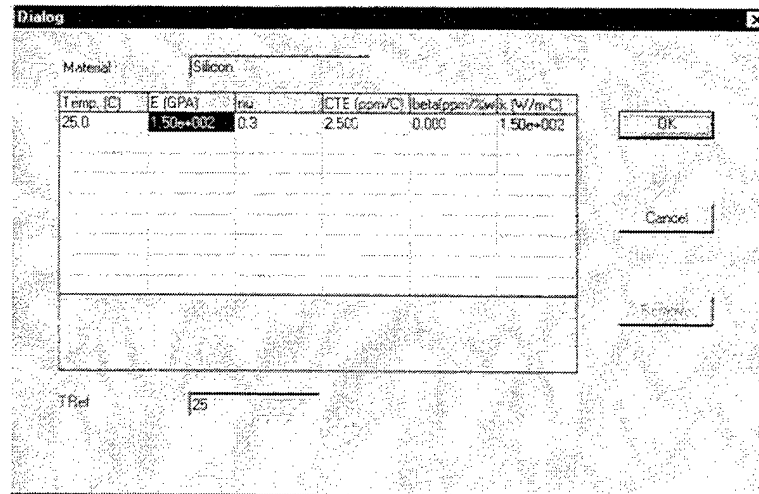
As illustrated near the bottom edge of the following figure, there are 15 sub-menus for PBGA packages: **Die**, **Die Attach**, **Metallization** (metallization in substrate), **Thermal via @ chip**, **LID**, **Package**, **Solder**, **Mask**, **Heat Sink**, **HS attach**, **Substrate Attach**, **PWB**, **PWB Metal**, **Loading**, and **Results**. Go through all the submenus to complete the analysis journey.

3.2.1 Die

- (1) Input die widths (**Dx** and **Dy**) and thickness (**Dz**) into the corresponding dialog boxes on screen.
- (2) Click Unit on top of the screen to switch between **Metric** and **English** units at any time.
- (3) Click the Material dialog box and choose a die material from the library.

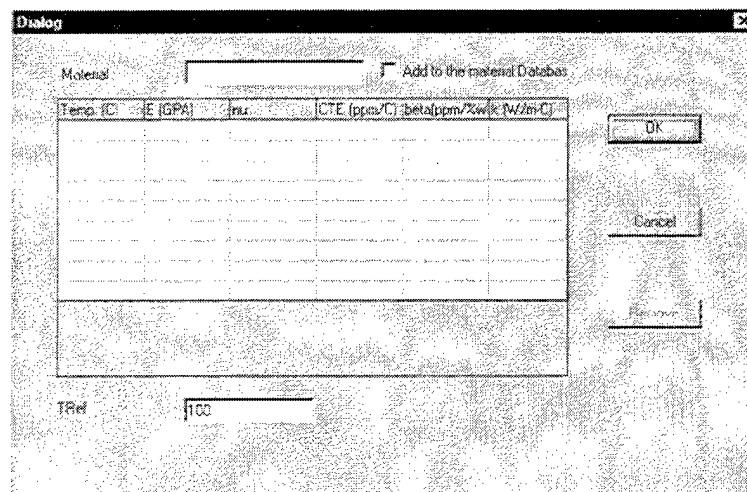


- (4) Click the Properties button to review the temperature material properties.



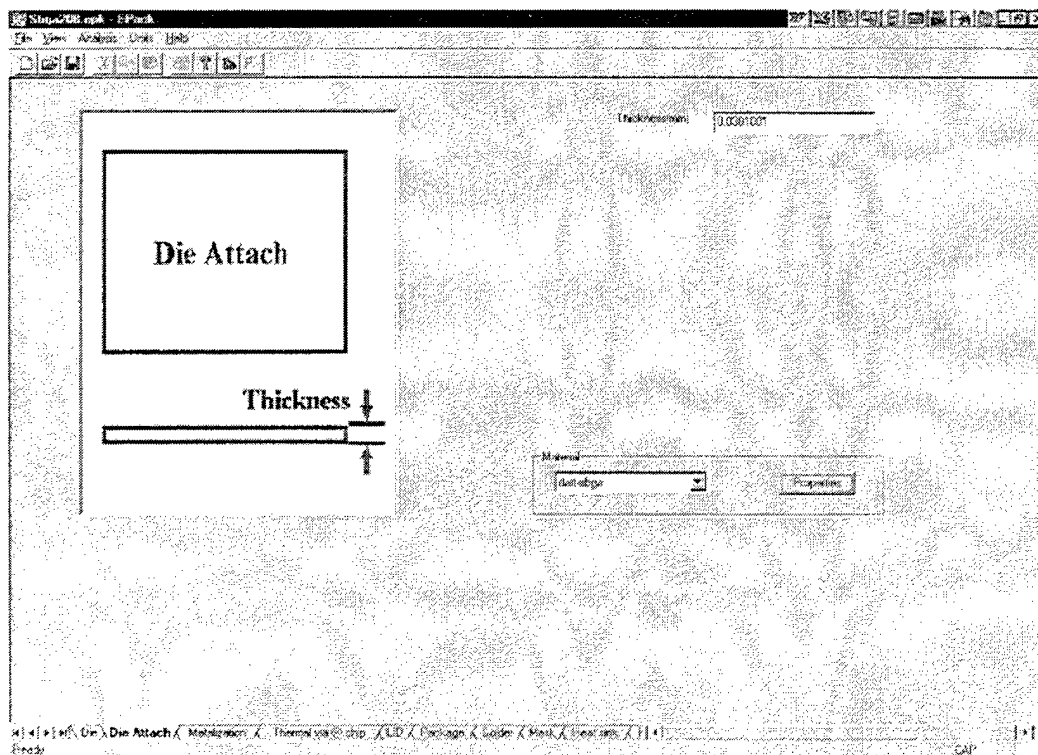
- (5) For new materials or materials not listed in the material library, choose User Defined as the material from the Material dialog box and click Properties to define the material properties.
- (6) Enter a name as the material ID and check the Add to the material Database box if you want to include the new material in the material database for future use.

- (7) Enter **Temp**, **E** (Young's modulus), **nu** (Poisson's ratio), **CTE** (coefficient of thermal expansion), **beta** (moisture swelling coefficient), and **TRef** (reference temperature) at up to nine different temperatures in an ascending order. For materials with constant material properties, simply complete one row of the table.
- (8) The newly defined material can be removed at any time by choosing the material and press the Remove button.



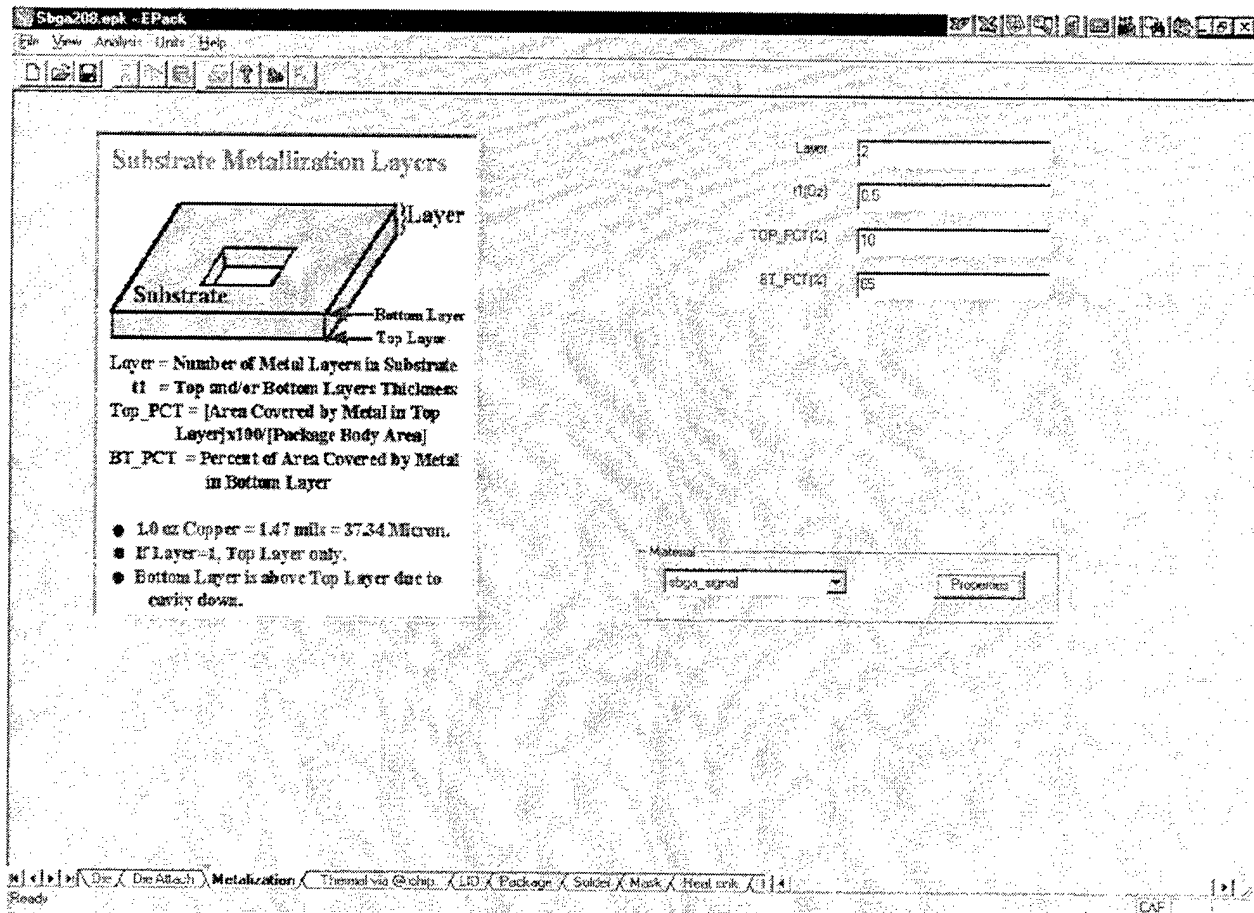
3.2.2 Die Attach

- (1) Input die attach thickness in the dialog box.
- (2) Select or define the die attach material with the same procedure as Step (2) to (8) in Section 3.2.1.



3.2.3 Substrate Metallization

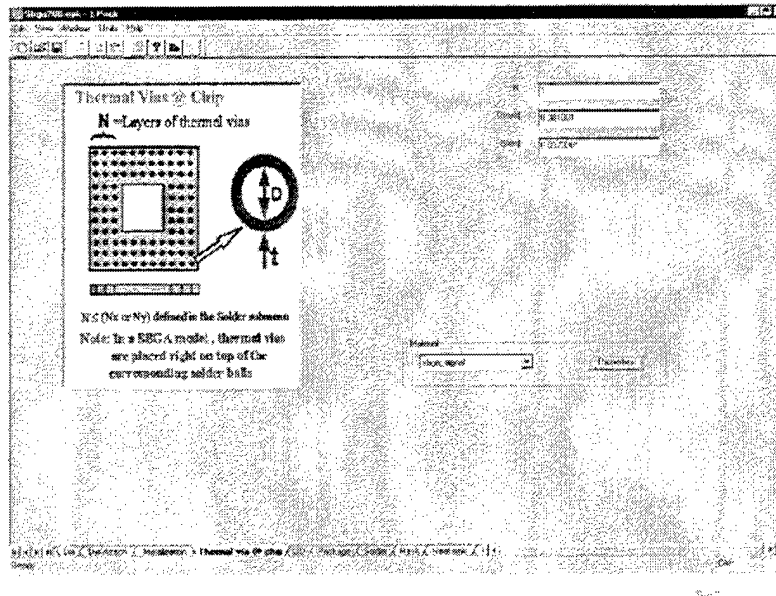
- (1) Input **Layer** (number of metalization layers enter either 2 or 4), **t1** (top and bottom layers thickness), **t2** (middle layers thickness), **Area1** (percent area covered by metal in the upper mid-layer), and **Area2** (percent area covered by metal in the lower mid-layer) in the dialog box. **t2**, **Area1** and **Area2** can be left empty if **Layer** equals to 2. The units for **t1** and **t2** are oz. As indicated in the on-screen illustration, 1 oz of copper (1 oz per square foot) equals to 1.47 mils (37.34 Microns) in thickness.
- (2) Select or define the substrate metalization material with the same procedure as Step (2) to (8) in Section 3.2.1.



In the present EPACK version, it is assumed that the substrate has either 4 or 2 metalization layers. It is also assumed that the top and bottom layers have the same thickness, and the two middle layers (if any) are in the same thickness.

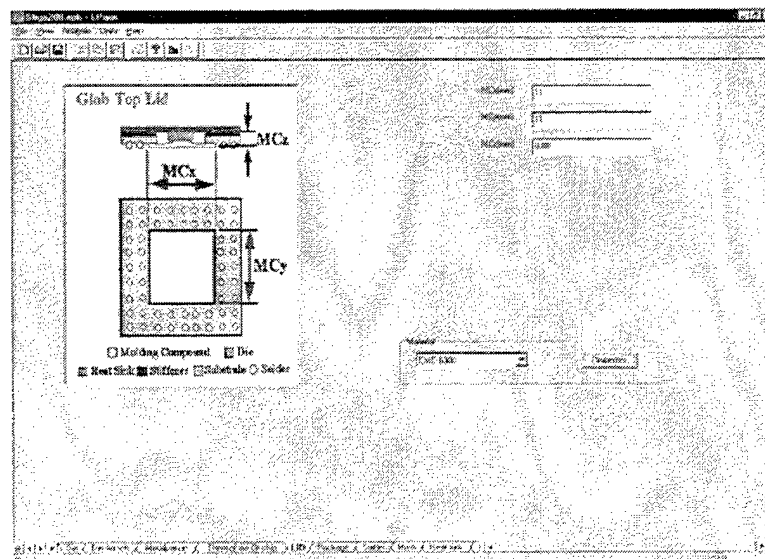
3.2.4 Substrate Thermal Via

- (1) Input **D**, **t** (inside diameter and thickness of the thermal via) and **N** (number of thermal vias in the substrate). Input **N** as 0 and ignore the inputs for **D** and **t** if there is no thermal via in the substrate. In the current EPACK version, the number of substrate thermal vias, **N**, must be the square of an even number if the outer row solder ball number is an odd number and the square of an odd number if the outer row solder ball number is an even number.
- (2) Select or define the substrate thermal via material with the same procedure as Step (2) to (8) in Section 3.2.1.



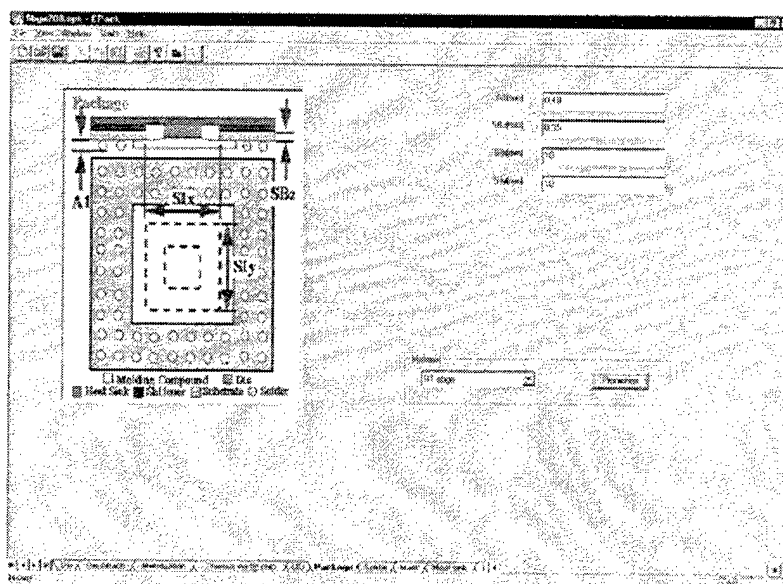
3.2.5 LID (Molding Compound Encapsulation)

- (1) Input **MCx**, **MCy** (widths of the encapsulation) and **MCz** (thickness of the encapsulation).
- (2) Select or define the encapsulation molding compound material with the same procedure as Step (2) to (8) in Section 3.2.1.



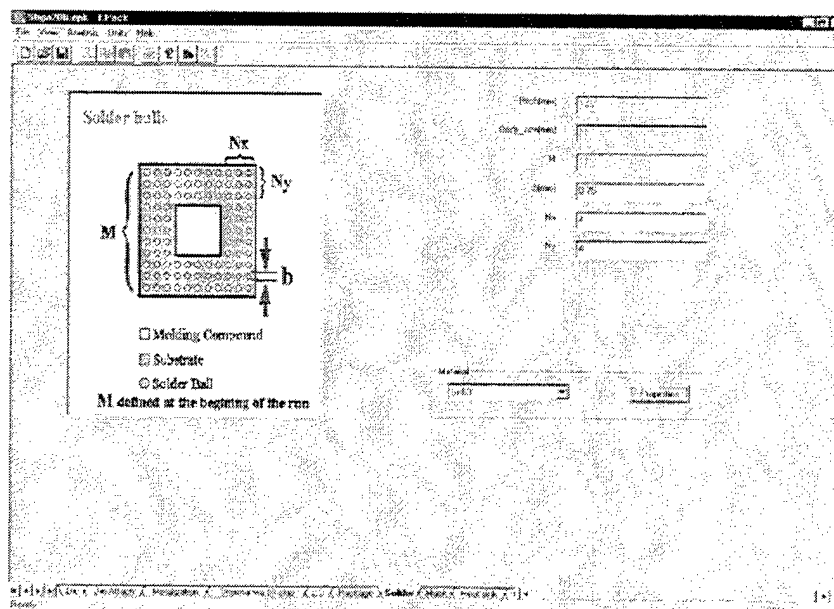
3.2.6 Package

- (1) Input **A1** (solder height after reflow collapse), **SBz** (substrate thickness), and **SIx** and **SIy** (substrate window widths). In other words, **A1** is the gap between the substrate and the PWB.
- (2) Select or define the substrate material with the same procedure as Step (2) to (8) in Section 3.2.1.



3.2.7 Solder Balls

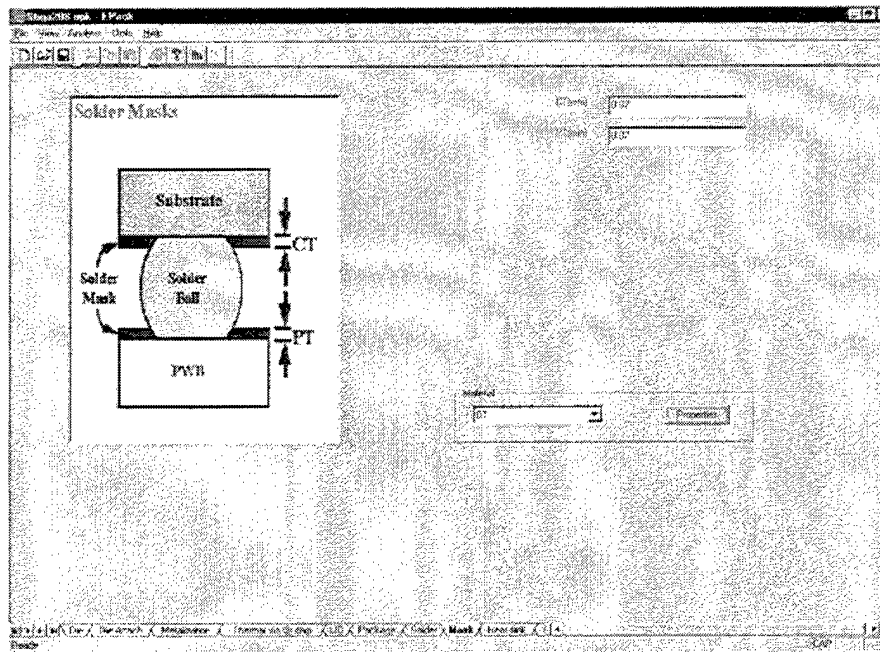
- (1) Input **b** (solder ball diameter) and **Nx**, **Ny** (column and row numbers of outer solder balls).
- (2) Select or define the solder/thermal ball material with the same procedure as Step (2) to (8) in Section 3.2.1.



Pitch, **Body_size**, and **M** can not be changed in this menu. However, for advanced users, these numbers of an existing EPACK model can be changed by modifying the *.EPK file. Please refer to Appendix IV for details.

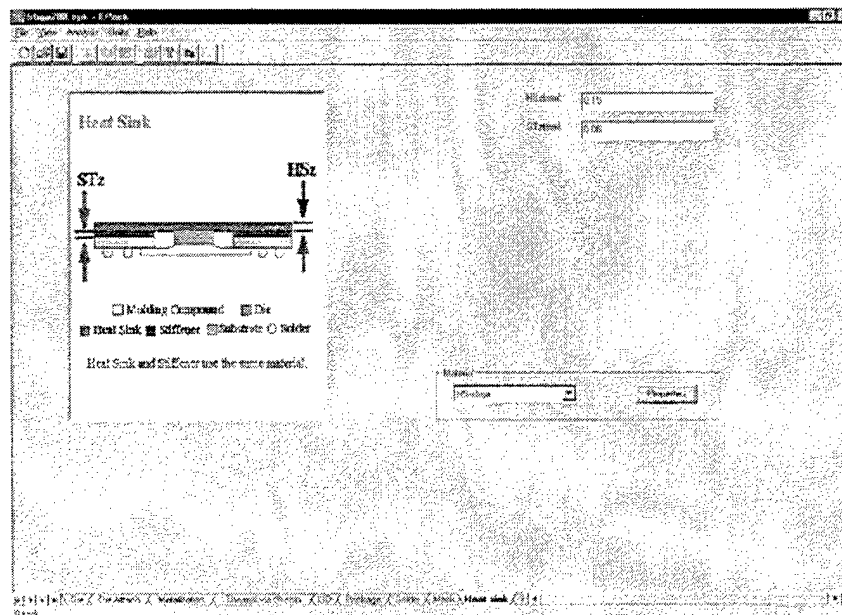
3.2.8 Solder Masks

- (1) Input **CT** and **PT** (solder mask thicknesses).
- (2) Select or define the solder mask material with the same procedure as Step (2) to (8) in Section 3.2.1.



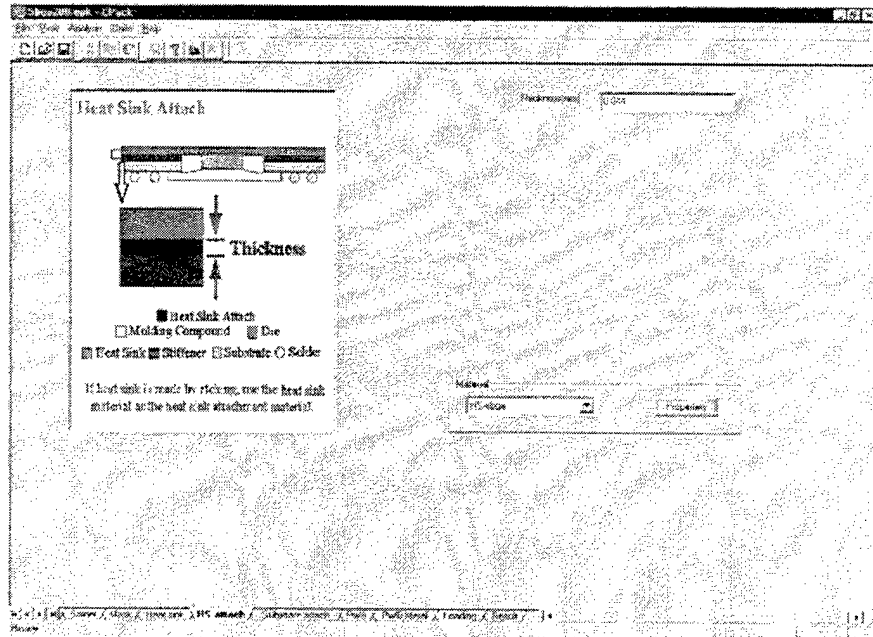
3.2.9 Heat Sink

- (1) Input **HSz** (heat sink thickness) and **STz** (stiffener thickness).
- (2) Select or define the heat sink ball material with the same procedure as Step (2) to (8) in Section 3.2.1.



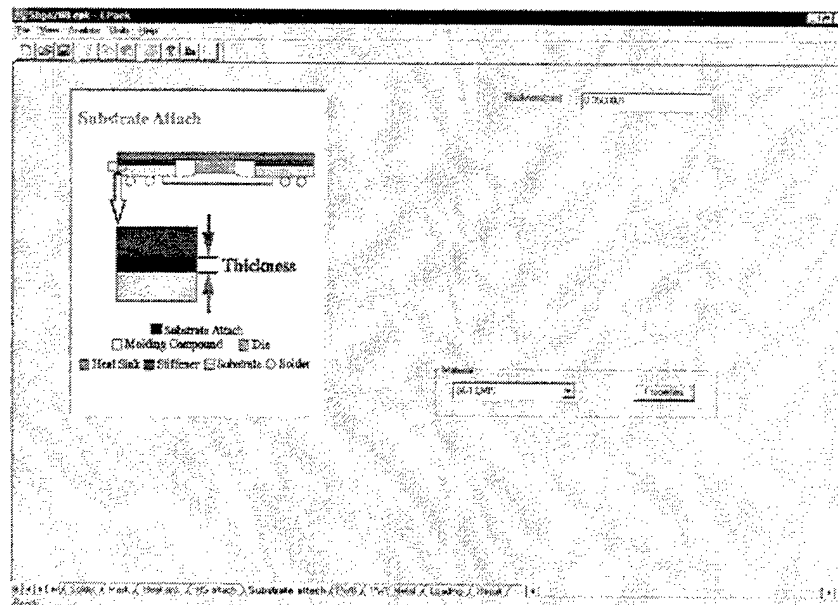
3.2.10 HS Attach

- (1) Input **Thickness** (heat sink attach thickness).
- (2) Select or define the heat sink attach material with the same procedure as Step (2) to (8) in Section 3.2.1.



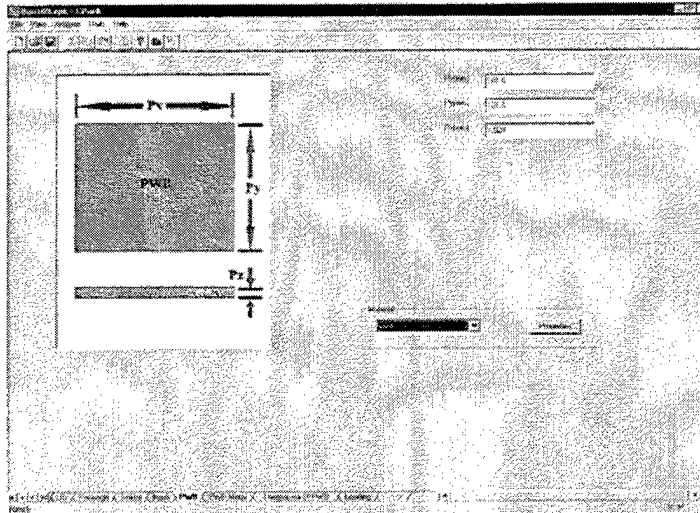
3.2.11 Substrate Attach

- (1) Input **Thickness** (substrate attach thickness).
- (2) Select or define the substrate attach material with the same procedure as Step (2) to (8) in Section 3.2.1.



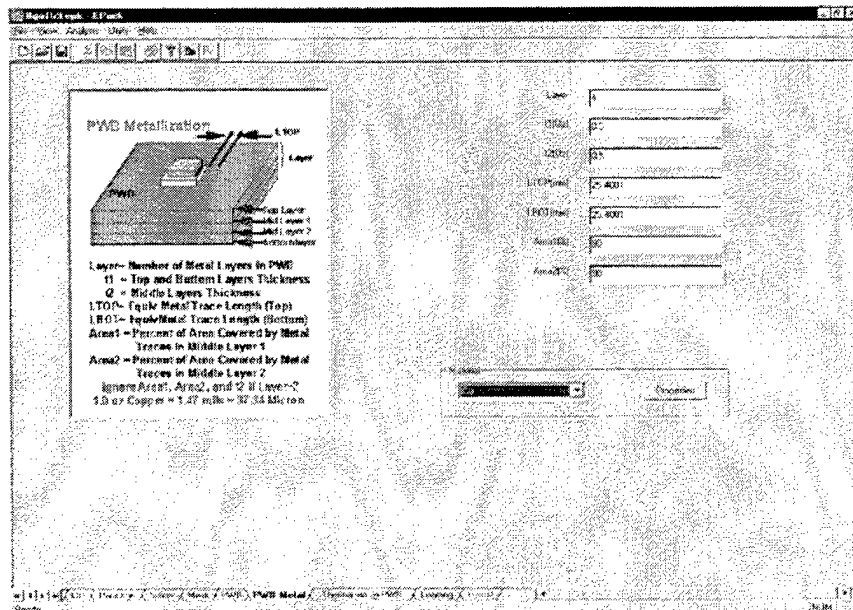
3.2.12 Printed Wire Board (PWB)

- (1) Input **Px**, **Py** (PWB widths) and **Pz** (PWB thickness).
- (2) Select or define the PWB material with the same procedure as Step (2) to (8) in Section 3.2.1.



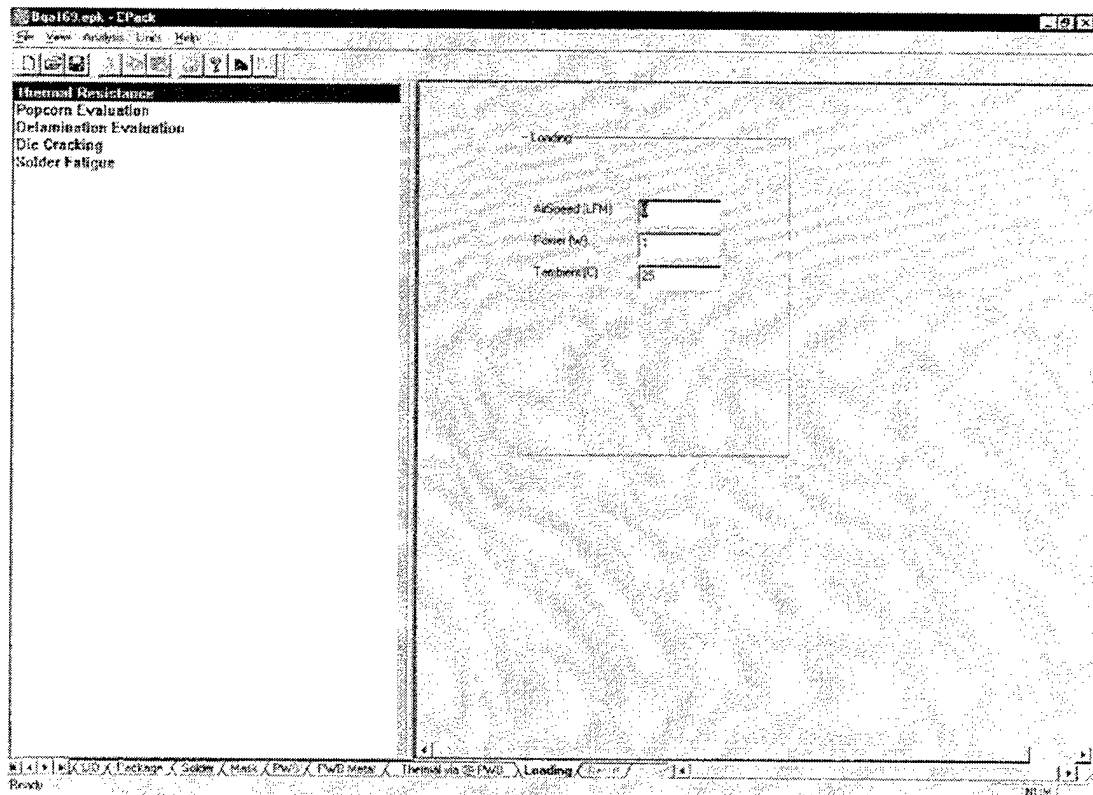
3.2.13 PWB Metallization

- (1) Input **Layer** (number of metalization layers enter either 2 or 4), **t1** (top and bottom layers thickness), **t2** (middle layers thickness), **LTOP** (equivalent metal trace length on the top surface of the PWB), **LBOT** (equivalent metal trace length on the bottom surface of the PWB), **Area1** (percent area covered by metal in the upper mid-layer), and **Area2** (percent area covered by metal in the lower mid-layer) in the dialog box. **t2**, **Area1** and **Area2** can be left empty if **Layer** equals to 2. The units for **t1** and **t2** are oz. As indicated in the on-screen illustration, 1 oz of copper (1 oz per square foot) equals to 1.47 mils (37.34 Microns) in thickness. For a typical thermal test board, **LTOP** and **LBOT** are usually between 0.5" to 1.0".
- (2) Select or define the PWB metallization material with the same procedure as Step (2) to (8) in Section 3.2.1.



3.2.14 Loading, Running, and Results

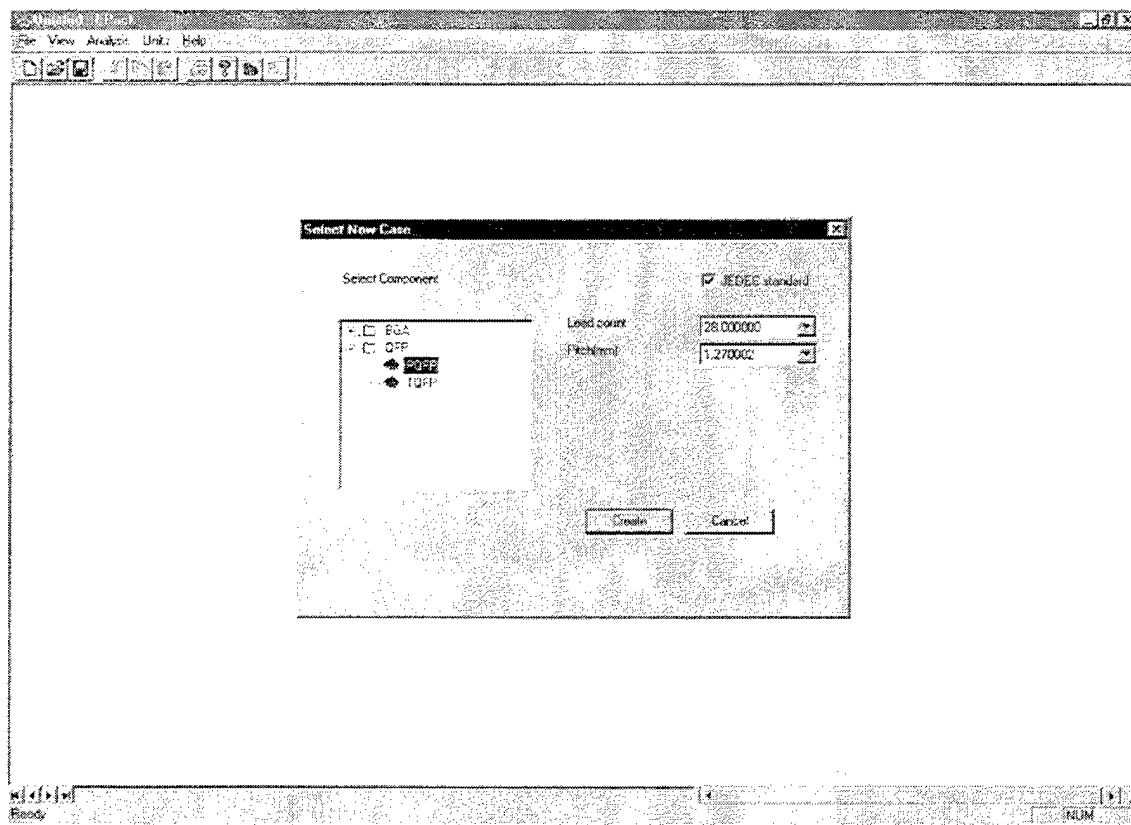
- (1) Pick the desired evaluation item from the on-screen menu.
- (2) Please refer to Appendix I for detailed input instructions of each analysis item.
- (3) Please refer to Appendix II for instructions of launching the analysis.
- (4) Please refer to Appendix III for results reviewing and plotting.



4. QFP

4.1 PQFP

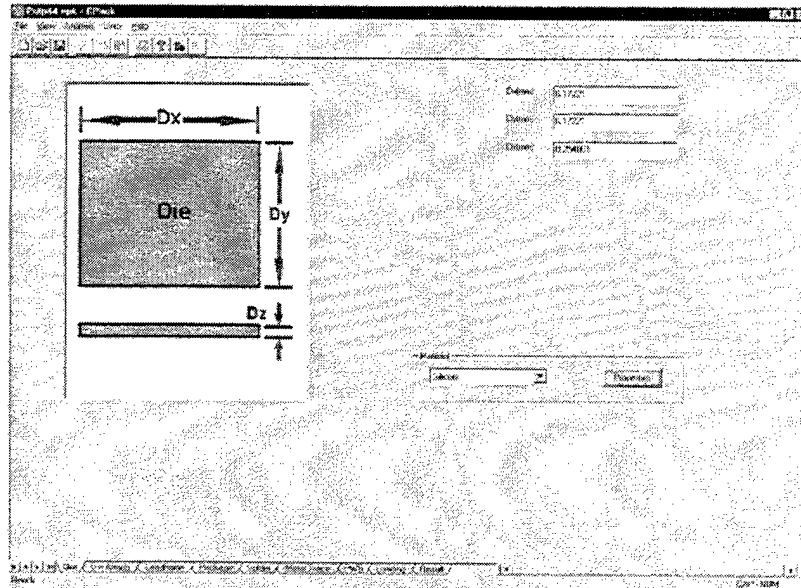
From **File-New** in the main menu, click **QFP-PQFP**, pick appropriate **Lead count** (package lead count) and **Pitch** (leadframe pitch) sequentially from the menu, and click **Create** to start the analysis. For PQFP packages no registered in JEDEC, simply click the **JEDEC Standard** dialog box to clear the check mark and enter **Lead count** and **Pitch** in the same way. A check mark in the **JEDEC Standard** dialog box means that the package is a JEDEC registered package, and an empty **JEDEC Standard** dialog box indicates that the package is a Non-JEDEC registered customized PBGA package.



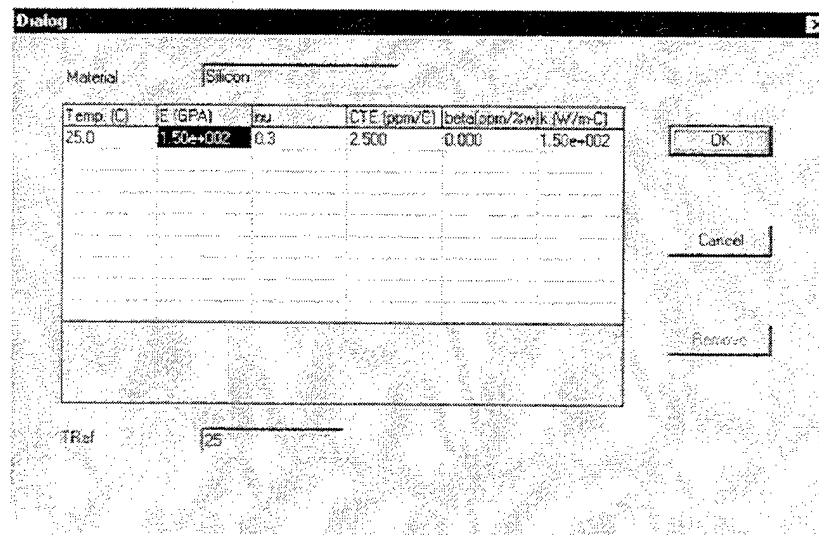
As illustrated near the bottom edge of the following figure, there are 10 sub-menus for PQFP packages: **Die**, **Die Attach**, **Leadframe**, **Package**, **Solder**, **PWB Metal Trace**, **PWB**, **Heat Sink**, **Loading**, and **Results**. Go through all the submenus to complete the analysis journey.

4.1.1 Die

- (1) Input die widths (**Dx** and **Dy**) and thickness (**Dz**) into the corresponding dialog boxes on screen.
- (2) Click Unit on top of the screen to switch between **Metric** and **English** units at any time.
- (3) Click the Material dialog box and choose a die material from the library.



- (4) Click the Properties button to review the temperature material properties.



- (5) For new materials or materials not listed in the material library, choose User Defined as the material from the Material dialog box and click Properties to define the material properties.
- (6) Enter a name as the material ID and check the Add to the material Database box if you want to include the new material in the material database for future use.

- (7) Enter **Temp**, **E** (Young's modulus), **nu** (Poisson's ratio), **CTE** (coefficient of thermal expansion), **beta** (moisture swelling coefficient), and **TRef** (reference temperature) at up to nine different temperatures in an ascending order. For materials with constant material properties, simply complete one row of the table.
- (8) The newly defined material can be removed at any time by choosing the material and press the Remove button.

The 'Dialog' window contains the following elements:

- Material:** A text input field.
- Add to the material Database:** A checkbox.
- Table:** A table with 6 columns: Temp. (C), E (GPa), nu, CTE (ppm/C), beta(ppm/%w/k (w/m-C)), and an empty column. There are 9 rows for data entry.
- Buttons:** 'OK', 'Cancel', and 'Random'.
- TRef:** A text input field with the value '100'.

4.1.2 Die Attach

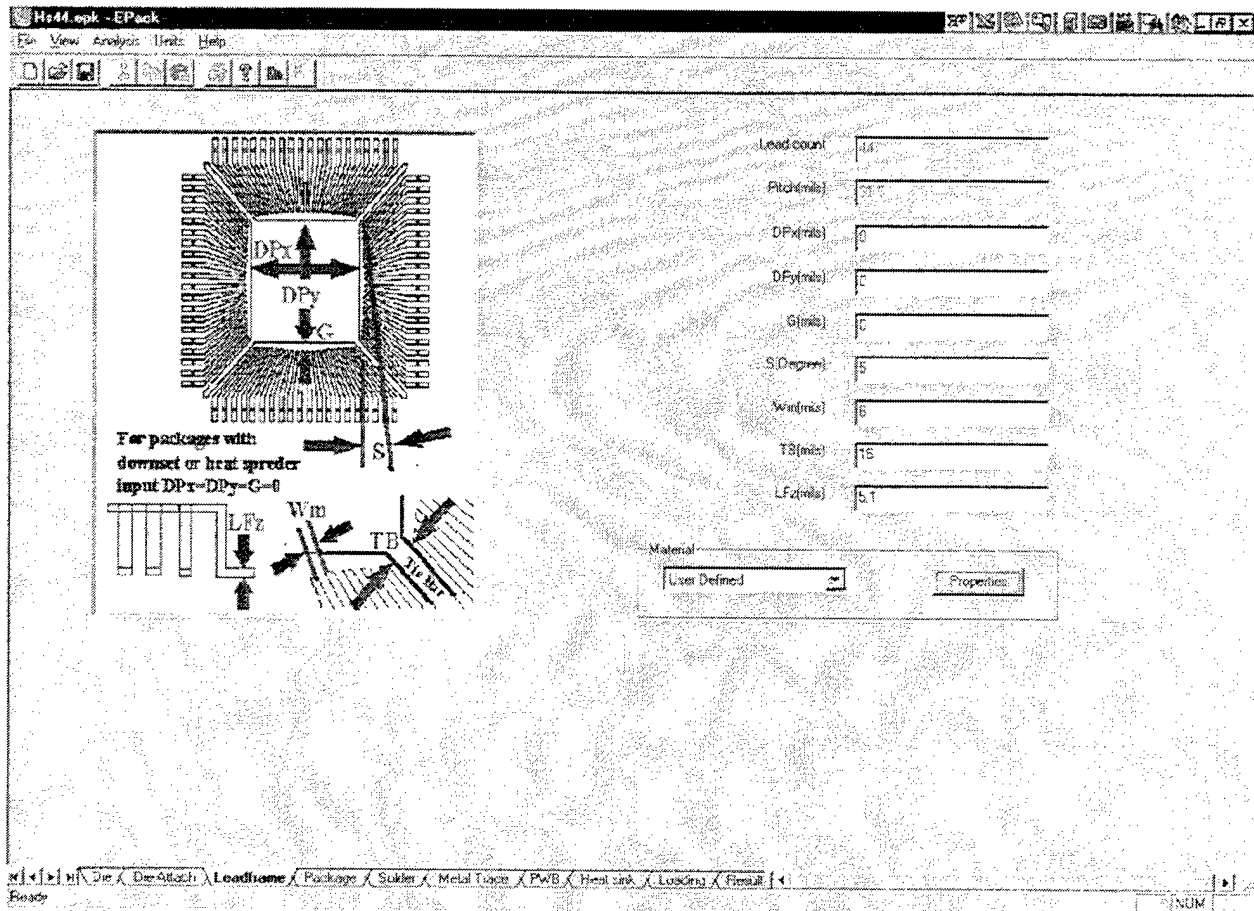
- (1) Input die attach thickness in the dialog box.
- (2) Select or define the die attach material with the same procedure as Step (2) to (8) in Section 4.1.1.

The 'Die Attach' dialog box includes the following elements:

- Diagram:** A schematic showing a square labeled 'Die Attach' above a horizontal bar labeled 'Thickness' with arrows indicating its extent.
- Thickness:** A text input field.
- Material:** A dropdown menu with 'Sn70Ag30' selected.
- Buttons:** 'OK' and 'Cancel'.

4.1.3 Leadframe

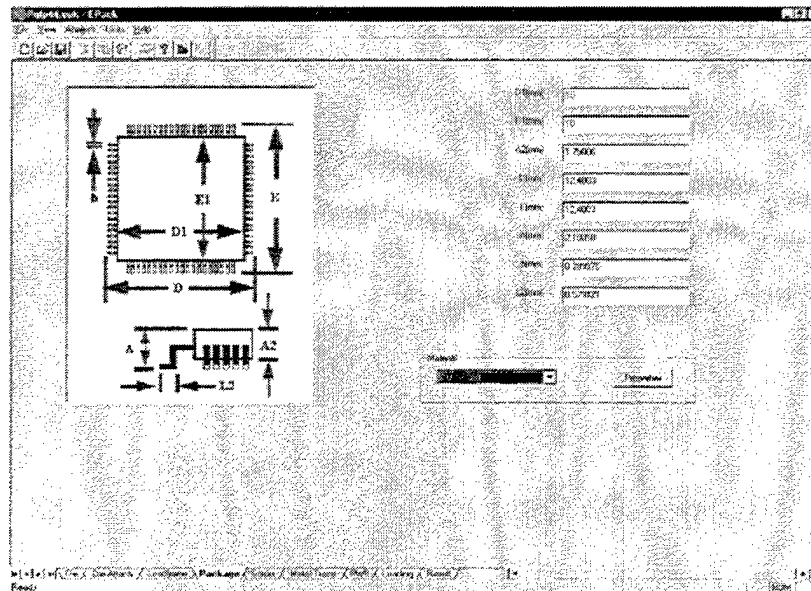
- (1) Input **DPx**, **DPy** (die attachment pad widths), **G** (the maximum gap between die pad and lead fingers), **S** (slope of die pad/lead finger gaps), **Wm** (lead figure width), **TB** (tie bar width), and **Lfz** (leadframe thickness) in the dialog box. **t2**, **Area1** and **Area2** can be left empty if **Layer** equals to 2. The units for **t1** and **t2** are oz. As indicated in the on-screen illustration, 1 oz of copper (1 oz per square foot) equals to 1.47 mils (37.34 Microns) in thickness. For packages with downset or heat sink, enter zero for **Dpx**, **Dpy**, and **G**. Additional details of the die pad and downset will be defined in the **Heat Sink** submenu.
- (2) Select or define the substrate metalization material with the same procedure as Step (2) to (8) in Section 3.1.



In the on-screen menu, the lead count and pitch of the selected PQFP package are also displayed in the dim dialog boxes. EPACK does not allow users to change numbers in the dim dialog boxes. However, for advanced users, these numbers can be changed by modifying the *.EPK file from a previous run. Details on how to modify the *.EPK file are described in Appendix IV.

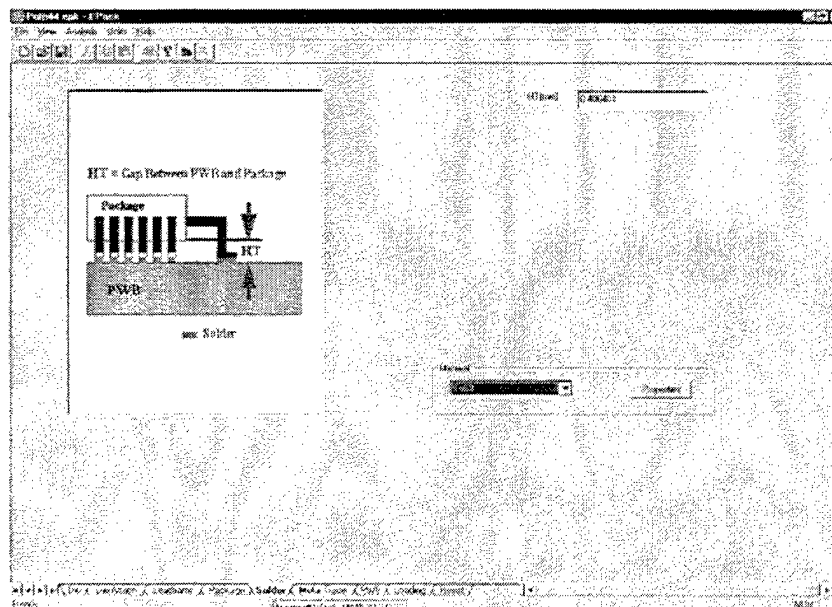
4.1.4 Package

- (1) Input **D1**, **E1** (package body widths), **A2** (package body thickness), **D**, **E** (overall package widths), **A** (overall package thickness), **b** (lead width) and **L2** (lead footprint length).
- (2) Select or define the encapsulation molding compound material with the same procedure as Step (2) to (8) in Section 4.1.1.



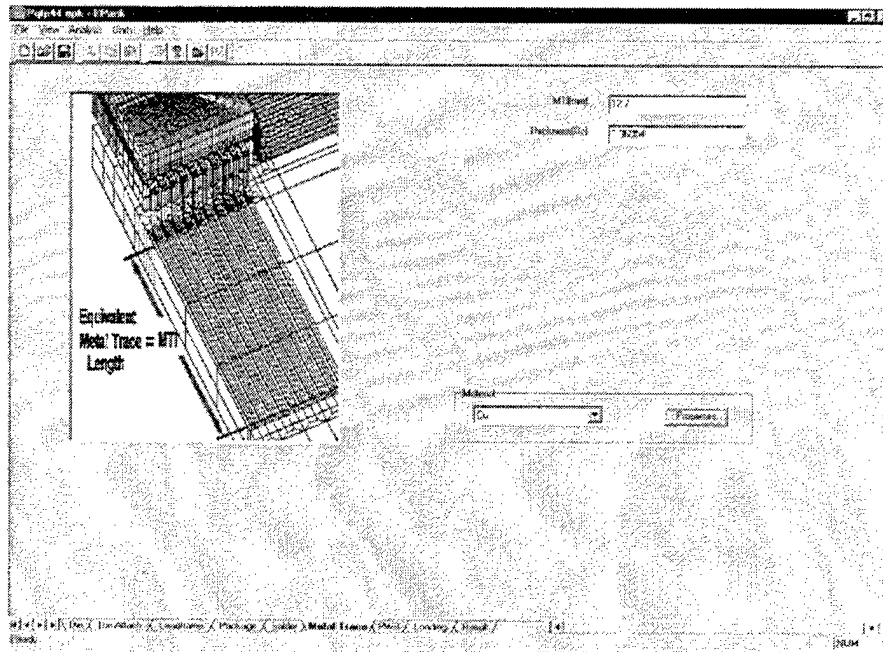
4.1.5 Solder

- (1) Input **HT** (gap between bottom surface of the package body and the PWB).
- (2) Select or define the solder material with the same procedure as Step (2) to (8) in Section 4.1.1.



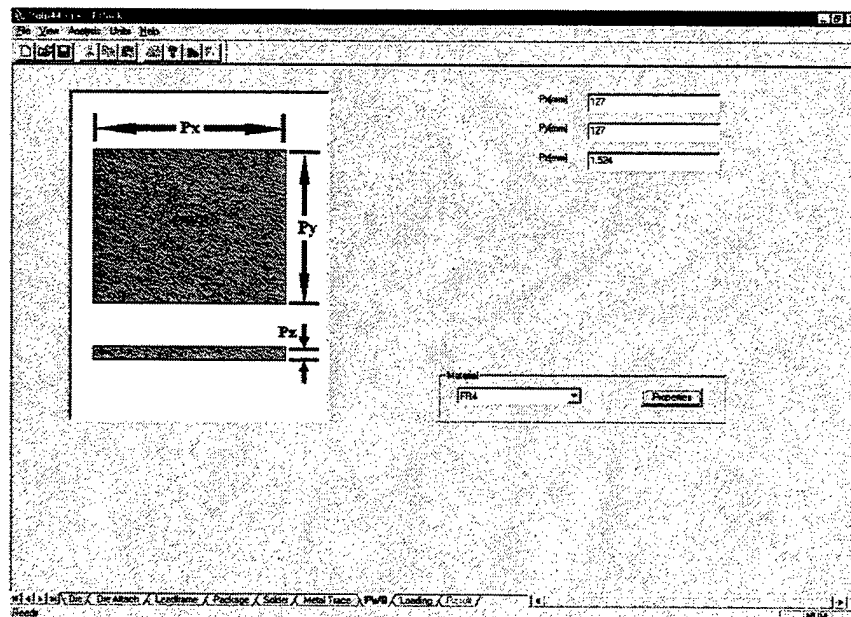
4.1.6 PWB Metal Trace

- (1) Input **MTL** (equivalent metal trace length on the PWB) and **Thickness** (thickness of the metal trace)
- (2) Select or define the metal trace material with the same procedure as Step (2) to (8) in Section 4.1.1.



4.1.7 PWB

- (1) Input **Px**, **Py** (widths of the PWB) and **Pz** (thickness of the PWB).
- (2) Select or define the PWB material with the same procedure as Step (2) to (8) in Section 4.1.1.



4.1.8 Heat Sink

- (1) Input **DS** (downset), **FI** (embedded lead finger length), **Bx**, **By** (die pad widths), **Bz** (die pad thickness), **Wx**, **Wy** (equivalent heat sink or heat spreader widths), **Az** (molding compound thickness underneath the heat sink), and **Mat_Pad** (die pad material index). For packages without die pad (i.e., die mounted directly to the heat sink), input **Bx**, **By**, and **Bz** as zero (0).
- (2) Select or define the PWB material with the same procedure as Step (2) to (8) in Section 4.1.1.

The screenshot displays the 'He44.epk - EPack' software window. On the left, a cross-sectional diagram illustrates the assembly layers: Die, Pad, LF (Lead Finger), Heat, and Spreader. Dimensions are labeled: **FI** (Lead Finger length), **DS** (Downset), **Az** (Molding compound thickness), **Bx**, **By**, **Bz** (Die pad dimensions), and **Wx**, **Wy** (Heat sink/spreader dimensions). A legend identifies the layers: Die (hatched), Pad (dotted), LF (solid black), Heat (white), and Spreader (white). Below the diagram, it states: 'Die Pad Material: M_Pad = 1 (hatched) = 2 (dotted)'. Instructions follow: 'Input Bz=0 for packages with no pad. Skip this sub-menu if no downset & LIS.'

On the right, a table of input parameters is shown:

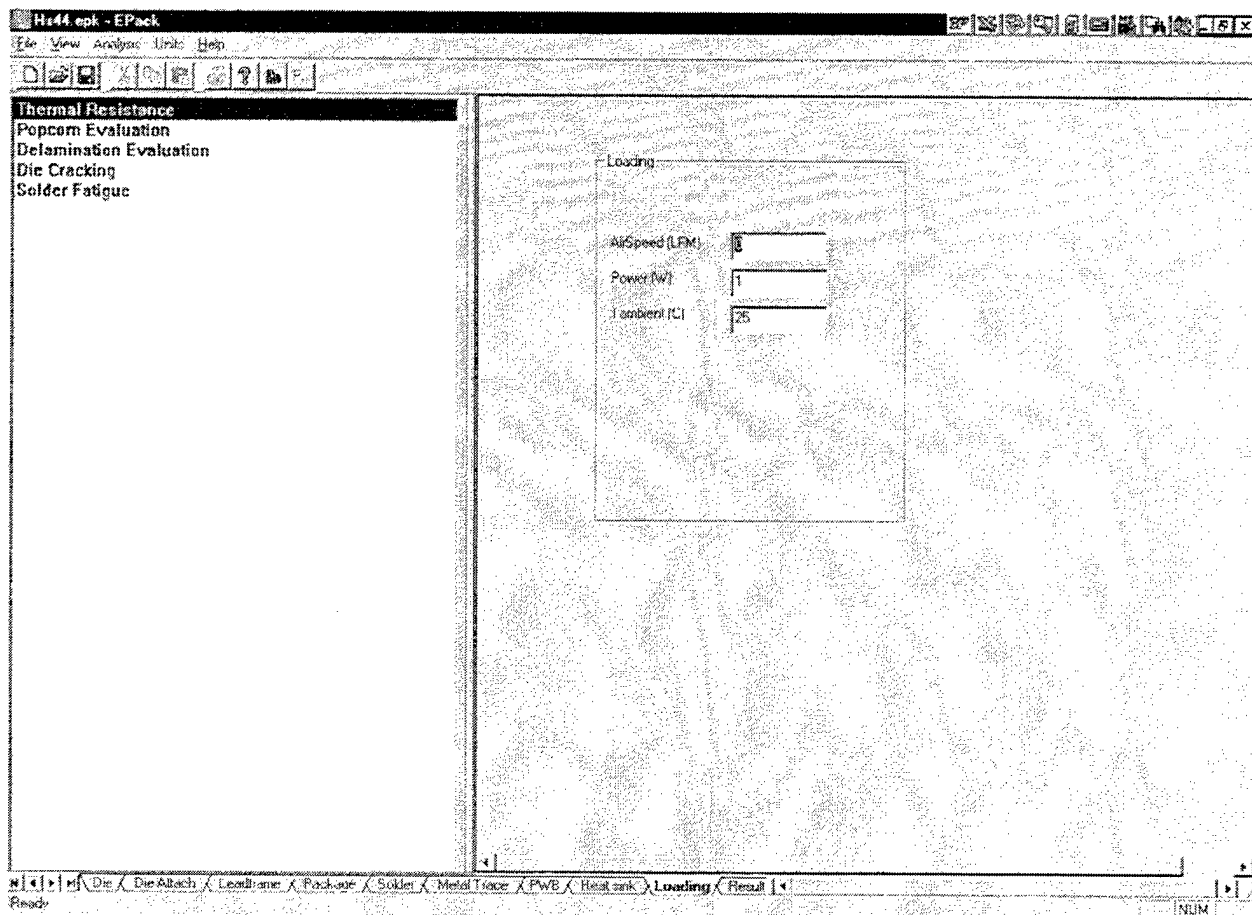
DS(mils)	7.5
FI(mils)	31.35
Bx(mils)	251
By(mils)	251
Bz(mils)	6
Wx(mils)	360
Wy(mils)	360
Az(mils)	10
Mat_Pad	1

Below the table, a 'Material' dropdown menu is set to 'Cu', with a 'Properties...' button next to it.

The bottom status bar shows the navigation path: 'Ready' | 'Die Attach' | 'Leadframe' | 'Package' | 'Solder' | 'Metal Fin' | 'PWB' | 'Heat sink' | 'Loading' | 'Finish' | 'NUM'.

4.1.9 Loading, Running, and Results

- (1) Pick the desired evaluation item from the on-screen menu.
- (2) Please refer to Appendix I for detailed input instructions of each analysis item.
- (3) Please refer to Appendix II for instructions of launching the analysis.
- (4) Please refer to Appendix III for results reviewing and plotting.



2.

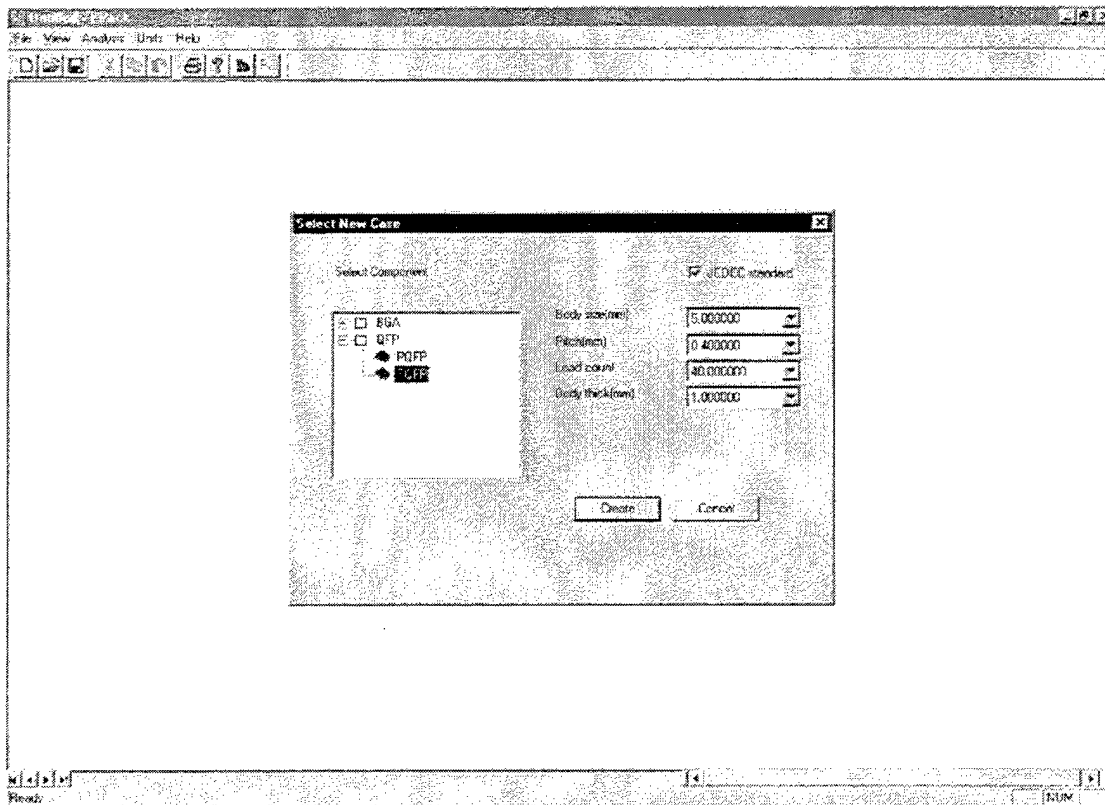
3. PBGA

4. QFP

4.1 PQFP

4.2 TQFP

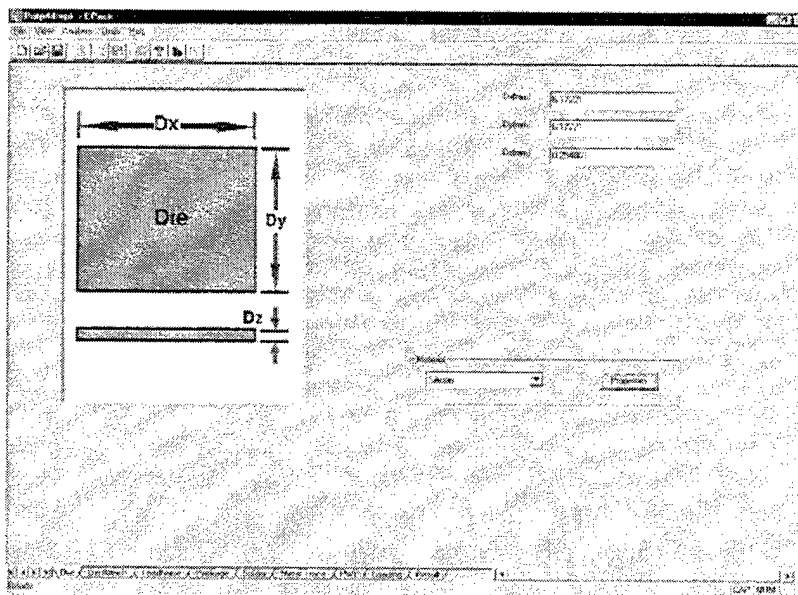
From **File-New** in the main menu, click **QFP-TQFP**, pick appropriate **Body size** (body widths), **Pitch** (lead pitch), **Lead count** (package lead count) and **Body thickness** sequentially from the menu, and click **Create** to start the analysis. For TQFP packages no registered in JEDEC, simply click the **JEDEC Standard** dialog box to clear the check mark and enter **Body size**, **Pitch**, **Lead count**, and **Body thickness** in the same way. A check mark in the **JEDEC Standard** dialog box means that the package is a JEDEC registered package, and an empty **JEDEC Standard** dialog box indicates that the package is a Non-JEDEC registered customized PBGA package.



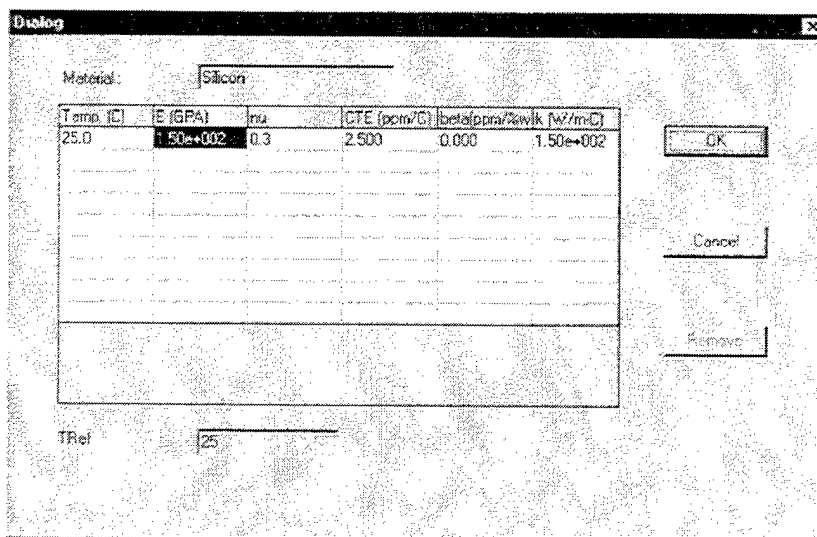
As illustrated near the bottom edge of the following figure, there are 10 sub-menus for TQFP packages: **Die**, **Die Attach**, **Leadframe**, **Package**, **Solder**, **PWB Metal Trace**, **PWB**, **Heat Sink**, **Loading**, and **Results**. Go through all the submenus to complete the analysis journey.

4.2.1 Die

- (1) Input die widths (**Dx** and **Dy**) and thickness (**Dz**) into the corresponding dialog boxes on screen.
- (2) Click Unit on top of the screen to switch between **Metric** and **English** units at any time.
- (3) Click the Material dialog box and choose a die material from the library.



- (4) Click the Properties button to review the temperature material properties.



- (5) For new materials or materials not listed in the material library, choose User Defined as the material from the Material dialog box and click Properties to define the material properties.
- (6) Enter a name as the material ID and check the Add to the material Database box if you want to include the new material in the material database for future use.

- (7) Enter **Temp**, **E** (Young's modulus), **nu** (Poisson's ratio), **CTE** (coefficient of thermal expansion), **beta** (moisture swelling coefficient), and **TRef** (reference temperature) at up to nine different temperatures in a ascending order. For materials with constant material properties, simply complete one row of the table.
- (8) The newly defined material can be removed at any time by choosing the material and press the Remove button.

Dialog

Material Add to the material Database

Temp (C)	E (GPa)	nu	CTE (ppm/C)	beta (ppm/%mk (W/mC))

OK

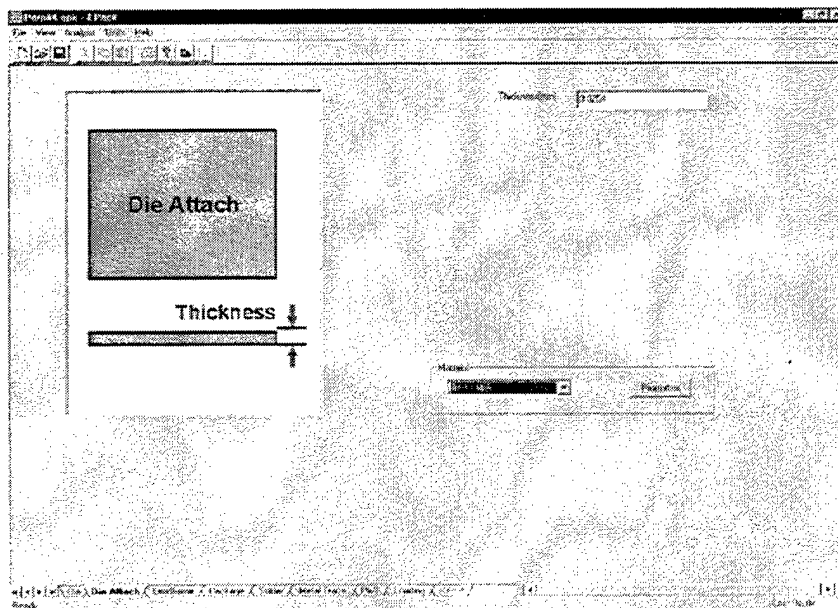
Cancel

Remove

TRef

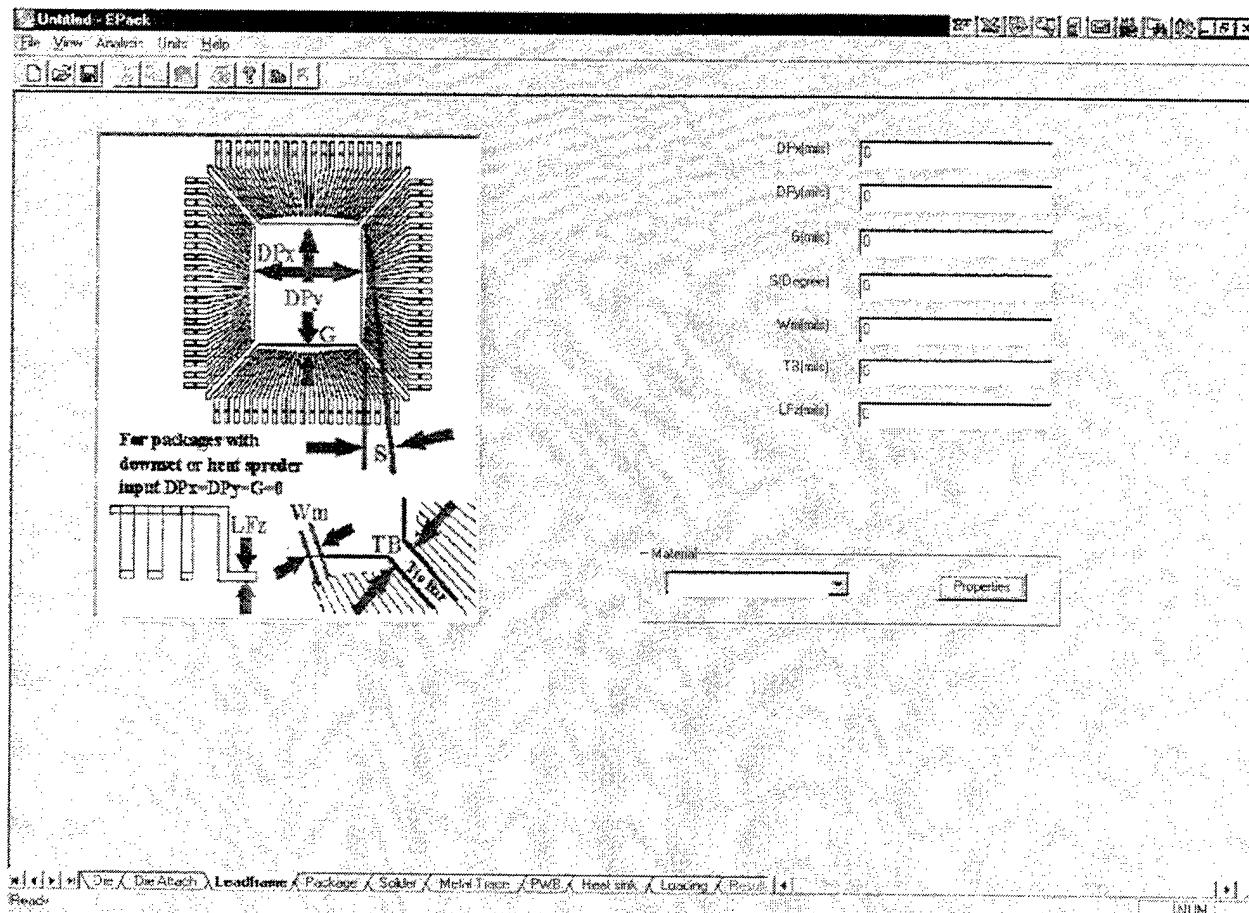
4.2.2 Die Attach

- (1) Input die attach thickness in the dialog box.
- (2) Select or define the die attach material with the same procedure as Step (2) to (8) in Section 4.2.1.



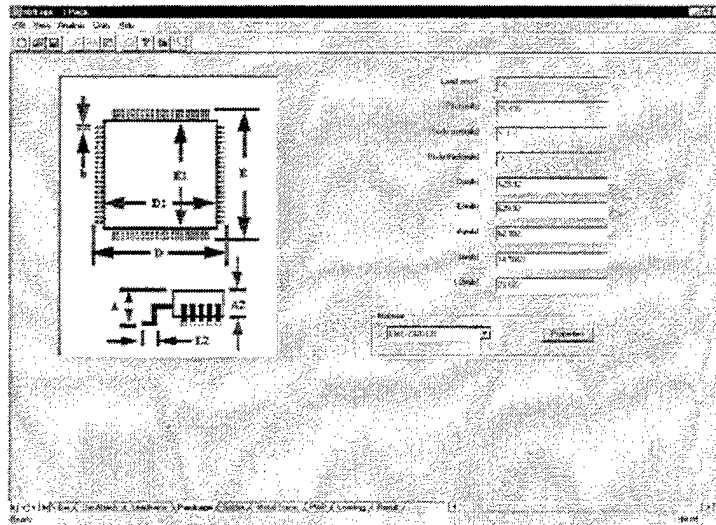
4.2.3 Leadframe

- (1) Input **DPx**, **DPy** (die attachment pad widths), **G** (the maximum gap between die pad and lead fingers), **S** (slope of die pad/lead finger gaps), **Wm** (lead fingure width), **TB** (tie bar width), and **Lfz** (leadframe thickness) in the dialog box. For packages with downset and heat sink (or heat spreader), input **Dpx**, **Dpy**, and **G** as zero (0). Detailed dimensions of the die pad and heat sink will be defined in the **Heat Sink** submenu.
- (2) Select or define the substrate metalization material with the same procedure as Step (2) to (8) in Section 3.1.



4.2.4 Package

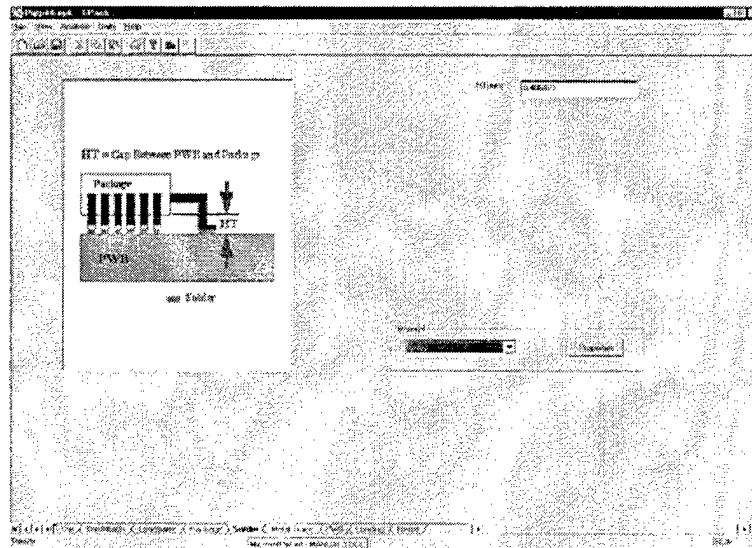
- (1) Input **D1**, **E1** (package body widths), **A2** (package body thickness), **D**, **E** (overall package widths), **A** (overall package thickness), **b** (lead width) and **L2** (lead footprint length).
- (2) Select or define the encapsulation molding compound material with the same procedure as Step (2) to (8) in Section 4.2.1.



In the on-screen menu, the lead count, pitch, body size and body thickness of the selected TQFP package are also displayed in the dim dialog boxes. EPACK does not allow users to change numbers in the dim dialog boxes. However, for advanced users, these numbers can be changed by modifying the *.EPK file from a previous run. Details on how to modify the *.EPK file are described in Appendix IV.

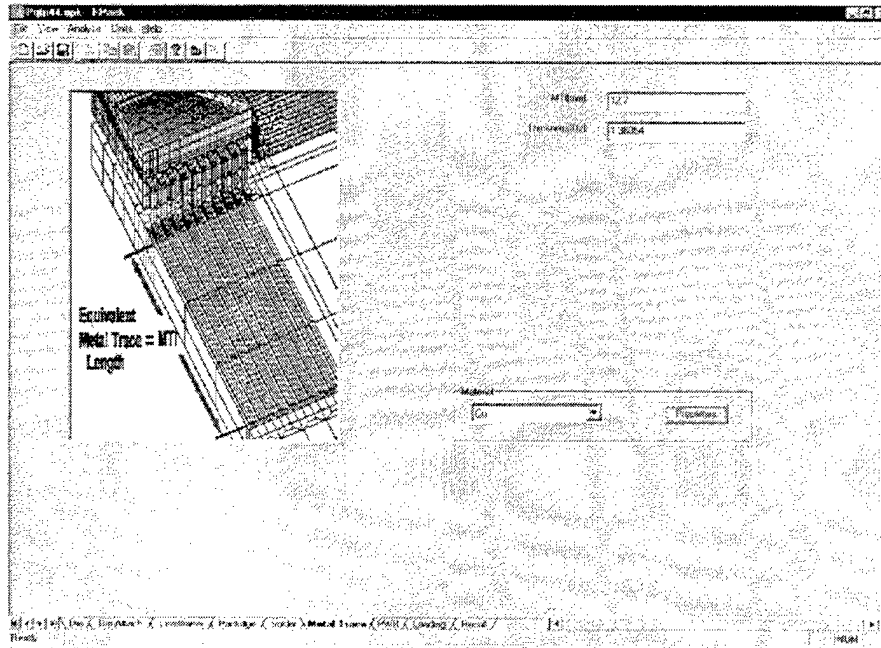
4.2.5 Solder

- (1) Input **HT** (gap between bottom surface of the package body and the PWB).
- (2) Select or define the solder material with the same procedure as Step (2) to (8) in Section 4.2.1.



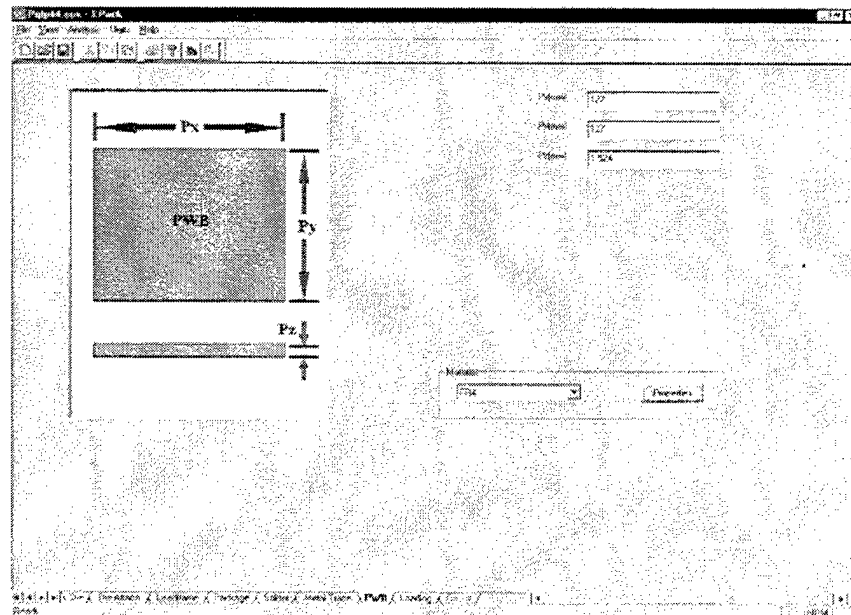
4.2.6 PWB Metal Trace

- (1) Input **MTL** (equivalent metal trace length on the PWB) and **Thickness** (thickness of the metal trace)
- (2) Select or define the metal trace material with the same procedure as Step (2) to (8) in Section 4.2.1.



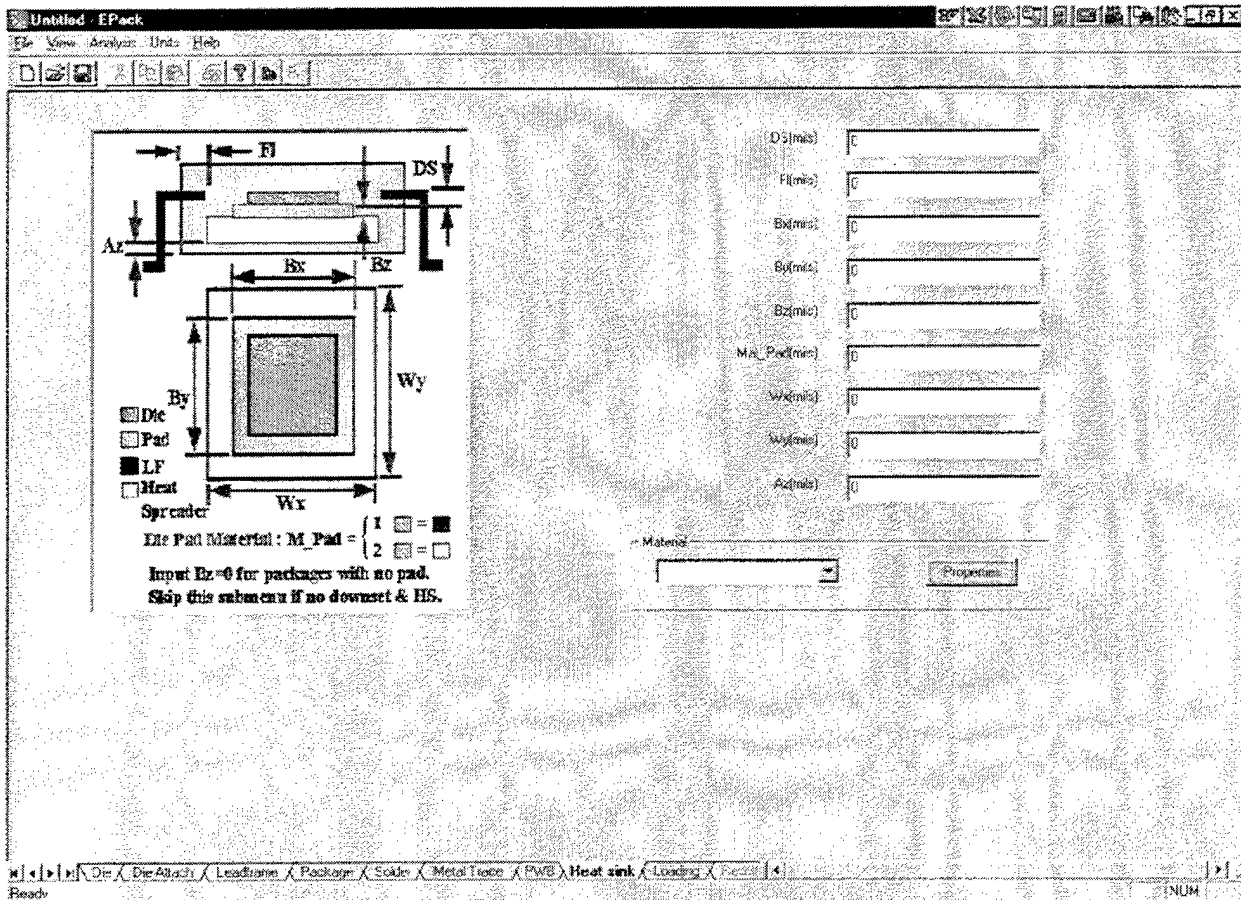
4.2.7 PWB

- (1) Input **Px**, **Py** (widths of the PWB) and **Pz** (thickness of the PWB).
- (2) Select or define the PWB material with the same procedure as Step (2) to (8) in Section 4.2.1.



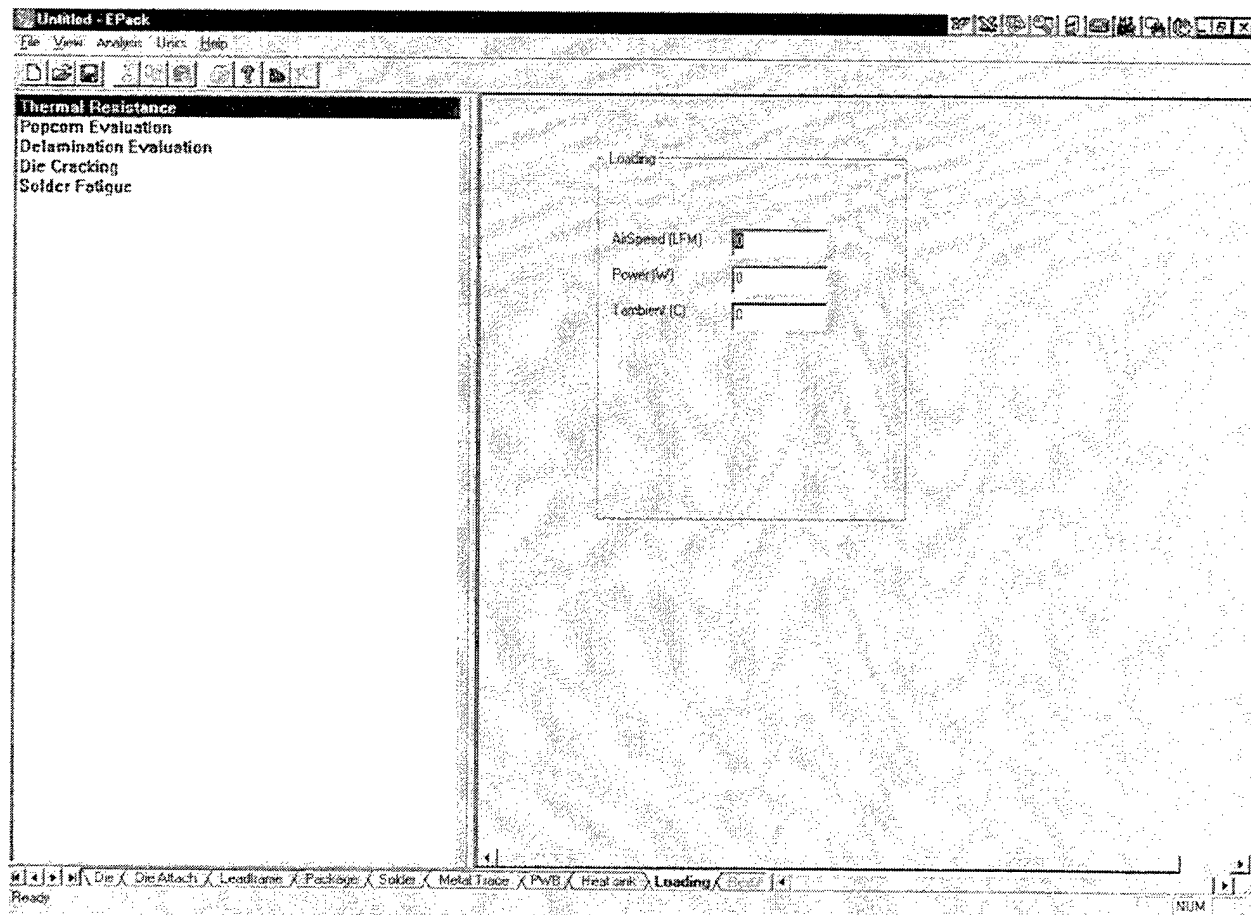
4.2.8 Heat Sink

- (1) Input **DS** (downset), **FI** (embedded lead finger length), **Bx**, **By** (die pad widths), **Bz** (die pad thickness), **Wx**, **Wy** (equivalent heat sink or heat spreader widths), **Az** (molding compound thickness underneath the heat sink), and **Mat_Pad** (die pad material index). For packages without die pad (i.e., die mounted directly to the heat sink), input **Bx**, **By**, and **Bz** as zero (0).
- (2) Select or define the PWB material with the same procedure as Step (2) to (8) in Section 4.1.1.



4.2.9 Loading, Running, and Results

- (1) Pick the desired evaluation item from the on-screen menu.
- (2) Please refer to Appendix I for detailed input instructions of each analysis item.
- (3) Please refer to Appendix II for instructions of launching the analysis.
- (4) Please refer to Appendix III for results reviewing and plotting.



Appendix I.2- Popcorn Evaluation

Under **loading** submenu, choose **Popcorn Evaluation** and enter **JEDEC Level** (JEDEC precondition levels between 1 and 6), and **Maximum Reflow Temperatur** (maximum solder reflow temperature) to start the popcorn evaluation with default moisture diffusion properties and material adhesion and fracture properties. For non-JEDEC preconditions, choose 0 for the **JEDEC Level** and uncheck the **Standard** box under **Preconditions** and enter **Temperature** (precondition temperature), **Humidity** (precondition humidity), and **Duration 'Hrs'** (precondition duration in hours). If the moisture diffusivity and moisture saturation level are known for the selected molding compound, uncheck the **Standard** box under **EMC Moisture Diffusivity**. Lastly, if the adhesion strengths (peel and shear), fracture toughness (K_{IC} and K_{IIC}) are known for the selected materials, uncheck the **Standard** box under **Delamination and Fracture Criteria** and enter Peel Strength (material interface strength under peeling), Shear Strength (material interface strength under shear), K_{IC} (mode I fracture toughness) and K_{IIC} (Mode II fracture toughness). If the **Standard** box is unchecked and a negative number is entered in a box in the table under **Delamination and Fracture Criteria**, the default number by EPACK will be used for that box. Therefore, when only part of the delamination and fracture criteria are known, the unknown values should be input as a negative number to use the program default values.

The screenshot shows the EPACK software interface with the 'Popcorn Evaluation' option selected in the sidebar. The main window contains the following settings:

- JEDEC Level:** 0
- Maximum Reflow Temp (°C):** 220
- Preconditions:**
 - ☒ Standard
 - Temperature (°C):** 165
 - Humidity (RH%):** 85
 - Duration (Hrs):** 168
- EMC Moisture Diffusivity:**
 - ☒ Standard
 - Diffusivity (cm²/s):** 8.45e-09
 - Moisture sat. (mg/cm³):** 7.2
- Delamination and Fracture criteria:**
 - ☒ Standard

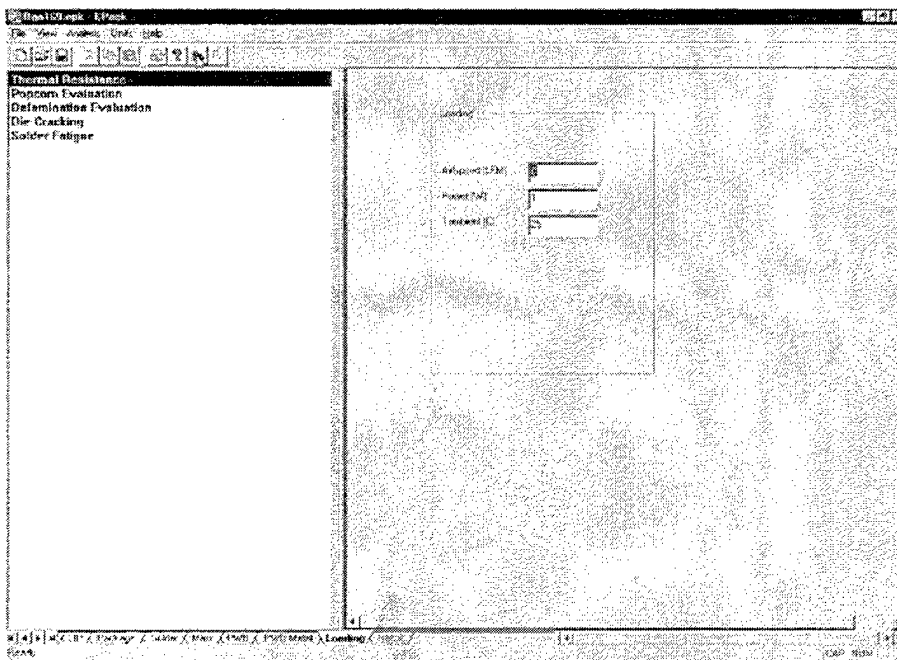
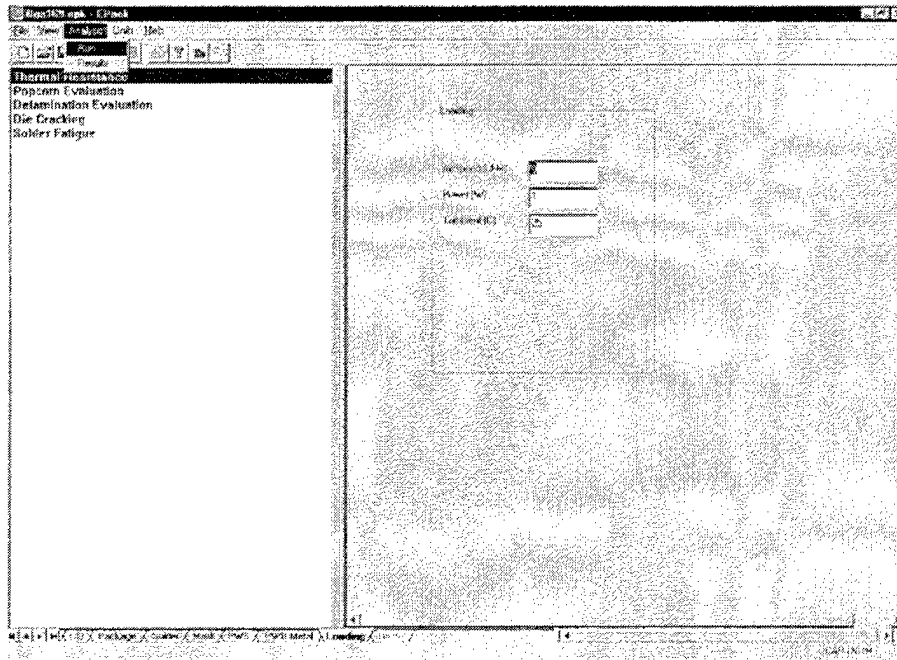
Below these settings is a table for 'Delamination and Fracture criteria' with the following data:

	Peel Strength (psi)	Shear Strength (psi)	K_{IC} (psi-in ^{3/2})	K_{IIC} (psi-in ^{3/2})
EMC/DIE	11.0	12.0	12.0	13.0
DIE/DA	21.0	22.0	23.0	24.0
PAD/EMC	31.0	32.0	33.0	34.0
EMC	N/A	N/A	43.0	N/A

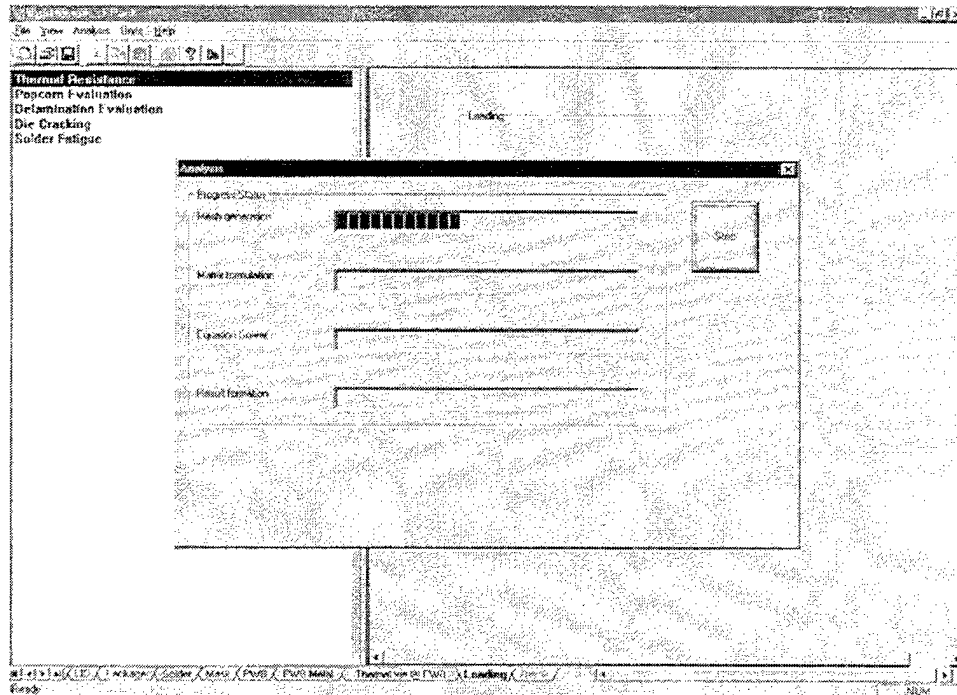
In the event of a multiple-pass reflow, for example, heatup and hold at 170 °C for 2 minutes before heating up again to 240 °C in a IR reflow, the input for **Maximum Reflow Temperature** may not be the absolute maximum temperature of the entire reflow process. If the hold time of the intermediate pass is long enough (longer than 1 minute), most of the moisture will have evaporated before reaching the maximum reflow temperature. It is recommended that, for intermediate temperature hold time longer than 1 minute, input the average of the intermediate temperature and the absolute maximum temperature as the **Maximum Reflow Temperature**. Epack will handle multiple pass reflow in the next release.

Appendix II. Launching an Analysis

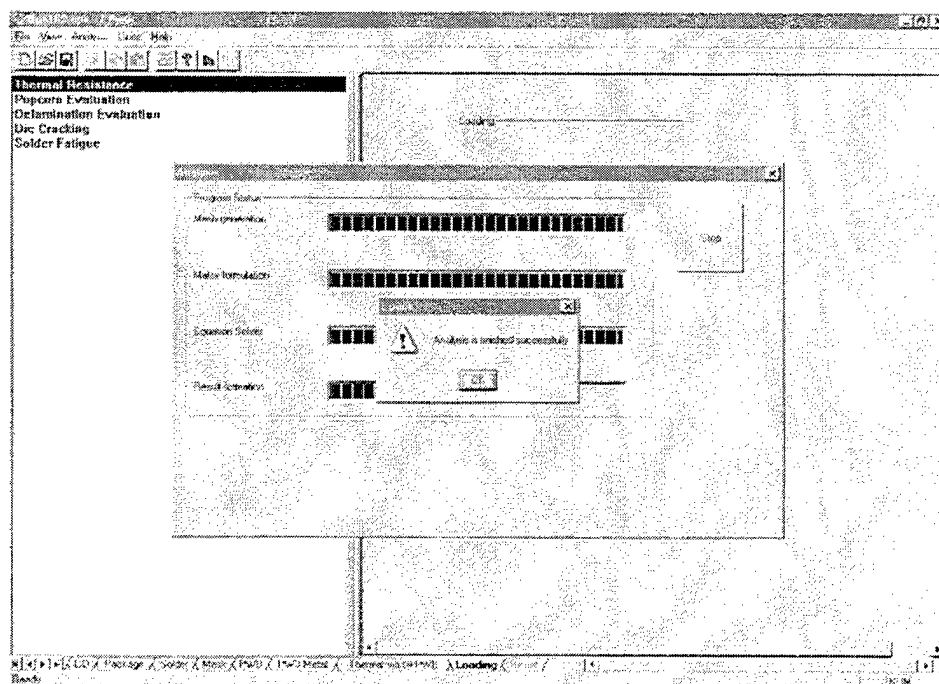
As illustrated in the following two figures, there are two ways to start the physics-based simulation after going through all the prior submenus for the problem input. One is clicking on **Analysis-Run** from the top row of the EPACK menu, and the other is simply clicking on the analysis shortcut icon, as illustrated in the bottom figure of this page.



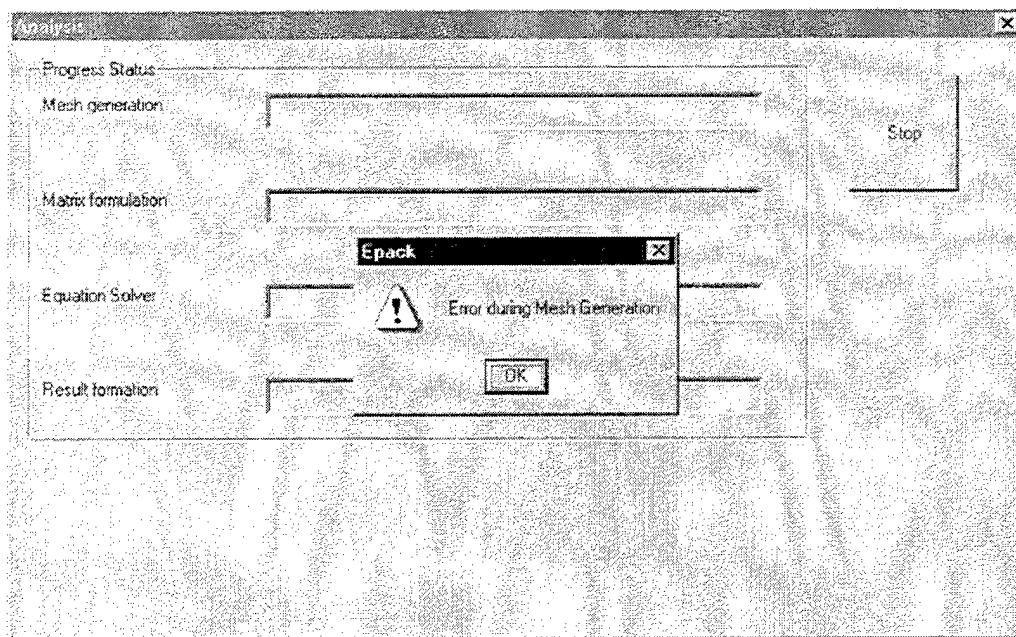
After launching the analysis, a submenu as illustrated in the following figure will pop out of the screen to indicate the analysis progress. Within EPACK, there are four major analysis steps: (1) finite element mesh generation, (2) finite element matrix formation, (4) equation solver (solving the finite element equations), and (4) result formation (writing tabulated and graphic results for review). To stop an analysis, simply click on the **Stop** button on screen at anytime.



After a successful calculation, simply click the **OK** button on screen (see the following figure) to go back to the main menu.



In case there are errors and mistakes in the data input, an error message as shown in the following figure will appear on screen.



Simply click the OK button and a diagnostic box with detailed error messages will appear near the bottom of the screen, as illustrated in the following figure. Double click each of the detailed error messages and the program will lead you to the corresponding submenu for input correction.

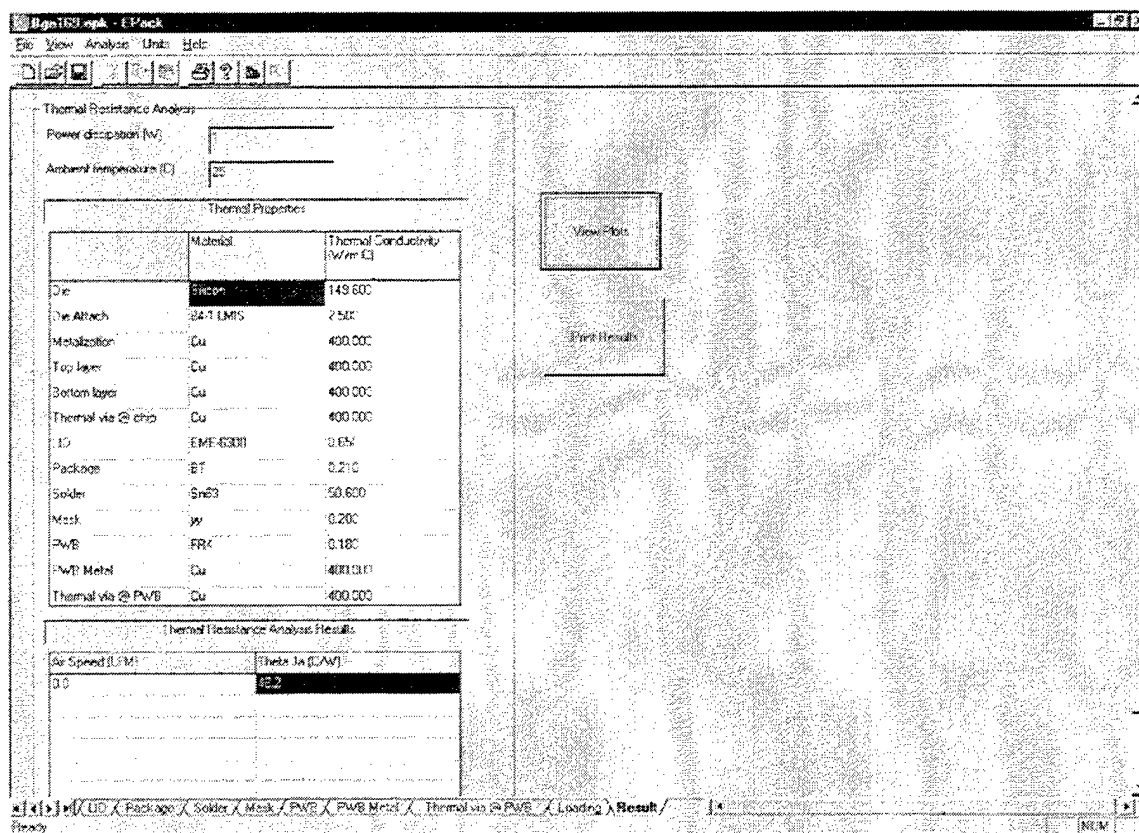


Appendix III. Results Reviewing and Plotting

Appendix III.1- Thermal Resistance Results

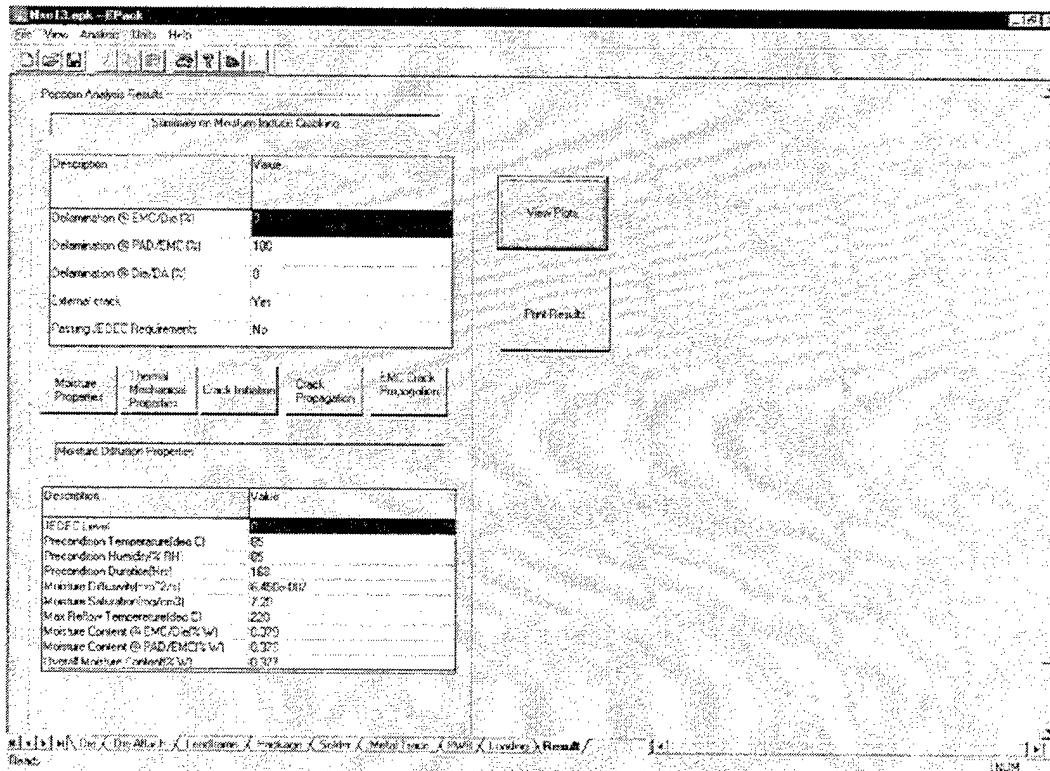
As illustrated in the figure below, the output screen for a thermal resistance analysis contains three parts. The upper part of the output echoes the input power dissipation and ambient temperature. The middle part tabulates material ID's and their thermal conductivities for each and every component of the package (die, die attach,....etc.). The bottom part of the output lists the input cooling air speed and the resulting thermal resistance, junction to ambient thermal resistance θ_{JA} .

To print the tabulated output, simply click on the **Print Results** button. To review the graphical results, click on the **View Plots** button. More details on the **View Plots** operation are described in Appendix II-3.



Appendix III.2- Popcorn Evaluation Results

As shown in the figure below, the popcorn evaluation output screen consists two parts. The upper part of the screen is the summary, while the lower part tabulates detailed information in five categories: **Moisture Properties**, **Thermal Mechanical Properties**, **Crack Initiation**, **Crack Propagation**, and **EMC Crack Propagation**. To see the detailed output under each of the five categories, click the corresponding button at the middle of the output screen.



Upon clicking on the **Moisture Properties** button, the following table will appear in the bottom half of the output screen. In this table, the **JEDEC Level** is usually between 1 and 6. A zero (0) in the **JEDEC Level** box means a user-defined package precondition has been chosen.

Description	Value
JEDEC Level	0
Precondition Temperature(deg C)	85
Precondition Humidity(% RH)	85
Precondition Duration(Hrs)	168
Moisture Diffusivity(mm^2/s)	6.450e-007
Moisture Saturation(mg/cm3)	7.20
Max Reflow Temperature(deg C)	220
Moisture Content @ EMC/Die(% w)	0.379
Moisture Content @ PAD/EMC(% w)	0.373
Overall Moisture Content(% w)	0.377

Upon clicking on the **Thermal Mechanical Properties** button, the following table will appear in the bottom half of the output screen. In this table, **E** is Young's modulus, **nu** is Poisson's ratio, **alfa** is coefficient of thermal expansion, and **beta** is moisture swelling coefficient. Although listed, the information on solder, metal trace, and PWB are not used in the popcorning evaluation and can be ignored.

Description	Material	E(GPa)	nu	alfa(ppm/c)	beta(ppm/%)
Die	nsc-die	150.00	0.30	3	0
Die Attach	Ablestik	4.30	0.30	82	0
Leadframe	nsc-lf	114.00	0.30	16	-1
Package	nsc-emc	12.20	0.30	57	-1
Solder	Sn63	14.90	0.30	25	0
Metal Trace	Cu	114.00	0.30	16	0
PWB	FR4	17.20	0.30	16	0

Upon clicking on the **Crack Initiation** button, average interface stresses and initial delamination percentage will be depicted in the bottom half of the output screen, as illustrated in the figure below.

Interface	Average peel stress (psi)	Average shear stress (psi)	Allowable peel stress (psi)	Allowable shear stress (psi)	Initial Delamination
EMC/Die	340	887	7299	7299	0
PAD/EMC	426	843	380	380	70
Die/DA	1172	930	7299	7299	0

Upon clicking on the **Crack Propagation** button, Mode I and Mode II stress intensities of the initial delamination under the hygrothermal loading and the mixed-mode interface fracture toughnesses will be listed in the bottom half of the output screen, as illustrated in the following figure. Crack propagation results of the initial delamination will be listed in the last column of the table.

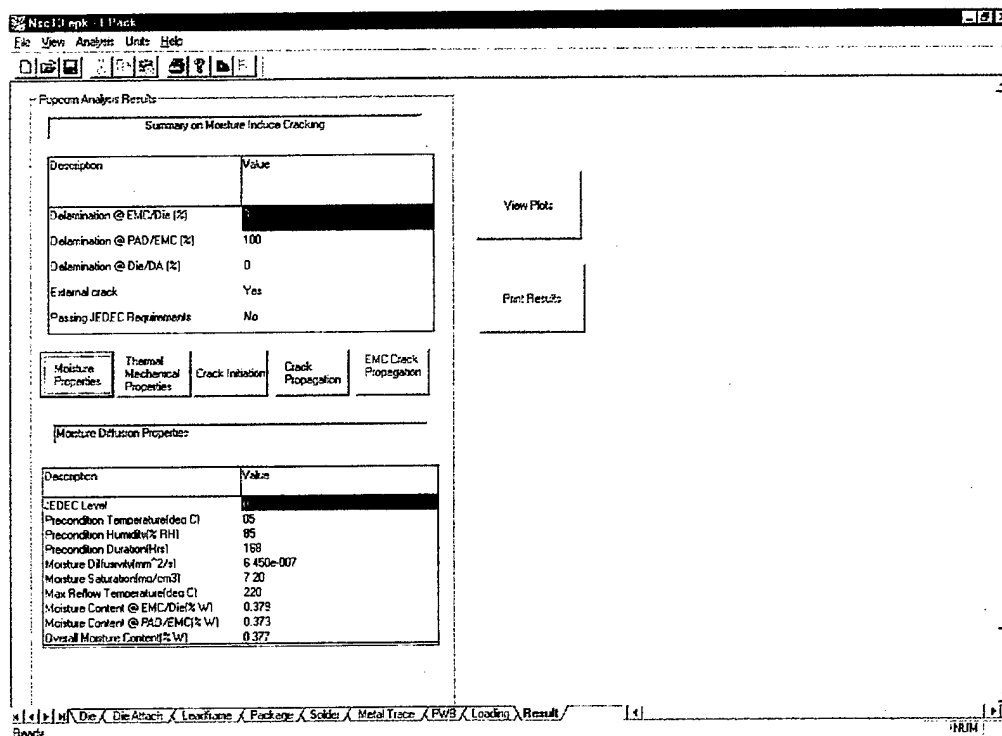
Interface	KI (psi(in ^{0.5}))	KII (psi(in ^{0.5}))	KIc (psi(in ^{0.5}))	KIIc (psi(in ^{0.5}))	Final Delamination (%)
EMC/Die	6.0	8.1	31.0	1110.2	0
PAD/EMC	157.3	180.6	118.5	529.5	100
Die/DA	13.6	8.5	310.3	11102.0	0

As illustrated in the following figure, after clicking on the **EMC Crack Propagation** button, steam pressure, Mode I stress intensity factor of the final delamination, and the molding Mode I fracture toughness will be tabulated in the bottom part of the output screen.

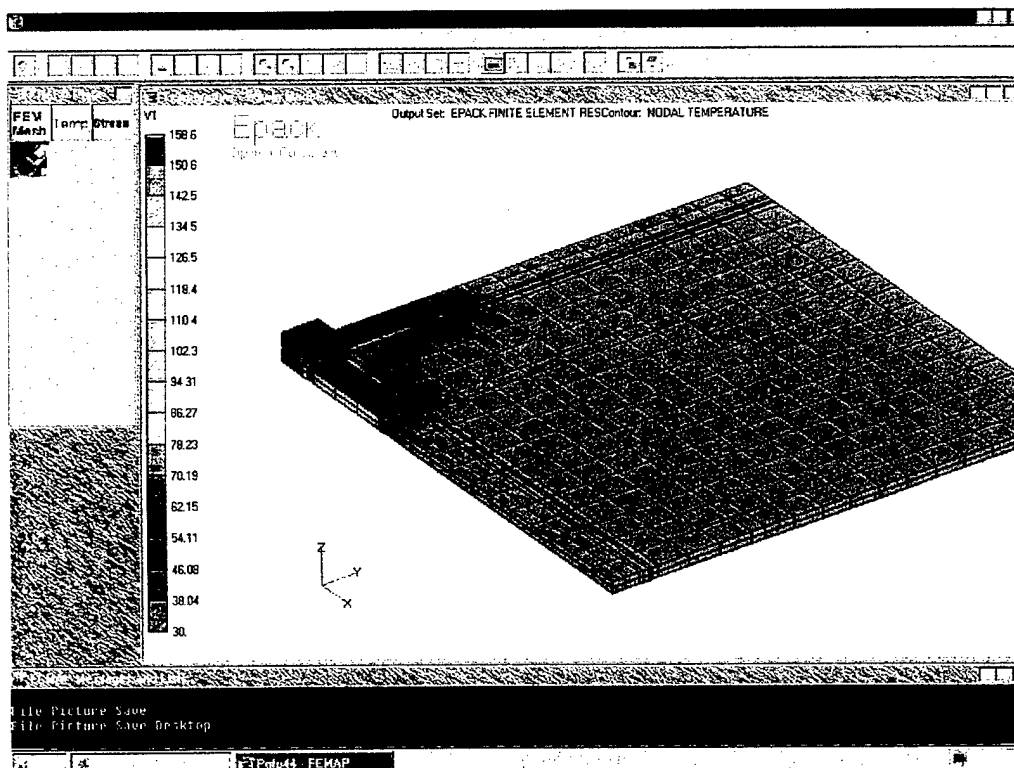
Description	Value
Steam Pressure (psi)	311.8
KI (psi(in ^{0.5}))	1518.2
KIc (psi(in ^{0.5}))	200.0
External crack	Yes

Appendix III.3- Graphic Results

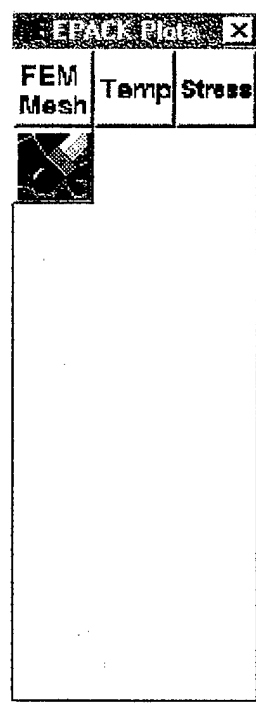
Under the Result submenu, click on the **View Plots** button to review graphical results of the EPACK analysis.




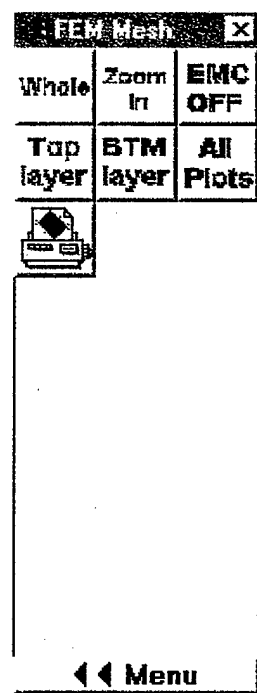
The following screen will appear after pressing the **View Plots** button.



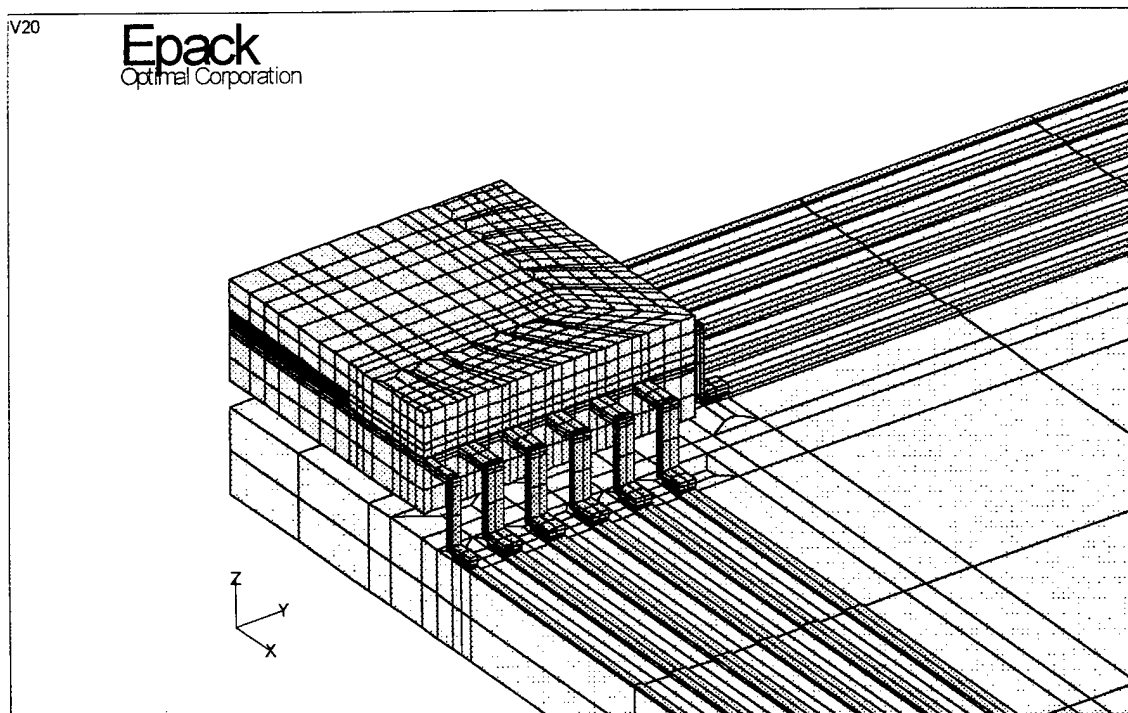
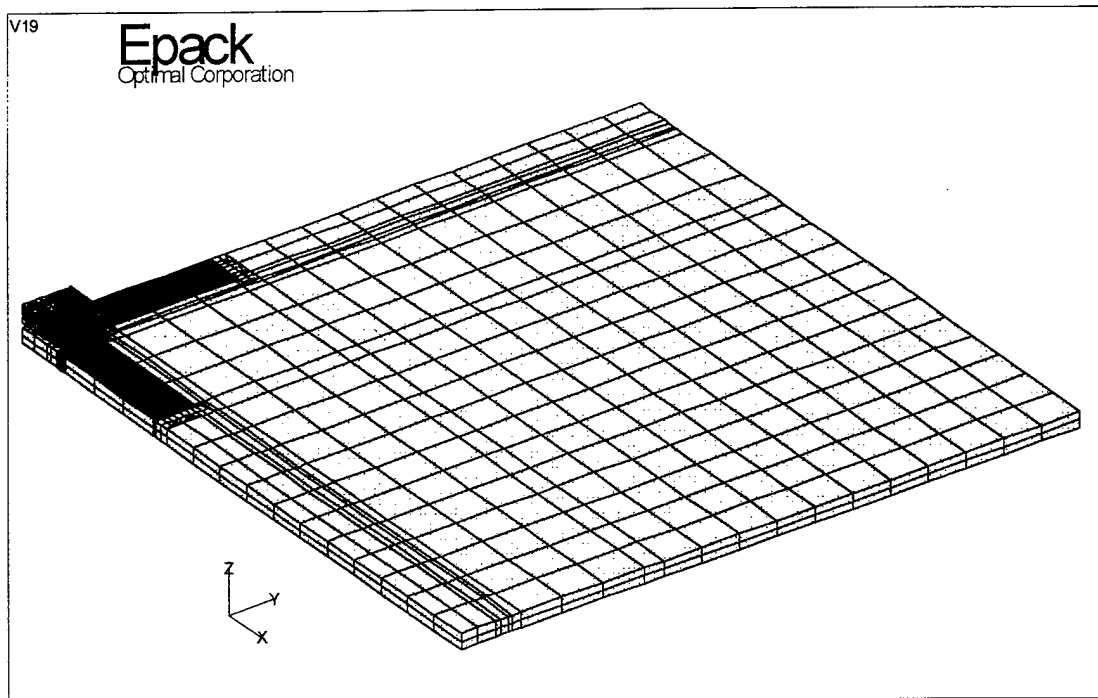
As illustrate in the following figure, the left side of the graphics screen contains a **EPACK Plots** shortcut menu for viewing and plotting the most commonly used figures. Under the **EPACK Plots** menu, there are three submenus, **FEM Mesh** (mesh of the finite element model), **Temp** (temperature plots), and **Stress** (interface stress plots).

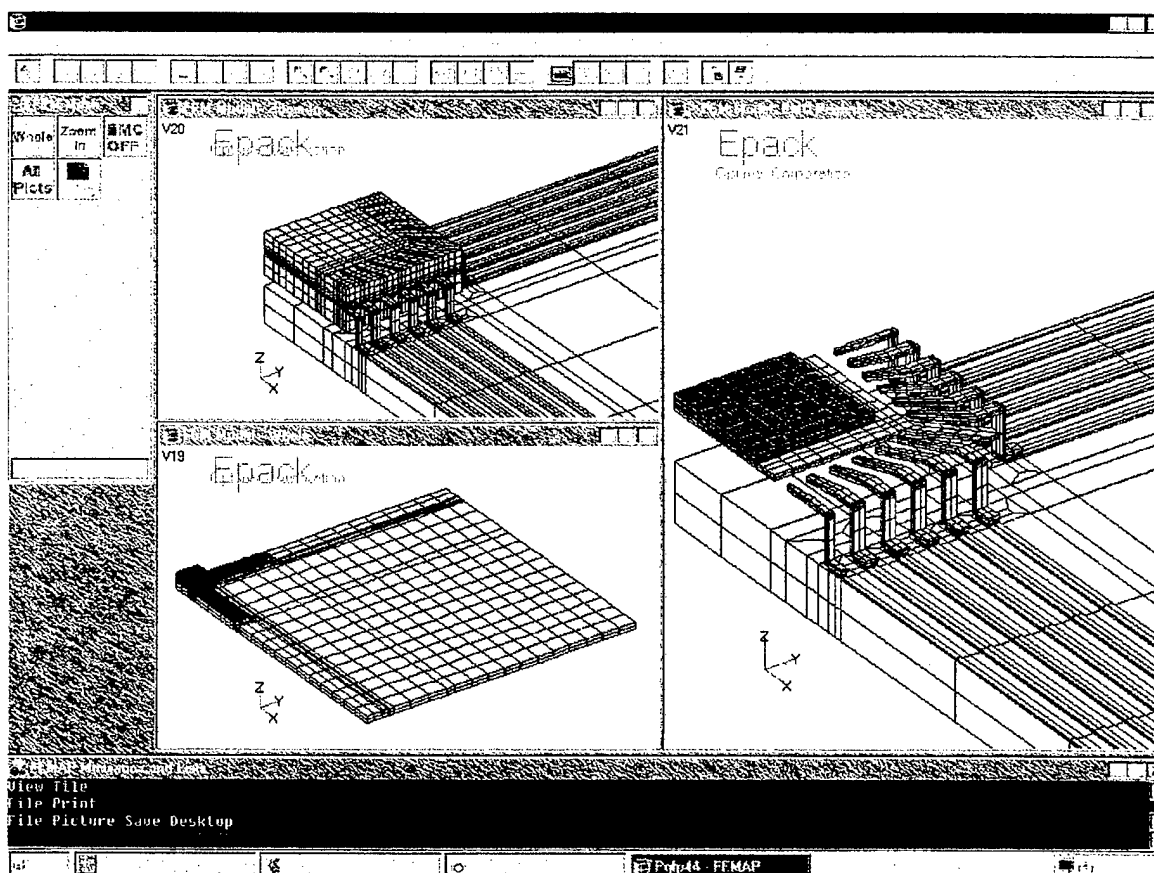
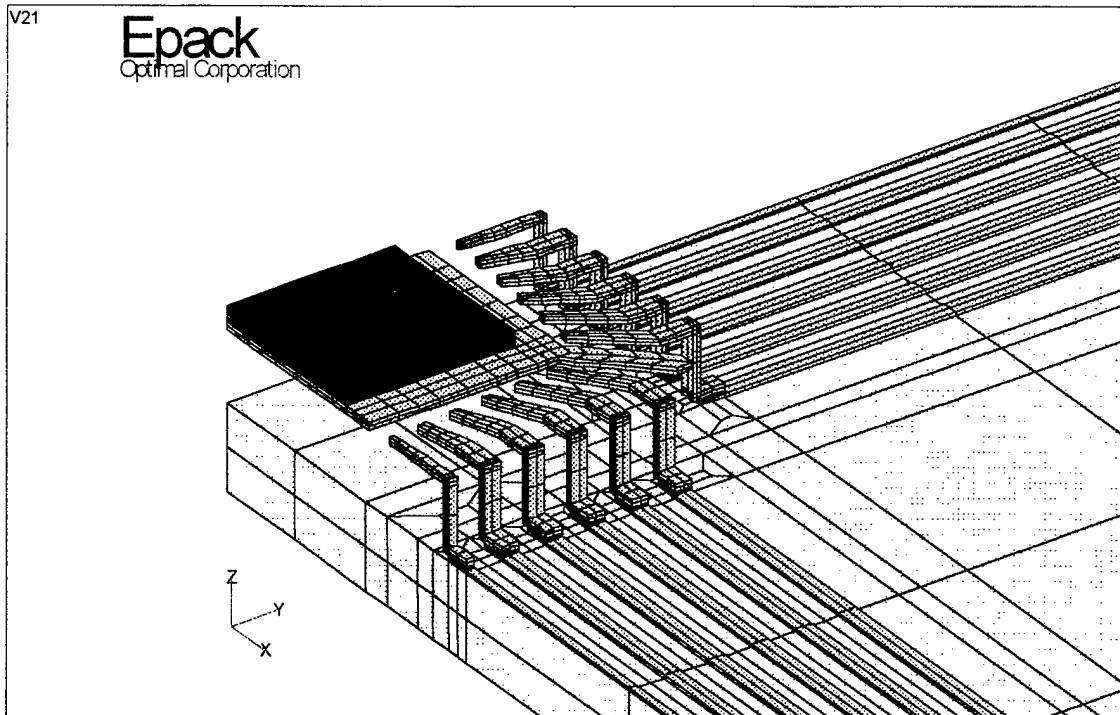


Clicking on the **FEM Mesh** button, the following submenu with five buttons: **Whole** (whole finite element model), **Zoom In** (zoom-in view of the finite element model), **EMC OFF** (zoom-in view of the finite element model without showing the molding compound material), **Top layer** (substrate metallization), **BTM layer** (substrate metalization)**All Plots** (showing the first three plots mentioned above on the screen simultantaneously), and  (a shortcut button for plotting out the figures on screen).

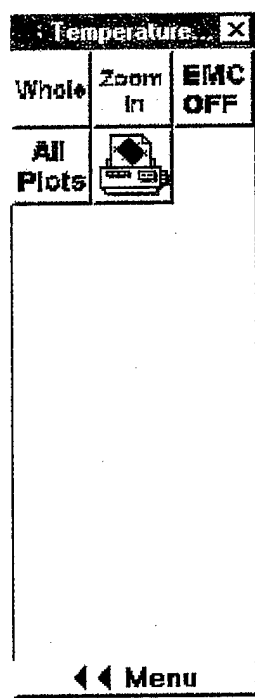


The following four figures are example plots of the figures under **Whole**, **Zoom In**, **EMC OFF**, and **All Plots** bottom.

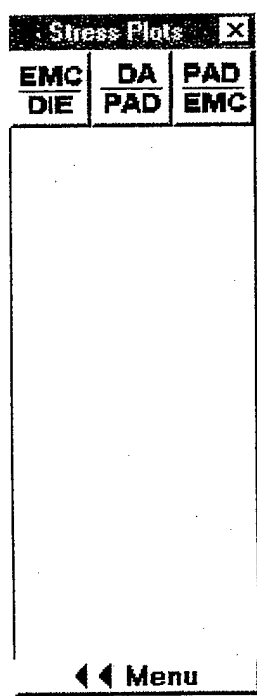




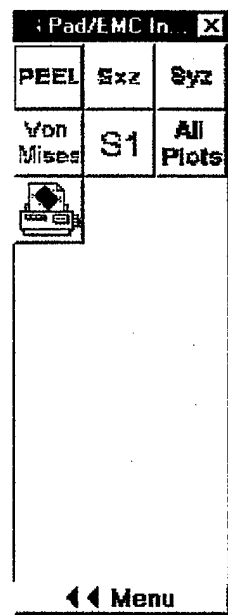
Similarly, upon clicking on the **Temp** button from the **EPACK Plots** menu, the following submenu will appear on screen. There are five buttons in this submenu and the functions of these five buttons are similar to those in the FEM Mesh submenu described above.



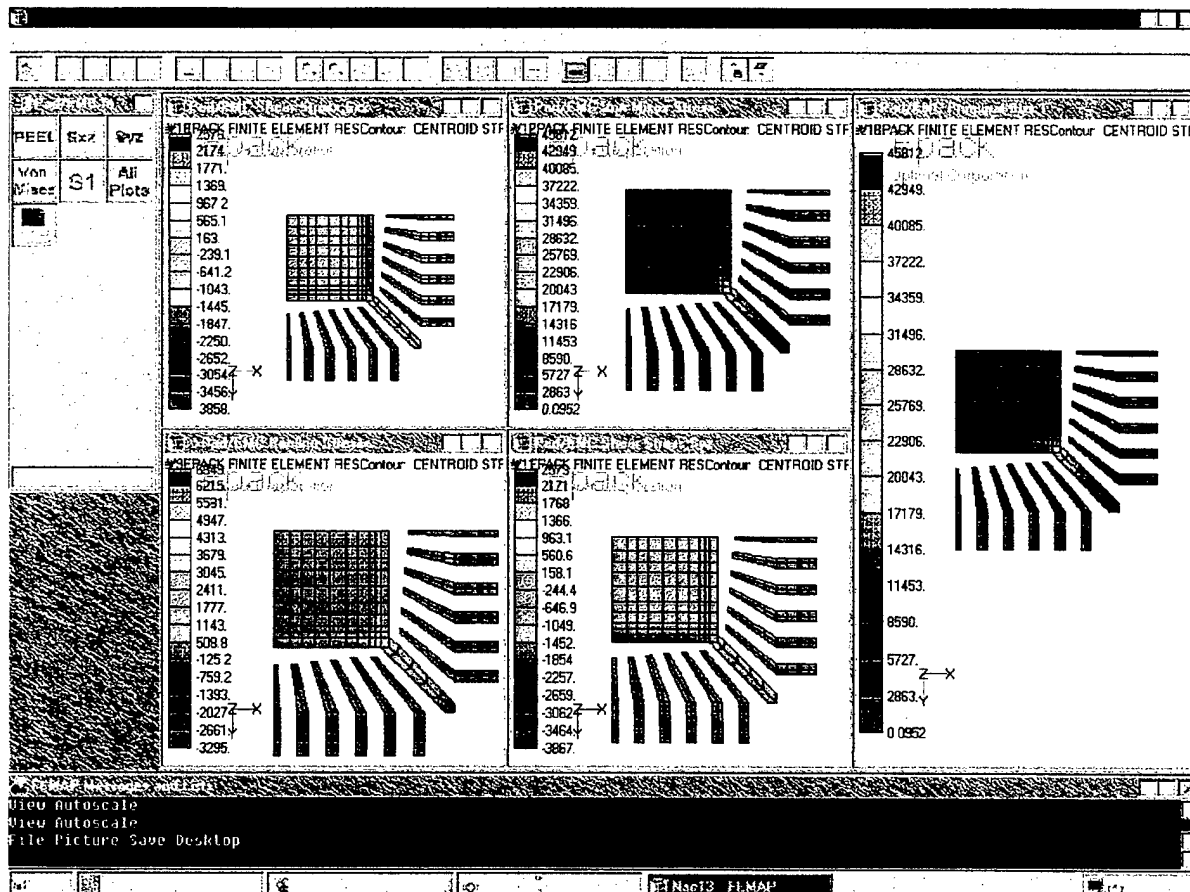
Upon pressing the Stress button from the **EPACK Plots** menu, the following submenu will appear on screen for interface stress plots. There are three buttons in this submenu, **EMC/DIE** (stresses at the EMC/die interface), **DA/PAD** (stresses at the die attach/die pad interface), and **PAD/EMC** (stresses at the die pad/EMC interface).



The following sub-submenu will appear on screen after pressing any of the three buttons in the **Stress Plots** submenu.

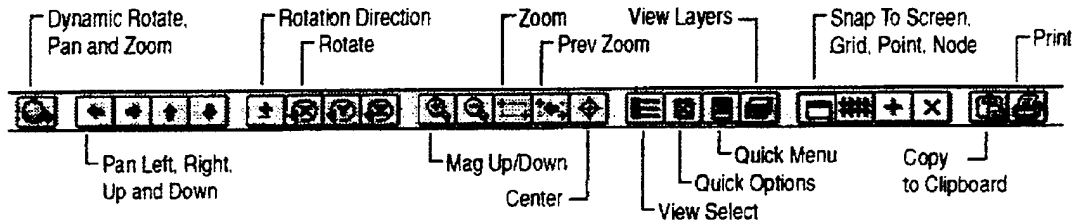


There are seven buttons in this sub-submenu: **PEEL** (peeling stress at the interface), **Sxz** and **Syz** (shear stresses at the interface), **Von Mises** (Von Mises stress at the interface), **S1** (the first principal stress at the interface), **All Plots** (all of the above five plots in one screen), and (a shortcut button for plotting out the figures on screen). The five different plots for an example problem are illustrated in the following figure.



Other Useful button on the graphics screen

EPACK uses FEMAP by Enterprise Software Products, Inc. for the graphic displays. There are many more graphics viewing tools and options under FEMAP. Advanced users please refer to the FEMAP User's manual for details of these advanced maneuvers. Some useful buttons on the FEMAP toolbar are illustrated in the following figure. Uses of these buttons on the FEMAP toolbar are self-explanatory.



Appendix IV. EPACK .EPK File Format

All of the input numbers in a EPACK are contained in the resulting *.EPK file. A sample *.EPK for the thermal resistance analysis of a 44-lead PQFP package is listed at the end of this appendix. For advanced EPACK users, it might be quicker to prepare the input file by editing an existing *.EPK file thwn to go through the input menus. As seen in the attached *.EPK file, the format of the EPACK input file is *<field> value1, value2,...*, where field is a character string describing the input quantities and *value1, value2,...*, are corresponding vakues of the input quantities. For the advanced users, modifying an existing *.EPK file with a text editor and opening the modified *.EPK file with **file-open** from the EPACK main menu may become a more efficient way to run many cases..

```
<COMPONENT> PQFP English
<PART> Die
<Dx> 243.000000
<Dy> 243.000000
<Dz> 10.000000
<MATERIAL> Silicon
<ENDPART>
<PART> Die Attach
<Thickness> 1.000000
<MATERIAL> User Defined
84-1
1
25.000000 1.000000 0.300000 16.000000 1600.000000 2.500000
25.000000
100.000000
<ENDPART>
<PART> Leadframe
<Lead count> 44.000000
<Pitch> 31.500000
<DPx> 291.000000
<DPy> 291.000000
<G> 20.000000
<S> 5.000000
<Wm> 5.999990
<TB> 15.000000
<LFz> 5.000000
<MATERIAL> User Defined
c7025
1
25.000000 1.000000 0.300000 16.000000 1600.000000 170.000000
25.000000
100.000000
<ENDPART>
<PART> Package
<D1> 393.700012
<E1> 393.700012
<A2> 68.899864
<D> 488.199799
<E> 488.199799
<A> 82.699837
<b> 11.810016
<L2> 22.799994
<MATERIAL> Nitto MP150
```

```

<ENDPART>
<PART> Solder
<HT> 16.000000
<MATERIAL> Sn63
<ENDPART>
<PART> Metal Trace
<MTI> 499.998993
<Thickness> 1.999994
<MATERIAL> Cu
<ENDPART>
<PART> PWB
<Px> 4999.990234
<Py> 4999.990234
<Pz> 59.999882
<MATERIAL> FR4
<ENDPART>
<Lead count> 44.000000
<Pitch> 31.500000
<ENDCOMPONENT>
<ANALYSISCASE> Thermal Resistance
0.000000 2.000000 30.000000
<ANALYSISCASERESULTS> 1
7
0.000000 64.305000
-1.000000 -1.000000
-1.000000 -1.000000
-1.000000 -1.000000
-1.000000 -1.000000
-1.000000 -1.000000
-1.000000 -1.000000

```

(note: JEDEC key parameter)

(note: JEDEC key parameter)